JAERI-M
87-025

PROCEEDINGS OF THE 1986 SEMINAR

ON

NUCLEAR DATA

February 1987

(Ed.) Tsuneo NAKAGAWA and Tetsuo ASAMI
JAPANESE NUCLEAR DATA COMMITTEE

日 本 原 子 力 研 究 所
Japan Atomic Energy Research Institute

Proceedings of the 1986 Seminar on Nuclear Data

(Ed.) Tsuneo NAKAGAWA and Tetsuo ASAMI

Japanese Nuclear Data Committee

Tokai Research Establishment

Japan Atomic Energy Research Institute

Tokai-mura, Naka-gun, Ibaraki-ken

The 1986 Seminar on Nuclear Data was held on November 26 and 27, 1986 at Tokai Research Establishment of Japan Atomic Energy Research Institute. This is an annual meeting which has been held since 1978, with the support of Japanese Nuclear Data Committee. The participants were about eighty including two scientists from China and Argentine who were just staying in Japan.

The seminar was made mainly focussing at the problems on the post-JENDL-3 activities on nuclear data and at the reactor constants and their sensitivitiy analyses. The poster session was carried out with the subjects on the post-JENDL-3 activities, recent measurements of neutron cross sections and computer codes for theoretical calculations.

The proceedings contain the papers presented in both the oral and poster sessions of the seminar. The texts are reproduced directly from the authors' manuscripts.

Programme and Executive Committee.

S. Igarasi	(Chairman, Japan Atomic Energy Research Institute)
T. Asami	(Japan Atomic Energy Research Institute)
A. Hasegawa	(Japan Atomic Energy Research Institute)
S. Iijima	(Nippon Atomic Industry Group Co., Ltd.)
M. Kawai	(Nippon Atomic Industry Group Co., Ltd.)
Y. Kawarasaki	(Japan Atomic Energy Research Institute)
K. Kitao	(National Institute of Radiological Sciences)
H. Matsunobu	(Sumitomo Atomic Energy Industries, Ltd.)
T. Nakagawa	(Japan Atomic Energy Research Institute)

R. Nakasima   (Hosei University)

M. Nakazawa   (University of Tokyo)

M. Sasaki   (Mitsubishi Atomic Power Industries, Ltd.)

H. Takano   (Japan Atomic Energy Research Institute)

1986 年核データ研究会報告書

日本原子力研究所東海研究所 シグマ研究委員会

（編）中川　庸雄・浅見　哲夫

　　1986 年核データ研究会は，1986 年（昭和 61 年）11 月 26・27 日の両日に日本原子力研究所の東海研究所において開催された。この研究会は 1978 年以来毎年，シグマ研究委員会の下で恒例の形で開催されているものであって，今回は国内の研究者約 80 名および日本に滞在中の中国とアルゼンチンからの研究者各 1 名が参加した。

　　研究会では (1) JENDL－3 後の核データ活動に関する問題，(2)炉定数と感度解析のテーマを中心に討議が行われた。ポスターセッションでは，(1)JENDL－3 以降 の核データ活動に関する問題の他に，(2)最近の測定，および (3) 理論計算コードについて発表があった。

　　この報告書には，研究会での講演・討議およびポスター発表にもとづく論文を収録してある。各報文は，著者の原稿をそのまゝ直接に写真印刷とした。

核データ研究会準備委員会委員

　　　　五十嵐信一（委員長・日本原子力研究所）

　　　　浅見　哲夫（日本原子力研究所）

　　　　飯島　俊吾（日本原子力事業（株））

　　　　川合　将義（日本原子力事業（株））

　　　　河原崎雄紀（日本原子力研究所）

　　　　喜多尾憲助（放射線医学総合研究所）

　　　　佐々木　誠（三菱原子力工業（株））

　　　　高野　秀機（日本原子力研究所）

　　　　中川　庸雄（日本原子力研究所）

　　　　中沢　正治（東京大学原子力工学研究施設）

　　　　中嶋　龍三（法政大学）

　　　　長谷川　明（日本原子力研究所）

　　　　松延　廣幸（住友原子力工業（株））

CONTENTS

目　　次

2. Post-JENDL-3 Activities

2.1 A Review of JENDL-3 Plan

T. Asasmi

Nuclear Data Center

Japan Atomic Energy Institute

Japanese Evaluated Nuclear Data Library, Version 3, JENDL-3 has planned to be used mainly for development of fusion reactors and studies of radiation shieldings as well as researches of fast breeder- and thermal reactors. Its compilation is now in progress, aiming at its completion in March 1987.

The outline of JENDL-3 plan and the features of JENDL-3 data are presented together with its historical passages of JENDL-3 plan.

1. Introduction

In the next paper, the problems on the post-JENDL-3 are discussed. The purpose of this paper is to show in advance the general futures of JENDL-3 plans which are now in progress. A plan of JENDL-3(Japanese Evaluated Nuclear Data Version 3) have been described by several authors[1)-3)] elsewhere. Therefore, only brief summary is given as well as its historical passages in this paper.

2. History of JENDL

The first version of JENDL(JENDL-1) was compiled in 1977, aming mainly at the uses for design calculations of fast reactors. The second version, JENDL-2 was compiled in 1982 to use not only for fission reactors but also for fusion researches which had been developed rapidly.

In JENDL-2, the range of the neutron energy was extended from 15 to 20 MeV, and the evaluated data were improved mainly for structural and fissile materials. In JENDL-2, however, the data of some nuclides important for fusion researches have not been compiled, and some data for high energies around 14 MeV were not satisfactory particularily for uses in fusion neutronics. Thought of such situation, Japanese Nuclear Data Committee (JNDC) started early a task force in March 1980 to

examine the JENDL-3 plans, although JENDL-2 had not yet been released at
that time. The task force collected the requests for JENDL-3 mainly from
the JNDC members by the questionaries. On the basis of those requests,
the task force gave the essences of the JENDL-3 plan, taking account of
the manpower and costs as well as the uses in wide fields for
nuclear-energy researches. These are roughly divided into the following
items.

1) to keep the upper limit of neutron energy at 20 MeV.

2) to hold the number of additional nuclides in minimum.

3) to adopt newly the nuclear data for photon production.

4) to improve the data on high-energy neutrons.

However, the task force was not able to give definite conclusiions for
both covariance data and special purpose files.

   In JNDC the work on data evaluation for JENDL-3 started in 1981 to
meet the demands mentioned above, aiming at the completion in 1987.

3. General Futures of JENDL-3

   An outline of the JENDL-3 plan is summarized as follows.

1) Nuclides stored in JENDL-3

   Only about 10 nuclides which were requested with high priorities in
the questionaries are added to JENDL-2 as new ones. Table 1 shows the
nuclides which will be stored in general file of JENDL-3. Table 2 also
shows the nuclides of fission products stored in JENDL-3. The comparison
of the nuclides stored in JENDL-3 between other large files in the world
is made in Table 3, classifiing in six mass-regions. From Table 3 it is
found that the number of nuclides in JENDL-3 is almost equal to that of
ENDF/B-V, and JENDL-3 has more nuclides with the mass lower than 30, in
comparing with that of ENDF/B-V. The latter due to the fact that JENDL-3
deal with the data of stable isotopes as well as the ones for element
and ENDF/B-V compiles mainly the data for natural element. Similarly
KEDAK-4 has comparatively more nuclides with low masses, because of
having the data for isotopes.

2) Adoption of the data for photon production

   The nuclear data for photon production, i.e. the ones for the
mulitiplicity(or the transition probability), the cross sections, and
the angular-and energy-distributions for gamma-rays emitted secondarily
are evaluated newly for JENDL-3. Twenty-seven nuclides will have the

evaluated data for photon production in JENDL-3, as shown shown by the asterisks in Table 1.

In order to examine the way for evaluating the photon-production data and for making these files, the working group on nuclear data for photon production has been organized in JNDC.

3) Improvement of the data for high-energy neutrons

The JENDL-2 data were improved largely for inelastic scattering and threshold reactions. In the evaluations of JENDL-2 data, however, the direct process in inelastic scattering was ignored for almost nuclides. Although this ignorance have not caused trouble for the cases to deal with neutrons with rather low energies, some tests for high-energy neutrons indicated that it gave a large effect.

In the data evaluations for almost all nuclides in JENDL-3, the cross sections and angular distribution for the direct process are calculated in the basis of either DWBA or coupled-channel model. All the data for threshold reactions significant below 20 MeV are evaluated in taking account of precompound effects, including the data of (n,n'p),(n,n'a), etc..

4) Double Differential Data

In the JENDL-3 data evaluation, we have made much efforts for the double differential data which play an important role in fusion neutronics. In the data evaluation, the recent measured data from both Osaka University and Tohoku University have been used effectively.

5) Data Refinement

In the data evaluations of JENDL-3 the calculations with theoretical model have been used in many part. Therefore, the model parameters such as optical potential, level density and so on have been examined in large extent. Almost all data of JENDL-2 have been looked over again and reevaluated as a whole. For example, the simultanous evaluation was made for the fission cross sections of ^{235}U, ^{238}U, ^{239}Pu, ^{240}Pu and ^{214}Pu and the capture cross sections of ^{197}Au and ^{238}U[4]).

4. Preliminary Version of JENDL-3

As described above, the JENDL-2 data, in particular the double differential cross sections deduced from JENDL-2 were insufficient for requirements from fields of fusion neutronics. In order to response an

urgent requests from the fusion neutronics group in JAERI, we decided to evaluate early for some nuclides important for fusion neutronics before the compilation of JENDL-3.

The evaluated data for ^{6}Li, ^{7}Li, ^{9}Be, ^{12}C, ^{16}O, Cr, Fe and Ni were reevaluated and compiled in the end of 1983. This temporary file is called JENDL-3PR1 (JENDL-3 Preliminary Version 1)[5)-8)]. After that these data were further revised and are referred as JENDL-3PR2. Furthur revisions will be made for a few data in JENDL-3PR2.

5. Futute Problems

As described above, there are some items which we were not able to adopt in JENDL-3 plan. That are covariance data and special purpose file including dosimetry data, activation cross section and so on. A part of these will be taken into account as tasks for the post-JENDL-3 plan which are discussed in the next paper.

References

1) Igarasi,S.:"Scope of JENDL-3",JAERI-M 9523 (1981) p.199
   (in Japanese).

2) Asami,T. and Igarasi,S.:"Plan for Compilation of JENDL-3",J. the
   Atomic Energy Soc. of Japan(Nihon-Genshiryoku Gakkai-Shi) 23,904
   (1981) (in Japanese).

3) Asami,T.:"Status of JENDL-3 Compilation",JAERI-M 83-041 (1983) p.171
   (in Japanses).

4) Kanda,Y., Uenohara,Y., Murata,T., Kawai,M., Matsunobu,H.,
   Nakagawa,T., Kikuchi,Y. and Nakajima,Y.: ibid. p.1567.

5) Asami,T.:"Status of JENDL-3PR1 and 3PR2", JAERI-M 86-029 (1986)
   p.15.

6) Chiba,S.:"Revision of the Neutron Nuclear Data of Lithium", ibid.
   p.32.

7) Kikuchi,Y., Shibata,K., Asami,T., Sugi,T. and Yamakoshi,H.: J. Nucl.
   Sci. Tech. 22, 499 (1985).

8) Shibata,K. and Kikuchi,Y.: Proc. of the Intern. Conf. on Nucl. Data
   for Basic and Applied Science (Santa Fe,1985)(Gordon and Breach
   Science Publishers, 1986) Vol.2, p.1585.

Table 1. Nuclides in the General Purpose File of JENDL-3. The underlines denote the nuclides stored newly in JENDL-3. The asterisks show the nuclides with the evaluated data for photon production.

Z	Nuclide	Z	Nuclide	Z	Nuclide
1	^{1}H, ^{2}H	21	^{45}Sc	63	*Eu, ^{151}Eu, ^{153}Eu
-	^{3}He, ^{4}He	22	*Ti, ^{40}Ti, ^{47}Ti, ^{48}Ti, ^{49}Ti, ^{50}Ti	72	*Hf, ^{174}Hf, ^{176}Hf, ^{177}Hf, ^{178}Hf, ^{179}Hf, ^{180}Hf
2		23	^{51}V	73	*^{181}Ta
3	*^{6}Li, *^{7}Li	24	*Cr, ^{50}Cr, ^{52}Cr, ^{53}Cr, ^{54}Cr	74	*W, ^{180}W, ^{182}W, ^{183}W, ^{184}W, ^{186}W
4	*^{9}Be	25	^{55}Mn	82	*Pb, ^{204}Pb, ^{206}Pb, ^{207}Pb, ^{208}Pb
5	^{10}B, ^{11}B	26	*Fe, ^{54}Fe, ^{56}Fe, ^{57}Fe, ^{58}Fe	83	*^{209}Bi
6	*^{12}C	27	^{59}Co	90	Th, ^{228}Th, ^{230}Th, ^{232}Th, ^{233}Th, ^{234}Th
7	*^{14}N	28	*Ni, ^{58}Ni, (^{59}Ni), ^{60}Ni, ^{61}Ni, ^{62}Ni, ^{64}Ni	91	^{231}Pa, ^{233}Pa
8	*^{16}O	29	*Cu, ^{63}Cu, ^{65}Cu	92	^{232}U, ^{233}U, ^{234}U, *^{235}U, ^{236}U, *^{238}U
9	^{19}F	30	Zr	93	^{237}Np, ^{239}Np
11	*^{23}Na	41	*^{93}Nb, (^{94}Nb)	94	^{236}Pu, ^{238}Pu, *^{239}Pu, ^{240}Pu, ^{241}Pu, ^{242}Pu
12	*Mg, ^{24}Mg, ^{25}Mg, ^{26}Mg	42	*Mo, ^{92}Mo, ^{94}Mo, ^{95}Mo, ^{96}Mo, ^{97}Mo, ^{98}Mo, ^{100}Mo	95	^{241}Am, ^{242g}Am, ^{242m}Am, ^{243}Am
13	*^{27}Al			96	^{242}Cm, ^{243}Cm, ^{244}Cm, ^{245}Cm, ^{246}Cm, ^{247}Cm, ^{248}Cm, ^{249}Cm
14	*Si, ^{28}Si, ^{29}Si, ^{30}Si	47	Ag, ^{107}Ag, ^{109}Ag	97	^{249}Bk
15	^{31}P	48	Cd	98	^{249}Cf, ^{250}Cf, ^{251}Cf
16	S, ^{32}S, ^{33}S, ^{34}S, ^{36}S				
17	Cl, ^{35}Cl, ^{37}Cl	51	Sb, ^{121}Sb, ^{123}Sb		
18	^{40}Ar				
19	K, ^{39}K, ^{40}K, ^{41}K				
20	*Ca, ^{40}Ca, ^{42}Ca, ^{43}Ca, ^{44}Ca, ^{46}Ca, ^{48}Ca				

Table 2. Fission Product Nuclides in JENDL-3.

The underlines denote the nuclides stored newly in JENDL-3.

Z	Nuclide
33	^{75}As
34	^{74}Se, ^{76}Se, ^{77}Se, ^{78}Se, ^{79}Se, ^{80}Se, ^{82}Se
35	^{79}Br, ^{81}Br
36	^{78}Kr, ^{80}Kr, ^{82}Kr, ^{83}Kr, ^{84}Kr, ^{85}Kr, ^{86}Kr
37	^{85}Rb, ^{87}Rb
38	^{86}Sr, ^{87}Sr, ^{88}Sr, ^{89}Sr, ^{90}Sr
39	^{89}Y, ^{91}Y
40	^{90}Zr, ^{91}Zr, ^{92}Zr, ^{93}Zr, ^{94}Zr, ^{95}Zr, ^{96}Zr
41	^{93}Nb, ^{95}Nb
42	^{92}Mo, ^{94}Mo, ^{95}Mo, ^{96}Mo, ^{97}Mo, ^{98}Mo, ^{99}Mo, ^{100}Mo
43	^{99}Tc
44	^{96}Ru, ^{98}Ru, ^{99}Ru, ^{100}Ru, ^{101}Ru, ^{102}Ru, ^{103}Ru, ^{104}Ru, ^{106}Ru
45	^{103}Rh, ^{105}Rh
46	^{102}Pd, ^{104}Pd, ^{105}Pd, ^{106}Pd, ^{107}Pd, ^{108}Pd, ^{110}Pd
47	^{107}Ag, ^{109}Ag, ^{110m}Ag
48	^{106}Cd, ^{108}Cd, ^{110}Cd, ^{111}Cd, ^{112}Cd, ^{113}Cd, ^{114}Cd, ^{116}Cd
49	^{113}In, ^{115}In
50	^{112}Sn, ^{114}Sn, ^{115}Sn, ^{116}Sn, ^{117}Sn, ^{118}Sn, ^{119}Sn, ^{120}Sn, ^{122}Sn, ^{123}Sn, ^{124}Sn, ^{126}Sn
51	^{121}Sb, ^{123}Sb, ^{124}Sb, ^{125}Sb
52	^{120}Te, ^{122}Te, ^{123}Te, ^{124}Te, ^{125}Te, ^{126}Te, ^{127m}Te, ^{128}Te, ^{129m}Te, ^{130}Te
53	^{127}I, ^{129}I, ^{131}I
54	^{124}Xe, ^{126}Xe, ^{128}Xe, ^{129}Xe, ^{130}Xe, ^{131}Xe, ^{132}Xe, ^{133}Xe, ^{134}Xe, ^{135}Xe, ^{136}Xe
55	^{133}Cs, ^{134}Cs, ^{135}Cs, ^{136}Cs, ^{137}Cs, ^{138}Cs
56	^{130}Ba, ^{132}Ba, ^{134}Ba, ^{135}Ba, ^{136}Ba, ^{137}Ba, ^{138}Ba, ^{140}Ba
57	^{138}La, ^{139}La
58	^{140}Ce, ^{141}Ce, ^{142}Ce, ^{144}Ce
59	^{141}Pr, ^{143}Pr
60	^{142}Nd, ^{143}Nd, ^{144}Nd, ^{145}Nd, ^{146}Nd, ^{147}Nd, ^{148}Nd, ^{150}Nd
61	^{147}Pm, ^{148g}Pm, ^{148m}Pm, ^{149}Pm
62	^{147}Sm, ^{148}Sm, ^{149}Sm, ^{150}Sm, ^{151}Sm, ^{152}Sm, ^{153}Sm, ^{154}Sm
63	^{151}Eu, ^{152}Eu, ^{153}Eu, ^{154}Eu, ^{155}Eu, ^{156}Eu
64	^{152}Gd, ^{154}Gd, ^{155}Gd, ^{156}Gd, ^{157}Gd, ^{158}Gd, ^{160}Gd
65	^{159}Tb

Table 3. The Comparison of the Numbers of Nuclides in JENDL-3 with Those
in JENDL-3 and in Other Library.

The figures in parenthesis stand for the number of nuclides with
photon-production data.

Nuclide Library	JENDL-2	JENDL-3	ENDF/B-V	KEDAK-4
light nuclides(z= 1 ~ 19)	1 1	3 8 (9)	2 3 (2 0)	1 2
structural material nuclides (z= 20 ~ 30)	3 0	3 7 (6)	9 (9)	1 8
FP nuclides (z= 31 ~ 69)	1 0 1	~ 1 7 0 (3)	1 9 6 (6)	9
medium weight nuclides (z= 70 ~ 89)	1 2	2 0 (5)	2 0 (7)	0
heavy nuclides (z= 90 ~ 94)	1 9	2 1 (3)	2 2 (9)	1 1
transplutonium (z= 95 ~)	8	1 8 (1)	1 9 (1 5)	6
TOTAL	1 8 1 (0)	~ 3 0 4 (2 7)	2 8 9 (6 6)	5 6 (0)

2.2 Proposals on Post-JENDL-3 Activity Programme
for Japanese Nuclear Data Committee

Working Group on Post-JENDL-3 Activity Programme,

M.Nakazawa[*] A.Hasegawa, J.Katakura, H.Mizumoto,

T.Nakagawa and T.Yoshida[**]

Japan Atomic Energy Research Institute

Tokai-mura, Naka-gun, Ibaraki-ken

The working group has made both survey on the present status of and future requirements to the Japanese nuclear data evaluation activities, and their recommendations as the post JENDL-3 activity are
(1) developments of special purpose file,
(2) start of new evaluations of high energy and charged particle data, and
(3) publications of useful data book.

1. Introduction

Production works of JENDL-3 (Japanese Evaluated Nuclear Data Library -3) are planed to be completed at the end of FY 1986 and will be open in the next year. What should be the next goal of Japanese nuclear data activities is the main concern for the steering committee of JNDC to make the working group on " Post-JENDL-3 activity programme" to answer such questions.

Between Dec.25,1985 and Aug.20,1986, the working group has got 8 meetings mainly to make survey in the following subjects,
(1) check and review of the present and previous nuclear data activity in Japan,

* Univ.of Tokyo
** NAIG

(2) research trends and nuclear data requirements in relating nuclear technology fields, and

(3) some other basic conditions supporting the nuclear data activity.

Ⅱ.Survey on Nuclear Data Needs

　　The working group has had many and meaningful discussions with respective researchers of many fields, where research trends of each fields and requirements to the JNDC have been discussed.

　　Summary of nuclear data requirements is given in Table 1, where it is clear what kind of nuclear data is thought necessary in each fields.

　　Another kind of requirements and/or comments to the JNDC activity have been given in the following points of

(1) improvements of the availability of JENDL by prepairing the standard group constants,

(2) easy use of JENDL or JNDC FP Decay Data File by publishing the data book or numerical table, and

(3) increase of the younger researchers of nuclear data measurements and evaluations.

Ⅲ.Proposals & Recommendations

　　Proposals for the Post-JENDL-3 activity of JNDC have been summarized on the three subjects,

(1) the near term goal should be recommended as the developments of special purpose files for mainly two application fields of nuclear fuel cycle technology of fission energy systems and fusion reactor technology, also should be included the preparation of standard group constants and the publication of data book.

(2) As the long term goal, new activities of nuclear data evaluations should
be started in the area of neutron reactions in the high energy region,ch-
arged particle reactions and atomic & molecular reactions.

(3) Additional and practical efforts should be increased to improve the base
of nuclear data activity, such as reinforcements of nuclear data
measurements activity , easy utilization of nuclear data.

Follow-up discussions of the present proposals on the Post-JENDL-3
activity in JNDC are expected on how to realize above-mentioned subjects,
espeally on the practical process to organize corresponding working group.

References

(1) "Survey of Research Trends in Nuclear Data relating Fields for Post-
JENDL-3 Activity ", H.Nakazawa, T.Yoshida, J.Katakura, A.Hasegawa,
H.Mizumoto and T.Nakagawa, JAERI-memo 61-330, Oct.1986

Table 1   Summary of Nuclear Data Requirements

Areas	Requirements
Light Water Reactor	Little for present LWR, Actinide and FP nuclear data for high burn core calculation Every nuclear data for high conversion LWR, especially in resonance region
Fast Reactor	Critical benchmark testing by standard group constant, Adjustments of group constant
Fusion Reactor	Blanket neutronics of tritium breeding, nuclear heating, gamma-ray productions, activation cross-section and radiation damage, gamma-ray Production, covariance matrices (maybe JENDL-4)
Nuclear Fuel Cycle	Safety of criticality problem, Production and decay data of relating radioactive nuclides(more than 1000) X-ray emission and internal conversion electron yield of actinide (α, n) reactions
Accelerator	Neutron Production cross section Shielding and activation for high energy accelerator Charged particle data for advanced utilization of accelerators
Decommissioning of Nuclear Power Reactor	Activation cross-section of structural and impurity materials of nuclear power reactors
Radiation Damage	DPA, Kerma factor
Medical Application	Neutron production cross-section such as Be(d,n), Li(d,n), cross-section of collimator materials and human body elements, KERMA Cross section for heavy ion, proton, pion
RI Utilization	Practical hand book of activation, emitted gamma-ray spectra, nuclear structure
Enrichment by Laser	Ultra fine level & Isotope shift data, excitation, ionization,de-excitation cross-sections, life time & branching ratio of excited atoms
Charged Particle Data	Fusion reactor developments (α, n) reaction for spent fuel

Table 2 Proposed Schedule of Post-JENDL-3 Activity in JNDC

Subjects	1	2	3	4	5	6	7	8	9	10(year)
Special Purpose File			1st step	→		2nd step	→			
Standard Group Constants			verification		utilization					
New Fields										
High Energy Region										
Charged Particle Data										→
Atom & Molecule Data										→
New Evaluation Method										
Promotion of Nuclear Data Utilitzaion										
Publication of Data Book			1st step			2nd step	→			
Value Added Data Base										→
The other Services										→
Comments		Grouping			Reassessment				Reassessment	

2.3 NEUTRON EMISSION FROM (α,n) REACTION IN NUCLEAR FUEL

T. MURATA

NAIG Nuclear Research Laboratory, Kawasaki, Japan

Nuclear fuels emit neutrons originated in spontaneous fission of heavy elements and in (α,n) reactions of light elements contained in the fuel.

These neutron emission data are required in the fields of radiation shielding design of various nuclear facilities and non-destructive measurement of nuclear materials concerning with the process control and safeguarding nuclear materials

The requested (α,n) data in these fields are thick target neutron yield and energy spectrum of emitted neutrons. The present status of the experimental data are reviewed briefly. As an example, thick target neutron yield and emitted neutron energy spectrum are calculated for the O-18(α,n)Ne-21 reaction, which is the most significant (α,n) reaction in oxide fuels.

1. Introduction

Neutrons are emitted from nuclear fuels originated in spontaneous fission of heavy elements and in (α,n) reactions of light elements with α-particles from α-decay of heavy elements.

These neutron emission data are required in the fields of

* neutron shielding design of nuclear fuel facilities such as enrichment, conversion, fabrication and reprocessing, and the design of transport casks between them.

* non-destructive assay of nuclear materials such as spent fuel burn-up determination, Pu/MOX fuel management, highly enriched UFG detection and so on, concerning the nuclear material safeguards and process control of the facilities.

* study of safety start-up of nuclear reactor without neutron source.

The requested (α,n) data in these fields are thick target neutron yields and energy spectra of emitted neutrons.

2. Present status of the data

Review of the data were made by R. NAKASIMA(1) in 1982. Scince then no versatile data were published. So, brief summary according to the report are described below for the experimental (α,n) cross sections and thick target neutron yields.

The (α, n) cross section measurements were reported by many authors for light and medium weight nucleus. Most of them aimed to study the resonance structures of the compound nucleus in the low energy region. Some of them are shown in Fig. 1

In the energy region below few MeV, cross sections show isolated resonance structures, and composite resonance structures in the energy region above that.

Thick target neutron yield measurements were made by BAIR and GOMEZ DEL CAMPO (2) for Li-6, Li-7, Li(nat.), Be-9, B-10, B-11, B(nat.), Pb·F2, Zn·F2, Mg(nat.), Al-27, Si-28 and Si-28·O2 in the energy region of Ea=3 ~9 MeV.

WEST and SHERWOOD(3) measured thick target neutron yields for Be, Be·O, B·N, C, U·C, U·O2, Mg, Al, Si, Fe and stainless steel in the energy range of Ea=3.6 ~ 10MeV. They compared their data with that of BAIR and GOMEZ DEL CAMPO and showed 10 ~20% discrepancies at most.

Examples of thick target neutron yields are shown in Fig. 2 and Fig. 3 for C and U ·O2, respectively.

3. Calculation of thick target neutron yield and energy spectrum of neutrons

The emitted α-particles are slowed down by the collision with constituent atoms of the fuel and make (α, n) reactions with light elements during the slowing down. So, the thick target neutron yield Yn is given by

$$ Yn = \sum_j \int_0^R \sigma j(Ea) \, dx = \sum_j \int_0^{Eao} \sigma j(Ea)/(-dEa/dx) \, dEa \qquad \text{neutrons/}\alpha $$

where $\sigma j(Ea)$ is the (α, n) cross section of nuclide j for α-particle of energy Ea, which depends on distance x from α-decayed nucleus. R is the range of α-particles of energy Eao. The integral variable x is changed to Ea in the second equation and (dEa/dx) is the stopping power of medium for α-particles of energy Ea.

As an example, thick target neutron yield of U·O2 caused by the O-18(α, n) Ne-21 reaction are calculated and the results are shown in Fig. 3. In the calculation, the cross sections measured by BAIR et al. (4) and revised in ref. (2) were used below Ea≈5.2 MeV. Above that energy, no experimental data with reasonable accuracy are not available, so, the experimental data of Ea<5.2 MeV were extrapolated with the statistical model calculation using ELIESE-2 (5). The stopping power was calculated using the semi-empirical formulae given in the book edited by ZIEGLER(6).

Emitted neutron energy spectrum are calculated by summing up the neutrons leaving the residual nucleus in ground and each excited states, taking into account the kinematical relation between emission angle and neutron energy, and

given by

$$dNn/dEn = \sum_{ij} \int_0^{Eao} d\sigma ij(Ea,En)/dEn / (-dEa/dx) \ dEa$$

where $d\sigma ij/dEn$ is the neutron emission cross section of nuclide j which was left in state i after emission of neutron, of which energy is between En and En+dEn. The emission cross section is not available presently. So, the term is changed as follows,

$$d\sigma ij/dEn = (d\sigma ij/d\Omega) \times (d\Omega/dEn) = 2\pi \sin\theta \ (d\theta/dEn) \ (d\sigma ij/d\Omega)$$

where $d\sigma ij/d\Omega$ is the angular distribution, θ emission angle, and $d\theta/dEn$ given by the kinematics of the reaction.

As an example, neutron energy spectrum of the O-18(α, n) reaction in thick U・02 was calculated. The angular distributions in the region of Ea<5.2 MeV were calculated with the BLATT-BIEDENHARN's formula using the resonance parameters obtained by analysis of the experimental cross sections of BAIR et al. The result of resonance analysis is shown in Fig.4 with some examples of calculated angular distributions. In the energy range of Ea>5.2 MeV, angular distributions were obtained by the statistical model calculations.

The result is shown in Fig.5 with solid line. For comparison, spectrum calculated with isotropic angular distributions is shown in the figure. Calculations were also made using the statistical cross sections in all energy range, and the results are shown in Fig.6.

4. Conclusion

For the experimental data of thick taget neutron yield, there are some discrepancy up to 10 ~20% between different measurements, however, the large discrepancy is localized in the energy region below few MeV, and it would not be a problem in practical use.

Experimental data of neutron energy spectrum are quite scarce, so, measurements of thick target neutron spectrum are required.

In neutron energy spectrum calculation, angular distribution data are not so important than excitation function of cross sections, for target nucleus which shows composite resonance structure.

For neutron energy spectrum, it should be studied how precise is precise enough in practical use.

As data file, thick target neutron yield and neutron energy spectrum are requested to be given in simple formulae.

REFERENCE

(1) NAKASIMA, R. : JAERI-M 82-117

(2) BAIR, J.K. and GOMEZ del CAMPO : Nucl.Sci.Eng.71,18 ('79)

(3) WEST, D. and SHERWOOD, A.C. : Ann.Nucl.Energy 9,551 ('82)

(4) BAIR, J.K. and WILLARD, H.B. : Phy.Rev. 128,299 ('62)

    BAIR, J.K. and HAAS, F.X. : Phy.Rev. C7,1356 ('73)

(5) IGARASI, S. : JAERI 1169 (1968)

(6) ZIEGLER, J.F. : "Helium:Stopping Power and Ranges in All Elements"

                    (Pergamon Press 1977)
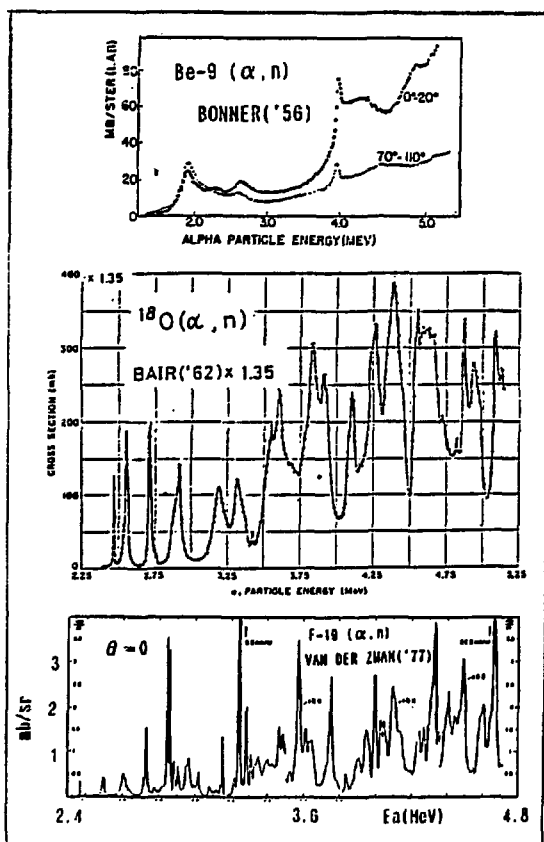
Fig.1 (α,n) cross sections for light nuclides
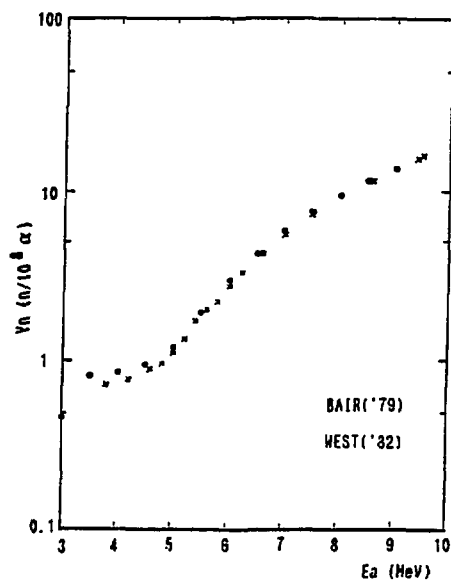
Fig.2 Thick target neutron yield for UC
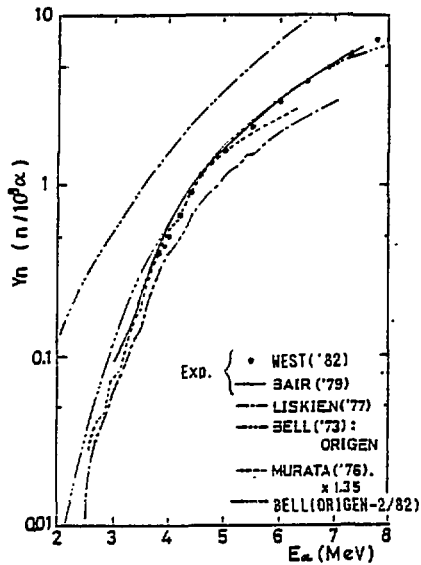
Fig.3 Thick target neutron yield for UO2

0-18 (α,n)Ne-21
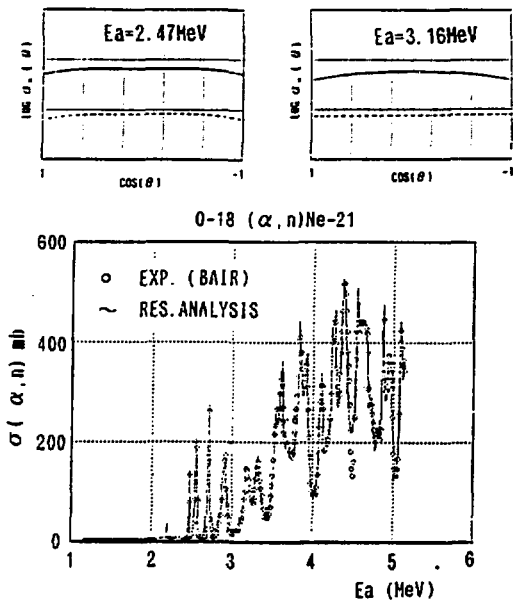
Fig.4 0-18 (α,n) resonance analysis
cross section analysis (center fig.)
relative ang.distrib. (upper&lower fig.)
⎧solid line : with all resonances
⎩dotted line : with single resonance
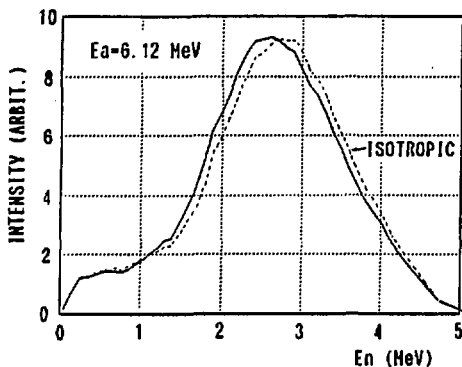
Fig.5
0-18 (α,n) neutron energy spectra in UO2
(with res.anal.+statistical cross section)
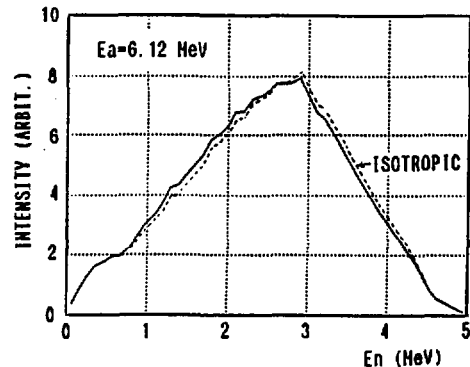
Fig.6
0-18 (α,n) neutron energy spectra in UO2
(with statistical cross section)

2.4 Actinide Nuclear Data for Nuclear Fuel Cycles

T. Yoshida and K. Hida

NAIG Nuclear Research Laboratory
Nippon Atomic Industry Group Co., Ltd.,

Roles of the neutron reactions in actinide-nuclide transmutation are reviewd briefly as well as the status of measured and evaluated data. Special attention is paid on the threshold reaction (n,2n), which is one of key reactions linking the actinide transmutation chains. Need for improving accuracy of the (n,2n) cross sections of Pu-239 and Np-237 is stressed.

1. Introduction

Generation of minor -but often unwelcome- actinides such as U-232, Pu-238, or Cm isotopes is of primary importance when we think about the problems of nuclear fuel cycles. Therefore the nuclear data related to formation and transmutation of these nuclides are essential to neutronic calculations which constitute the basis of planning, realization and control of nuclear fuel cycles. In the following, we review the status of the nuclear data needed in these calculations and try to find a way to improve the accuracy of the actinide transmutation calculations.

2. Actinides in Nuclear Fuel Cycles

First of all we try to make a brief summary of each minor actinide nuclide. The formation chains of these nuclides are shown in Fig. 1.

(1) Uranium-232 : One of the most "unwelcome" actinides because of the high energy gamma-ray emitted by its far descendant Tl-208. Generated mainly via Pu-236 and via Pa-232. A small portion produced by U-234(n,3n) reaction (ref.1).

(2) Uranium-236 : A representative neutron poison which deteriorates the neutron economy in LWR core. Accumulated considerably by repeat of fuel recycling (ref. 2).

(3) Plutonium-236 : A parent of hazardous U-232 above mentioned (alpha-decay)

(4) Plutonium-238 : A strong alpha-emitter. Produced by
the reactions Np-237(n,r) and Pu-239(n,2n) and by
alpha-decay of Cm-242. The emitted alpha-particle causes
radiolysis of the organic solvent which is essential in the
reprocessing plant.

(5) Americium isotopes : Alpha-emitters (especially
Am-241). Also important as the parents of Cm isotopes.
Formed mainly by the beta-decay of Pu-241 and the (n,r)
reaction of Pu-242 followed by beta-decay. Am-241 becomes
an "unwelcome" neutron poison when aged plutonium is
recylcled to LWRs.

(6) Curium isotopes : Strong alpha-emitters. Spontaneously
fissioning. Conspicuous as the sources of spontaneous
fission neutrons and the (alpha,n) neutrons. Formed by the
neutron capture and the beta-decay of Am isotopes.

The above explains briefly the origins and the functions
of the minor actinides from the view point of nuclear fuel
cycles. As is suggested there and is seen in Fig.1, the
alpha- and the beta-decays and the reactions (n,r), (n,2n)
play critical roles in generating the minor actinides. The
data related to the decays (half-lives, branching ratios)
are fairly well known compared to the reaction data. We
review restrictively the reaction data in the next section.

3. Reactions Leading to Actinide Transmutation

Important neutron reactions responsible for generation of
the minor actinides introduced in the preceding section are
listed in Table I. These are the (n,r), (n,2n) and the
(n,3n) reactions.
Fig. 2 is a typical comparison of the (n,r) cross section
in the actinide region, where the experimental data is
accumulated rather well. This reaction, Pu-242(n,r), is
responsible for formation of Am-243. Although the
reliability of the (n,r) reaction data is not so bad in a
relative sense, there left several problems. One example
is the case of U-236. In a very recent Russian report
(ref. 3) almost 50% reduction of the (n,r) cross section is
suggested in keV - MeV region in spite of an overall
agreement seen in old data (Fig. 3).
The present accuracy of the threshold reactions (n,2n)
and (n,3n) is far from satisfaction though the importance
of these reactions compares quite well with the (n,r)
reaction in transmutation of the actinides. Table II shows
the fission-spectrum averages of the important threshold
reactions (ref. 4). For U-238 and Th-232 the five major
libraries give one-group values quite consistent each
other. For these two cases the experimental data are well

accumulated as is exemplified in Fig. 4. On the contrary the (n,2n) reactions of Np-237 (responsible for formation of Pu-236) and Pu-239 (Pu-238 as well) differs largely among the libraries. The difference reaches a factor of three at most. Though there are measured data (ref. 5) persistent discrepancy remains in Pu-239 (Fig. 4). The apparent agreement in the U-234(n,3n) reaction among three libraries seems to be a chance occurrence. This reaction, responsible for formation of U-232 in part, draws little attention in any application field other than the nuclear transmutation in fuel cycles and there has been no extensive study on this special reaction.

From the status review above it may be concluded that the reliability of the threshold reactions represented by (n,2n) should be improved further. These reactions give rise to key passages linking important actinides in the nuclear transmutation.

4. One Group Cross Sections

COMRAD and ORIGEN-2 are among versatile nuclear transmutation codes widely used in fuel cycle problems (refs. 6 and 7). In these two codes the neutron cross sections are applied in the form of one-group constants, which make compact storage and easy access possible. In the case of ORIGEN-2, nearly 50 sets of one-group constants are prepared for users, who deal with various types of reactors in various operation conditions. By virtue of this elaborate one-group cross-section library, ORIGEN-2 calculates the actinides transmutations fairly acculately. Figure 6 compares the ORIGEN-2 result with that of BWR lattice code TGBLA (ref. 8) which makes the most use of sophisticated physics model and many-group constants. As is seen here the overall behavior of actinide inventory is in agreement though some inconsistencies are observed, for example, in Pu-241 and Cm-244.

Collapsing of threshold cross sections reveals one problem. Figure 7 shows an example of threshold cross sections, a typical LWR flux and their product (the response). As is seen here, only the low energy part of the cross section (6-9 MeV) contributes to the flux-averaged one-group cross section. In general the low-energy part of a threshold cross section is sensitive to model parameters when it is calculated, and suffers often from large statistical error when measured. These factors tend to deteriorate the accuracy of the evaluated low-energy cross-section in comparison with the higher energy part or the plateau. This fact gives rise to substantial lowering of accuracy when threshold cross-section data is applied to actual reactor problems. One is recommended to keep this fact in mind when evaluating threshold, especially (n,2n), cross sections.

5. Branching

The ground to isomeric-state ratio in the reaction product nuclide often plays a decisive role in nuclear formation and transformation. A typical example is the case of Np-237, one of the key nuclides, produced by the reactions U-236(n,r) and U-238(n,2n). When this nuclide undergo a (n,2n) reaction, a portion proceeds to an isomeric state and the rest to the ground state. The 22.5 hour isomeric state decays into U-236 and Pu-236, half-and-half. On the contrary the ground state has a very long life-time (115000 years) and then the production rate of Pu-236, an ancestor of "unwelcome" U-232, is very small. In this way the branching ratio determines essentially the productivity of U-232.

As well as a cross section itself, a branching ratio is a function of the incident neutron energy. This dependence must be evaluated with a high accuracy. Especially, as was mentioned in the preceding paragraph, the low energy part just above the threshold play a critical role. Fortunately a recent measurement (ref. 9) provided us with a good guideline for evaluating the (n,2n) cross section of Np-237 and the branching ratio.

6. Concluding Remarks

From the above discussion it may be concluded that improving the accuracy of the (n,2n) cross-section data is the most important step toward betterment of the prediction accuracy of actinide formation and transmutation. Accurate measurement the (n,2n) csoss sections of Pu-239 and Np-237 are pertinent answers for the above purpose.

Acknowledgements

References

1) K.Hida, T.Kusuno and S.Seino, Nucl.Technol, 75,148(1986)
2) T.S.Zaritskaya et al., Sov.At.Energy, 54,332(1983)
3) O.T.Grudzevich, et al.,"Radiative Capture Cross Section of U-236 for 0.15 - 1.1 MeV Neutrons", INDC(CCP)-220/L (1984) IAEA
4) H.Takano, private communication (1986)
5) D.S.Mather,et al., AERE-072/72 (1972): J.Frehaut et al. Proc.Conf.on Nucl.Data for Basic and Appl. Sic., Santa Fe (1986) p.1561
6) Y.Naito, T.Hara, H.Ihara and J.Katakura, "Development of Nuclear Decay Data Library JDDL and Nuclear Generation and Decay Code COMRAD", JAERI-M 86-121 (1986)
7) A.G.Croff, Nucl.Technol., 62.335(1983)
8) M.Yamamoto, H.Mizuta, K.Makino and R.T.Chiang, Proc. Topical.Mtg. on Reactor Phys. and Shielding, Chicago (1984) American Nucl. Society
9) N.V.Kornilov, Proc. Mtg on Transactinium Nucl Data, Uppsala, (1984) IAEA
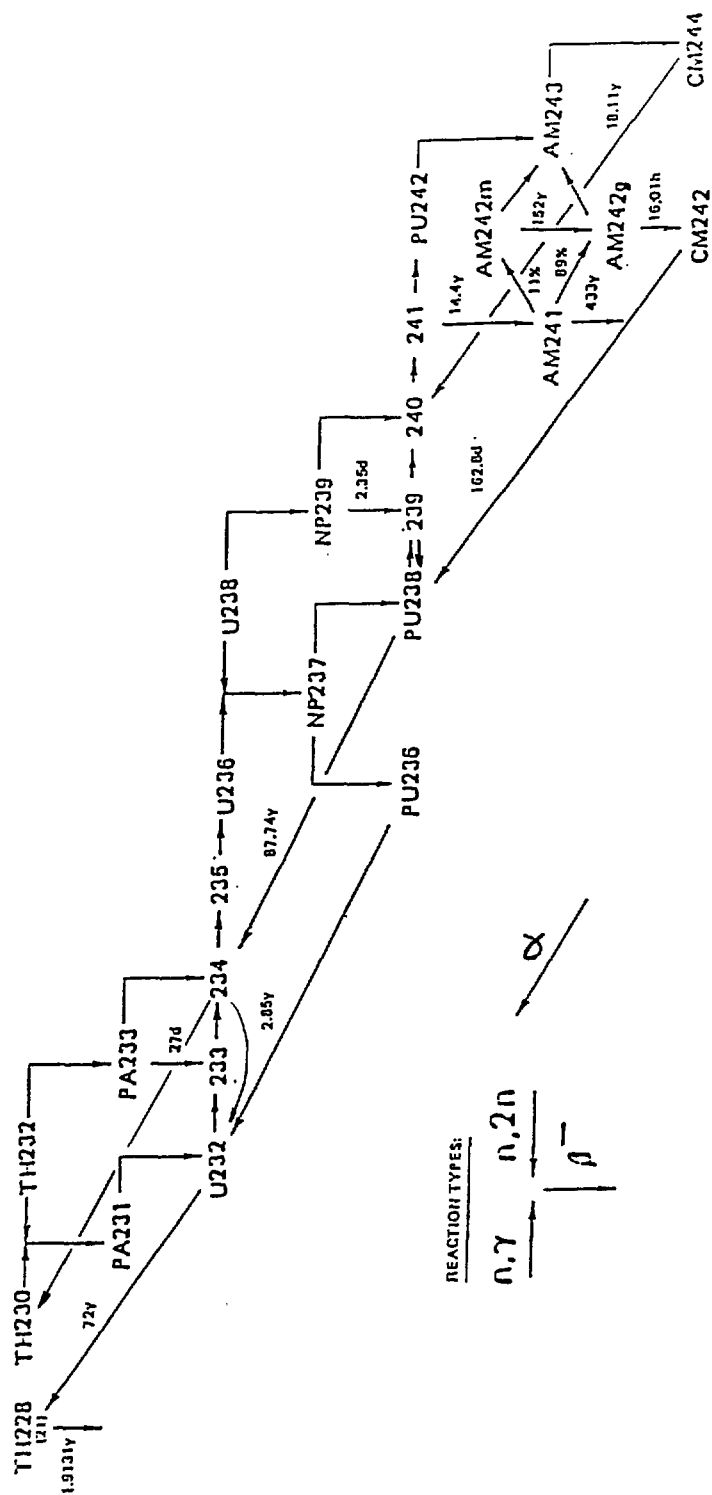
Fig. 1 Transmutation Chains of Actinide Nuclides
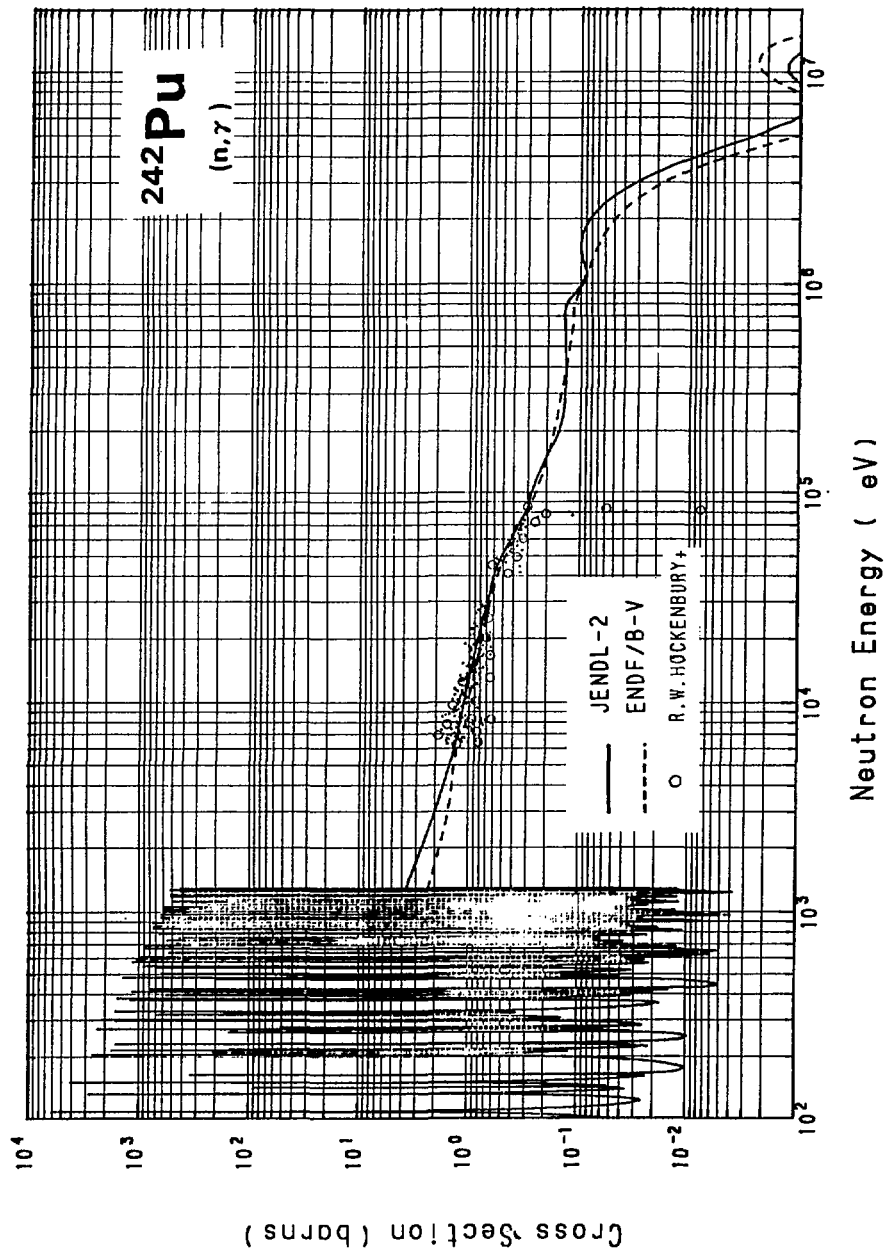
Fig. 2   Neutron Capture Cross Section of Pu-242
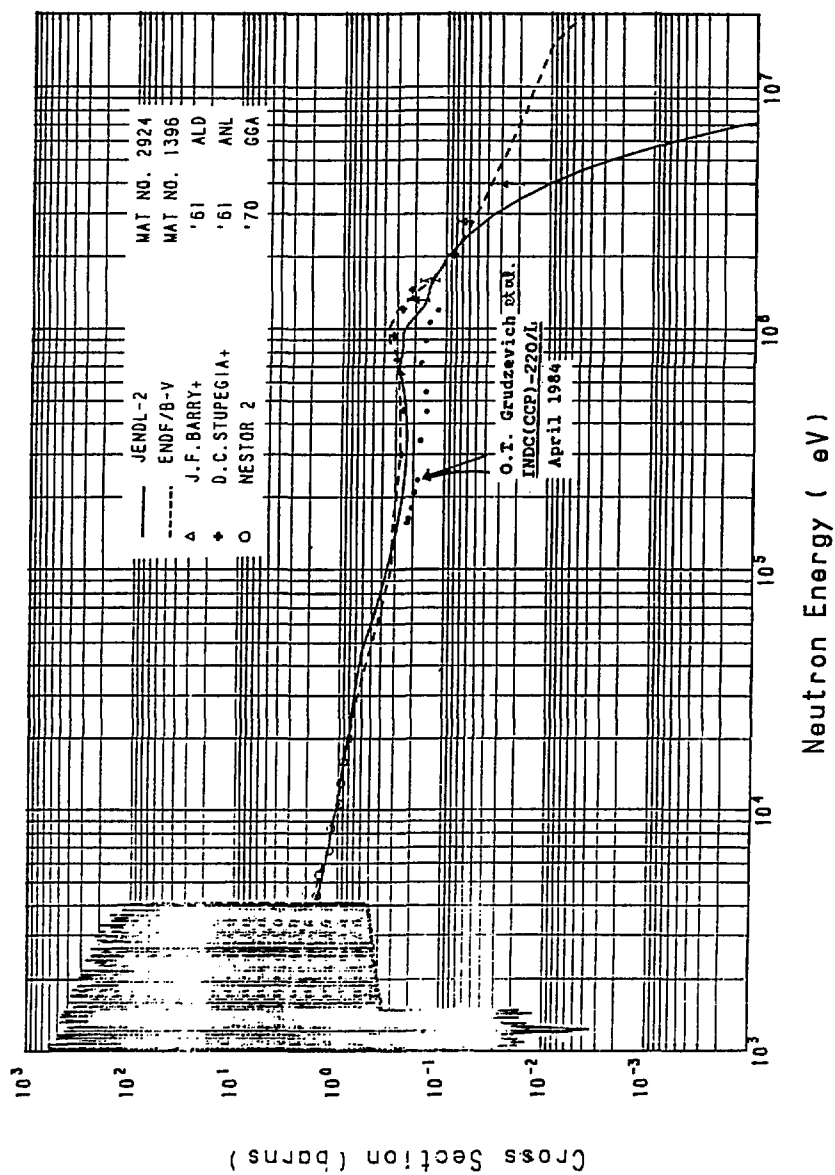
Fig. 3 Neutron Capture Cross Section of U-236
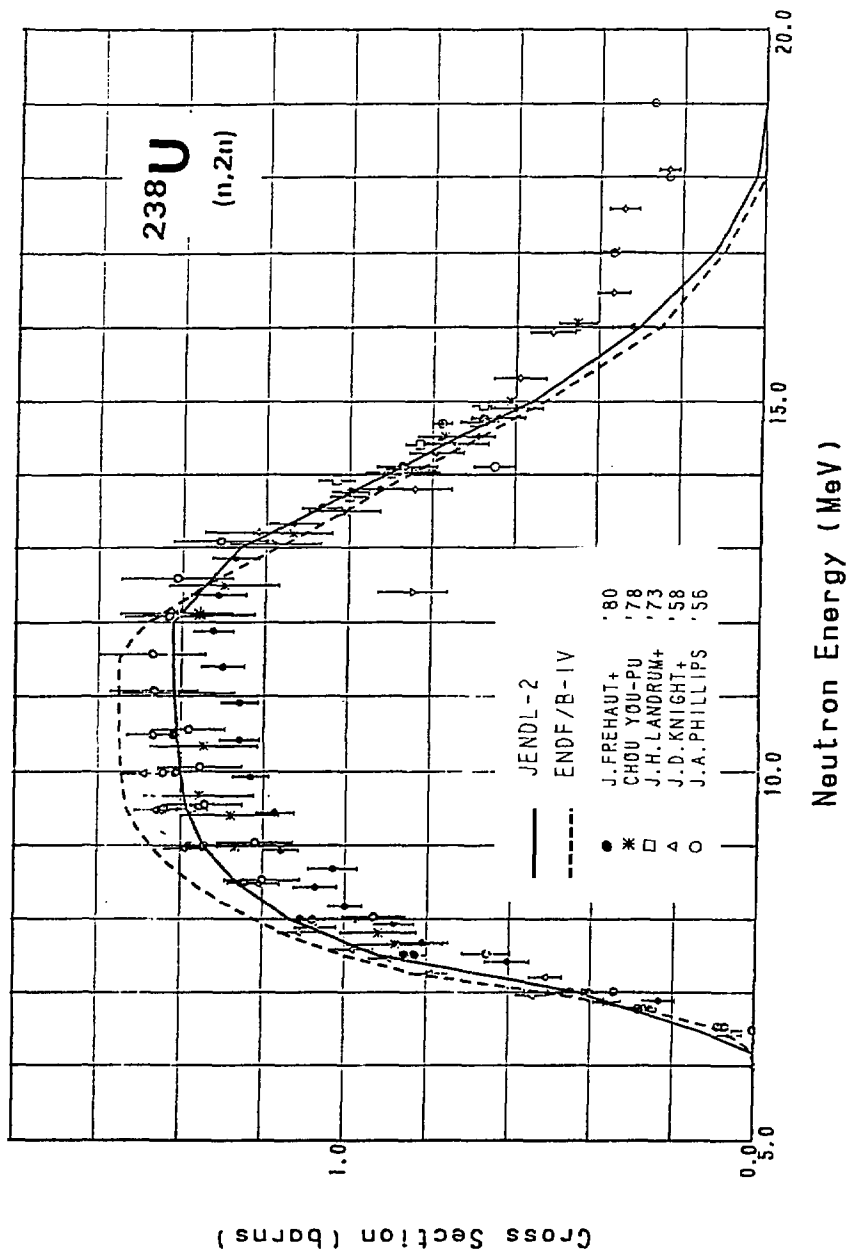
Fig. 4   (n, 2n) Cross Section of U-238

Pu239 (n.2n)

ENDF/B4   1264
JENDL2   2943
Frehaut
Mather
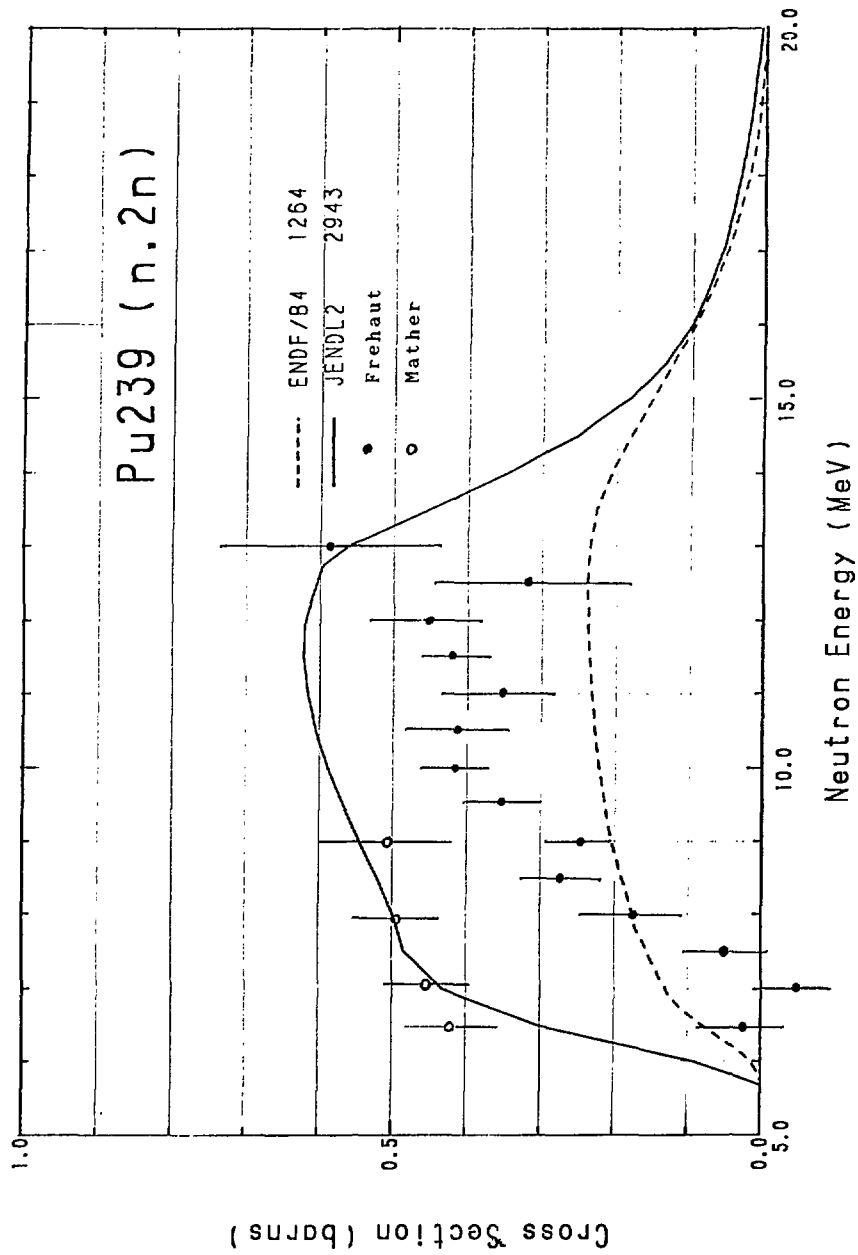
Fig. 5   (n.2n) Cross Section of Pu-239

Neutron Energy (MeV)

Cross Section (barns)
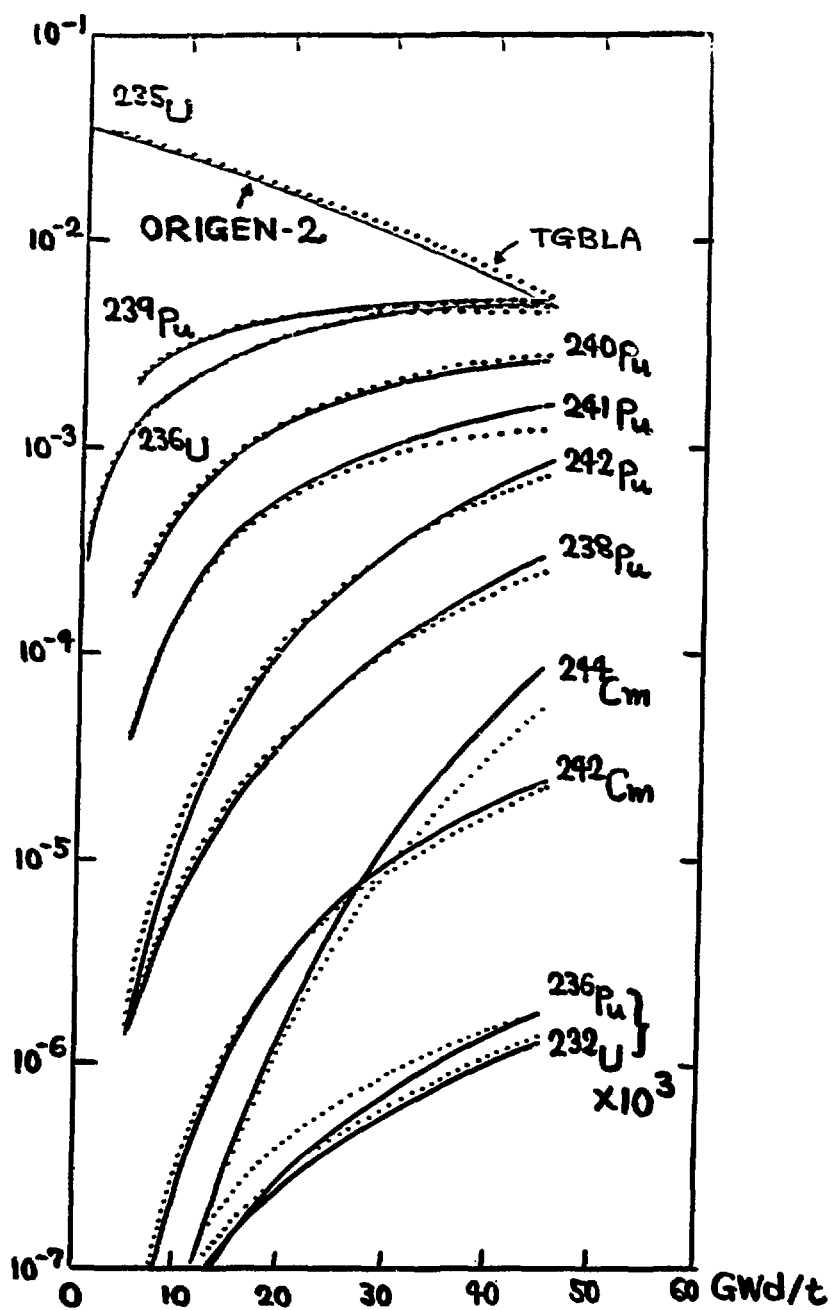
Fig. 6

Generation and Depletion of Actinide Nuclide in BWR Fuel
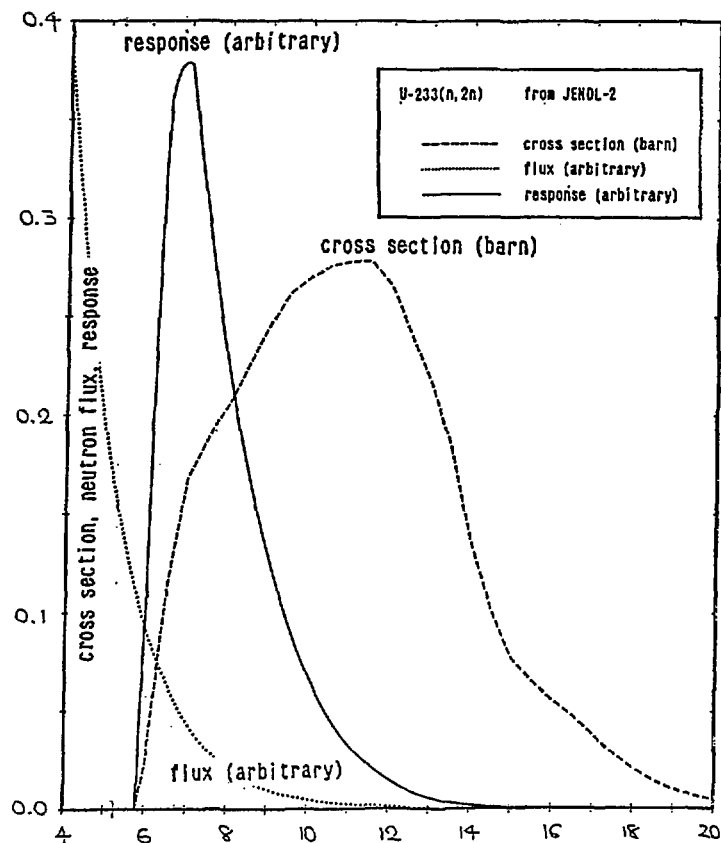
Fig. 7
U-233 (n, 2n) Cross Section and its Response
to a Typical LWR Neutron Flux

Due to Y. Okuda
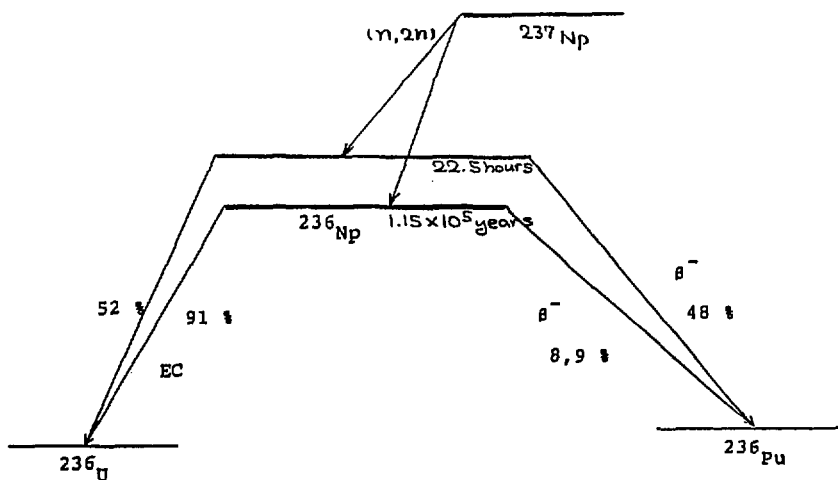
Fig. 8   Branching of the (n, 2n) Reaction of Np-237

Table I Key Reactions for Important Actinide Formation

Nuclide	Data Needed	Final Products	One-Group Constant
Th−230	(n.γ) Cross Section	U−232	24.0
−232	(n.2n) ″	″	0.0038
Pa−231	(n.γ) ″	″	65.0
U −234	(n.3n) ″	″	1.0E−5
−235	(n.γ) ″	″	10.39
−236	(n.γ) ″	U−232,U−236	8.39
−238	(n.2n) ″	U−232	0.0041
Np−237	(n,2n) to ground state	U−236	3.6E−4
	(n,2n) to isomeric state	U−232	3.2E−4
	(n.γ) Cross Section	Pu−238	33.0
Pu−239	(n.γ) ″	″	33.3
−242	(n.γ) ″	Am, Cm Isotopes	33.3
Am−241	(n.γ) to ground state	Cm−244	100.0
	″ to isomeric state	Cm−242	12.0

note) One group constants were taken from the ORIGEN-2 library only for the purpose of giving a rough idea on its size.

Table II
        Fission Averaged (n, 2n) and (n, 3n)
        Cross Sections

Reaction	Library	Fiss. Av. (b)
Th232 (n, 2n)	JEF-1 ENDF/B-5 ENDL-82 JENDL-2 KEDAK-4	16. 57-3 15. 60-3 16. 71-3 14. 46-3 16. 57-3
U-234 (n, 3n)	JEF-1 ENDF/B-5 ENDL-82 JENDL-2	16. 11-6 16. 12-6 34. 36-6 14. 39-6
U-238 (n, 2n)	JEF-1 ENDF/B-5 ENDL-82 JENDL-2 KEDAK-4	15. 37-3 15. 49-3 16. 59-3 15. 37-3 16. 84-3
Np237 (n, 2n)	JEF-1 ENDF/B-5 ENDL-82 JENDL-2 KEDAK-4	2. 37-3 1. 43-3 4. 20-3 3. 30-3 3. 83-3
Pu239 (n, 2n)	JEF-1 ENDF/B-5 ENDL-82 JENDL-2 KEDAK-4	9. 63-3 3. 32-3 5. 12-3 10. 63-3 11. 88-3

Due to H. Takano

2.5 Discussion on Post-JENDL-3 Activities

2.5.1 For the Enhancement of the Utilization of Nuclear Data Prepared by JNDC (Comments for the Recommendation of the Action for the Post JENDL-3 Project of JNDC)

Akira HASEGAWA

Japan Atomic Energy Research Institute
Tokai-mura, Naka-gun, Ibaraki-ken, Japan

The evaluated nuclear data , typically represented by JENDL-2, JENDL-3, has been prepared continuously by the number of enthusiastic evaluaters/supporters of Japanese Nuclear Data Committee (JNDC). But relatively low priority had been given to the effort for the promotion of the utilization of these data.

Here I comment about how to enhance the utilization of the nuclear data prepared by JNDC. Stresses in the discussion are placed on the following Points;

1. preparation of common/standard group constants library,
2. development of JENDL value added data base,
3. Bulletine Board System for the feed back information data base of the experiences of JENDL,
4. Utilization of communication net-works system,
5. nessecity of organization of users, of holdind a meeting / conference for the communication between users and evaluators.

1. Preparation of common/standard group constants library

Considering the technical trends in the atomic energy industry for the forthcoming 10 or 20 years, the big user of the nuclear data would be still the fields of the design calculation of core or shielding of the nuclear reactors (FBR, LWR, AWR, HCLWR, GCR, Fusion). Though the application filelds of the nuclear data will spread continuously to non-energy fields, such as medical therapy or activation analysis etc., it is hardly to think these fields become the majority of the users. Thus the nuclear data prepared by JNDC (Japanese Nuclear Data Committee) are meaningfull when they are used in the above stated design fields.

For the design calculation, nuclear data are generally used as in the form of group constants. Following characteristics are picked up for the usage of group constants in the design stage.

* The change of group constant library should be evaded whenever possible to maintain the consistency between chronological design history. The assigned group constants libray are always used whenever some big defects are not found. Thus the catchfrases " the newest evaluations or revised data " are not strong reasons for users to change the library.

* The method used in the design stage gains the long life once the method is established. It is used repeatedly as the standard design. Therefore, changing the method used in the design stage is very difficult as it has a large inertia.

* The library can be used as easily as possible, otherwise it will be avoided to use.

* The library passed by the assessment or much popurarity gained are preferably used by the user. Thus the newcomer is not always well-comed even if it is the latest and the best one. New one is always handicapped.

* Completeness is requested for the library, for example a wide coverage of materials or completeness of covered energy.

* At the adopting stage of the library, it will be adopted very smoothly as the library when the super-power such as authority, government or orderer, orders to use.

* The data (library) and the method (program) does not stand independently, in the design stage, in onother word method and data is very tightly coupled.

From the characteristics stated above, following strategies will be recommeded to enhanse the utilization of JENDL data.

Coupled JENDL group constants library and the programs should be timely introduced to the design calculation of some specific reactors. For the adoption of the library, the authority's suggestion to use JENDL would be very helpfull. The group constants and method to be adopted should be very common / standardized one considering user's cost. And the library should be very easily manipulated by users, for example, only necessary thing is to change the library. Or code system with JENDL group constants should be offered. When the library is used, the applicability or problems in the library should be clear for the users. To this point, the later described 'feed back information data base of JENDL' will be enough.

For the high grade users or specialists, it is also necessary to offer a standard processing code system for group constants productions.

To summarize, It is inevitable to supply the group constants library commonly used for the users in the core/shielding design calculations based on the JNDC data. For example, JFS-3-J2 type library /1/ in FBR application or VITAMIN-E libray /2/ in Shielding application for Sn code (ANISN, DOT). These group constants libraries should be supplied as soon as possible when the JENDL file is available. For the high grade users, it is also recommended to open the standardized processing code system for the production of group constants of their-own.

2. Development of JENDL value added data base

For some users, it may not be worth-while when they receive all data of JENDL stored in MT. From the experiences, we know that the data are hardly used unless the requesting data are easily to get in the requesting media for the users.

For the enhancement of the utilization of JENDL, development of a data base is inevitable so as to be able to supply any data requested by users. At the same time this data base should also retrive some deduced values by processing of the original data , such as
  * average cross sections weighted by some specific weights in
    0.5 lethargy widths,

* resonance peak value or minimum value of Fe-natural elastic cross sections,

* thermal (2200 m) value, Maxwellian averaged value, 14 MeV value, resonance integral etc.

And at the same time requested data should be output to required media of the users , such as, to terminal, to the printer, to the graphic plotter and to the graphic display.

Thus for the general users, a value added data base of JENDL is the most requested one. By using this data base, they can retrive not only any information stored in the data base but also some deduced values from their desk top computers whenever they need. In this data base, the data should be available via information net-work system connected to the telecommunication line. For the moment, it takes relatively long time to communicate by the telephone line due to very low data transfer speed (300 bps), however, it will be greately improved if digital packet communication net-work is available. At the same time, it is very important for the value added data base to equip the capability of connecting to the usual personal computers.

For the big users to use the data continuously, data transfer by media is also necessary. We can list up for the media for example floppy disk, magnetic tape, optical disk (CD-ROM),... etc. Especially the last one is very attractive future media for the nuclear data due to it's enormous capacity of the storage. If we have a 30 cm optical-disk, there is still enough space to remain even if we store all of the JENDL data and the utility program for handling. We are convinced that in the future this media will play an important role for the nuclear data fields. For all about JENDL data, such a day will come soon only an optical-disk is enough, into which all data and software are packed.

As already stated, the data services requesting to the data center via telephon, telex, letters will be out of date soon, because the time delay should be unavoidable. We would like to insist here that the value added data base is inevitable so as to serve promptly all data to users whenever they requested. The prototype version is already ready to open, i.e., EDFSRS /3/ (Evaluated Data Files Storage and Retrieval System). Starting from this system, it is rather easy to make up full system in a short time. Introduction of the value added data base will also contribute significantely to ease the man-power shortage of the nuclear data center.

3. Bulletine Board System for the feed back information data base of
   the experiences of JENDL across the application fields

   Before opening of the JENDL file to the publics, applicability is
always cheched by some integral tests by the JNDC . But it is not
possible for data supplied side (JNDC) to check data against all
application fields. Thus this data base is planned to share all
experienced results / informations obtained from the nuclear data
utilized by users. Because of the extension of the application fields
and of the users, such feed back information data base of the JENDL is
necessary. This data base will work as follows; For the user he can get
information beforehand about the data which he intend to use. For the
evaluaters who evaluate the data they can get informations across the
fields, so as to provide the indication to the problems of the data or
to know the necessity for the re-evaluation work. Thus it is expected
to play a role like a hot-line between the evaluater and users.
   This system will be realized by a bulletine board system / electric
conference system using computer comunications net-work linked with
personal computers. The data in this data base will be constructed from
the following entries, nuclide, MAT number (material id.), reaction,
energy range, application field, results or feed back information,
problems and recommendations, and name of entered persons for responsi-
bilty. This data base is furnished with the following functions,
accumulation of the information with relevant indexes, retrievals of
these informations, resisteration of new entries or some answers to the
existing informations. This system is now investigating in the Working
Group on Integral Tests for JENDL under Subcommittee of Reactor Con-
stant of JNDC(Japanese Nuclear Data Committee).

4. Utilization of communication net-works system

   The data bases stated previous sections, JENDL value added data
base or the feed back information data base of the experiences of
JENDL, are thought to be operated via tele- comunication net work
services implicitely. If we suppose not to be able to use the net-
works, the merits of the utilization of these data bases will be
greately reduced for the public users. The users scattered over the
whole country of JAPAN must come to JAERI to use these data bases. In
such a case the demerits are inestimably large comparing the opposite

case such that they can use the data from their desk top computers.

Up to now the JAERI's main frame computers operated in the computing center cannot connect to the outside(commertial tele-communication) net-works. This will be a big problem for these data base services. We want to say here to connect them to the net-woks immediately. When the JAERI's computers cannnot connect to the net-works even in the future due to the institutional codes, keeping the secrecies or budget problems .. etc., it is recommended to start the services directed to the net-work oriented by Nuclear Data Center itself installing a new mini computer. When it is not feasible either, the third plan is to set up a new organization (company) like a third sector to serve the nuclear data.

The trends of the present days, the services via communication net-works like LAN(local Area Net-works), VAN(Value Added Net-works), FAX, are very common to the nations. Why we cannot get such good harvests by using thesenet-works?

5. Nessecity of organization of users, or of holdind a meeting / conference for the communication between users and evaluators

An organization of users may be necessary to promote the utilization of the nuclear data. It is requested for the data center to grasp the users fields and using form of the data or to send a news for new release etc. Evidently this is not considered for the purpose of controlling the users. For the data base services the registeration of users are inevitable to the security of the data base.

A meeting or a conference organized by users and evaluators is also necessary in order to discuss and to clarify the problems found from the screening of the discussions on the bulletine board system of the feed back information data base. The selection of attendants for the meeting will be performed quickly according to this data base. Different from the mechanical and cold discussions presented on the bulletine board of computers , it is also necessary between users and evaluaters to comunicate and to conclude the discussions on the round table presented by themselves.

References

/1/ H.Takano and Y.Ishiguro : "Production and Benchmark Tests of
    Fast Reactor Group Constant Set JFS-3-J2," JAERI-M 82-135 (1982).
/2/ C.R.Weisbin, et al.: "VITAMIN-E: An ENDF/B-V Multigroup Cross-
    Section Library for LMFBR Core and Shield, LWR Shield, Dosimetry
    and Fusion Blanket Technology," ORNL-5505 (ENDF-274) (1979).
/3/ A.Hasegawa. : "Development of EDFSRS:Evaluated Data Files Storage
    and Retrieval System," JAERI-1295 (1985).

2.5.2 Some Comments on Post JENDLE-3 Activity Program

— At the Point of Safety Evaluation of Fuel Cycle Facilities —

'Yoshitaka NAITO

Japan Atomic Energy Research Institute
Tokai-mura, Naka-gun, Ibaraki-ken

At the point of safety evaluation of fuel cycle facilities, some important problems to be taken into account are discussed, and some proposals are also offered to obtain more accurate isotopic compositions in fuel cycle systems relating with improvement of the computer code COMRAD.

1. Introduction

Safety evaluation of fuel cycle facilities becomes very important recently according to the realization of high burn-up of LWR fuel and burn-up of MOX fuel in ATRs and FBRs. One of the important problems is to obtain reliable isotopic compositions of fuel cycle systems. For calculating generation and decay of isotopes, the computer code COMRAD has been dwvwloped.

To obtain reliable computed results by COMRAD on isotopic compositions in spent fuel, more accurate data are required.

In this report, will be shown some problems on safety evaluation of fuel cycle facilities and some proposals to improve COMRAD.

2. Problems on safety evaluation of fuel cycle facilities

1) Due to high burn-up of LWR fuel and burn-up of MOX fuel in ATRs and FBRs, neutron shielding from spent fuel will become an important problem. To evaluate neutron source intensity, accuracy evaluation on the quantities of ^{238}Pu, ^{244}Cm etc. is very important.

2) For utilization of depleted Uranium and Plutonium produced by reprocessing plants, it is important to evaluate accurately isotopic composition of Uranium and Plutonium. Estimation of ^{232}U which is

strong radiation source, is desired to be more accurately.

3) As for waste disposal of reprocessing plants, it is important to understand the characteristics of TRU, especially, ^{237}Np.

As shown in Fig. 1, many of actinides which are important for safety evaluation of fuel cycle facilities, are produced by (n,2n) or (α,n) reaction whose accuracies have not been taken so much care formerly.

3. Proposals to improve the COMRAD code

Generation and decay of isotopes are often calculated with the ORIGEN-2 code. The accuracy of the code is not so completely evaluated. The COMRAD code has been developed to take into account of Japanese evaluation work on nuclear data. Calculational flow diagram for COMRAD is shown in Fig. 2. Following tasks are required to improve the code.

1) Modification of the decay data library JDDL of COMRAD by adapting data which are not in ENSDF.

2) Production of one enrgy group neutron cross sections with JENDL-3.

3) Evaluation of accuracy and calculation model for (n,2n) and (α,n) reactions.

4) Evaluation of adequacy of generation and decay chains of actinide.

5) Evaluation of average number of neutrons emitted by spontaneous fission.
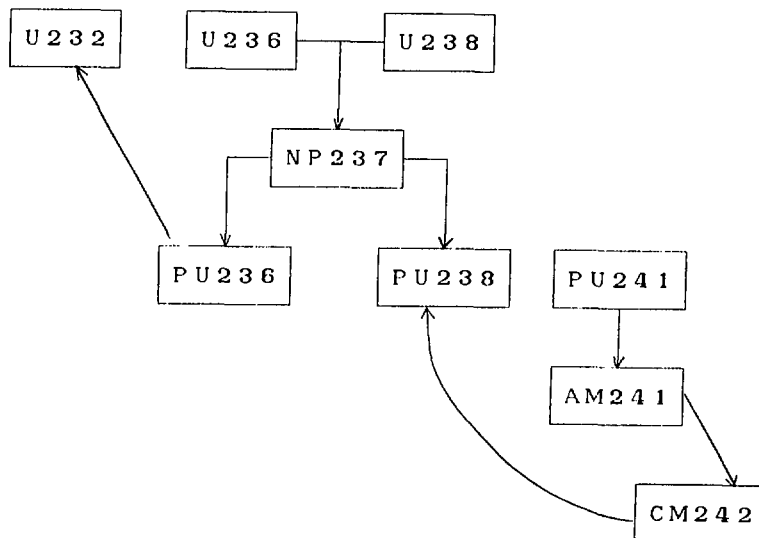
Fig. 1 Important chain for safety evaluation
of fuel cycle facilities
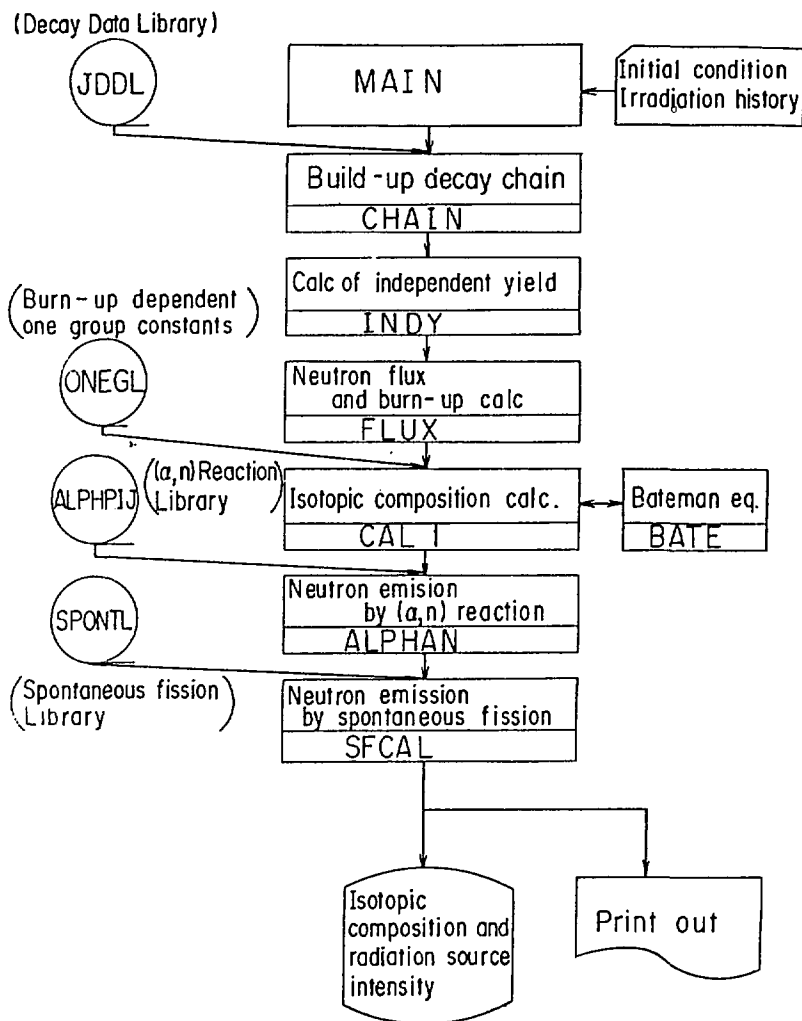
Fig.2 Flow digram for the COMRAD code

2.5.3 Doubly-differential Reaction Product Data
for High Energy Neutrons

M. Baba

Department of Nuclear Engineering, Tohoku University

Aramaki, Sendai-shi, Miyagi-ken

A comment is presented on the needs and status of energy-angular doubly-differential data for high energy neutrons in relation with the neutronic calculations and radiation effects assessment for fusion reactor and accelerator-based high energy neutron source.

1. Introduction

Nuclear data for high energy neutrons (En ≧ 10 MeV) will be of growing interest as the basis for development of fusion reactor, and accelerator-based high energy neutron source[1]. The latter is expected to find a variety of application such as material irradiation test facility, medical application, and accelerator-breeder and/or incineration system[1]. Therefore, future nuclear data program should cover the high energy range up to GeV as well as fusion related areas below tens MeV.

For the development of the systems, comprehensive nuclear data are required including charged particle induced reaction[1,2]. Among them, the neutron emission spectra and scattering cross sections are the most basic quantities characterizing the neutron field. The neutron emission spectra are strongly angle-dependent at higher energies, and doubly-differential type cross section (DDX) data are important[3,4]. One of the critical features of high energy neutron field is the high rate of radiation-induced material-damage, which is caused by composite effects of atomic displacement, gas production and nuclear transmutation. Therefore, the nuclear data pertaining radiation damage are of general importance in high energy region. The neutron DDX are important also for the assessment of radiation damage and nuclear heating because they determine the energy distribution of primary knock on atom (PKA) due to

neutron emission reaction. The energy and angular distribution data of charged particle emission reactions are also necessary for the assessment of radiation effects[5]. These data are not provided, however, by the existing data file, and "conventional" assumptions are applied resulting in unreasonable results such as negative KERMA values[5].

Thus the DDX data of secondary neutrons and charged particles are of great importance in high energy neutron field. In addition, DDX data are useful to examine the model parameters in theoretical calculations for nuclear data evaluation.

2. Neutron DDX Data.

The neutron DDX data around 14 MeV showed marked improvement recently as the result of active efforts in measurements and theoretical model refinement[3,4], although they are still unsatisfactory. However, for neutron energies other than 14 MeV, the experimental data containing continuum neutrons are very few due to scarcity of appropriate neutron source. This is just the case for 8-13 MeV region, where special apparatus or techniques are required to obtain the DDX data. At LANL, the H(t,n) reaction has been used to obtain mono-energy neutrons at 10 MeV, and provided precious data, although they are limited to light elements[6]. At Geel[7] and ORNL[8], a combination of "white" neutron beam and spectrum unfolding technique has been applied. This method has deficiency of limited energy resolution in both primary and secondary neutrons. Anyway, in this region, the evaluated data have not been examined in detail, and more efforts are needed including technical developments and integral experiments.

Above 15 MeV, the T(d,n) reaction can be applied for DDX measurement using MeV range deuteron beam. Fig.1 illustrates the experimental neutron DDX of iron at 18 MeV[9] together with the corresponding values by the evaluations. In this energy, there exists marked discrepancy, while the evaluations provide very good description for 14 MeV neutrons [3,4]. Such a deficiency in evaluated data may cause uncertainties in both neutronics and radiation damage calculations. This example suggests the needs of experimental data at several incident energies. In higher energy region, much larger discrepancies up to factors to

decade are reported between the experiments and calculations
for recoil spectra[10] and neutron emission spectra[11]. Fig.2 shows the
comparison between the experiment and calculation for the neutron
emission spectra by the (p,n) reactions at ~300 MeV[11].

3. Secondary Charged Particle Data and Damage Calculation

The neutron induced charged particle emission reactions such as
(n,p),(n,α),(n,nα) reactions play important role in calculation of
radiation damage and heating. For the calculation of PKA due to these
reactions, energy distribution and reaction kinematics are to be known,
especially for (n,α) reaction because of large recoil energy. For
example, the recoil energy of ^{56}Fe in the ^{58}Ni(n,γ)^{59}Ni(n,α)^{56}Fe
reaction which is used for helium production in thermal-reactor
irradiation test, produces additional ~20% atomic displacement[12].
Several studies have shown that the energy and angular distribution
of the reaction have significant effect on PKA and damage energy.
However, due to lack of such information in the evaluated data, and to
insufficient status of experimental data, the energy and angular distri-
bution are assumed rather conventionally without sound basis. Fig.4
illustrates the α-spectra for ^{58}Ni(n,α) reaction calculated by different
models[5]; this indicates large uncertainties associated in modeling the
spectrum. These modeling does not necessarily prove the energy conserv-
ation and leads to non realistic results. Of course, γ-ray production
cross sections and spectra are indispensable to satisfy the energy
conservation. MacFahren & Foster[5] have reported an "exact" calculation
using DDX type and energy-balanced data obtained by a theoretical calcu-
lation; they showed significant change from "conventional" calculation
in damage energy and drastic improvement in nuclear heating. Takahashi
et al.[13] also proposed a method for realistic calculation of PKA based
on the neutron DDX.

Thus the energy-angular DDXs for secondary charged particles are
also required in high energy region. It is noted that the charged
particle data even at thermal energy are not well known and to be
improved for establishment of "simulation rule" of material test irradi-
ation.

4. Summary

The high energy ($\geq$ 10 MeV) nuclear data are to be one of the principal areas in future nuclear data program, for the development of fusion reactor and accelerator-based neutron systems. These high energy region is an unexplored field and will provide various new items in experimental and theoretical areas of nuclear data works. Recent activities in Japan for fusion nuclear data are thought to be favorable factors for the program.

Among various data needed, the DDX type ones of reaction products will be of prime importance as the basis for neutronics calculation and radiation effects assessment. The experimental data are the primary source of the information, then further activities in experimets are expecetd. It should be noted that suitable neutron generators based on tandem accelerator or cyclotron are indispensable to promote the activities. The DDX data are not represented correctly in the single-differential format using file-4 and 5, then appropriate data formating such as file-6 or pseudo-level method is also important for the improvement of the evaluated data file.

Reference

1. M.Nakazawa et al., Internal Report (in japanese)

2. S.Iijima et al., Internal Report (in japanese)

3. M.Baba, JAERI-M 86-029 (1986) p.119

4. A.Takahashi, ibid., p.99

5. R.E.Macfarlen et al., J. Nucl. Mat., 122 & 123 1041-1047 (1984)

6. D.M.Drake et al., N.S.E., 63 401 (1977), LA-8342(1980), LA-10665-MS

7. E.Dekempeneer et al., Rad. Effects 92-96 133 (1986)

8. G.Morgan ORNL/TM-6247

   Yabuta et al., NETU-47 (Nucl. Eng., Tohoku Univ.,1986) p.10

10. W.Amian et al., Rad. Effects 92-96 1643 (1986)

11. M.M.Meir et al., BNL-NCS-37699 (1986) p.93

12. L.K.Hansur et al., J. Nucl. Mat., 139 228 (1986)

13. A.Takahashi et al., Proc.1985 Fall Meeting of Atomic Energy Soc. Japan, p.171
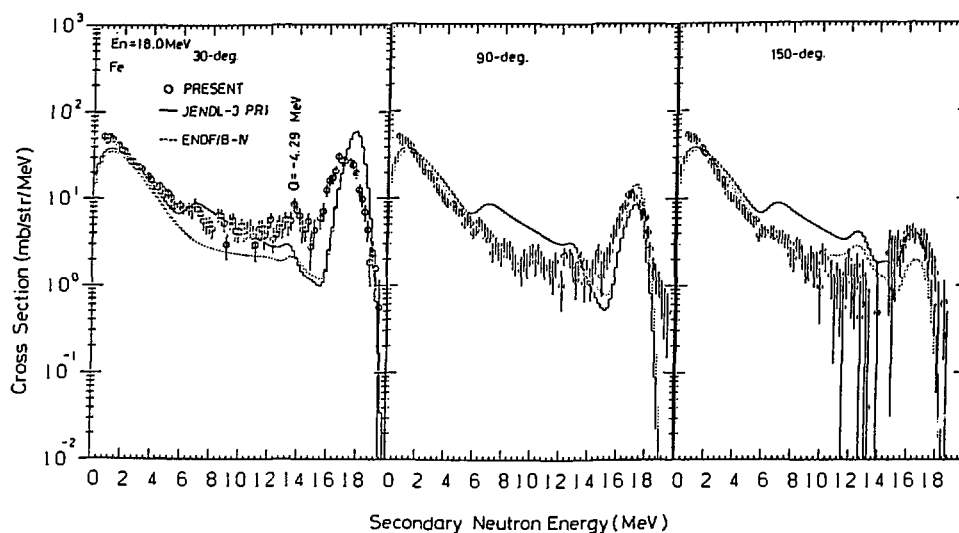
Fig.1 Neutron DDX of iron for 18MeV neutrons.[9]
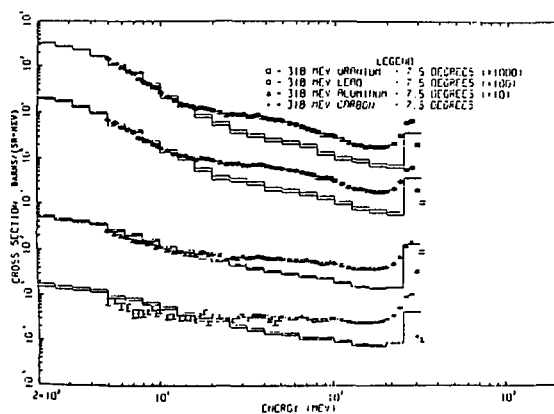
Fig.2 Neutron Emission
spectra for proton
induced reaction
at 318 MeV.[11]
The solid lines
show HETC calculation.

Ni-58 (n,α), α SPECTRUM FOR 14 MeV n
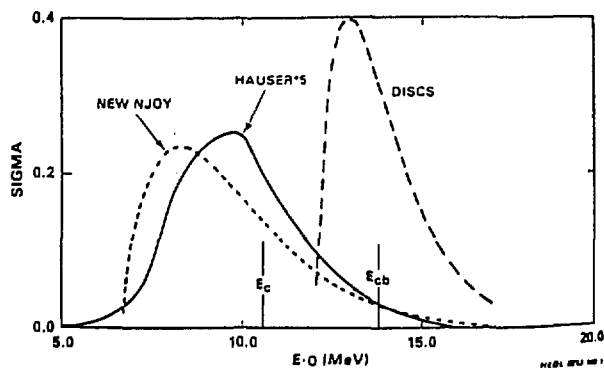
Fig.3 Calculated
α-spectrum for
^{58}Ni(n,α) reaction.[5]

2.5.4 Comments from the view point of fusion neutronics experiments

T. Nakamura

Japan Atomic Energy Research Institute

Tokai-mura, Naka-gun, Ibaraki-ken

Some comments are presented for the post-JENDL3 activities from the view point of fusion neutronics experiments.

A number of experiments, both differential and integral, have been conducted recently in Japan for the verification of the nuclear data for the design of fusion reactors; some data in the JENDL3 pre-liminary versions have been examined by using these experimental results.

Some comments and proposals are stated for the activities after the release of JENDL3, referring to the works at FNS as examples for explanation.

1)   Testing of JENDL3 by integral neutronics experiments.

A well-planned integral experiment provides good means to test nuclear data for elements of interest. The recent experiment on the angle-dependent leakage neutron spectra from Be slabs by Oyama et al.is referred as a typical example[1]. As is shown in Fig.1, the calculated values with different nuclear files show deviations from the measured one in different ways, indicating the necessity of the re-examination in the evaluation of this element.

Benchmark experiment data have been and being accumulated for important elements other than Be at FNS and at other facilities. Using these data, an activity should be encouraged to make the systematic testing of nuclear data files putting a prime priority on JENDL3. The information extracted through the study is to be fed back to the JENDL3 revision or incorporated in the post-JENDL3 file.

2) Provision for sensitivity/uncertainty analysis

Sensitivity/uncertainty analysis is a powerful tool both in planning experiment and interpreting the results obtained in regard to nuclear data base. Recently Ikeda et al. performed a two-dimensional senitivity/uncertainty analysis on FNS experimental systems in the geometry shown in Fig. 2[2]. This is to assess uncertainty in tritium production rate distribution due to the current cross-section unceirtainties by using ENDF/B-V, File 33. One of the results is given iin Fig.3.

The corresponding error file in JENDL is is not incorporated yet. But it is keenly requested for the sensitivity/uncertainty calculation to make best use of the domestic nuclear data file both for nuclear design research and the analysis of the integral experiments.

3) Provision for gamma-ray production cross section

Nuclear energy deposition in a fusion blanket is the important neutronic quantity next to tritiumm production. Substantial experimental efforts are directed to this area. Hence, reliable cross section data on gamma-ray production is needed for the analysis of integral experiments. They are also indispensable in nuclear design works to make a consistent prediction of neutron and gamma ray doses using a single file.

4) Activation cross section data

At FNS a program is in progress to measure activation cross sections around 14MeV systematically for the various nuclides used in fusion reactor materials covering over 200 reactions. A part of the results is presented in this seminar by Ikeda[3]. As there is no other activity as exhaustive as this one, these data are strongly recommended to be incorporated in JENDL activation and dosimetry files in due course.

References

(1) Y. Oyama and H. Maekawa: Angular Neutron Flux on Beryllium Slab
    Irradiated with DT Neutrons and Comparison with Calculations
    To be submitted to Nucl.Sci. and Eng.

(2) Y. Ikeda and M. Z. Youssef: Two-Dimensional Cross-Section
    Sensitivity and Uncertainty Analysis for Tritium Production
    Rate in Fusion-Oriented Integral Experiments
    To be published in Fusion Tecnol.

(3) Y. Ikeda et al.: A Program of Cross Section Measurements on
    Fusion Structural components for 14 MeV Neutrons Using
    FNS Facility
    This Seminar
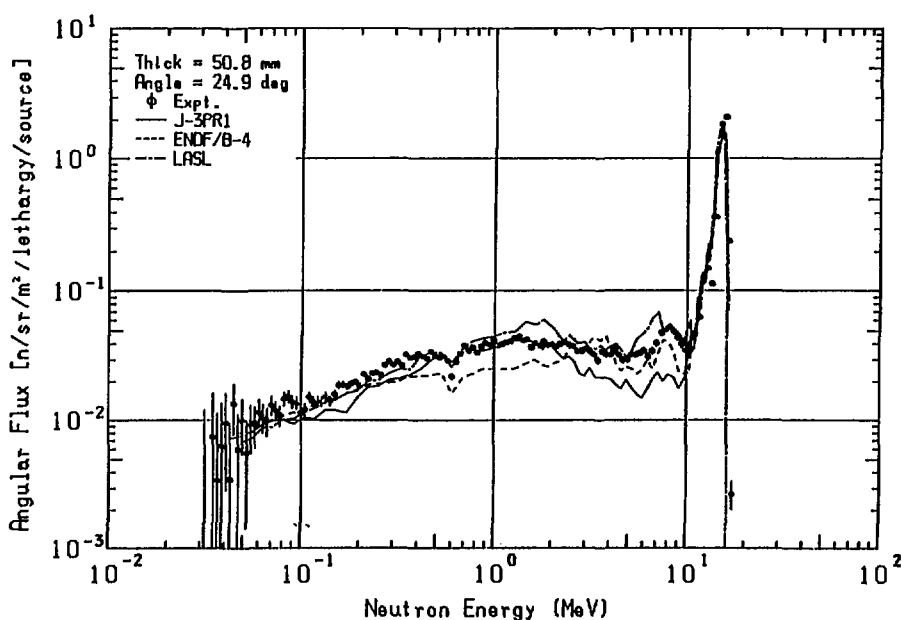
Fig. 1 The comparison between the measured and the
calculated neutron spectra of Be slab
experiment (Ref.1)
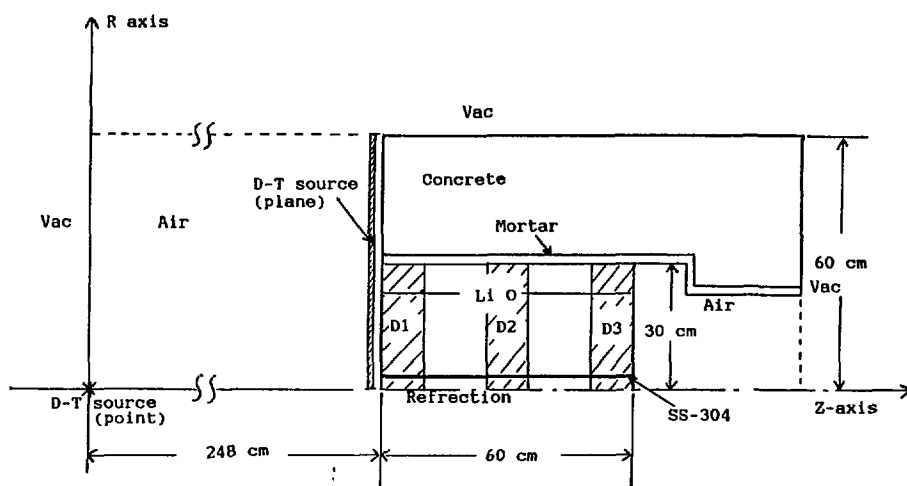
R-Z model for the reference system
D1, D2, D3 indicate detector zones of T-6

Fig.2   The R-Z two-dimensional geometrical model

for the analysis (Ref.2)
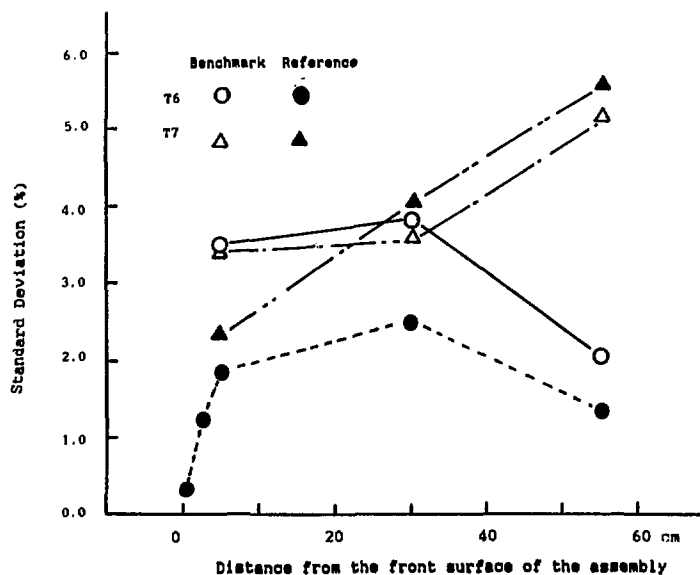
Fig.3   The total relative uncertainty in TPR-6(T6)

and TPR-7(T7) in two diferrent systems

(Ref.2)

2.5.5   Some Comments on Post−JENDL−3 Activity Programme for

Japanese Nuclear Data Committee

Atsushi Zukeran

Energy Research Laboratory, Hitachi ltd.

1168, Moriyama-cho, Hitachi-shi, Ibaraki-ken, Japan

I . INTRODUCTION

Fourty-three years have past since the first nuclear
reactor CP-1, a graphite moderated critical assembly at Ar-
gonne National Laboratory(ANL),was critical. But, scientists
and engineers are still in a situation of evaluating
nuclear data for nuclear energy production. Certainly
nuclear data evaluation is a difficult and time consuming
task.

The ad hoc committee for the post JENDL-3 program has
made a presentation of proposals. Then, this report gives
some comments from a quite different view-point i.e., con-
sidering the circumstances surrounding nuclear data evalua-
tion, including a historical review. While these are my per-
sonal comments, I hope others will find some merit in them.

II . NATURE OF NUCLEAR DATA

Nuclear data, at present, are mainly for neutron in-
duced reactions covering an energy range cold neutron (
about 10^{-3} eV) to fast neutrons (around 14 MeV) providing
the fusion neutron sources as shown in Fig. 1.   In this
figure typical neutron spectra in the core of the fission
reactors and in the first wall of fusion torus are shown. As
evident from the figure, the nuclear data given to the
evaluators cover a wide range (13 cycle in logarithmic
scale), and there are severe requirements for data accuracy
from reactor designers. Then, nuclear data must be recog-
nized as key quantities for constructing a reactor with high
safety and core performance, although their evaluation task
is difficult.

In the lower energy region (below a few eV), nuclear-
molecular interactions affect the neutron population and
thus not only nuclear properties, but also a molecular bind-
ing effect are important issues in order to evaluate physi-
cal behavior of neutrons. As a historical example, the in-
elastic scattering of slow neutrons in ZrH crystal might be
an important phenomenon which ensures the inherent safety of

the TRIGGER reactor.

Nuclear data for critical fission reactors, for which the neutron spectra are schematically shown in Fig.1, have to achieve a neutron balance. Therefore, from a practical viewpoint, the simultaneous grade-up of nuclear data, with a consistency between nuclei and their reactions seems to be an effective approach. Simultaneous evaluations being carried out by the heavy nuclei nuclear data evaluation group are expected to be promising, in the sense mentioned above.

However, for the fusion reactor with a neutron flux due to leakage of neutrons from the neutron production region, the nuclear reactions are only weakly correlated between the blanket and the neutron source region of plasma. Thus, the need for balance in nuclear data does not seem so great as for fission reactors. Rather, high energy (14Mev) induced reactions such as gas productions reaction, secondary particle induced activity, and the nuclear data for damage evaluation of the first wall are emphasized for future engineering requirements.

Nuclear data including charged particle induced reactions by GeV particles have been excluded in the current nuclear data evaluation. These data are potentially needed for accelerator breeders based on spallation reactions. Therefore, propose such pioneering work should be promoted by specialists.

III. SITUATION OF NUCLEAR DATA EVALUATION

Consider the number of different nuclei to be evaluated, such a "giant" task should be undertaken as a world-wide task for evaluators, experimenters and theoreticians. Fortunately, international collaboration in the field of nuclear data is well established and information has been efficiently exchanged. Although there are many national evaluated nuclear data files such as JENDL, ENDF/B, UKNDL, KEDAK, JEF, CENDL and SOKRATOR, no "international nuclear data file" exists. Such a file may be considered in the future as the goal of a world-wide evaluation task. It might take the form of an unified files based on current domestic data and a file including evaluated data based on the international division of tasks.

However, considering current activity for nuclear data evaluation, it seems that working scientists and student are not interested in the nuclear data evaluation, since it is a laborious and less glamorous than other areas of nuclear physics. The current situation for nuclear data evaluators

is as subcontractors in nuclear energy development although
nuclear data have been a key issue. Thus, a new, better ap-
proach must be developed positively as the result of great
need to apply nuclear data and encourage young people to un-
dertake evaluation work. As a historical example , the so-
called "high α -value" problem comes to mind. This involved
why the realization of the fast breeder reactor depended
upon whether the magnitude of ^{239}Pu α -value was higher or
not. Recently,for a high compact lattice light water reac-
tor the same situation has arisen in relation to void reac-
tivity prediction.

Ⅲ. HISTORICAL REVIEW

A graphic chronology for evaluated nuclear data files
is depicted in Fig.2. The first version of the American
evaluated nuclear data file ENDF/B- I was completed in
1968. After 9 years from ENDF/B- I , The first version of
Japanese Evaluated Nuclear Data Library JENDL-1 was compiled
in 1977. Evaluations for the third version are now in
progress and it should be completed around May 1987. Among
seven national files listed, the ENDF/B files have gone
through the largest number of versions. The usable lifetime
of each version seems to get longer with each succeeding
one. Defining "file-life" as the time between the incep-
tion of the file and the next new version, and "cumulative
life " of a particular evaluated file like ENDF/B as a
staircase plot of these file lifes. then cumulative file
lifes for ENDF/B and KEDAK are shown in Fig.3. Although this
is a rough plot, there seems to be a systematical trend
which can be approximated by a parabola. Then, a "eye-guid
line" indicates that the next version ENDF/B-Ⅵ , beginning
in 1986, would be viable up to the beginning of the next
century 2003. In general, file life tends to get longer as
reliability or data accuracy are improved.

In Table 1, U235 fission cross sections, chosen as a
typical nuclei, are processed from ENDF/B and JENDL-2 files,
and the other one (ABBN) of Bondarenko cross section set
which was the first cross section set used in Japan before
the first version of ENDF/B, are shown. The deviation from
JENDL-2's are also shown as a percent. From this comparison
the following trends can be obtained.

1) A significant difference between the oldest data
of the Bondarenko set and other data exits in the KeV
region. The most recent data agree within several per-

cent against the maximum 31 % deviation in the oldest one.

2)   Another difference is found around 21.5 eV to 2.15 eV. There is about a 13% difference between ENDF/B's and JENDL-2's.

3)   In general, the mutual differences have decreased with time or version-up of files as shown in ENDF/B's and JENDL-2's.

As can be deduced from the above example, by repeating (i.e.,refining) the evaluation of data, the locations of data is seemed to go to some limited region which means one of saturation phenomena. In this sense, a statistical treatment such as simultaneous evaluation using covariance matrix will be welcome.

In order to quantify Japanese activities in nuclear data, the number of oral presentations at biannual Japan Atomic Energy Meetings is used. Oral presentations can give an indication of overall activity better than the publications since the former includes preliminary results before formal publication at the end of task.

The number of oral presentations in the meetings are shown in Fig.4. The presentations are categorized into total number, the presentations from companies and institutions , national and private universities, Japan Atomic Energy Institute and the others. In order to indicate the man power contributing to nuclear data activities from experimental, theoretical analysis and evaluation areas, the total number of authors listed for presentations are also shown in the figure. This figure points up the following tendencies.

1)   Nuclear data activity, as measured by the total numbers of presentations and persons, have increased with passing time.

(2)   In analyzing the sources of contributions, activity in institutions is dominant, in particular, university activities have become gradually larger, while company activities have been nearly constant.

As shown in Fig.4, the total number of persons at the 1986 meeting was 127 men as obtained by a double counting

method, i.e., if the same person was listed for two articles, the number is two. In the 1967 fall meeting (20 years ago), no session for "Nuclear Data", however a few presentation related to nuclear data. These activities focused on an application of nuclear data to reactor analysis, such as a calculational model of resonance integral using the resonance parameters. However,

(3) recent presentations tends to be for the nuclear data related to higher energy (14 MeV) neutron induced reactions such as double differential cross section, threshold and/or gas production cross sections, which are aimed forwards fusion reactor interests.

But overall, it is unfortunately true that

(4) presentations related to the nuclear data "evaluations" are much fewer few than expected, or desirable.

The last point is particularly serious when viewed in terms of the amount of work being extended to complete JENDL file. This tendency should be examined by all of us, working as evaluators or related areas.

VI . CONCLUDING REMARKS AND COMMENTS.
    I have given some comments for Post JENDL-3 activities which are quite different viewpoints from just technical considerations. These are my own private opinions, but I feel they are valid talking points to determine future directions and tasks.

Table 1 U235 Fission Cross Sections in comparison to the Cross Section based on JENDL-2

Group NO	Upper Energy		U235 Fission Cross Sections (barn)				
			ABBN Set (1964)	ENDF/B-III‡) (1971)	ENDF/B-IV‡) (1973)	ENDF/B-V‡) (1979)	JENDL-2‡) (1982)
1	10.5	MeV	1.75 (6.68)‡)	1.57 (-4.27)	1.63 (-0.62)	1.64 (-0.07)	1.64
2	6.5		1.15 (3.24)	1.07 (-3.58)	1.12 (0.71)	1.10 (-0.89)	1.11
3	4.0		1.25 (2.04)	1.20 (-1.95)	1.22 (-0.46)	1.21 (-1.37)	1.23
4	2.5		1.28 (-0.44)	1.29 (0.40)	1.27 (-1.42)	1.28 (-0.56)	1.29
5	1.4		1.25 (2.54)	1.22 (-0.03)	1.22 (0.40)	1.22 (-1.14)	1.22
6	0.8		1.23 (5.20)	1.16 (-0.60)	1.16 (-0.60)	1.16 (-0.91)	1.17
7	0.4		1.41 (9.50)	1.29 (-0.13)	1.28 (-0.69)	1.28 (-0.56)	1.29
8	0.2		1.70 (13.39)	1.51 (0.95)	1.48 (-1.58)	1.48 (-1.55)	1.50
9	100.	keV	2.10 (19.01)	1.85 (5.06)	1.75 (-0.90)	1.71 (-3.06)	1.76
10	46.5		2.65 (27.29)	2.24 (7.42)	2.05 (-1.50)	2.01 (-3.58)	2.08
11	21.5		3.40 (31.37)	2.74 (5.85)	2.78 (-4.21)	2.46 (-4.37)	2.59
12	10.0		4.40 (24.82)	3.56 (-3.95)	3.59 (-3.95)	3.38 (-4.10)	3.53
13	4.6		5.40 (5.86)	5.12 (3.51)	4.95 (-2.92)	4.92 (-3.51)	5.10
14	2.15		7.30 (0.68)	7.52 (3.63)	7.29 (0.47)	7.13 (-1.73)	7.25
15	1000.	eV	11.0 (3.05)	11.58 (8.49)	11.55 (8.20)	11.26 (5.49)	10.67
16	465.		16.0 (-4.17)	16.31 (-2.30)	16.42 (-1.68)	16.30 (-2.35)	16.70
17	215.		22. (1.49)	21.16 (-2.38)	21.19 (-2.26)	20.35 (-6.15)	21.68
18	100.		35. (1.39)	34.90 (1.09)	35.20 (1.96)	35.52 (2.90)	34.52
19	46.65		45. (4.39)	43.10 (-0.02)	43.10 (-0.02)	43.10 (-0.02)	43.11
20	21.5		45. (-0.69)	51.15 (12.88)	51.15 (12.88)	51.15 (12.88)	45.31
21	10.0		37. (-20.26)	48.37 (4.25)	48.37 (4.25)	48.37 (4.25)	46.40
22	4.6		20. (18.14)	17.12 (1.14)	17.12 (1.14)	17.12 (1.14)	16.93
23	2.15		35. (-2.83)	35.98 (-0.11)	35.98 (-0.11)	35.98 (-0.11)	36.02
24	1.0		64. (-3.17)	65.51 (-0.90)	66.09 (-0.01)	65.31 (-1.20)	66.10
25	0.465		155. (-1.63)	157.05 (-5.06)	158.45 (-4.21)	158.31 (-4.30)	156.42

‡) prepared by the same processing code for this work.   ‡) percentage deviations from JENDL-2'S
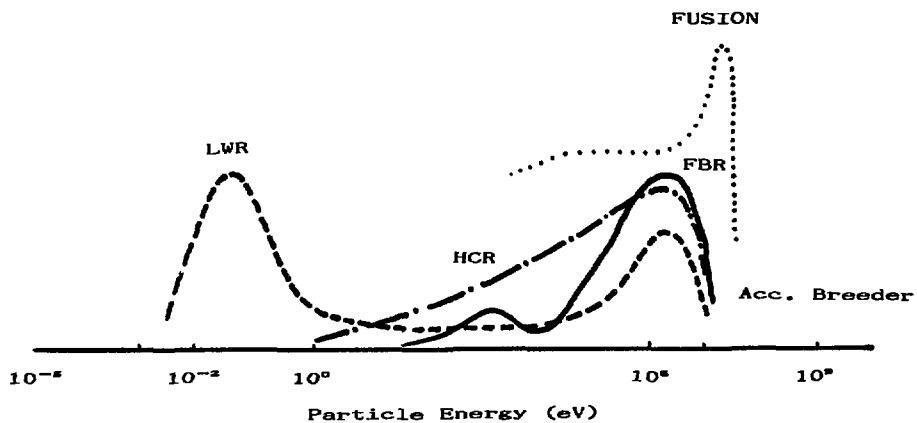
Fig. 1   Neutron Energy Spectra of Typical Reactors
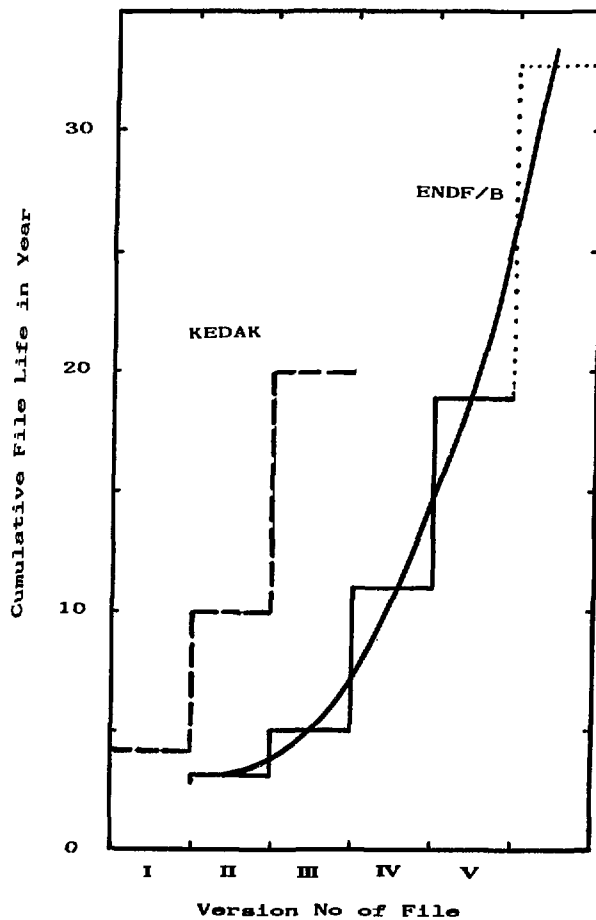
Fig. 2   Life Time of Evaluated Nuclear Data File
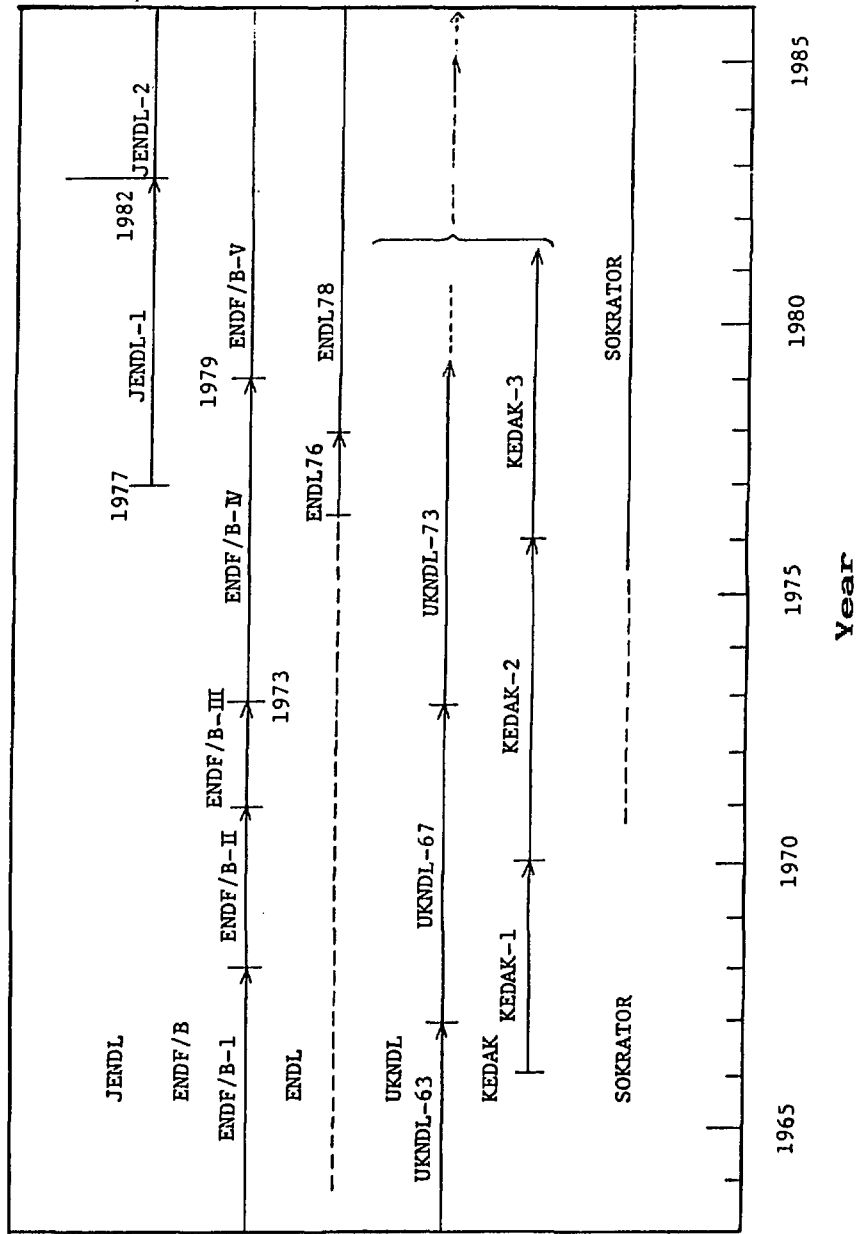
Fig. 3 Histories of Evaluated Nuclear Data Files

Fig. 4 Numbers of Oral Presentations and Persons contributing to Nuclear data Activities in the Biannual Meetings of Japan Atomic Energy Society.
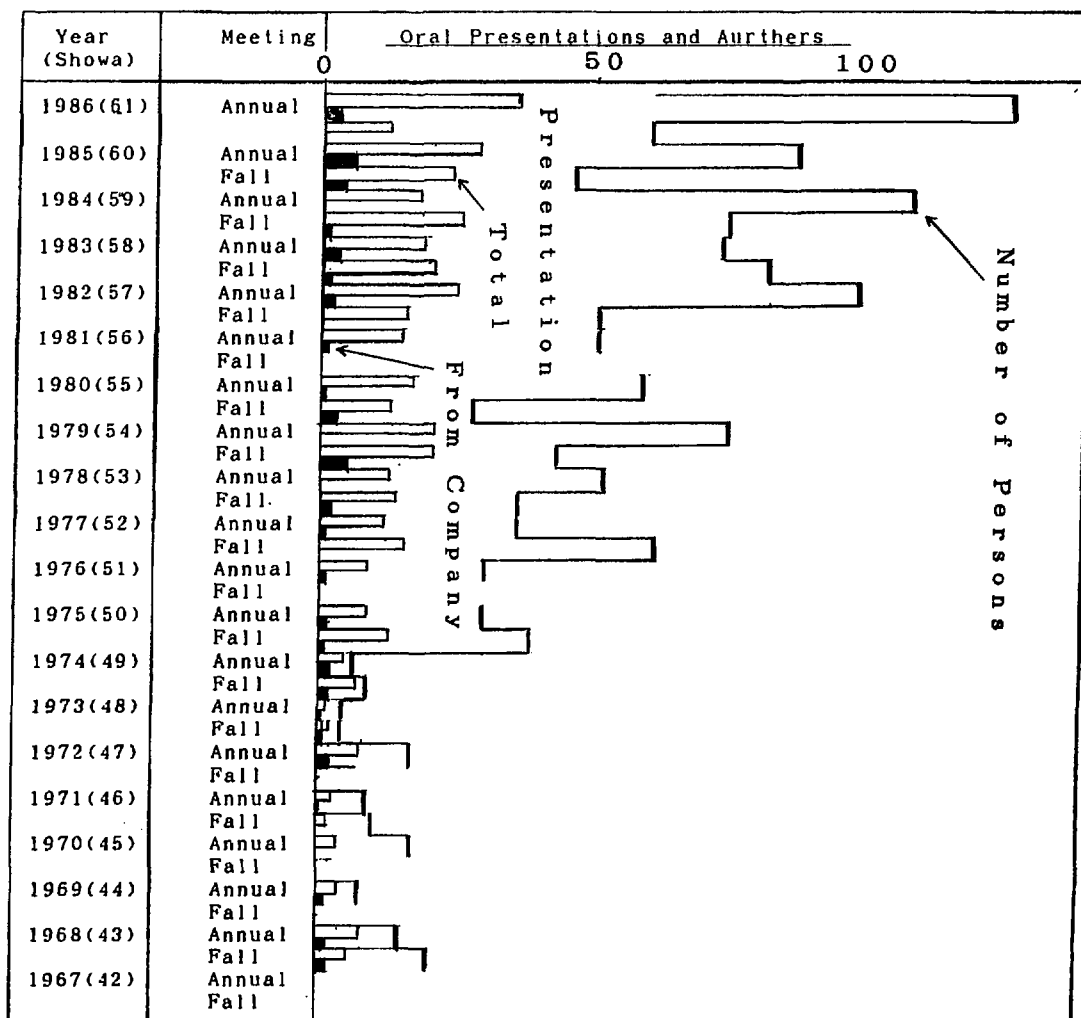
2.5.6 Comments to JENDL-3

Hiroshi Tochihara
Mitsubishi Atomic Power Industries, Inc. (MAPI)

Experience of JENDL-2 application and comments
to JENDL-3 were reported from standpoint of an
user in water reactor nuclear design field.

I am not directly engaged in nuclear cross section data evaluation work.
Following comments are those from standpoint of a nuclear design engineer,
that is, an user of JENDL.

In MAPI nuclear cross section data library are needed mainly for nuclear
and shielding design of PWR, APWR, HCPWR, FBR and fissile material storage
facilities.

As to PWR, there are many startup physics test data and operating data of
real PWR plants. Using these data, we can totally verify our nuclear de-
sign calculations (ENDF/B based LEOPARD code) and recently there is rather
good agreement between measurement and prediction.

Several important isotopes JENDL-2 library data were used to replace our
original library data to check the reactivity difference in benchmark prob-
lems between both library data.

There are rather small difference, so we think that it is not necessary to
replace our library data right now.

The detailed results will be reported in the next poster session by
Mr. M. Sasaki of MAPI.

But according to the recent trends towards longer cycle operation, high
burnup operation, Plutonium recycle and new type reactor development such
as HCPWR, there are increasing necessity for transuranium higher isotopes
and fission products cross section data based on the originally evaluated
library data such as JENDL-3. The merit of Japanese library data is its
easiness to access. But in the user's standpoint, the problem is that
preparation of the new library data is very time and money consuming work
but the benefit is not so much. Easy to make but much benefit is our aim.

Preparation of JENDL standard library data set for several standard nuclear
design codes such as MUFT and TEMPEST are very useful for many industry
nuclear people. Also preparation of automatic computer system for easy
access to JENDL library data is important to users of JENDL. Many people
will use JENDL library according to increase of reliability and easiness
to use JENDL library.

3. Topics

3.1 Fast Neutron Scattering in the Energy Range between 10 and 40MeV

Y. Yamanouti

Department of Physics, Japan Atomic Energy Research Institute
Tokai, Ibaraki 319-11, Japan

Abstract: The neutron scattering cross sections in the energy range
from 10 to 40MeV are reviewed. The theoretical analyses in terms of
the phenomenological global optical potential and the microscopic
optical potentials are disccussed in this report.

1.   Introduction

   During the last ten years, fast neutron facilities and programs have
been established for systematic studies of neutron scattering over a
wide energy range, so that the differential neutron scattering
measurements in the energy range from 10 to 40MeV have been made in
several laboratories. The accumulated scattering data have been
reported mainly with neutron energies up to 26MeV. Scattering cross
sections above 26MeV are available only for five target nuclei at 30 and
40MeV. These data were measured by the now-terminated MSU neutron
facility[1]. The availability of facilities for carrying out various
types of experiments including neutron elastic and inelastic scattering
was summarized by Zafiratos[2]. In the following sections the status of
the measured scattering cross sections and the recent optical model
analyses of the elastic scattering cross sections are presented.

2.   Measured cross sections

   For neutron scattering data, all presently available neutron
scattering cross sections measured with the neutron energies above 20MeV
have been surveyed and graphical tabulation of scattering and reaction
data has been presented by Rapaport[3]. And Hansen has reported

measurements and calculations of neutron scattering angular distributions over a wide mass and energy range[4]. The neutron scattering data have been measured mainly in TUNL(10 to 17MeV), Ohio University (11,20 to 26MeV), Livermore(14.6 and 24MeV) and Michigan State University(30 and 40MeV). The elastic scattering cross sections of ^{208}Pb at incident neutron energies between 7 and 40MeV are shown in fig.1 as a typical examle in neutron scattering from heavy nuclei in this energy range[5].

3. Global optical model potential

   The measured angular distributions for the elastic scattering are usually analyzed in terms of the optical model, and the individual best fit optical parameters are obtained for each angular distribution. The optical model provides the basis not only for the analyses by nuclear reaction theories but also for the technological calculations in which nuclear data are used for applications.

   From the elastic scattering cross sections information for the phenomenological global optical model can be obtained. Global optical model potentials assuming macroscopic approach with Saxon-Woods and derivative Saxon-Woods radial shape have been proposed by Wilmore and Hodgson[6], Becchetti and Greenlees[7], Rapaport[8], and Walter and Guss[9]. In the most recent work of the global optical potential by Walter and Guss, A spherical optical potential for neutron scattering has been parametrized for the mass region larger than 53, and the energy range between 10 and 80MeV. Although some of the results are still tentative, reasonable fits have been achieved in the restricted mass and enery range by this global optical potential. The quality of the fits for A>53 and 10<E<26MeV is shown in fig.2.

4. Microscopic optical model potential

   Different approach to the optical model potential from a more fundamental microscopic theory based on the nucleon-nucleon interaction has been investigated, i.e. the nuclear matter aproach of Jeukenne, Lejeune and Mahaux[10,11], and the folding model of Brieva and Rook[12-14]. Hansen has reported the results of the test of the microscopic optical potentials over a wide mass range from Be to Bi. The predictions of

both JLM and BR microscopic potentials were compared with the elastic
cross sections at 14.6MeV.

For the test over the energy range from 8 to 26MeV the measured neutron
elastic cross sections for ^{54}Fe were compared with calculations with
the microscopic optical potentials. Comparison between the microscopic
optical model and measured cross sections are shown in fig.3.
Predictions of the two microscopic models are remarkably good. The JLM
model gives better agreement with the neutron scattering cross sections
over the whole mass range.

5. Conclusions

The neutron scattering data were reviewed and the theoretical
predictions in terms of the global optical potential and the microscopic
optical potentials were presented. The neutron scattering data seem to
be well described by the recent global optical potential in the
restricted mass range A>53. The microscopic optical potentials also
well predict the scattering data at 14.6MeV.

Although untiring efforts have been devoted to accumulate nuclear data
in a wide mass range, neutron scattering data are still sparse and
there are many target nuclei which remain to be measured.
Neutron scattering measurements at higher energies up to 40MeV should be
made in order to obtain the best global optical potential for describing
neutron scattering, test the microscopic optical potentials as a tool to
predict neutron scattering cross sections, and respond to the nuclear
data needs for technological applications hereafter.

References

1) DeVito, R.P., Dissertation, Michigan State University 1979

2) Zafiratos, C.D., AIP Conference Proceedings Vol 124, p327 (1985).

3) Rapaport, J., Proc. Int. Conf. Nucl. Data for Basic and Applied Science, Santa Fe, N.M., p1229 (1985).

4) Hansen, L.F., Proc. Int. Conf. Nucl. Data for Basic and Applied Science, Santa Fe, N.M., p83 (1985).

5) Finlay, R.W., Annand, J.R.M., Cheema, T.S., and Rapaport, J., Phys.Rev.,C30, 796 (1984).

6) Wilmore, D., and Hodgson, P.E., Nucl.Phys.,55, 673 (1964).

7) Becchetti, F.D., and Greenlees, G.W., Phys. Rev., 182, 1190 (1969).

8) Rapaport, J., Kulkarni, V., and Finlay, R.W., Nucl.Phys., A330, 15 (1979).

9) Walter, R.L., and Guss, P.P., Proc. Int. Conf. Nucl. Data for Basic and Applied Science, Santa Fe, N.M., p1079 (1985).

10) Jeukenne, P., Lejeune, A., and Mahaux, C., Phys.Rep., 25C, 83 (1976).

11) Jeukenne, P., Lejeune, A., and Mahaux, C., C16, 80 (1977).

12) Brieva, F.A., and Rook, J.R., Nucl. Phys., A291, 299 (1977).

13) Brieva, F.A., and Rook, J.R., Nucl. Phys., A291, 317 (1977).

14) Brieva, F.A., and Rook, J.R., Nucl. Phys., A297, 206 (1978).
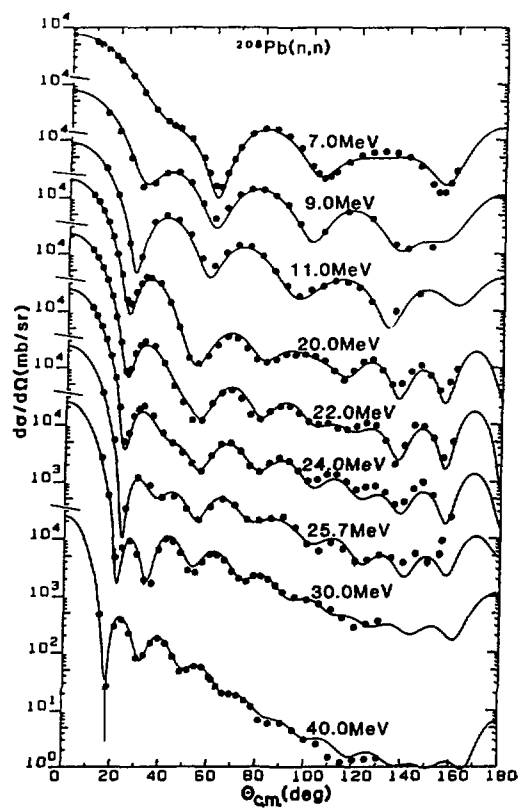
Fig.1   Differential neutron scattering cross sections for
        the ^{208}Pb(n,n) reaction at incident neutron energies
        between 7 and 40MeV. Data are from the following
        sources: 7,20 22 and 26MeV-present measurement;
        9,11 and 25.7MeV-Rapaport et al.(N.P.A296,95(1978));
        30 and 40MeV-DeVito et al.(MSUCL-363,(1981)).
        Ref.5).
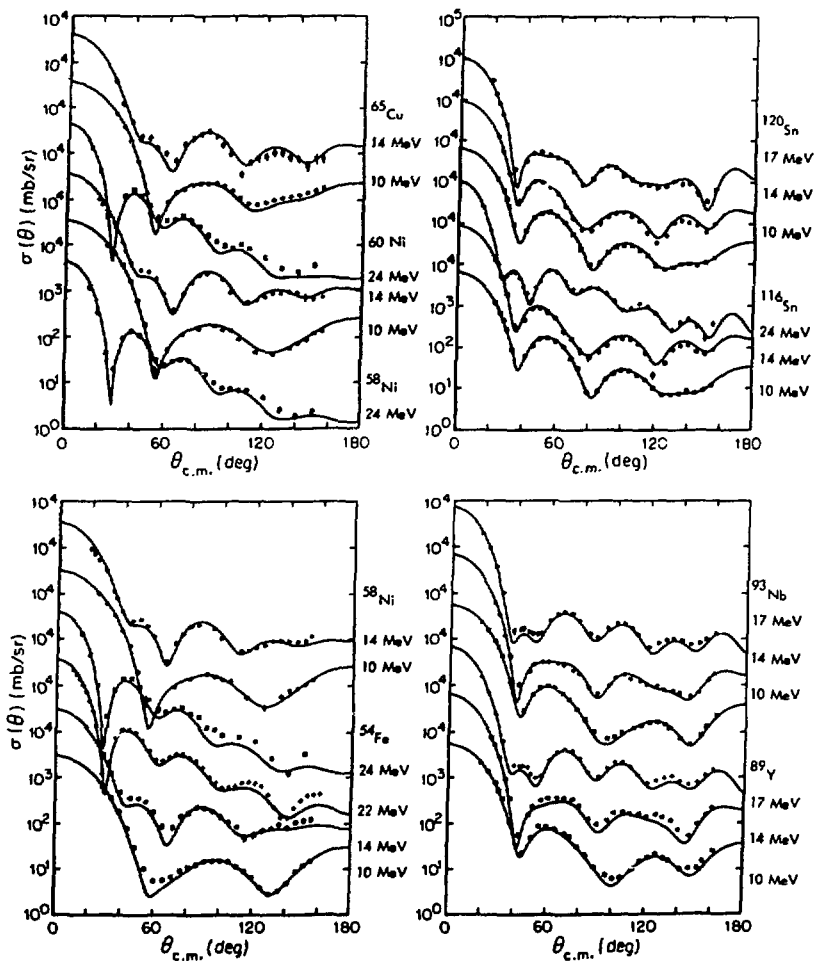
Fig.2a Differential neutron scattering cross section data
and global optical model calculations for
neutron—nucleus scattering in tne mass range from [54]Fe
to [120]Sn. Ref.9).
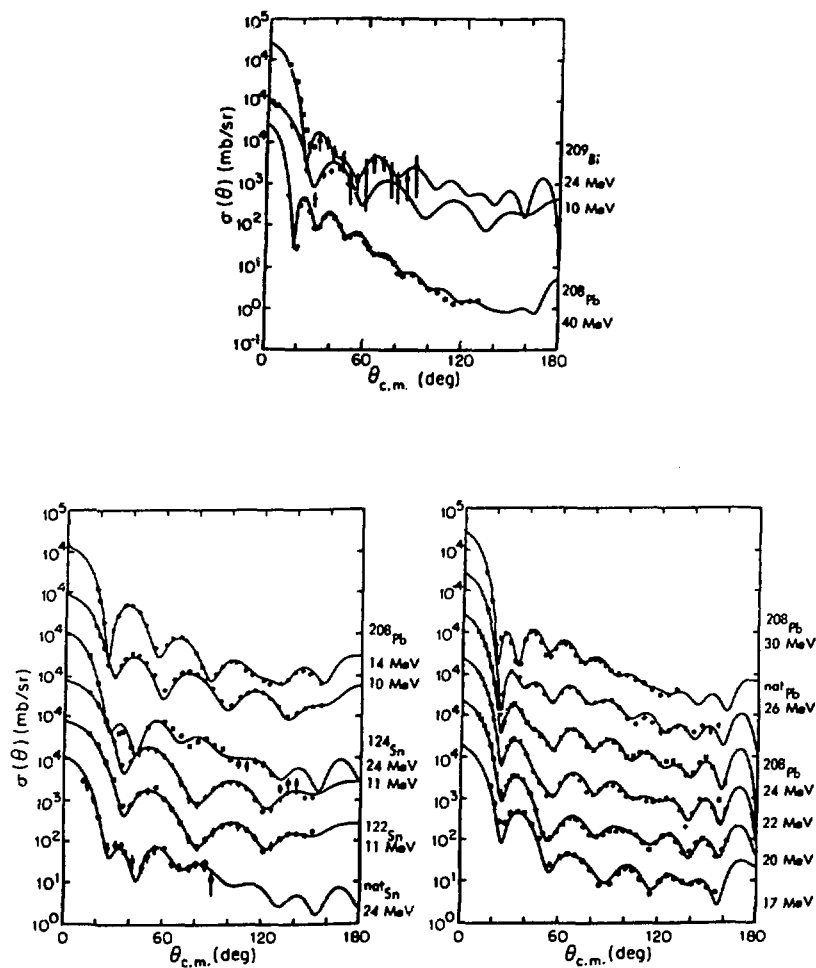
Fig.2b   Differential neutron scattering cross section data
and global optical model calculations for
neutron-nucleus scattering in the mass range from ^{nat}Sn
to ^{209}Bi. Ref.9).
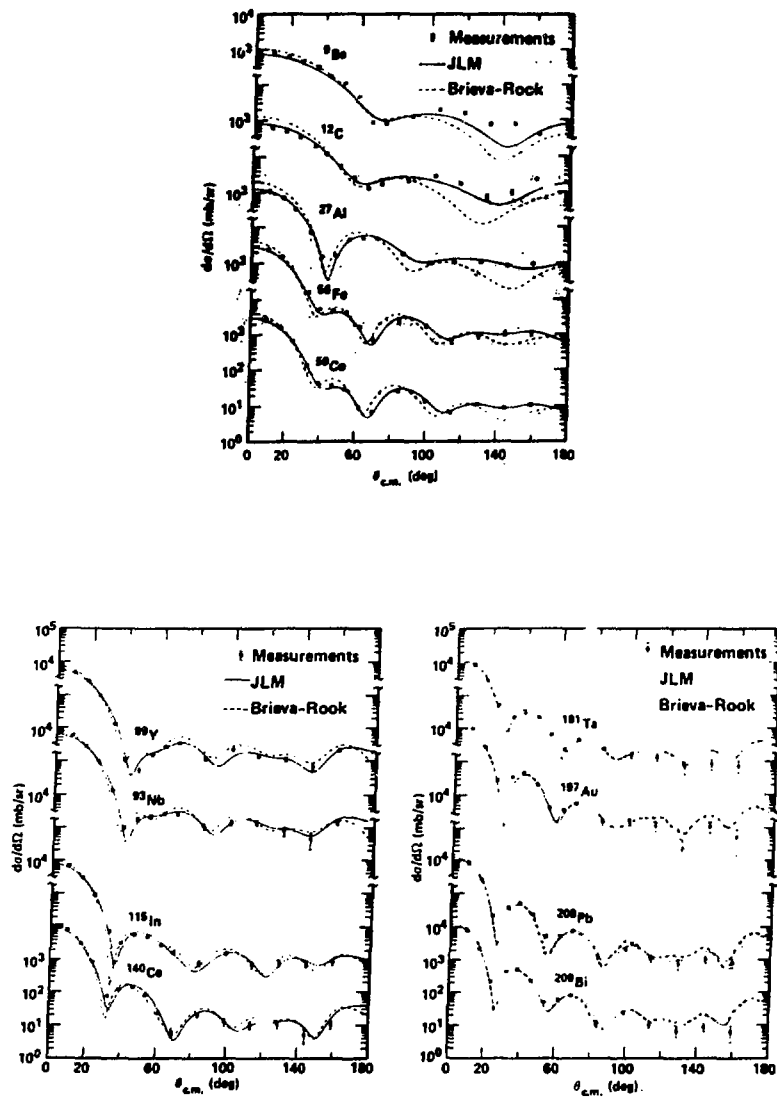
Fig.3   Measurements of neutron elastic scattering at 14.6MeV
         and calculations with the JLM and BR microscopic optical
         potentials. Ref.4).

3.2 Nuclear data related to accelerator applications

Motoharu Mizumoto

Japan Atomic Energy Research Institute

Tokai-mura, Naka-gun, Ibaraki-ken

The use of particle accelerators for applied purposes becomes very common in recent year. The measurement and evaluation for nuclear data related to these applications are expected as one of the main activities after the evaluation works for the JENDL-3 file will be completed. In this report, some of the aims of accelerator applications will be discussed and the characteristics, in particular, of neutron data in the high energy region will be briefly described. As an example of such nuclear data needs, residual radio activities in the accelerator due to the operation of the JAERI Electron Linac will be presented.

1. Introduction

Since particle accelerators were first developed about 50 years ago, they have been exclusively used for fundamental researches such as nuclear physics, particle physics and material sciences. But accelerators are now used for many applied purposes, because the maximum beam energy and current have been increasing very rapidly and various kinds of particle beams have become available with sophisticated beam operation. It is also expected that the accelerator technology will be used in the field of energy productions in future. Recent advanced technologies, including electronics, new materials, high frequency and superconduction, make it possible to construct accelerators more economically and efficiently.

The development of intense neutron sources is considered to be one of the most important accelerator applications, where comprehensive nuclear data will be required. Nuclear data needs range from several MeV to 1 GeV with respect to the neutron energy, and include many charged particle reaction data. But at present, various existing techniques for data handling and calculation may be partly applicable to those regions. The research fields related to the

accelerator applications will stimulate activities both for nuclear
data evaluations and experiments.

2. Fields for accelerator applications

Table 1 shows the various fields in the applications where
particle accelerators are used. These fields may be classified into
two groups: one has already been put to practical use and another
needs more researches for future uses. Medical and industrial uses
have been already widely spread[1]. More than 400 small electron
linear accelerators are used for medical applications and 100 are used
for radiographies all over the country. About 10 cyclotrons are used
in hospitals for the radiation therapy and radioisotope productions
for medical treatments and diagnostics. On the other hands, proton
(or deuteron) accelerators of large scale are still under development.
In addition to the intense neutron sources, they are expected to be
used for various future applications such as transmutation of
radioactive wastes, breeding of fissile fuels and irradiation test of
fusion materials. These research fields have close relationship to
the nuclear energy researches, of which existing activities can be
easily expanded for these purposes.

Table 2 shows the regions where data are necessary to evaluate
for accelerator applications. These are categorized into four main
items: determination of source properties, source and accelerator
shielding, safety and maintenance, and radiation damage and dosimetry.
As apparently known from this table, the necessary properties of the
data are very similar as those required for the fission and fusion
reactor developments. As already pointed out, the only differences
are that the energy regions are high and the various charged particle
reactions have to be considered

3. High energy neutron data

The purpose of this chapter is to review high energy neutron
cross section data above 20 MeV. But this review is not comprehensive
and is only intended to show the main characteristics of the data in
this energy region. There have been many review works which described
the data status in more detail[2-6]. There are still very

insufficient data available between 20 to 50 MeV and practically no
data above 100 MeV except total cross sections. In spite of the
immediate data need, the increase of the references in CINDA[7] is
slow because the number of the experimental facilities, which are
capable to do this kind of high energy neutron experiments, is limited.

The Davis cyclotron, Electron Linac at ORNL(ORELA) and KFK
cyclotron have obtained total cross section data in the 10-50 MeV
range for several elements. In addition to these laboratories, the
WNR facility at Los Alamos have provided total cross section data
above 100 MeV region using the 800 MeV spallation neutron source.
They constructed the new facility in 1986 by adding PSR (Proton
Storage Ring) and are expected to produce new data of better quality
with more intense neutron source. Figure 1 shows the example for Fe
total cross sections where a significant discrepancy exists among the
Davis, ORELA and KFK data. The only 10-15 % accuracy was obtained so
far and additional work is necessary to satisfy the required need of
about 5 %[3]. Figure 2 shows the comparison of the Cr data[4]. When
the conventional optical model parameter sets are used for the
calculation, predicted total cross section values are found to be
quite different from the experimental results.

The elastic and inelastic scattering cross sections have been
extensively measured in Ohio and TUNL University. The present status
and systematic studies of optical model calculation were reviewed by
Yamanouti in this seminar[8]. The reasonable optical parameters are
required to fit also total cross sections, proton induced cross
sections and analyzing power as shown in Fig. 3.

The examples of neutron emission data such as (n,2n) and (n,3n)
cross sections are shown in Figs. 4a and 4b, which were measured at
Los Alamos[9]. For the light element, the cross section value
increases only in the high energy region while for the heavy element
the cross section rises in the lower energy region due to the mass
dependence of neutron binding energies. The statistical model
including preequilibrium effects can predict reasonably well these
data.

Activation cross sections are also very important in the high
energy region but there are no convenient monoenergetic neutron

sources. Therefore the d-Be source, which is not fully monoenergetic, was used at Julich[10] to obtain such data as shown in Fig. 5. Double differential cross sections for emitted charged particles (proton, deuteron, triton, helium-3 and alpha) were measured at Davis[6] using 27.4, 39.7 and 60.7 MeV neutrons from the p-^{7}Li reaction. These data on human tissue elements (H, C, N and O) are very useful to know the energy dissipation in the body (kerma) for the neutron therapy. In Fig. 6, data for 60.7 MeV neutrons on Carbon are shown. The gamma-ray production cross sections have been measured for many elements below 20 MeV for fusion application using the ORELA white neutron source. They extended their energy region up to 40 MeV and provided the data for calculations of gamma-ray heating and radiation shielding. Figure 7 shows the recent discrete gamma-ray data for Cr[11].

In many laboratories, much efforts have been made to obtain high energy data. Several neutron sources for this purpose are being investigated.[12].

Theoretical calculations of high energy neutron data have been also carried out below about 50 MeV in order to supplement the insufficiency of experimental data. They are generally based on the multi-step Hauser Feshbach model combined with preequilibrium and direct reaction model. Those models utilize optical potential parameters, average level densities and discrete level information. Figure 8 shows the example of the ^{59}Co evaluation calculated with the Los Alamos computer code GNASH[13], where a large number of reactions were taken into account.

4. Intense neutron source

The main types of nuclear reactions, which can be used for neutron production, are given in Table 3.[14] The numbers of neutrons per particle or reaction and the heat deposition per source neutron are shown. The shape of the emitted neutron energy spectrum is also important for each purpose of usage. The d-T neutrons and photo neutrons (W(e,n)) can be used only for the basic researches because of the low neutron intensity and difficulty to cool the target. The fission neutron is not suitable for the high energy neutron experiments due to the thermal neutron spectrum. The D-T fusion

neutron may possibly be used in future as very intense neutron sources after fusion reactors will be realized.

Figure 9 shows the energy distribution of neutrons emitted at various angles when 40 MeV deuterons hit a thick Li target[15]. From deuteron break-up reaction, the neutron with an energy of about half that of the incident deuteron is emitted in the forward direction. Figure 10 shows the emitted neutron flux shapes from the spallation reactions of 590 MeV protons incident to Pb and ^{238}U target[16]. Low energy part below about 10 MeV is due to neutron evaporations which have an isotropic angular distribution, while high energy part is due to knock-on reactions with a strong forward peak. Because of intense high energy neutrons, these two sources can be suitable for investigation of radiation damage in the first wall of a D-T fusion reactor. An exposure of 14 MeV neutrons are needed for this test with a flux of the order of $10^{14} ncm^{-2}s^{-1}$.

Table 4 shows the comparison of the nuclear data requirements between the break-up neutron of d-Li and the spallation neutron source. With regard to the accelerator technology and the availability of nuclear data, the construction of deuteron accelerators may be easier than high energy proton accelerators. But, as already mentioned, spallation sources have possibilities for many other applications. Moreover, spallation reactions provide the highest number of neutrons per proton (up to 40 n/p) and cause the smallest heat deposition per neutron. In recent year, several projects of large scale for spallation neutron sources have been proposed and several new facilities have started operation.

The nuclear reaction mechanism in the high energy region above 50 MeV is not fully understood, but to some extent, this reaction can be described by multiple collisions between the incident particle and free nucleons in the target. This is called an intranuclear cascade model. This process is too complicated to be calculated by analytical methods. Therefore, Monte Carlo technique is applied in combination with the transport calculation of the cascade and particle evaporation from target nuclei. Figure 11 show the comparison between the experiment and such calculation at the incident proton energy of 800 MeV[17]. The good agreement was obtained between the calculation and

experiment at this energy.

5. Residual activities at the JAERI electron accelerator

Accurate information and reduction (if possible) of residual radio activities in the accelerator structure and shielding material are important for operation and maintenance of particle accelerators. The calculations to estimate such activities were carried out, for example, in the case of the FMIT (Fusion Material Irradiation Test Facility) project[18]. But up to now such estimations have been scarcely done because accelerator components are very complex and radio activities are difficult to be generalized due to the strong dependence on each arrangements of each facility.

At the JAERI electron linear accelerator, neutron time-of-flight experiments have been carried out for more than 15 years. Schematic arrangement of the accelerator is shown in Fig. 12. Residual radio activities were accumulated in the accelerator structure, beam transport system and neutron target. At the high energy electron linac, activities are produced mainly by photo reactions such as (Υ,n) and (Υ,p) due to bremsstrahlung and neutron absorptions due to secondary emitted neutrons. Components activated are stainless steel, aluminum, copper and concrete shield.

Measurements of gamma-ray activities were made with a portable Ge detector at several positions along the accelerating tubes as shown in Fig. 12. The electron energy, which causes activations, increases along the accelerating tube from 2 to 120 MeV. Observed gamma-ray spectrum at position #5 is shown in Fig. 13. Induced activities in the figure have relatively long lives because measurements were made 48 hours after the accelerator operation was stopped. Table 5 shows the major reactions to be considered with ratios of intensities to the ^{60}Co gamma-rays. The FMIT estimations are also shown for reference. Though they were calculated for deuteron induced reactions, it was found that similar activities were produced. Figure 14 shows the dependence of gamma-ray intensities on the measured positions, which should be correlated with accelerated electron energies. It is necessary to calculate these activations based on the intensity and energy of the accelerated particle and evaluated reaction cross

sections of structural and shielding materials of accelerators. But
it should be also noted that these data are strongly dependent on the
operation condition of the particular period. The accumulation of
this kind of information from various accelerators is very important
and useful to construct new accelerator and facility.

6. Summary

The data evaluation related to accelerator applications is the
new field for nuclear data activities. The nuclear model calculations
are in general only methods to produce data for evaluations in the
high energy region. However they are often based on assumptions which
cannot be fully justified. Therefore, model predictions must be
checked from comparisons with reliable experimental data. Productions
of new experimental data are urgently needed using advanced techniques
and new facilities. Collaboration between experimentalists and
evaluators among many laboratories will be effective to improve the
data status.

References

(1) J. Tanaka and H. Kamitsubo, J. Phys. Soc. Japan, 39 (1984) 235

(2) R.C. Haight, Proc. Sym. on Neutron Cross Sections from 10 to 40 MeV, BNL, p201 (1977)

(3) ᵤ.C. Browne and P.W. Lisowski, Proc. Sym. on Neutron Cross Sections from 10 to 50 MeV, BNL, p215 (1980)

(4) D.C. Larson, ibid. p277

(5) R.L. Walter and P.P Guss, Proc. Int. Conf. on Nuclear Data for Basic and Applied Science, Santa Fe, p1079 (1985)

(6) J.L. Romero, F.P. Brady and T.S. Subramanian, ibid, p687

(7) CINDA86, Index to Literature and Computer Files on Microscopic Neutron Data, IAEA, Vienna (1986)

(8) Y. Yamanouti, Proc. the 1986 Seminar on Nuclear Data, Tokai (1986)

(9) L.R. Veeser, E.D. Arthur and P.G. Young, Phys. Rev. C16 (1977) 1792

(10) S.M. Qaim, C.H. Wu and R. Wolfle, Nucl. Phys. A410 (1983) 421

(11) D.C. Larson, Proc. Int. Conf. on Nuclear Data for Basic and Applied Science, Santa Fe, p71 (1985)

(12) IAEA Advisory Group Meeting on Properties of Neutron Source, Leningrad (1986)

(13) E.D. Arthur, P.G. Young and W.K. Matthes, Sym. on Neutron Cross Sections from 10 to 50 MeV, BNL, p751 (1980)

(14) S. Cierjacks, Proc. KTG/ENS Int. Sem. on Nucl. Data, Cross Section Libraries and Their Application in Nucl. Technology, Bonn, p315 (1985)

(15) M.J. Saltmash et al., Nucl. Instrum. Methods, 145 (1977) 81

(16) S. Cierjacks et al., Proc. Int. Conf. on Nuclear Data for Science and Technology, p383 (1983)

(17) M.M. Meier et al., Proc. Int Conf. on Nuclear Data for Basic and Applied Science, Santa Fe, p1415 (1985)

(18) L.L. Carter, R.J. Morford and A.D. Wilcox, Proc. Sym. on Neutron Cross Sections from 10 to 50 MeV, p431 (1980)

Table 1. Fields for accelerator applications

Accelerator	Fields for use
Proton (Deuteron)	Neutron source, Transmutation of radioactive waste, Breeding of fissile fuel, Material irradiation, Meson production, Muon catalyzed fusion, RI production, Medical use, Material analysis
Electron	Free electron laser, Synchrotron radiation, Inertial confinement fusion, Food irradiation, RI production, Material irradiation, X-ray source, Medical use
Heavy ion	New material developments, Biology, Inertial confinement fusion, Medical use, RI production

---

Table 2. Nuclear data related to accelerator applications

---

(1) Source reaction	Particle and mass yield (incident of proton, deuteron, electron, heavy ion), Emitted neutron intensity, spectrum, angular distribution, Charged particle reaction cross section, Neutron cross section.
(2) Shielding	Total, Scattering, Nonelastic, Gamma-ray production cross sections (Double differential)
(3) Maintenance	Radiation cross section (induced by proton, deuteron, neutron), Reaction yield
(4) Damage and Dosimetry	DPA, Gas production, Transmutation, Radiation cross section

---

Table 3.   Neutron producing reactions

Reaction	Yield n/particle or event	Deposited Heat MeV/n	Type of Spectrum
T(d,n) (0.2MeV)	8×10^{-5} n/d	2500	14 MeV
W(e,n) (100MeV)	3.2×10^{-2} n/e	3100	evaporation
Li(d,n) (40 MeV)	6.7×10^{-2} n/d	600	d-break-up
Fission (^{235}U)	1 n/fission	200	fission
D-T Fusion	1 n/fusion	3	14 MeV
Pb spallation (1GeV)	20 n/p	23	evap.+cascade
^{238}U Spallation (1GeV)	40 n/p	50	evap.+cascade

Table 4   Comparison of required nuclear data between break-up and spallation neutron sources.

	Deuteron break-up source	Spallation source
Accelerator	AVF cyclotron Alvarez linac FMIT(Proposed)	Cyclotron TRIUMP, SIN Coupled cavity linac LAMPF, SNQ(Proposed)
Reaction	d + Li, d + Be	Spallation
Status of nuclear data		
Source	Data exist except Ed<2MeV	Data at TRIUMP, SIN, LAMPF exist but insufficient and depend on calculations
Shielding	Need of total, angular, nonela data Require of 10-15% for Fe,0,Si,Ca,C Goal 5 %, Data from Davis, ORNL, KFK, WNR exist but are insufficient	HILO(ORNL) file contains n-66 and Γ-21 groups up to 400 MeV, LANL file contains data up to 800 MeV, No data exist above 800 MeV, No angular distribution above P_5
Maintenance	Data need for stainless, beam tube, air concrete, drift tube but are insufficient	Data need for all cross sections including high and low energy fission, spallation, $(n,\Gamma)+(n,2n)+(n,3n)$
Dosimetry	Data need for He, H production but no data exist except 14 MeV	Data exist for He, H production of C,0,Si, but do not agree with calculations

Table 5. Induced residual activities in the JAERI electron linac

Activated Nuclides	Half life	γ-ray Energy (keV)	Major reaction	Ratio to ^{60}Co	FMIT estimation
^{22}Na	2.6 a	1275	$^{23}Na(\gamma,n)$, $^{24}Mg(\gamma,np)$	0.11	
^{24}Na	14.96 h	1369,2754	$^{24}Mg(n,p)$, $^{27}Al(n,\alpha)$		
^{48}V	15.97 d	984,1312	$^{50}Cr(\gamma,np)$		
^{51}Cr	27.70 d	320	$^{52}Cr(\gamma,n)$, $^{50}Cr(n,\gamma)$	0.14	
^{54}Mn	312.2 d	835	$^{54}Fe(n,p)$, $^{55}Mn(\gamma,n)$	3.5	14.4
^{59}Fe	44.6 d	1099,1292	$^{62}Ni(n,\alpha)$		
^{56}Co	78.76 d	847,1238,	$^{58}Ni(\gamma,np)$	0.14	0.07
^{57}Co	271.3 d	122,136	$^{58}Ni(\gamma,p)$		
^{58}Co	70.78 d	811	$^{58}Ni(n,p)$, $^{59}Co(\gamma,n)$	1.3	0.84
^{60}Co	5.272 a	1173,1332	$^{59}Co(n,\gamma)$, $^{60}Ni(n,p)$	1.0	1.0
^{57}Ni	36.0 h	1378,1920	$^{58}Ni(\gamma,n)$	0.18	

FE TOTAL CROSS SECTION
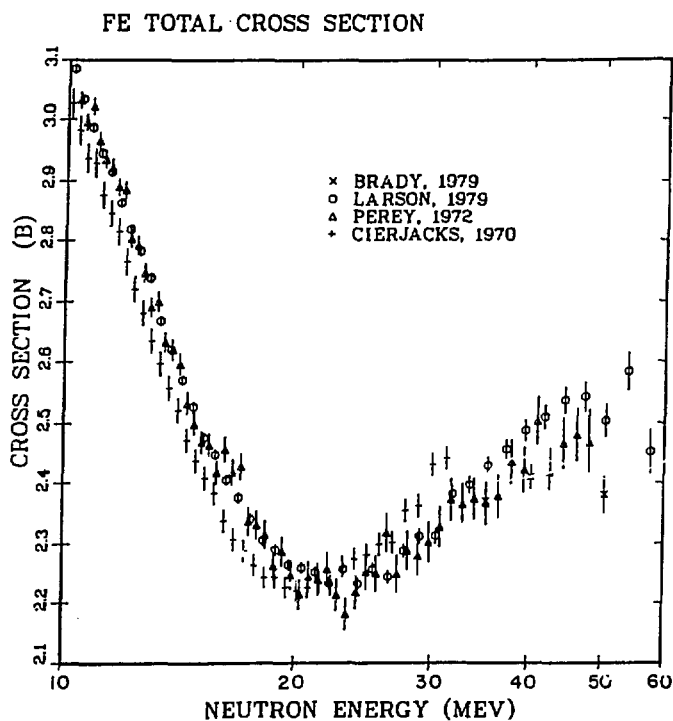
Fig. 1.   A comparison of total cross section results for Fe.
For details, see Ref.3.
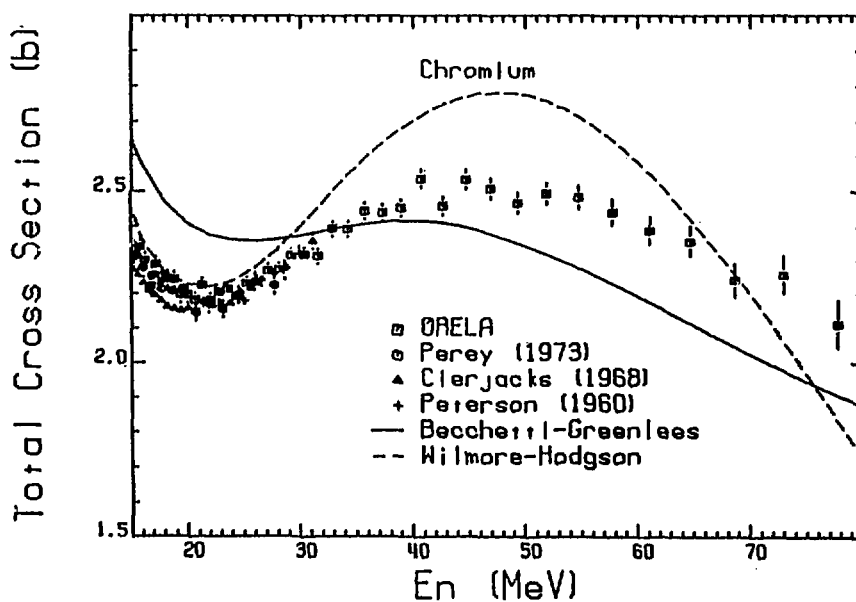
Fig. 2.   Comparison of total cross section data for Cr. For
details, see Ref.4.
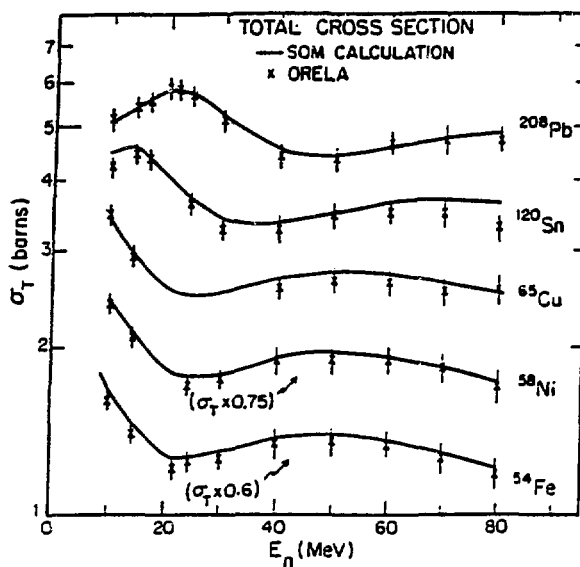
Fig. 3a. Neutron total cross section data and optical model
calculations (Ref.5)
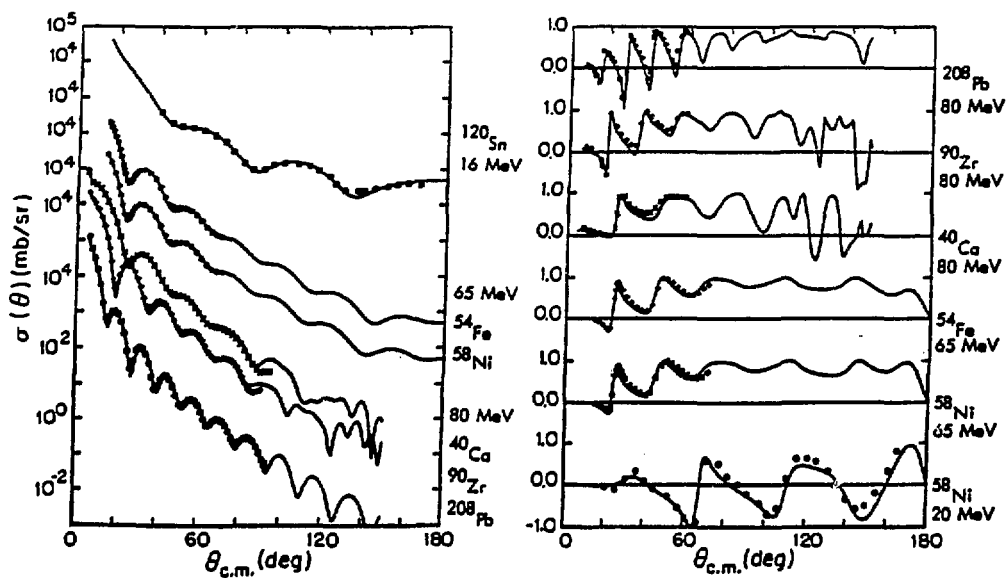
Fig. 3b. Cross section and analyzing power data and SOM
calculations for proton-nucleus scattering (Ref. 5)
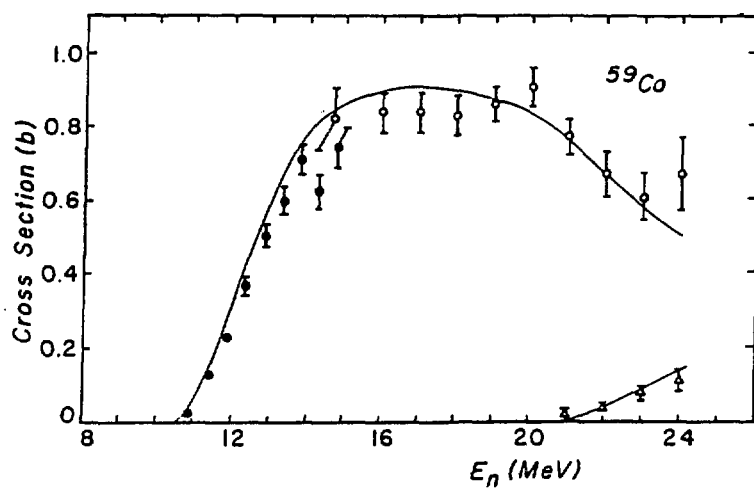
Fig. 4a. Cross sections for ^{59}Co(n,xn). For details, see Ref.9.
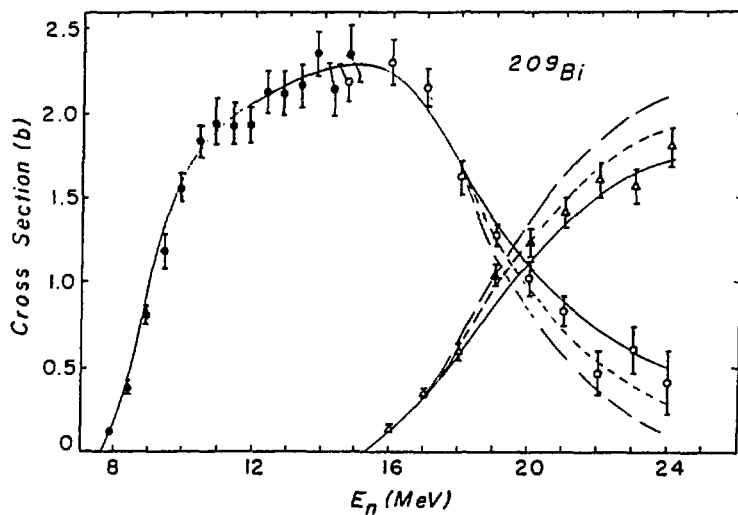
Fig. 4b. Cross sections for ^{209}Bi(n,xn). For details, see Ref.9.
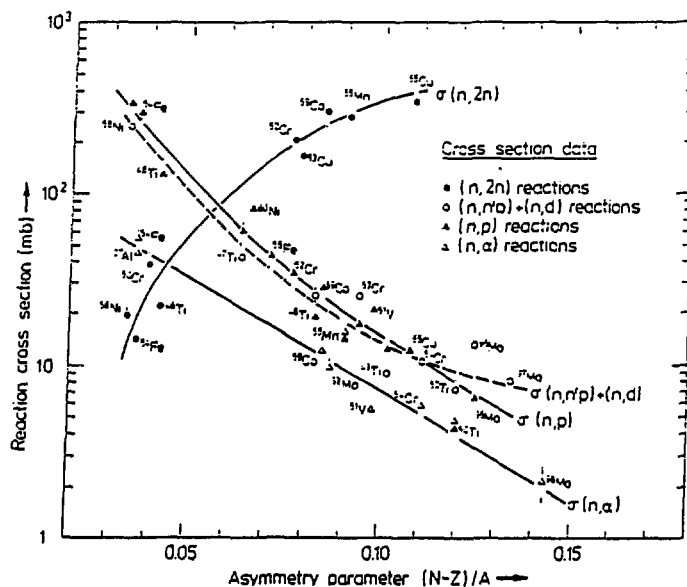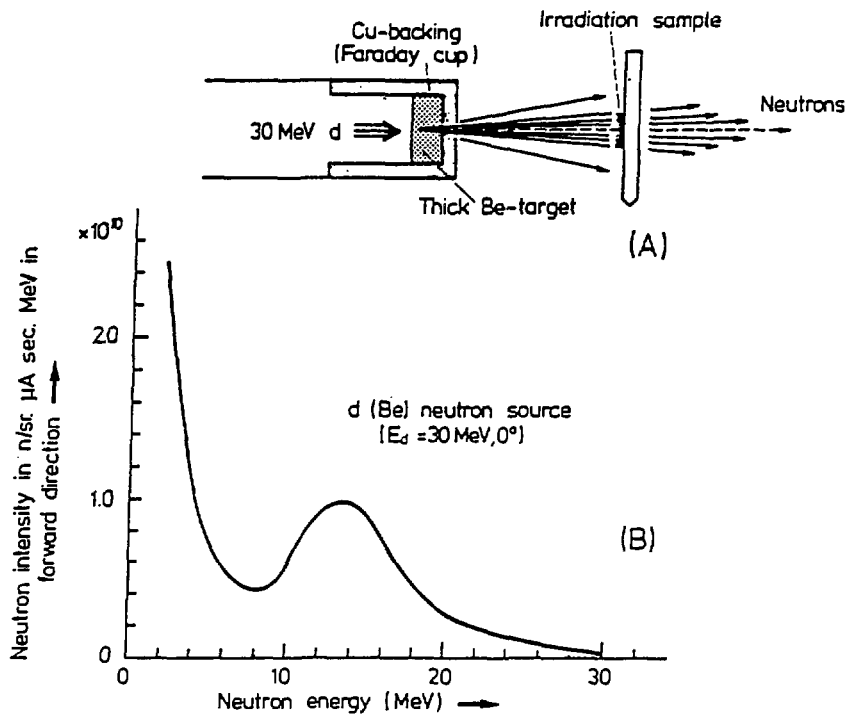
Fig. 5.   Systematic trends in cross sections of (n,2n), (n,p),
((n,n)+(n,d)) and (n,) reactions induced by 30 MeV
d-Be neutrons on some structural materials. (Ref.10)
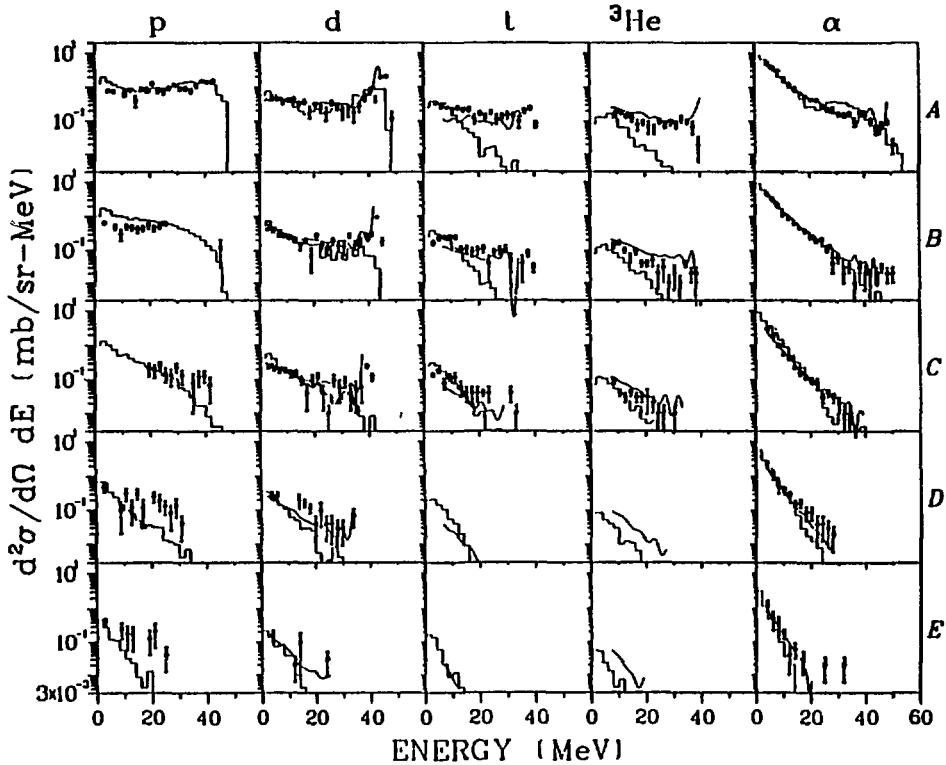
Fig. 6.   Double differential cross sections (laboratory) for
          60.7 MeV neutrons on Carbon. Key: A=20, B=40, C=65,
          D=90 and E=150. For details, see Ref.6.
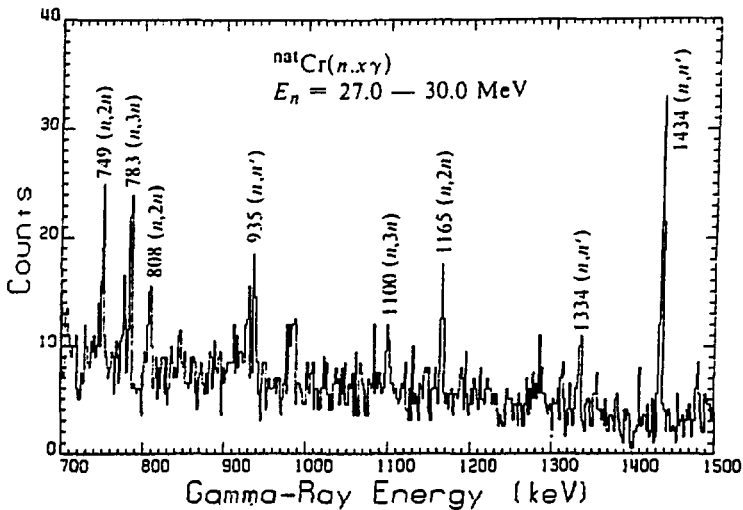
Fig. 7.   Portion of gamma-ray spectrum for $^{nat}Cr(n,x)$. Gamma
          rays from various reactions of n + ^{nat}Cr are labeled.
          (Ref.11)
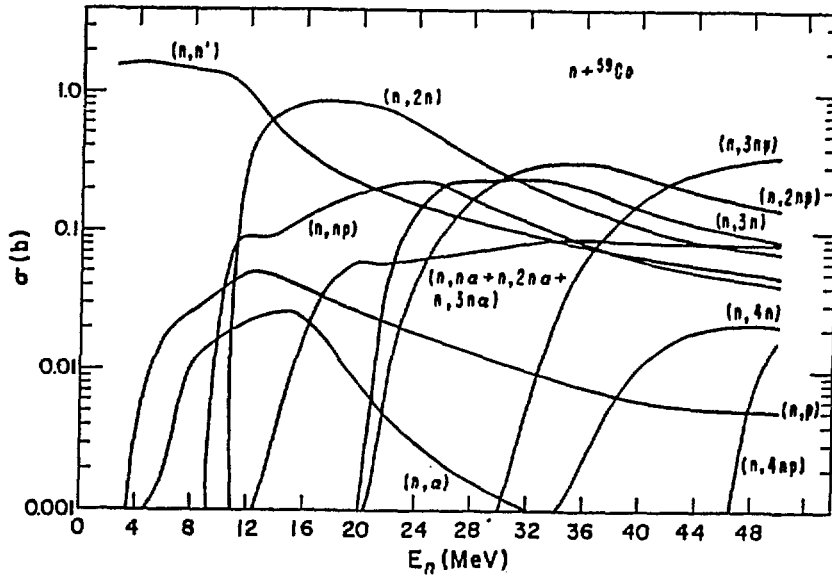
Fig. 8.　Trends in cross sections calculated for ^{59}Co.　(Ref.13)
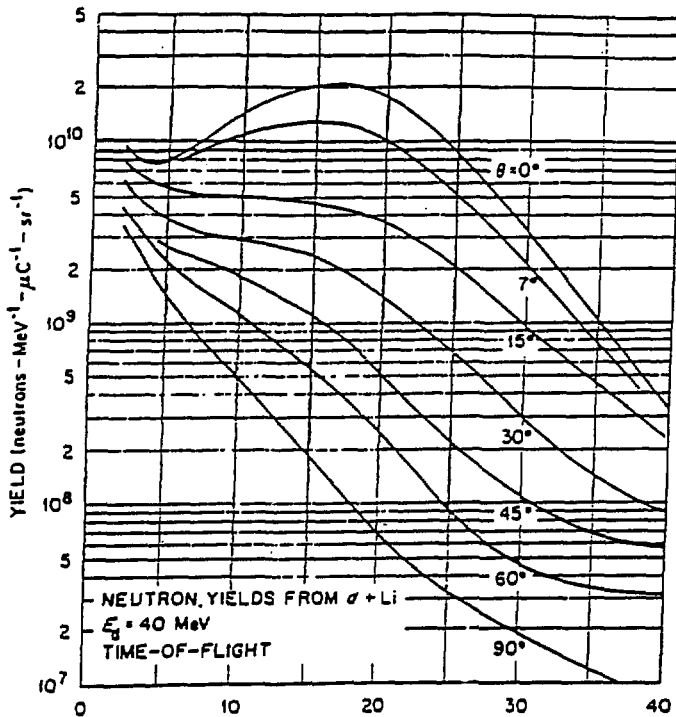
Fig. 9.　Energy distribution of neutrons emitted at various
angles with respect to the incident beam when 40 MeV
deuterons are incident on a thick Li target. (Ref.15)
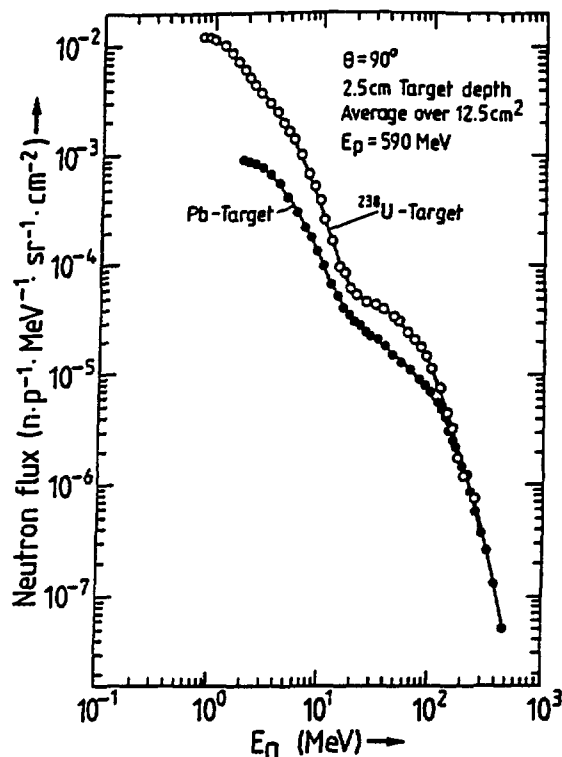
Fig. 10. Neutron spectra for Pb and depleted U targets (Ref.16)
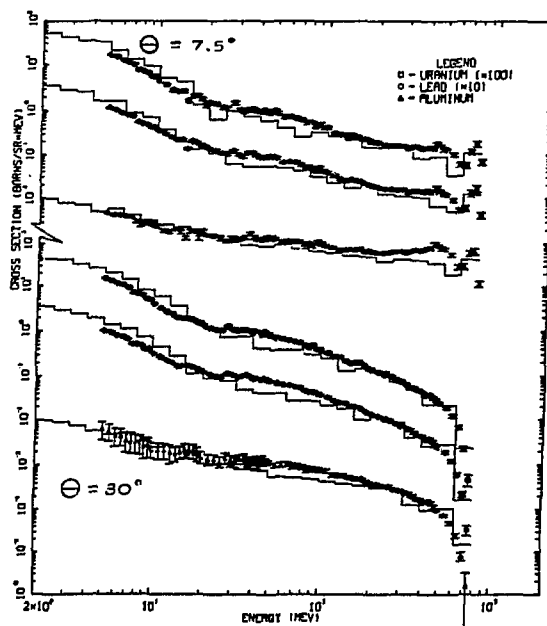
Fig. 11. Comparison of experiment and Calculation at 800 MeV.
(Ref.17)
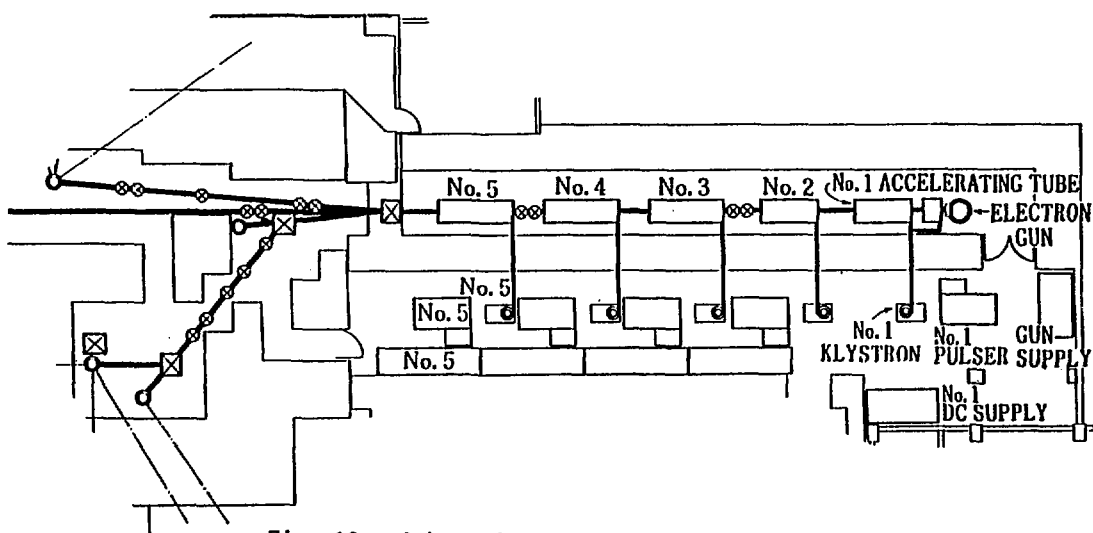
Fig. 12.   Schematic arrangement of the JAERI electron linear accelerator.
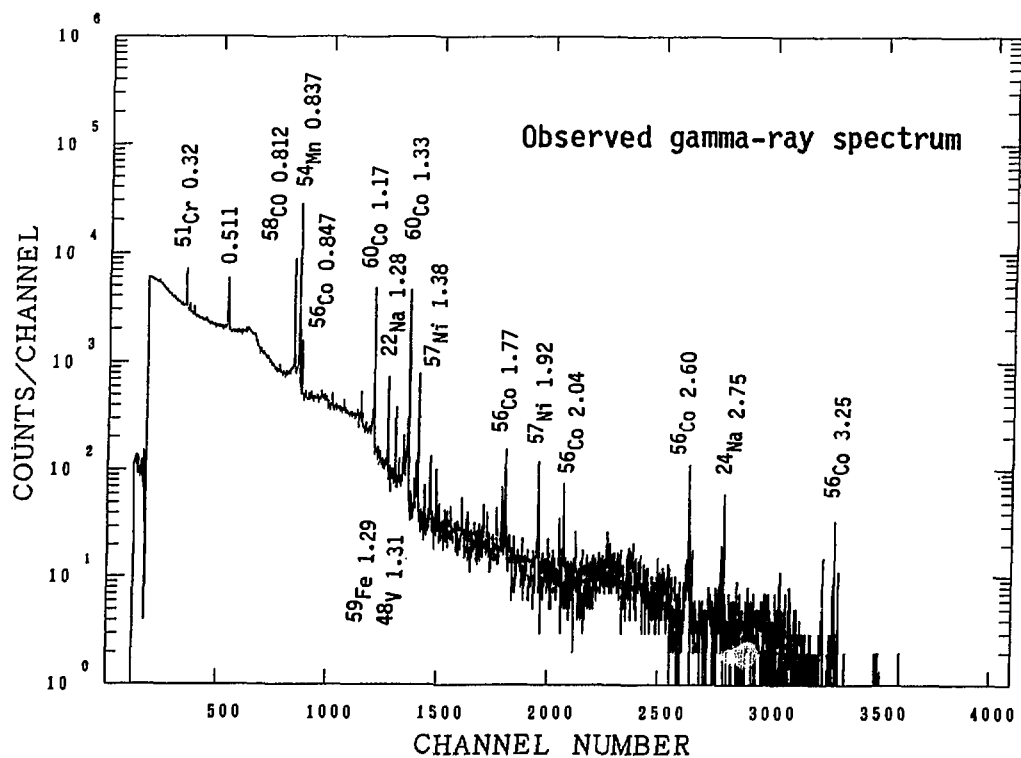
Fig. 13.   Observed gamma-ray spectrum at the position #5.
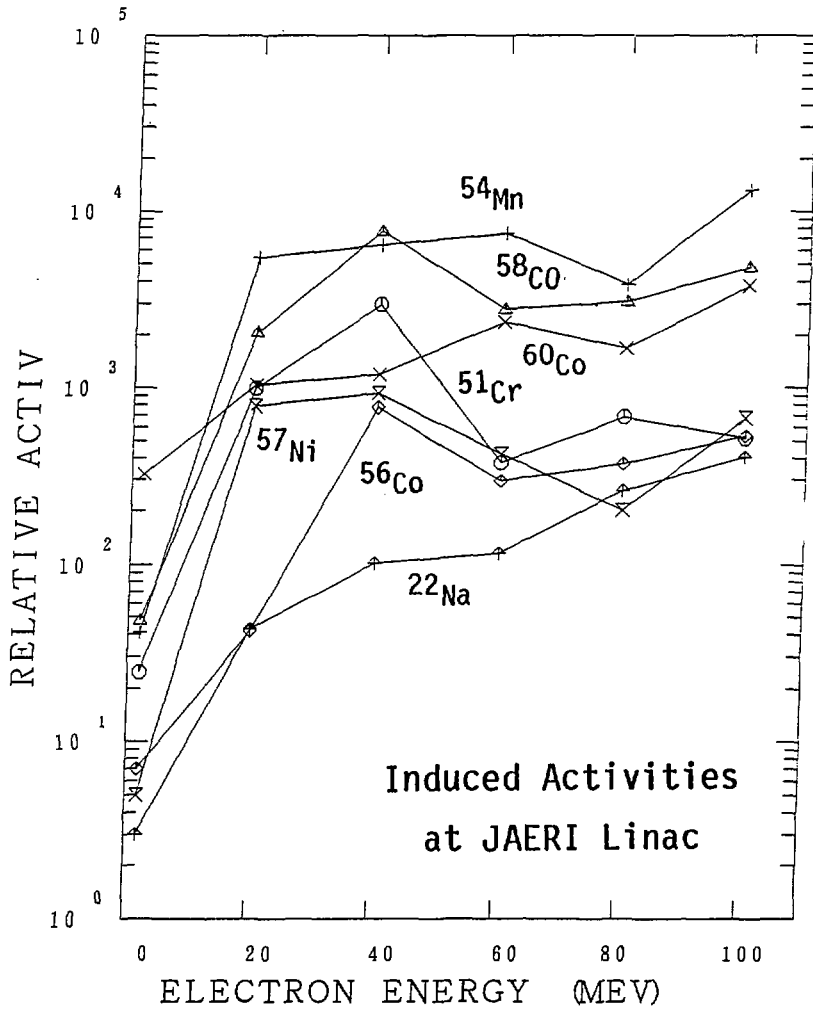
Fig. 14. The dependence of gamma-ray intensities on the measured positions, which should be correlated with accelerated electron energy.

3.3 Charged Particle Induced Reactions
(Standard Reaction)

RIKEN   A. Hashizume

Since 1984, we made the compilation of the cross section data of charged particle induced reactions useful for production of radioactive isotopes in biomedical use. Our primary interest is in the reaction cross sections which are concerned with production of the following isotopes:

^{11}C, ^{13}N, ^{18}F, ^{28}Mg, ^{52}Fe, ^{67}Ga, ^{67}Ga, ^{74}As,
^{77}Br, ^{77}Kr, ^{81}Rb, ^{82m}Rb, ^{111}In, ^{123}Xe, ^{127}Xe, ^{123}I,
^{124}I, and ^{125}I.

In general, these integral cross sections of charged particles are obtained by the foil activation method. In the experiment, one have to determine the energy and numbers of incident particles on a target and also to determine the induced activities. The uncertainties of stopping power and straggling of incident energy in the target assembly are also the factors which affect the accuracy of measurements. In charged particle induced nuclear reactions the accuracies of experiment are not always good. It is usual case that the experimental values obtained independently shows some discrepancies. A example is shown in Fig.1 which indicates the reaction cross section of ^{123}Xe by $^{127}I(p,5n)$. The daughter of ^{123}Xe, ^{123}I, is considered one of the best radionuclides for in vivo diagnostic nuclear medical studies using single-photon emission computed tomography. At the enrgy of 51 MeV where the cross section become maximum, the values are distributed about 60 %. These situation is can be pointed out for other reactions. One way to avoid these discrepancies is to use the standard reaction and dtermine relatively the cross section.

The use of these monitor reactions have also advantage where Faraday cups for beam flux monitoring is difficult to use in case of using internal beam such as high energy accelerator machine.

Idealy the monitor reactions used for standard should satisfy the following factors:

(1) The absolute cross section should be known precisely in wide range of energies of incident particles.

(2) The cross section should change rather smoothly as incident particle energies increase. It is not desiable to have sharp resonances.

(3) Other reaction channels should be small

(4) The effects of secondary particles due to primary reaction should be small.

(5) The half-life of reaction product should not to be too short compaired to irradiation time.

(6) The quantitiative determination of activity can be easily made.

(7) Target material and foil should be obtained without difficulty.

(8) The target shoud be stable during the irradiation.

Though there are lots of reactions, there exist very few reactions which can be adopted for standard monitor reactions. One of the restriction comes from the criterion (7). If one looks for the isotopes which have natural abundance more than 98 %, there are 28 isotopes in nature in which 6 isotopes are in gas phase at normal temperature. If one examines further the other criterions one realizes that the $^{12}C(p,pn)^{11}C$ reaction can be used as a primary standard for the proton induced reactions. Specially the absolute cross sections of this reaction have been measured in wide range of incident energies. For other reactions $^{27}Al(p,3np)^{24}Na$, $^{63}Cu(p,2n)^{62}Zn$, $^{65}Cu(p,n)^{65}Zn$, $^{65}Cu(p,pn)^{64}Cu$, are used for the monitoring. For deutron induced reactions $^{27}Al(d,x)^{24}Na$ is used. For alpha induced reactions, aluminum target is also used by making the reaction $^{27}Al(\alpha,x)^{24}Na$.

The cross sections of $C(p,pn)^{11}C$ are summarized in Fig 2. Typical errors are distributed between 3 to 5 % in the energy range between 20 MeV and 28 GeV. In Table 1, an example of the cause of errors in the measurement of $^{65}Cu(p,pn)$ is shown. The errors of other reactions are summarized in Table 2.
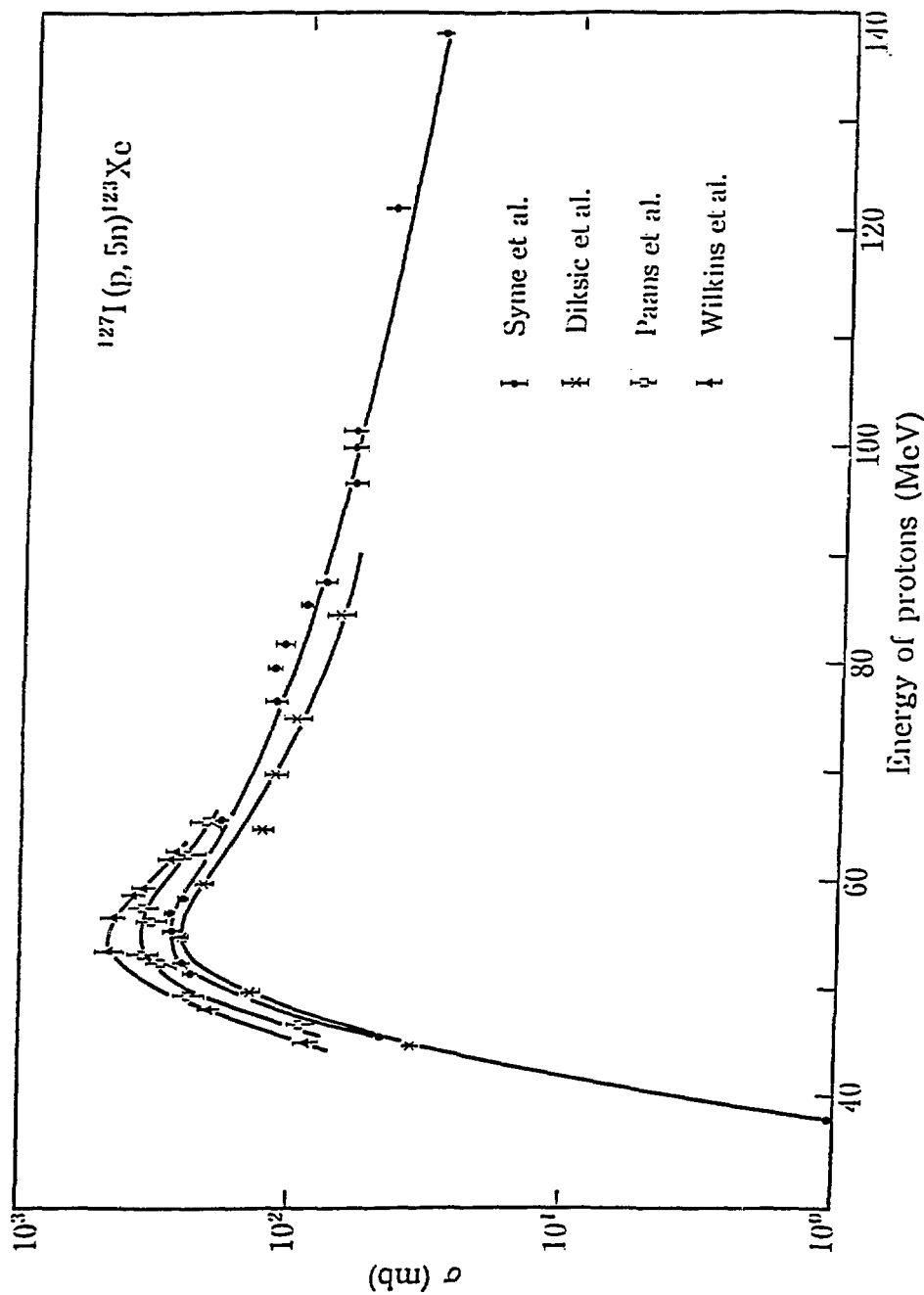
Fig. 1 Comparison of excitation functions of the $^{127}I(p,5n)^{123}Xe$ reaction
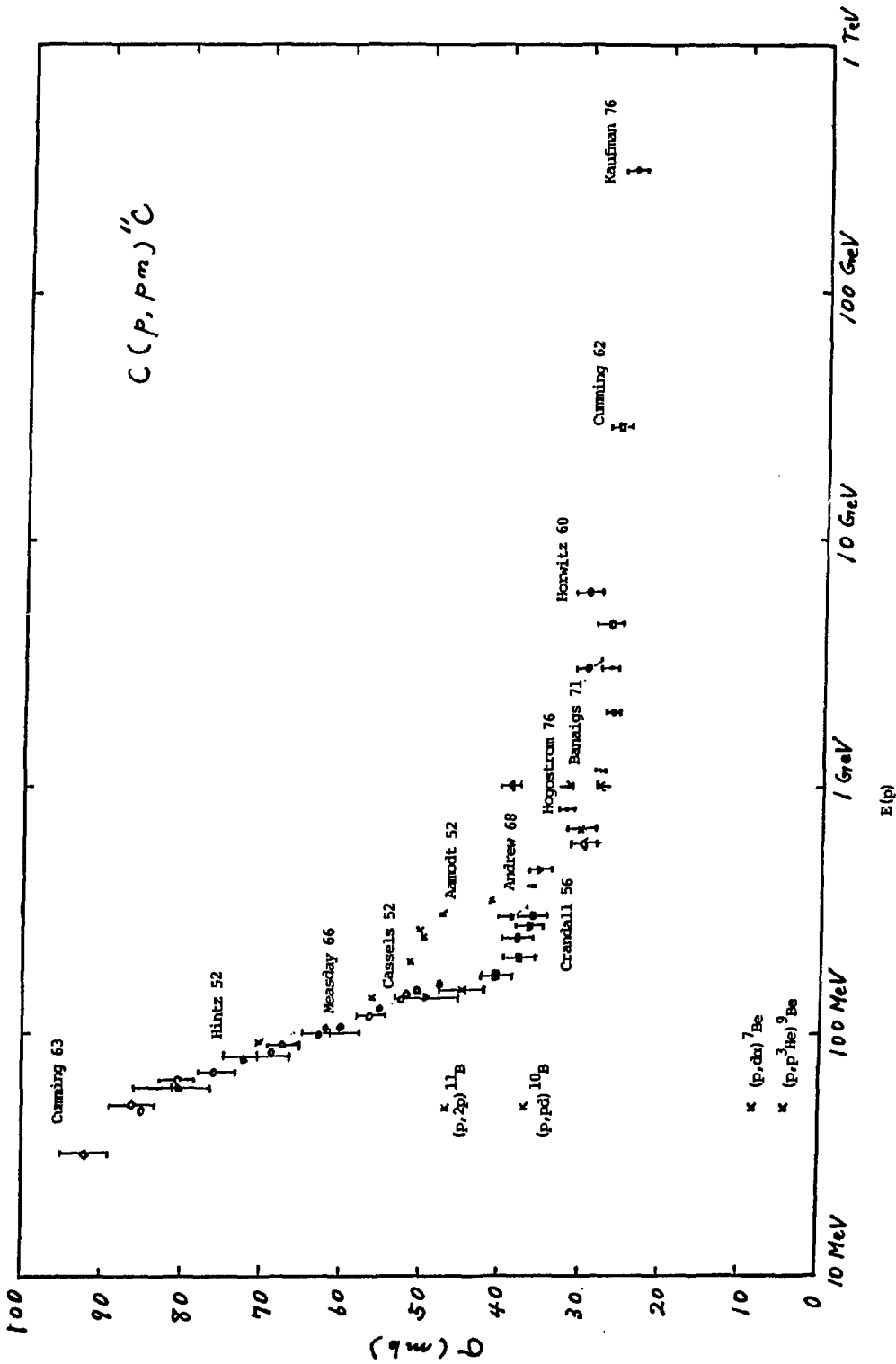
Fig. 2 The cross sections of C(p,pn)[11]C which is used for the standard of proton induced reaction.

Table 1. An example of indicative and systematic errors in
the $^{65}Cu(p,pn)^{64}Cu$ reaction.

Randum error	±%	Systematics	±%
Chemical yield	3.0	Number of protons	1.0
Activity measurements	2.5	Standard calibration	1.6
Live time estimations	1.5	Counter efficiency	1.5
Pipeting, dilution,weighing	1.0	Decay Scheme	1.0
Decay curve analysis	1.0		
Photopeak areas	3.0		
Uncertainty	5.0		2.6

Table 2. The errors of cross sections of the standard and/or
monitor reactions.

Reactions	Energy range	Errors
$C(p,pn)^{11}C$	20 MeV – 28 GeV	3–5 %
$^{27}Al(p,x)^{24}Na$	30 MeV– 28 GeV	~ 5 %
$^{65}Cu(p,pn)^{64}Cu$	23 MeV – 102 MeV	6 %
$^{27}Al(d,3p2n)^{24}Na$	13 MeV – 23 MeV 40 MeV – 88.5 MeV	8–10 % < 3 %
$^{27}Al(\alpha,x)^{24}Na$	60 MeV – 156 MeV	6 %
$^{27}Al(\alpha,x)^{22}Na$	60 MeV – 156 MeV	6 %

4. Group Constants and Sensitivity Analysis

4.1 Uncertainty analysis of neutron transport calculation

Y.Oka,*K.Furuta and *S.Kondo

Department of Nuclear Engineering,

*Nuclear Engineering Research Laboratory

University of Tokyo

Hongo, Bunkyo-ku, Tokyo.

Abstract

A cross section sensitivity-uncertainty analysis code, SUSD was developed. The code calculates sensitivity coefficients for one and two-dimensional transport problems based on the first order perturbation theory. Variance and standard deviation of detector responses or design parameters can be obtained using cross section covariance matrix. The code is able to perform sensitivity-uncertainty analysis for secondary neutron angular distribution(SAD) and secondary neutron energy distribution(SED).

Covariances of ^{6}Li and ^{7}Li neutron cross sections in JENDL-3PR1 were evaluated including SAD and SED. Covariances of Fe and Be were also evaluated.

The uncertainty of tritium breeding ratio, fast neutron leakage flux and neutron heating was analysed on four types of blanket concepts for a commercial tokamak fusion reactor. The uncertainty of tritium breeding ratio was less than 6 percent. Contribution from SAD/SED uncertainties are significant for some parameters.

Formulas to estimate the errors of numerical solution of the transport equation were derived based on the perturbation theory. This method enables us to deterministically estimate the numerical errors due to iterative solution, spacial discretization and Legendre polynomial expansion of transfer cross-sections. The calculational errors of the tritium breeding ratio and the fast neutron leakage flux of the fusion blankets were analysed.

1. Introduction

The solution of the transport equation has the errors associated with the cross section uncertainty and also with the computational

method. We have developed the method for the cross section sensitivity
and uncertainty analysis of the nuclear performance of fusion reactor
blankets[1-3]. We have also studied the errors of the numerical solution
of the transport equation[4-6].

2. Cross-section sentivity and uncertainty analysis

2.1 Theory

The relative variance of response R such as tritium breeding ratio
can be evaluatated from the following relation.[1,2]

$$RVAR(R) = \sum_{xy} \sum_{gh} P_x^g RCOV\left(\sigma_x^g, \sigma_y^h\right) P_y^h,$$

, where $RCOV(\sigma_x^g, \sigma_y^h)$ is the relative covariance matrix for
the multigroup cross sections of reaction x and y. P is the relative
sensitivity coefficient, and g and h are indexes for energy groups. The
sensitivity coefficient is calculated based on the first-order perturba-
tion theory.

The uncertainty of secondary neutron energy and angular distribu-
tion (SED and SAD) is very important for fusion neutronics problems.
Methods and formats to express SAD/SED uncertainties in nuclear data
files such as ENDF/B have not yet been standardized. The only effort so
far to specify SED uncertainties quantitatively is the work done by
S.A.W. Gerstl[7]. He has introduced a spectral shape uncertainty parameter
which means the relative standard deviation of integrated area of SED
function below or above the median energy of secondary neutrons.

Every SAD/SED uncertainty cannot be expressed exactly with a
spectral shape uncertainty parameter. As an example, Fig.1 shows the
composite SED of ^{6}Li(n,n') reaction to the continum level and ^{6}Li(n,2n)
reaction at an incident neutron energy of 14.2 MeV. The SED function is
underestimated below 2.1 MeV, overestimated between 2.1 and 7.3 MeV, and
underestimated again above 7.3 MeV by the JENDL-3PR1 evaluation. This
uncertainty pattern cannot be expressed with a spectral shape uncer-
tainty parameter.

To overcome this drawback of a spectral shape uncertainty
parameter, the authors have introduced a covariance matrix for integrated
area of SAD and SED. The intervals of integration can be determined for
each reaction type. For example the SED uncertainties shown in Fig.1 are

described in table 1. The relative standard deviations (RSD) in this table have been evaluated by the following formula:

$$RSD_m = \frac{\left| \int_m P_x(E \to E')\,dE' - \int_m P_e(E \to E')\,dE' \right|}{\int_m P_e(E \to E')\,dE'}.$$

where P_x and P_e are measured and evaluated SED function respectively. Fully correlated and fully anticorrelated offdiagonal elements in the correlation matrix of Table 1 are required to maintain a normal SED function.

In the case of SAD, given by Legendre polynomial expansion, a covariance matrix for Legendre coefficients is also used. This new expression of SAD/SED uncertainties is more flexible than the previous method and exact enough for most purposes.

The relative variance of response R, for an incident energy group g, is calculated with the SAD/SED relative covariance matrix $RCOV_g(f_m, f_n)$ by the formula:

$$RVAR_g(R) = \sum_m \sum_n P_{mg} RCOV_g(f_m, f_n) P_{ng},$$

where P is the SAD/SED sensitivity coefficient consistent with the SAD/SED covariance matrix, and f_m is an integrated probability for the m-th integration interval or a Legendre coefficient for the m-th order.

As for correlation between different energy groups, only full-correlation or non-correlation have been assumed in the present study, because there is little knowledge of the energy correlation of SAD/SED uncertainties. SED data in JENDL3-PR1 has been applied to SED covariance matrices. On the other hand, non-correlation has been applied to the covariance matrices of SAD represented by Legendre expansion, because Legendre coefficients determined by fitting experimental data have weak correlations between different energy groups. SAD/SED sensitivity coefficients are also calculated based on the first-order perturbation theory.

2.2 Computational procedures

We have developed the code system, SUSD for the sensitivity and uncertainty analysis including SAD/SED effect.[2] The structure of the code system is shown in Fig.2. The forward and adjoint flux are calculated by ANISN, BISON[8] and DOT3.5. BISON is the one dimensional tranport and bur-

nup calculation code developed by us. GROUPR and ERRORR are the module of NJOY code system. They are used for the geration of group cross sections and group covarriance matrix respectively. PUFF-2 is the module similar to ERRORR. We have newly developed GROUPSR and SEADR for generating SAD partial transfer matrix and multigroup SAD/SED covariance matrices respectively. The code stores the moment matrix and the sensitivity cefficients and the calculation can be restarted using the data.

2.3 Cross-section and covariance data

While only three nuclides, ^{12}C, ^{14}N and ^{16}O, have a covariance file in ENDF/B-IV, cross-section covariance data of several nuclides are contained in the latest version, ENDF/B-V. ENDF/B-V is unavailable in Japan except for some tapes for special purposes. Even if all tapes of ENDF/B-V were available, however, covariance data of some important nuclides for fusion reactors, such as ^7Li or ^9Be, are for limited distribution.

The authors have evaluated covariance data for ^6Li, ^7Li, ^9Be and Fe based on the evaluation for JENDL-3PR1. Details of the covariance evaluation for ^6Li and ^7Li are described in ref.[3]. The evaluation for ^9Be and Fe has been based primarily on the comparison of evaluated and experimental data. This method is simpler than for lithium isotopes, but is expected to give conservative results because strong correlations between different neutron energies have been assumed in the evaluation. Covariance data of SAD and SED for lithium isotopes have been evaluated by comparing the evaluated curves with measured SAD or SED data.

Table 2 shows the reference of cross-sections and covariance data used for the present study.

2.4 Errors of nuclear performance of commercial tokamak
     fusion reactor blankets

The analysis has been carried out on four types of blanket concepts for a commercial tokamak reactor with a plasma major radius of 7 m. The one-dimensional cylindrical models used are shown in Fig.3. The models, except for the $Li_2O/Be/H_2O$ concept, have been based on the Blanket Comparison and Selection Study by Argonne National Laboratory. Short descriptions of these models follow.

Li/Li blanket

Liquid lithium is used as both a tritium breeding material and coolant. The blanket comprises a 1 cm thick first wall, a tritium breeding zone, and a reflector which is followed by a shield 30 cm thick. The thickness of the tritium breeding zone and the reflector are 40 cm and 20 cm inboard, and 60 cm and 30 cm outboard.

Li/Li + He blanket

The inboard blanket of the Li/Li blanket is replaced with a non-breeding blanket cooled with helium. This concept has been proposed to avoid serious MHD problems expected in maintaining lithium flow through the inboard blanket. Another merit of this concept is the high thermal efficiency which may be attained by producing superheated steam using high temperature helium from the inboard blanket.

Li_2O/H_2O blanket

In this blanket, lithium oxide cooled with water is used as tritium breeding material. A double-wall coolant tube is adopted in order to reduce tritium leakage into the water. The blanket comprises a 1.2 cm thick first wall, a tritium breeding zone, and a plenum or a hot-shield, followed by a shield 30cm thick. The thickness of the tritium breeding zone is 28.8 cm inboard, 50.8 cm outboard.

$Li_2O/Be/H_2O$ blanket

A neutron multiplier of beryllium is installed instead of the second tritium breeding bank of the Li_2O/H_2O blanket. The 0.9 cm thick tritium breeding bank is left between the first wall and the neutron multiplier to capture neutrons backscattered from the beryllium layer.

The atomic components of materials used are listed in Table 3. A ferritic steel, HT-9, is used as structural material for all of the blanket models.

The design parameters investigated in the analysis include the tritium breeding ratio, the neutron heating and the fast neutron leakage flux from the inboard shield. The details of the results described in reference[1].

Relative standard deviations in the total tritium breeding ratio (TBR) are shown in Table 4. If the cross-section data of different

nuclides are uncorrelated, collective RSD are equal to the square root of accumulated square of RSD for each nuclide, which is listed as total in the table. If they are fully correlated, on the other hand, collective RSD is simple sum of RSD for each nuclide, which is listed as sum. The real values of collective RSD will exist between these two limits, total and sum.

As can be seen in the table, collective RSD of the TBR is 2-4%. In the $Li_2O/Be/H_2O$ blanket, beryllium contributes most to RSD, but in the other blankets iron has the largest contribution to RSD. Lithium-7 also has a large contribution, especially in the blankets with liquid lithium.

Table 5 shows the reaction types which have a large contribution to TBR uncertainties. Neutron multiplying reactions, such as $^7Li(n,n'_c)T$, $Fe(n,2n)$ or $^9Be(n,2n)$, and their competitive threshold reactions, such as $Fe(n,He)$ or inelastic scattering of iron, have a large impact on the TBR. Threshold reactions of iron, as well as lithium, seem to be important for an accurate TBR assessment. The direct effect of $^7Li(n,n'He)T$ reaction is also significant, especially for the blankets with liquid lithium breeder. In Table 6, RSD, due to uncertainties in excitation functions, are compared with those for SAD/SED. As for some reactions of ^7Li, more contribution comes from SAD/SED uncertainties than from excitation function uncertainties. It is essential to include the SAD/SED uncertainties for the analysis of fusion reactor blankets.

3. The errors of transport calculation by the deterministic
    method

The numerical solution of the transport equation has the errors associated with the computational method. As for deterministic methods to solve the transport equation, the primary sources of such errors include

(1) incomplete convergence of iterative solution,

(2) discretization of space variables

(3) Legendre polynomial expansion of the transfer cross
    sections

(4) discretization of angular variables

(5) multigroup approximation.

Emprical estimation of the errors is very cost and time consuming, where calculation is repeated varying the order of approximations and the

results are compared with each other. We have developed the method for estimating the errors[4]. It is based on the perturbation theory and is applied to the first three sources of the errors.

We have estimated the errors of the discrete ordinates transport calculation such as ANISN for fusion neutronics problems. The details of the study are described in the reference 4 and 5. The blanket models are the same as those for the cross section sensitivity uncertainty analysis. The errors of the tritium breeding ratio and the fast neutron leakage flux from the inboard shield have been analysed.

The results are listed in Table 7. The errors associated with iteration, round-off, spacial discretization and P_L expansion of the transfer cross sections has been calculated using the perturbation theory. The convergence criterion was 10^{-3}(point) and 5×10^{-3}(volume). The mesh spacing was 1 cm and the diamond difference scheme was used. The order of P_L expansion was P_3. Those errors are generally small. The errors of tritium breeding ratio associated with the P_L expansion of the scattering cross sections is found to be less than 1 %. Direct representation of the angular dependence or the use of the DDX is not necessary for the estimation of the tritium breeding ratio. The errors associated with the cross section uncertainty is the largest as for the tritium breeding ratio.

The errors attributed to the multigroup approximation has been estimated by comparing the calculations by BISON and MCNP. BISON is one-dimensional transport and burnup calculation code developed by us. The transport calculation scheme is the same as that of ANISN. Three types of multigroup cross sections for BISON have been generated from ENDF/B-4 using NJOY code system. They are the infinite dilution 42 group cross sections of the GICX-40 structure, 171 group cross sections of VITAMIN-C structure and the 42 group cross sections with space dependent self-shielding factors. They are denoted 42 group, 171 group and S42 group in the next figure. For MCNP, the continuous energy, point-wise cross sections have been used.

The ratio of the total neutron fluxes of the multigroup BISON calculation to the point-wise calculation by MCNP, G/P is shown in Fig 4. In the blankets the multigroup calculation agrees well with the point calculation. However, the flux is underestimated by the multigroup calculation in the reflectors and in the shields, where iron is the most abundant component. Neutrons are slowed down by water in the plenum and

removed from the resonance region of iron, so that comparatively a good agreement is obtained in the outboard shield of the Li_2O/H_2O blanket. The fast neutron leakage flux from the inboard shield has also been greatly underestimated by the multigroup calculation as shown in Table 7. The energy group structure and the self-shielding factors take a very important role for the accuracy of multigroup calculation.

4. Summary

1. We have developed SUSD code system for the cross section sensitivity uncertainty analysis including SAD/SED effect.
2. We have evaluated covariance data for ^6Li, ^7Li, ^9Be and Fe based on the evaluation for JENDL-3PR1. SAD/SED uncertainty is evaluated for ^6Li and ^7Li.
3. The error of the tritium breeding ratio associated with cross section uncertainty is about 6 percent for the commercial tokamk fusion reactor blankets. SAD/SED uncertainty has the same order of contribution to the error as that of the excitation function. Types of the reactions contributing the error have also been clarified.
4. We have derived the formulas based on the perturbation theory to estimate the errors due to iterative solution, spacial discreti- zation and Legendre polynomial expansion of the transfer cross sec- tions. The errors of the tritium breeding ratio using the P_L expan- sion method is less than 1 % for the commercial tokamak fusion reac- tor blankets.
5. The leakage flux through the fusion reactor reflector and shield are largely underestimated by the multigroup calculations using the 42 group GICX-40 type infinite dilution cross sections. The energy group structure and the self-shielding factor take a very important role for the accuracy of the multigroup calculation.

References

1. FURUTA.K. et al., Nucl.Eng.Design/Fusion 3 287 (1986).
2. FURUTA.K. et al., UTNL-R-0185 (1986).
3. FURUTA.K. et al., UTNL-R-0167 (1984).
4. FURUTA.K. et al., " Development of Method for Estimating

Errors in Numerical Solution of Transport Equation Based on Perturbation Theory " J.Nucl.Sci.Technol. to be published.

5. FURUTA.K. et al., " Accuracy of Multigroup Transport Calculationin D-T Fusion Neutronics " J.Nucl.Sci.Technol. to be published.

6. OKA.Y.et al., " Experiment on Neutron Transmission through Depleted Uranium Layers and Analysis with DOT 3.5 and MCNP " Proc. Top. Conf. on Theory and Practices in Radiation Protection and Shielding, April 22-24, 1987, Knoxville, to be published.

7. GERSTL.S.A.W. et al. " LA-8333-MS (1980).

8. FURUTA.K. et al. " UTNL-R-0141 (1982).

9. SMITH.D.L. et al., ANL/FPP-84-1 (1984).

Table 1
SED uncertainties for ^{6}Li(n, n$'_c$) and ^{6}Li(n, 2n) reactions at 14.2 MeV incident neutron energy

Interval (MeV)	SED[a]	RSD(%)[b]	Correlation Matrix (X100)		
0.0 − 2.1	0.197	13.3	100	−100	100
2.1 − 7.3	0.667	18.7	−100	100	−100
7.3 − 14.2	0.136	5.4	100	−100	100

a) Integrated SED probability for the interval.
b) Relative standard deviation of the integrated SED.

Table 2
Nuclear data file used

Nuclide	File	Covariance
^{1}H	ENDF/B-V	ENDF/B-V
^{6}Li	JENDL-3PR1	Evaluated
^{7}Li	JENDL-3PR1	Evaluated
^{9}Be	JENDL-3PR1	Evaluated
^{12}C	ENDF/B-V	ENDF/B-V
^{16}O	ENDF/B-IV	ENDF/B-IV
Fe	JENDL-3PR1	Evaluated
Ni	ENDF/B-IV	None
Cr	ENDF/B-IV	None
Mo	ENDF/B-IV	None
^{55}Mn	ENDF/B-IV	None

Table 3
Material composition

Material	Nuclide	Density (1/b cm)
Li	^{6}Li	3.430-3[a]
	^{7}Li	4.286-2
Li_2O[b]	^{6}Li	4.816-3
	^{7}Li	6.010-2
	O	3.246-2
H_2O	H	6.686-2
	O	3.343-2
Beryllium	Be	1.236-1
HT-9	Fe	7.058-2
	Ni	3.950-4
	Cr	1.070-2
	Mo	4.833-4
	Mn	4.643-4
	C	7.722-4
Fe1422	Fe	6.953-2
	Ni	1.580-3
	Cr	1.848-3
	Mn	1.219-2

a) Read as 3.430×10^{-3}.
b) 80 % of T.D.

Table 4
Relative standard deviation (%) in the tritium breeding ratio due to uncertainties in cross-section data

Nuclide	Li/Li	Li/Li+He	Li_2O/H_2O	$Li_2O/Be/H_2O$
^{6}Li[a]	0.435	0.372	0.156	0.109
^{7}Li[a]	1.15	1.01	0.795	0.426
^{1}H	neg.[b]	neg.	0.012	0.017
^{16}O	neg.	neg.	0.646	0.405
Fe	1.15	1.47	1.27	0.942
^{9}Be	-	-	-	1.73
Total	1.7	1.8	1.6	2.1
Sum	2.7	2.9	2.9	3.6

a) SAD/SED contribution is included.
b) Less than 0.001 %

Table 5.
Reactions which have a large contribution to uncertainties in the tritium breeding ratio

	Li/Li			Li/Li+He	
Reaction	RSD (%)	Sensitivity	Reaction	RSD (%)	Sensitivity
^{7}Li(n,n'He)T$^{a)}$	1.3	3.225-1$^{b)}$	^{7}Li(n,n'He)T$^{a)}$	1.2	2.903-1
Fe inelastic	0.75	-5.795-2	Fe(n,He)	0.83	-3.151-2
^{7}Li(n,n'$_c$) SED	0.66	1.758-1$^{c)}$	Fe(n,2n)	0.75	7.529-2
Fe(n,He)	0.63	-2.463-2	Fe inelastic	0.70	-5.423-2
^{7}Li(n,n'$_c$)	0.60	-6.807-2	^{7}Li(n,n'$_o$)	0.56	-6.446-2
Fe(n,2n)	0.44	4.395-2	^{7}Li(n,n'$_c$) SED	0.51	1.427-1$^{c)}$
^{6}Li(n,n$_c$)	0.40	-1.132-2	^{6}Li(n,n'$_c$)	0.38	-1.066-2

	Li$_2$O/H$_2$O			Li$_2$O/Be/H$_2$O	
Reaction	RSD (%)	Sensitivity	Reaction	RSD (%)	Sensitivity
Fe(n,2n)	0.88	8.846-2	^{9}Be(n,2n)	1.8	2.142-1
Fe(n,He)	0.77	-2.856-2	Fe(n,He)	0.60	-2.231-2
^{7}Li(n,n'He)T$^{a)}$	0.71	1.799-1	Fe inelastic	0.57	-4.751-2
^{16}O(n,He)	0.62	-5.360-2	^{7}Li(n,n'He)T$^{a)}$	0.40	1.004-1
Fe inelastic	0.43	-3.300-2	Fe(n,2n)	0.36	3.651-2
^{7}Li(n,2n)	0.37	1.866-2	^{16}O(n,He)	0.35	-3.231-2

a) Direct effect only.
b) Read as 3.225 X 10^{-1}.
c) Values listed are the total gain terms.

Table 6.
Comparison of RSD (%) in the tritium breeding ratio due to uncertainties in excitation functions and SAD/SED

	Li/Li		Li/Li+He	
Reaction	Exci.Func.	SAD/SED	Exci.Func.	SAD/SED
^{6}Li elastic	3.7-2a)	4.4-3	4.1-2	4.9-3
^{6}Li(n,n'$_c$)	0.40	0.18	0.38	0.14
^{7}Li elastic	0.11	0.14	0.14	0.13
^{7}Li(n,n'$_2$)	0.31	0.17	0.28	0.18
^{7}Li(n,n'$_c$)	0.60	0.66	0.56	0.51

	Li$_2$O/H$_2$O		Li$_2$O/Be/H$_2$O	
Reaction	Exci.Func.	SAD/SED	Exci.Func.	SAD/SED
^{6}Li elastic	5.3-3	9.4-4	3.1-3	4.9-4
^{6}Li(n,n'$_c$)	8.9-2	0.10	7.3-2	6.2-2
^{7}Li elastic	1.7-2	3.7-2	1.3-2	2.5-2
^{7}Li(n,n'$_2$)	7.8-2	4.5-2	7.6-2	2.6-2
^{7}Li(n,n'$_c$)	0.14	0.36	1.2-2	0.26

a) Read as 3.7 X 10^{-2}.

Table 7. Comparison of errors and uncertainties (in %) of
          two design parameters estimated for fusion reactor blankets

| Design parameter | TBR | | Leakage flux | | Order of |
Blanket type	Li/Li	Li$_2$O/H$_2$O	Li/Li	Li$_2$O/H$_2$O	approximation
Cross-section uncertainty[a]	±5.4	±5.8	±26	±34	
Iteration and round-off	0.003	0.02	0.04	0.02	Point convergence < 10^{-3}
Spacial discretization	−0.19	−0.14	3.5	3.2	Mesh spacings ≤ 1 cm
Angular discretization	<0.1	<0.03	<0.5	<0.3	S6
Pℓ expansion	0.67	0.31	6.1	9.1	P3
Multi-group approximation	1.6	−0.8	factor 3 ~ 4	factor 2 ~ 3	42-group

a) Twice of the standard deviations
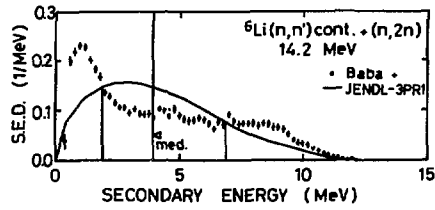
Fig. 1. Secondary energy distribution of ^{6}Li(n, n$'_c$) and ^{6}Li(n, 2n) reactions at 14.2 MeV incident neutron energy.
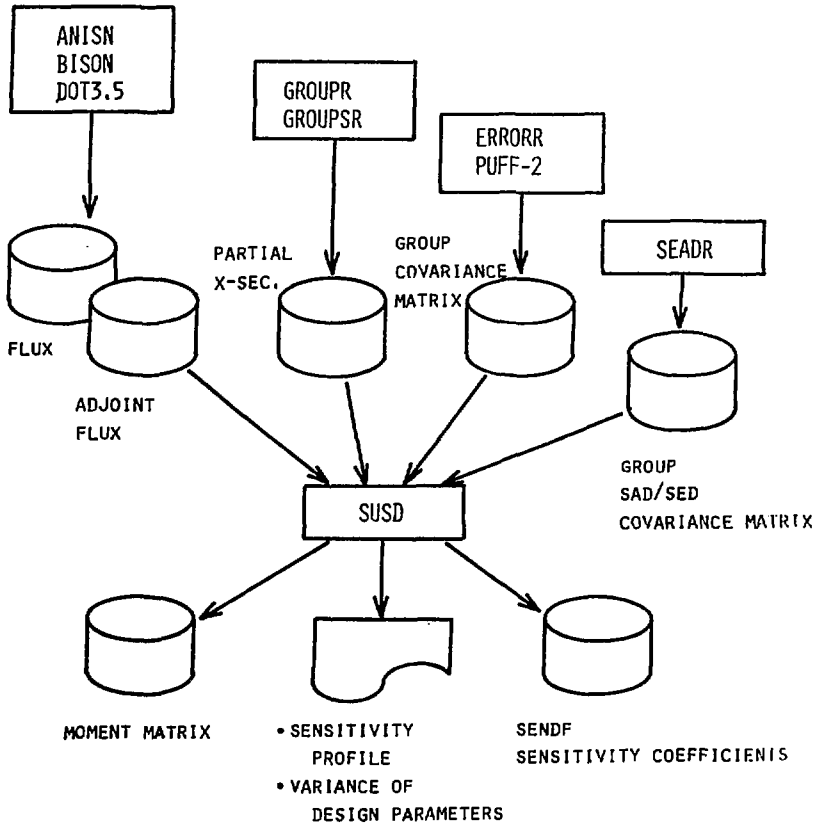
Fig.2. SUSD code system

Li/Li blanket

Distance from toroidal axis (cm)

Li/Li+He blanket

Distance from toroidal axis (cm)
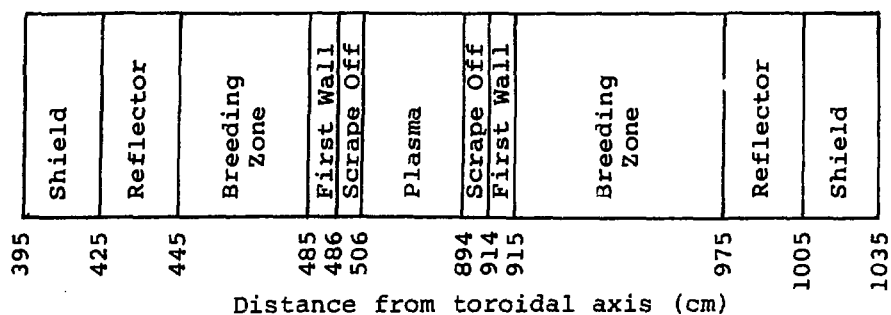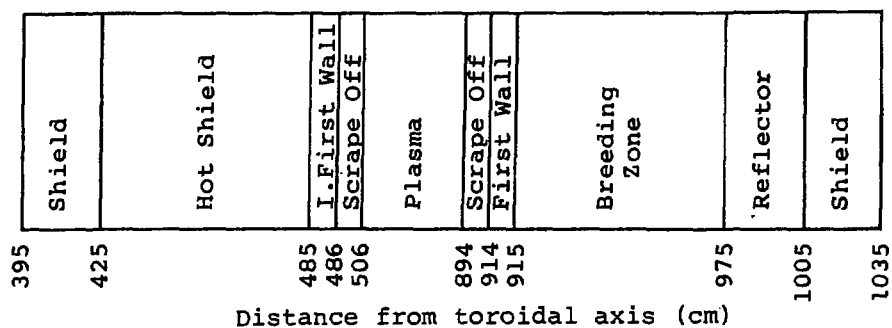
Volume Fraction (%) of Materials

	Li	HT-9	H_2O	Fe1422
First Wall	50.0	50.0	-	-
Breeding Zone	92.5	7.5	-	-
Reflector	10.0	90.0	-	-
Shield	-	-	10.0	90.0
I. First Wall	-	50.0	-	-
Hot Shield	-	90.0	-	-

Fig.3. Blanket models used in the analysis

Li$_2$O/H$_2$O blanket

| Shield | Hot Shield | B.Bank-4 | B.Bank-3 | B.Bank-2 | B.Bank-1 | First Wall | Scrape Off | Plasma | Scrape Off | First Wall | B.Bank-1 | B.Bank-2 | B.Bank-3 | B.Bank-5 | Plenum | Shield |

401 431 456 466 478.5 483.9 484.8 486 506 894 914 915.2 916.1 921.5 934 966 984 1014

Distance from toroidal axis (cm)

Li$_2$O/Be/H$_2$O blanket

| Shield | Hot Shield | B.Bank-4 | B.Bank-3 | Multiplier | B.Bank-1 | First Wall | Scrape Off | Plasma | Scrape Off | First Wall | B.Bank-1 | Multiplier | B.Bank-3 | B.Bank-5 | Plenum | Shield |

401 431 456 466 478.5 483.9 484.8 486 506 894 914 915.2 916.1 921.5 934 966 984 1014

Distance from toroidal axis (cm)

Volume Fraction (%) of Materials

	Li$_2$O	HT-9	H$_2$O	Fe1422	Be
First Wall	–	80.6	19.4	–	–
Breeding Bank-1	97.5	1.6	0.9	–	–
Breeding Bank-2	54.1	19.0	18.1	–	–
Breeding Bank-3	69.1	13.1	12.1	–	–
Breeding Bank-4	79.8	8.8	7.8	–	–
Breeding Bank-5	85.8	6.4	5.5	–	–
Hot Shield	–	90.0	10.0	–	–
Plenum	–	25.0	75.0	–	–
Shield	–	–	10.0	90.0	–
Multiplier	–	4.2	3.4	–	91.0

Fig. 3. Continued.
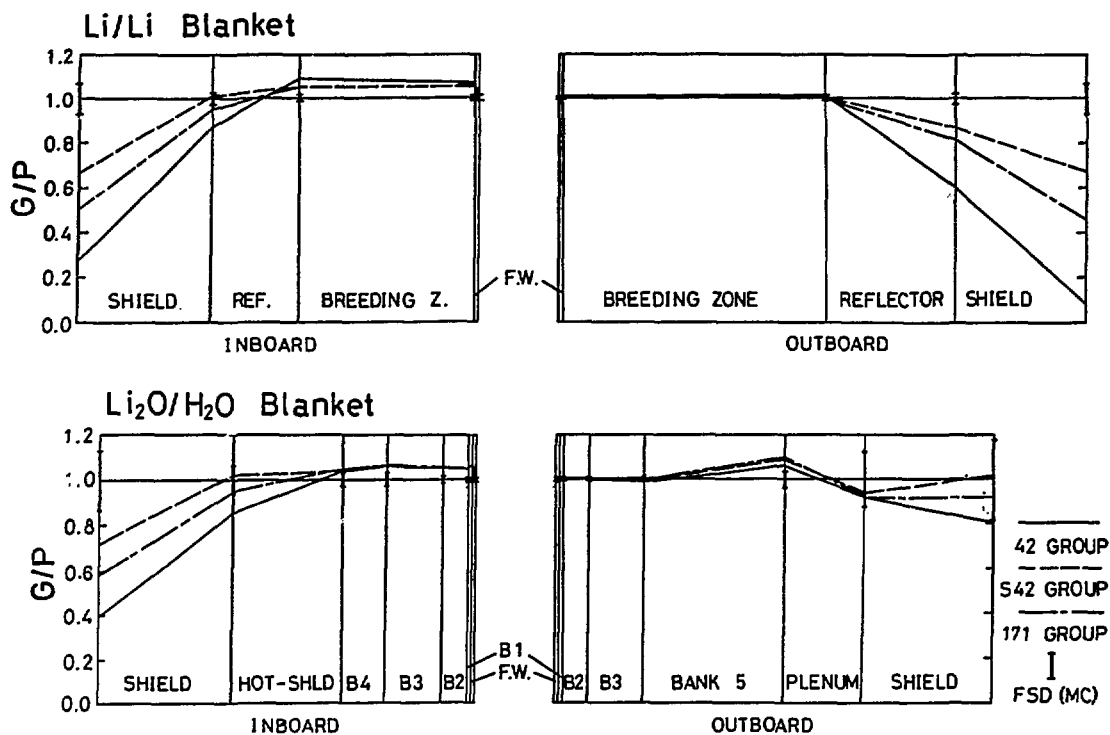
Fig.4. Comparison of total flux in fusion reactor blankets
between multi-group and point-wise calculation

4.2 Comparison of Multigroup and Pointwise Cross Sections Used in Transport Calculations

Hiroyuki HASHIKURA and Shunsuke KONDO

Nuclear Engineering Research Laboratory
Faculty of Engineering, University of Tokyo
Tokai-mura, Naka-gun, Ibaraki

Neutron transport calculations have been made using the computer codes of discrete ordinate methods. The evaluated nuclear data are necessary to be processed into the multigroup data for these calculations and the energy boundaries are determined in order to reproduce well the original nuclear data. A number of multigroup data libraries such as GICX40, JSD-100 and VITAMIN-C have been made for the neutron transport calculations. There are some uncertainties in the results of the neutron transport calculations. The uncertainties mainly come from (1) error of nuclear data, (2) error of multigroup cross section and (3) numerical error. The results that are calculated by the point Monte Carlo code, MCNP, using pointwise and multigroup cross sections are compared. The discrepancy depends on the use of pointwise or multigroup cross sections. Because the code utilizes pointwise and multigroup data of the reaction cross sections with the same angular and energy distributions of the secondary neutrons. The energy boundaries used for multigroup cross sections are 42, 100 and 171 groups which correspond to those of GICX40, JSD-100 and VITAMIN-C data libraries, respectively.

1. Introduction

Discrete ordinate transport codes are widely used for the nuclear calculations of fast reactor shielding and fusion reactor designs[1-2]. They adopt the multigroup cross sections that are generated by the nuclear data processing codes such as SUPERTOG and NJOY[3-4]. The multigroup data are compiled for data libraries such as GICX40, JSD100 and VITAMIN-C that are 42, 100 and 171 energy group structures, respectively[5-7]. There are sometimes large uncertainties in the results of transport calculations. They come from 1) the error of nuclear data, 2) the numerical error and 3) the error of the multigroup cross sections. Since the uncertainties caused by the errors of nuclear data and numerical methods have been already reported in this meeting[8], the uncertainty of the calculated results caused by the error of the multigroup cross sections are discussed. For

the purpose of this study, it is necessary to remove the
uncertainty caused by the errors of the nuclear data and
numerical methods from the calculated results. So we have not
carried out the analysis of the experiments and the comparison of
the calculated results by different transport codes but numerical
experiments using the Monte Carlo code, MCNP[9]. The advantage of
MCNP is to utilized the pointwise nuclear data and the multigroup
cross section data with the same angular and energy distributions
of the secondary neutrons. The calculated result by pointwise
data is compared with that by the multigroup data. The dicrepancy
between two results depends on the use of pointwise or multigroup
data.

2. Data and calculational geometry

Iron nuclear data of ENDF/B-IV are processed by NJOY code
system[10]. The flow of generating cross sections for MCNP is
shown in Fig.1. The iron nuclear data are converted to the
pointwise data. The pointwise date are directly processed into
data format for MCNP. The multigroup data are generated from the
pointwise data by GROUPR module of NJOY code system and processed
into data format for MCNP. Infinitely dilute and Bondarenko self-
shielded sets of 42, 100 and 171 group cross sections are
generated using the $1/E$ and $1/\sigma_t \cdot E$ weighting functions,
respectively[11]. The nuclear data of iron are processed into one
pointwise and six multigroup data sets for MCNP.

The pointwise data and infinitely dilute 171 group cross
sections are shown in Fig.2 and Fig.3, respectively. 171 group
cross sections reproduce the peak and valley structures of the
pointwise data.

The calculational geometry is shown in Fig.4. 14.1 MeV mono-
energy neutrons are emitted isotropically in the sphere center.
The thickness of the iron is 40cm. The neutron fluxes are counted
at the inner surfaces (No.1-No.5 as shown in Fig.4) using surface
crossing estimator in the energy range from 14.1 MeV to 10 keV.

3. Calculational results and discussions

The ratios (G/P values) of the calculated integral fluxes (E>10keV) using pointwise and multigroup cross sections are shown in Fig.5. The solid and dashed lines are obtained by the calculated results using infinitely dilute and Bondarenko self-shielded sets, respectively. G/P values increase within the iron sphere and decrease around 1.0 at the iron surface. G/P values become close to 1.0 when the group numbers increase. But the sensitivety of the weighting function to the G/P values is larger than that of the group numbers. The comparisons of the calculated energy spectra using pointwise with these using infinitely dilute and Bondarenko self-shielded 171 group structures are shown in Fig.6 and Fig.7, respectively. In Fig. 6, the discrepancy becomes large at the peak that corresponds to the valley of the nuclear data. Bondarenko self-shielded factors are shown in Fig.8. The self-shielding effects of 171 energy group structures are large in the energy range between 0.1 and 1.0 MeV. The better improvement is found in the energy range between 0.1 and 1 MeV when the spectra are calculated by Bondarenko self-shielded cross sections.

Neutron transmission in the resonance region has been already discussed by Kawai[12]. Fig.10 shows the angular flux in the vicinity of 24 keV resonance valley. At 27 keV resonance peak, the flux is almost isotropic but in the valley at 24 keV strong anisotropy is found. The anisotropy of the neutron flux varies in the energy region and is very large at the valley. This indicates that fine energy structures should be incorporated in the valley of the resonance region when the multigroup cross sections are generated.

4. Summary

The results of this study are summarized as follows:
1) The choice of the weighting function is more important than that of group numbers.
2) The valley structures of nuclear data should be incorporated well in the multigroup structures.
3) G/P value is 1.14 at maximun in the iron sphere when

the Bondarenko self-shielded 171 group cross sections
are used.

Reference

1) W.W.Engel,Jr.,:A user's manual for ANISN, A One
   Dimensional Discrete Ordinate Transport Code with
   Anisotropic Scattering, K-1693, Oak Ridge Gaseous
   Diffusion Plant (1967).
2) Rhodes W.A., et al.: the DOT-III Two-Dimensional
   Transport Code, ORNL-TM-4280, Oak Ridge National
   Laboratory (1983).
3) Wright,R.Q., et al.,:SUPERTOG A program to Generate Fine
   Group Constant and Pn Scattering matrix from ENDF/B-IV,
   ORNL-TM-2679 (1969).
4) MacFarlane,R.E., et al.,: The NJOY nuclear data
   processing system; User's manual,LA-9303-M, (1982).
5) Y. Seki et al.,:Coupled 42 group Neutron and 21 Group
   Gamma-Ray Cross Section Sets for Fusion Reactor
   Calculations, JAERI-M-8818 (1980).
6) Koyama,K., et al.,: Multigroup cross section sets for
   shield materials-100 neutron groups and 20 gamma-ray
   groups in P5 approximation, (in Japanese), JAERI-M-
   6928,(1977).
7) Roussin R.W. et al.,: The CTR Processed Multigroup
   Cross Section Library for Neutronics studies, ORNL/RSIC-
   37, Oak Ridge National Laboratory (1977).
8) Oka, Y. et al.,: Uncertainty analysis of Neutron
   transport Calculation, This meeting (1986).1
9) Los Alamos Radiation Transport Group (x-6): MCNP-A
   general Monte Carlo code for neutron and photon
   transport, LA-7396-M, Rev. (1981).
10)Drake,M.K.(ed.),: Data formats and procedures for the
   ENDF neutron cross section library, BNL-50274 (T-
   601,TID-4500),ENDF 102, Vol. 1,(1970), Revised 1974.
11) Bondarenko, I.I. et al.,: Group Constants For Nuclear
   Reactor Calculations, Consultants Bureau, New York,
   (1964).
12) Kawai M, UTNL-R-0098 (in Japanese).

ENDF/B-IV

IRON

Point-wise data

Pointwse data
for MCNP

Multigroup data
(42,1ØØ,171 group)

Group data
for MCNP
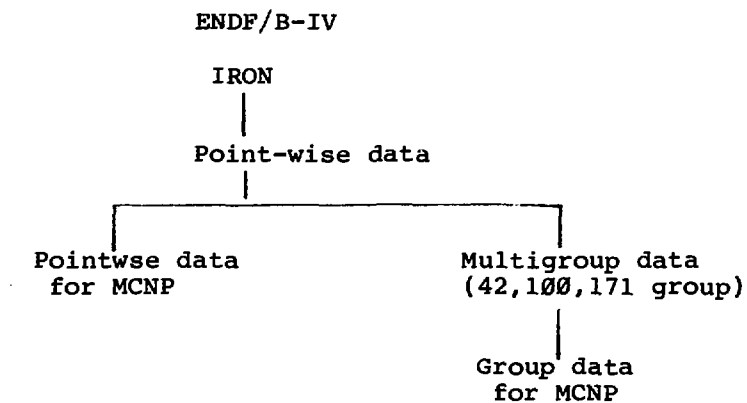
Fig.1   Flow of the generation of cross sections
        For MCNP.
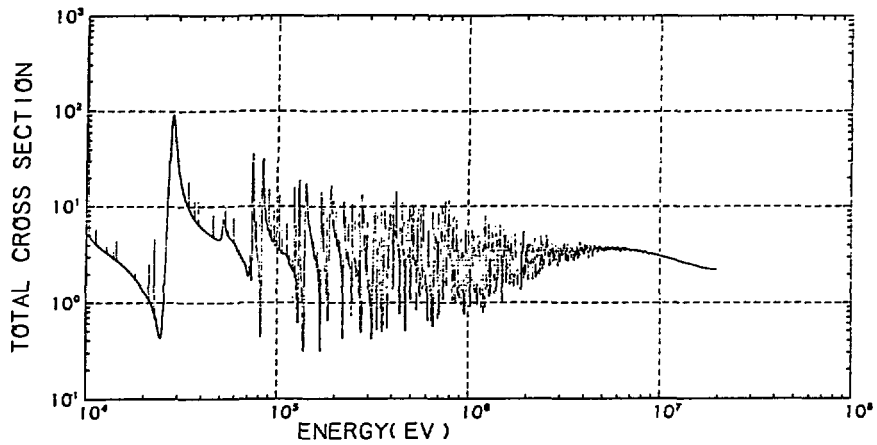
Fig.2   Pointwise cross section data used in MCNP.
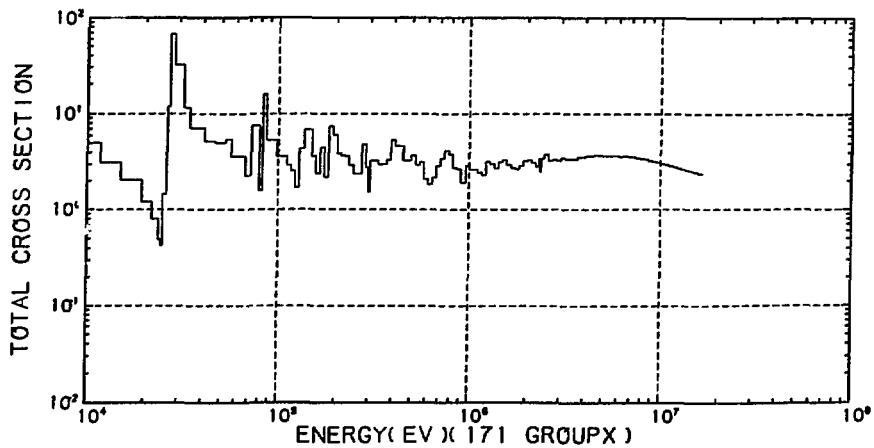
Fig.3   171 Group cross section data used in MCNP.
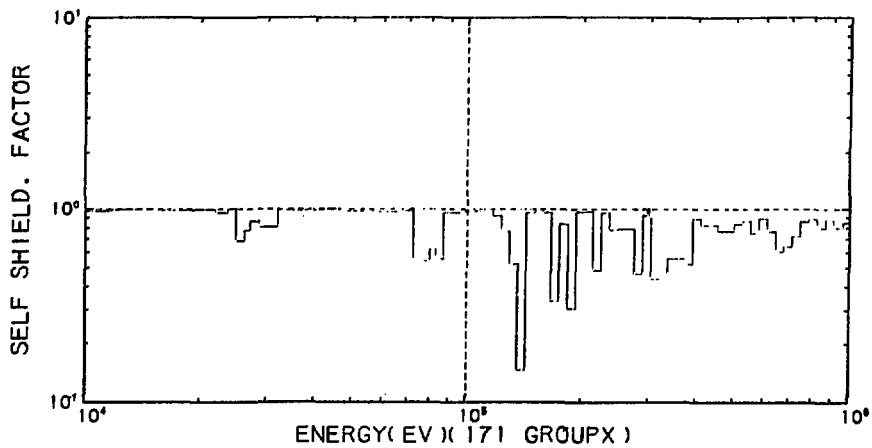
Fig.4   Shelf-shielding factor.
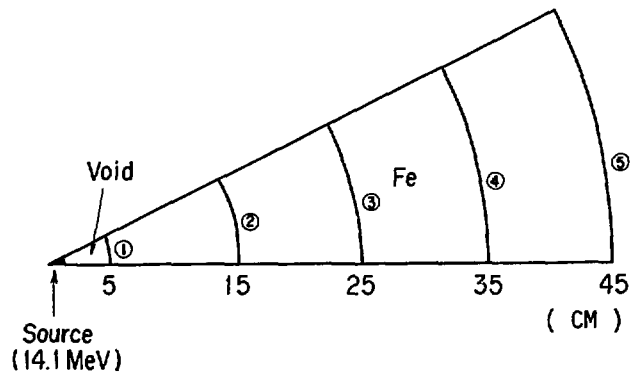
Fig.5 Calculatinal geometry.
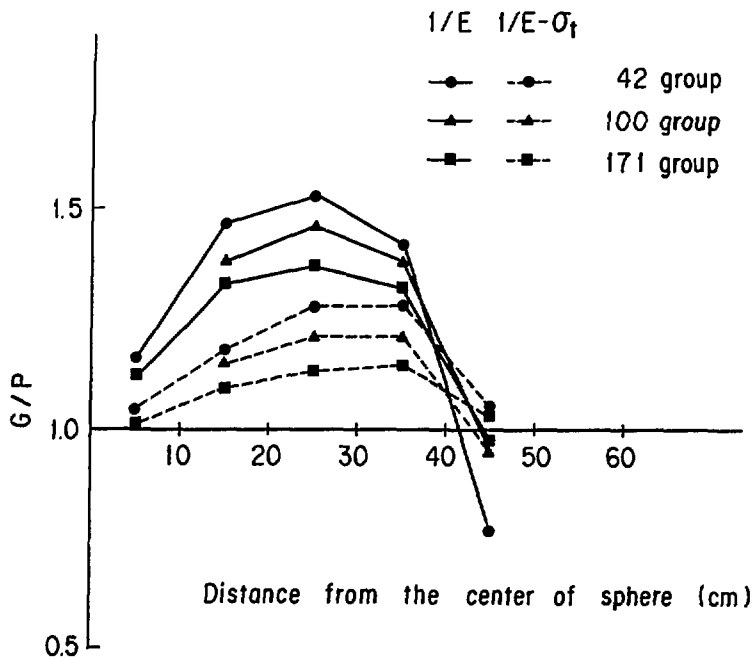
Fig.6 G/P values in the iron sphere.
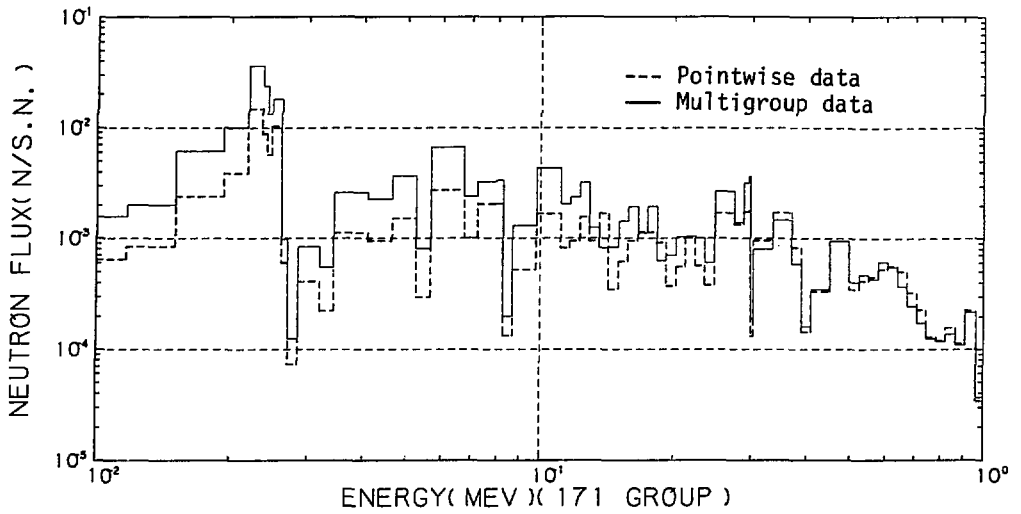
Fig.7 Comparison between the calculated results using pointwise
and infinitely dilution cross sections.
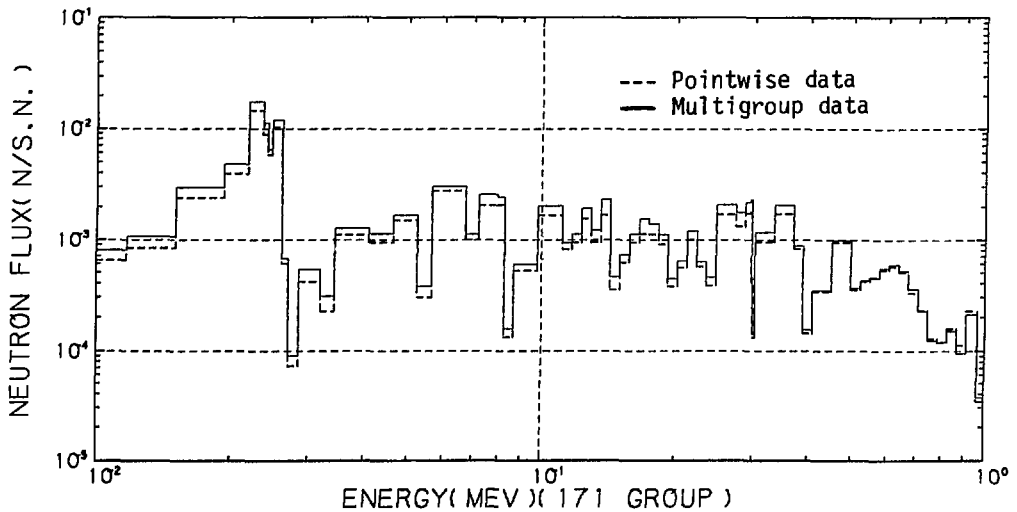
Fig.8 Comparison between the calculated results using pointwise
and Bondarenko self-shielded cross sections.
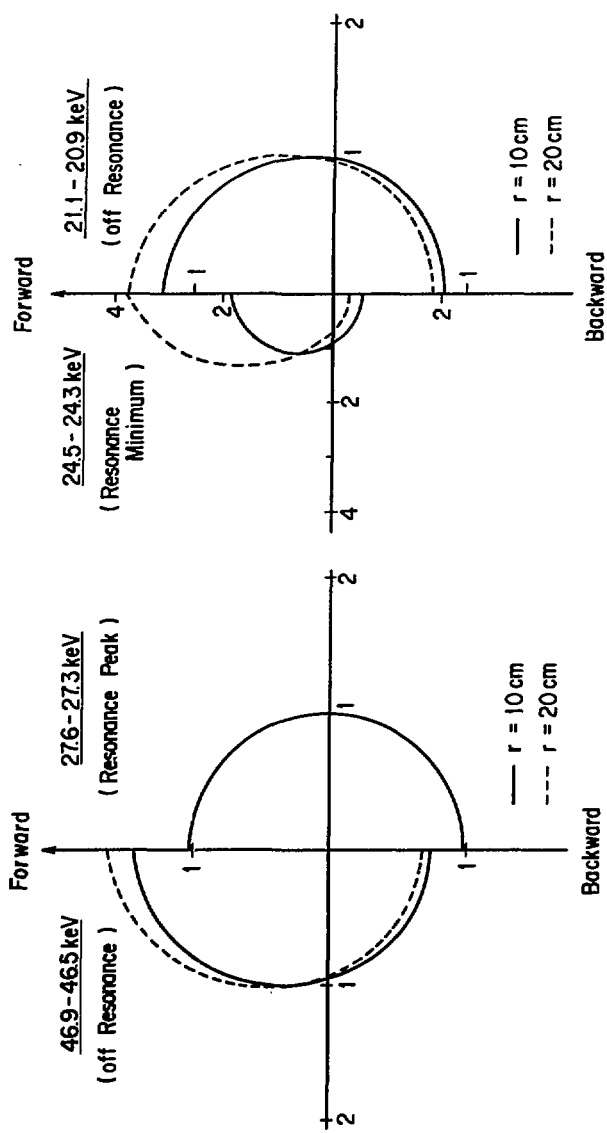
Fig. 9 Angular distribution of neutron flux in iron sphere.12)

4.3 Group Cross Sections of Fission Products and Minor Actinides

Hideki Takano, Hithoshi Ihara and Hiroshi Akie

Japan Atomic Energy Research Institute
Tokai-mura, Naka-gun, Ibaraki-ken

Group cross section library for fission products and minor actinides has been generated with the TIMS-PGG processing code on the basis of the evaluated nuclear data file JENDL-2.

For fast reactor calculations, the lumped group cross sections of fission products for mother nuclides U-235, U-238, Pu-239 and Pu-241 were generated by taking into account burnup dependence and fission gas release. This group constant library is called JFS-3-J2/FP2.

For thermal reactor calculations, the fission product chain model in which the 65 nuclides are explicitly treated have been studied and the pseudo group cross sections with the 107 energy group structure were generated. The group constant library generated is called SRACLIB-JENDL2.

Resonance self-shielding effect of fission products on burnup reactivity loss has been investigated by using the SRACLIB-JENDL2 library in high conversion light water reactors.

The effect of nuclear data uncertainties of fission products and minor actinides on the burnup reactivity change has been examined by comparing the results obtained with four evaluated nuclear data files; JENDL-2, JEF-1, ENDF/B-IV and -V. The effect of the minor actinides such as Am and Cm on burnup reactivity loss has been also examined by performing the burnup calculation for the HCLWR lattice.

1. Introduction

Recently, to improve effective utilization of uranium source, much efforts are made to raise burnup and conversion ratio in advanced light water reactors, tight lattice light water reactors and fast breeder reactors. Fission product and actinide nuclides have an important role in predicting burnup characteristics in design study of these power reactors. The prediction accuracy primarily depends on the quality of nuclear data for these nuclides, the calculational methods of group

cross sections and burnup chain models.

Burnup calculations of fast reactors are conventionally performed by using group cross sections lumped for all fission product nuclides for each mother nuclides.[1] The lumped cross sections were generated without considering capture reaction when build up of fission product nuclides are calculated by solving decay chains.[2-3] It is assumed that the burnup dependence of the lumped cross sections is negligibly small.[2-3] In this report, the lumped cross sections are generated on the basis of the FP data of JENDL-2 which have been evaluated by the FP Working Group of Japanese Nuclear Data Committee, and the burnup dependence of the lumped cross sections is examined by considering capture chains in burnup calculation.

In burnup calculations of thermal reactors are normally used the FP chain models in which several FP nuclides are explicitly treated and one pseudo FP nuclide is generated.[4] In high conversion light water reactors(HCLWR), reactivity change with burnup is very flat as compared to that for conventional LWRs. The reactivity loss is caused predominantly by fission product absorptions, being about sixty percent of the total loss, with the relatively low consumption of fissile materials being of minor importance. Discrepancies between nuclear data of fission product nuclides are more remarkable than those for fuel materials. Large discrepancies are observed for the primary data, such as the cross sections at 2200 m/s and resonance integrals for many fission product nuclides obtained from large evaluated nuclear data libraries, JENDL-2, RCN-3, ENDF/B-V and JEF-1. In the present report, the effects of the nuclear data uncertainty for the fission products on burnup reactivity change are examined by performing cell burnup calculations for an undermoderated hexagonal fuel pin lattice.

The fission product absorptions are calculated conventionally by using infinitely dilute capture cross sections without taking into account for resonance self-shielding effects, because atomic number densities of fission products accumulated with burnup are much less than those of resonant fuel materials. However, a number of fission product nuclides have very large resonance capture cross sections in the intermediate neutron spectrum region. In the present report, the resonance self-shielding effect on the reactivity change with burnup is studied by calculating the self-shielding factors of Bondarenko scheme [1]

Uncertainties of nuclear data of minor actinides such as Am and Cm

are more larger than those of major actinides such as U-235 and Pu-239 . The minor actinides contribute considerably reactivity loss in the burnup calculations of HCLWRs and FBRs. The effects of the nuclear data uncertainty of these minor actinides on the burnup reactivity loss are studied in this report.

2. Generation of Lumped Group Cross Sections of Fission Products for Fast Reactor Calculations

The JAERI-Fast Group Constant Sets JFS-2 and JFS-3-J2 include the lumped group cross sections [2-3] for fission products based on the JENDL-1. The 100 fission product (FP) nuclides have been evaluated by the FP Working Group of Japanese Nuclear Data Committee and they have been adopted in the JENDL-2 file. To generate the lumped group cross sections based on the JENDL-2 FP data, group cross sections for each FP nuclide were required. They were calculated for the 100 and 55 nuclides of JENDL-2 and ENDF/B-V with the TIMS-PGG [5] codes. These FP nuclides are shown in Tables 1 and 2. The energy structure was the 70-group one used in the JFS-3-J2 set[6] .

Concentrations of the 155 nuclides are obtained by using the DCHAIN code[7] which solves build up and decay chains for the 1170 nuclides. The summation of the fractional concentrations for the 155 nuclides is 99.95 percent to the total concentration at the burnup time of 360 days. The DCHAIN code[7] was modified so as to treat capture chains for the these nuclides with the 70-group capture cross sections. The capture chains are shown in Fig. 1. The calculations were performed on the basis of the following input parameters: the 70-group neutron spectrum obtained for a typical large fast reactor, constant flux of 3.5×10^{15} n/cm^2 /s and burnup time of 30 - 1800 days.

The lumped cross sections for capture, elastic scattering, inelastic scattering, (n,2n) and total reactions were generated corresponding to the fission products due to four mother nuclides of U-235, U-238, Pu-239 and Pu-241. These cross sections were calculated for the burnup time of 30, 60, 180, 360, 540, 720, 1080, 1440 and 1800 days.

The dependence of the lumped cross sections on burnup was examined by calculating one group cross sections collapsed with the 70-group neutron spectrum. The burnup time dependence of the one group cross sections calculated for the four mother nuclides are shown in Fig. 2. The difference between the one group cross sections for the burnup of

400 and 1800 days is about 5 percent.

The burnup time dependence of the one group cross sections calculated by taking account of various chain models are compared in Fig. 3. The model $\sigma_c \varphi = 0$ shows the results calculated without considering capture chains for the FP nuclides. This was the same model as the one used in Refs. (2) and (3). The one group capture cross sections obtained with this model increase with the burnup time. The model (Xe=0) assumes that all the Xe gas are released at each burnup stage. The model (Xe=0, Cs=0.5) assumes that all the Xe and the half of Cs gas are released at each burnup stage. We can observe from this figure that accurate treatment for fission gas release should be considered for burnup calculations.

3. Burnup Characteristics in HCLWRs

3.1 Production of Group Cross Section Library for Thermal Rector Analysis Code SRAC

Infinite dilute cross sections and self-shielding factors for actinides and fission products were calculated with the TIMS-PGG system [5]. The self-shielding factors calculated were tabulated as a function of background cross sections and temperatures. In cell burnup calculations, effective cross sections are calculated by using the self-shielding factors interpolated by background cross sections:

$$\sigma_{0,i} = \frac{1}{N_i} \sum_{i=j} N_j \sigma_{t,j} + \sigma_h$$

where N_i is the atomic number density of fission product nuclides i considered for calculating self-shielding factor, $\sigma_{t,j}$ the total cross section of nuclide j included in fuel region and σ_h the heterogeneity effect obtained by using Dancoff factor and mean chord length. This calculation is called " Table-look-up " method.

The four different libraries have been generated on the basis of the ENDF/B-IV, JENDL-2, ENDF/B-V and JEF-1 files, and these are called SRACLIB-ENDFB4, -JENDL2, -ENDFB5 and -JEF1, respectively.[8]

3.2 Fission Product Chain Model

Several FP chain models have been prepared in the SRAC code. [9] The model proposed by Garrison and Roos [10] is a very simple one which

consists of 3 lumped FP groups (rapidly saturating. slowly saturating and non-saturating) and two explicit nuclides of Xe-135 and Sm-149. This model is available to low burnup calculations. A more accurate model with 45 explicit and one-pseudo nuclides have been proposed by Iijima et al. [4] for BWR burnup calculations and been accepted in the SRAC system. The FP chain scheme of this model is shown in Fig.4. However, the HCLWRs have intermediate neutron spectra and are considerably different from those of current LWRs. Therefore, it is useful to examine that this model is enough applicable to the HCLWRs burnup calculations.

Burnup calculations were performed by using the cell burnup routine in the SRAC system. A following typical tight hexagonal lattice of HCPWRs was selected : the diameter of fuel pin is 1.0 cm, the thickness of cladding with stainless steel 0.04 cm, the volume ratio of the moderator to fuel region 0.74 and the enrichment of Pu-fissile 8.0 percent. The temperatures for the fuel, cladding and moderator are 900, 600 and 600 K, respectively. A linear power rating 160 W/cm was assumed.

Figure 5 shows the orders of importance for the fractional absorption rates calculated for individual FP nuclide using the 45 FP chain model. The order of the pseudo FP shown by PSD is very high and the absorption rate is 0.8 % at the burnup stage of 50 GWD/t. The capture cross sections for three pseudo FP are compared in Fig.6. The pseudo cross section(PSD) used in the SRAC code was generated conveniently so as to conserve the resonance integral of 10.6 barns recommended by Iijima et al. Those for SRACLIB-JENDL2 and -ENDFB5 were produced on the basis of the FP data of JENDL-2 and ENDF/B-V, respectively.

The cell burnup calculations were performed with the 45 FP chains and three different pseudo FP cross sections in Fig. 6. The reactivity changes are compared in Fig.7. The PSD cross section used in SRAC considerably overestimates the reactivity loss by about 1%Δk comparing the result obtained with ENDFB5 at the burnup stage of 50 GWD/t. It should be noticed that the resonance integrals for the ENDFB5 pseudo cross section is 10.7 barns and is almost equal to that of the PSD cross section. It is moreover observed at the burnup 50 GWD/t that there is the difference of 0.5 %Δk between the results calculated with the pseudo cross sections of JENDL2 and ENDFB5. Furthermore, the pseudo cross sections for the 45 FP model contains another problem for resonance self-shielding effect by several FP nuclides such as Zr-93,

Mo-95, In-113 and so on as shown in Fig.9.

Therefore, the 45 FP chain model was improved by considering several reasons described above. The new model explicitly treats 65 FP nuclides and one pseudo nuclide as shown in Fig.8. Figure 9 shows the comparison of the pseudo cross sections calculated for the 45 and 65 FP models. It is observed from this figure that some large resonances for several nuclides are excluded from the pseudo cross sections of the 45 FP model. The pseudo resonance integral for the 65 FP model was 4.1 barns.

Figure 10 shows the comparison of the burnup reactivity loss calcu-lated with the different pseudo cross sections of the 65 FP model. These pseudo cross sections were obtained on the basis of the JENDL-2 and ENDF/B-V data. The effect of the nuclear data uncertainty on the burnup reactivity loss is not observed from this figure.

3.3 Resonance Self-Shielding Effects of Fission Products

In the cell burnup calculations, the effective cross sections for the 65 fission products which are explicitly treated in the burnup chain are calculated at each burnup stage by using the self-shielding factors described in Section 3.1. The dependence of fractional absorp-tion rate for fission products on burnup is studied in this section.

The contribution of individual fission product nuclide to the total reaction absorption rate is shown in Fig.11 at the burnup stage of 50 GWD/t. It is observed from this figure that the self-shielding effects of Xe-131 and Cs-133 are remarkable in comparison with those of the other nuclides.

The dependence of the multiplication factors on burnup is compared in Fig. 12. The reactivity loss by burnup is reduced considerably by taking into account for the self-shielding effects of the fission products. As seen in Fig.13, the effect of the fission products causes the differences·of about 0.6 percent on the effective multiplication factor at the burnup stage of 50 GWD/t. In this figure, another example of the moderator to fuel volume ratio of 1.4 is also shown, where the zircaloy with 0.064 cm thickness is used as the cladding material.

3.4 The Effects of Nuclear Data Uncertainty on Burnup Reactivity Changes

Fission Products

Discrepancy among nuclear data of fission products are more remarkable than those for fuel materials. Table 3 shows the comparison of the primary data, the cross sections at 2200 m/s and resonance integrals for several fission product and minor actinide nuclides obtained from the evaluated nuclear data files, JENDL-1, JENDL-2, ENDF/B-V and JEF-1. Large discrepancies for these primary cross section data are observed from this table. The nuclear data uncertainty of the fission product nuclides is striking especially for resonance cross section data. As typical example, the resonance cross sections for Eu-155 and Ru-103 are compared among the four evaluated files in Figs.14 and 15 . From these figures, it can be observed that the discrepancies among the evaluated capture cross sections for Eu-155 and Ru-103 are incredibly large.

In order to examine the effects of the nuclear data uncertainty for the fission products on burnup reactivity change, the cell burnup calculations were performed with the SRAC code system for a undermoderated hexagonal tight lattice described in Section 3.2.

The contributions of fractional absorption rate of the individual fission product nuclide to the total one were calculated for the three evaluated files, JENDL-2, ENDF/B-V and JEF-1. They are compared with each other in Fig. 16. The differences between the absorption fractions are observed for several nuclides, in particular being remarkable for Tc-99, Pd-108, Cs-135, Ru-103 and Eu-155.

The burnup reactivity changes were calculated using these different evaluated files. The relative values of multiplication factor calculated with the other files to that obtained with JENDL-2 are shown as a function of burnup in Fig. 17. Significant discrepancy between the reactivity changes obtained with JENDL-2 and ENDF/B-V is observed, while the discrepancy between those for JENDL-2 and JEF-1 is very small . This is due to an accidental cancellation as seen from Fig. 16.

Minor Actinides

In the burnup routine of the SRAC code, minor actinides such as Am and Cm were not taken into account the actinide chain model.[9]

However, this model remarkably underpredict the reactivity loss for high burnup reactor calculation such as APWR and HCLWR. Therefore, this model was improved and Am and Cm chains were added as shown in Fig. 18. The effects of these minor actinides on the burnup reactivity loss are studied by performing the cell burnup calculation for the HCLWR lattice described in Section 3.2.

It is observed from Fig.19 that the contribution of Am-241 and Am-243 on the burnup reactivity loss is very large and about 2 %Δk at the burnup 50 GWD/t. This effect is almost equal to reduce the burnup rate of 10 GWD/t. There are considerable nuclear data uncertainties for these nuclides as seen in Table 3. The capture and fission cross sections of Am-243 are compared respectively in Figs. 20 and 21. Remarkable discrepancies are observed among the data for the four files, JENDL-2, JEF-1, ENDF/B-IV and -V. Several fission resonances in the low energy region are evaluated in the JENDL-2 and JEF-1 files. Therefore, it is important that the effect of the data uncertainty on the reactivity loss is examined.

Figure 22 shows the comparison of the fractional absorption rates calculated for the minor actinides of the four files. The difference between the Am-243 absorptions obtained with JENDL-2 and ENDF/B-IV is lager than 0.2 %. However, the results obtained with JENDL-2, ENDF/B-V and JEF-1 are in good agreement with each other. It is only observed from Fig. 23 that the multiplication factors calculated with the minor actinide data of ENDF/B-IV become lager than those obtained with the other data.

4. Concluding Remarks

For burnup calculations of fast breeder reactors, the lumped group cross sections for four mother fission nuclides of U-235, U-238, Pu-239 and Pu-241 have been generated on the basis of the JENDL-2 FP data. The burnup dependence of the lumped cross sections has been studied by considering the transfer to another beta-decay chain by neutron capture reaction. It was showed that the burnup dependence was considerably observed at high burnup stage. The effect of fission gas release for Kr, Xe, Cs and I on the lumped cross sections has been also examined and was remarkable. In the near future, the effects of the burnup dependence and fission gas release on burnup characteristics in fast reactor will be investigated by core burnup

calculations.

For thermal reactor calculations, the group constant library SRACLIB-JENDL2 has been generated on the basis of the JENDL-2 file. Using this library, fission product chain and actinide chain models have been studied for burnup calculations. In order to predict accurately burnup performance in high conversion light water reactors, the 45 FP chain model proposed for BWR calculation was improved by deriving the 65 FP model.

Resonance self-shielding effect of fission products on burnup characteristics has been investigated in high conversion light water reactors. The self-shielding effects caused the differences of about 0.6 and 0.75 percent on the effective multiplication factors at the burnup stage of 50 GWD/t for the cases of the moderator to fuel volume ratios of 0.74 and 1.4, respectively. The self-shielding effects of Xe-131 and Cs-133 were remarkably.

The effect of nuclear data uncertainties of fission products on the burnup reactivity change has been examined by comparing the results obtained with four evaluated nuclear data files; JENDL-2, JEF-1, ENDF/B-IV and -V. Fractional absorption rates for individual fission product nuclide were considerably scattered among these files. Although significant difference between the reactivity changes calculated with JENDL-2 and ENDF/B-V was observed, the discrepancy between those obtained with JENDL-2 and JEF-1 was small due to an accidental cancellation.

The simple ac....ide chains used in the SRAC code was improved to treat minor actinides such as Am and Cm. The cell burnup calculation for the HCLWR lattice showed that the effect of these minor actinides on the burnup reactivity loss was remarkable. The effect of nuclear data uncertainty of the minor actinides on the reactivity change was also studied. It was shown that the result calculated with the ENDF/B-IV· data was scattered by comparing the results obtained with the other data of JENDL-2, JEF-1 and ENDF/B-V.

Anyway, a consistent reevaluation work will be needed to the nuclear data of the fission products and minor actinides for a better estimate of the HCLWR burnup characteristics.

References

1) Abagyan L.P., et at.:"Group Constants for Nuclear Reactor Calculations", Consultants Bureau, New York (1964).

2) Kikuchi Y., et al.:" Fission Product Fast Reactor Group Constant System of JNDC," JAERI 1248 (1976).

3) Takano H.and Sato W.:"Lumped Group Constants of Fission Products," JAERI-M 83 129, Reactor Engineering Department Annual Report, p15, (1983).

4) Iijima S., Yoshida T. and Yamamoto T. : J. Nucl. Sci. Tecnol.,19, 96 (1982).

5) Takano H., Hasegawa A. and Kaneko K.:" TIMS-PGG : A Code System for Producing Group Constants in Fast Neutron Energy Region," JAERI-M 82-072 (1982).

6) Takano H. and Ishiguro Y.:"Production and Benchmark Tests of Fast Reactor Group Constants Set JFS-3-J2," JAERI-M 82-135 (1982).

7) Tasaka K.:" DCHAIN Code for Analysis of Build-up and Decay of Nuclides," JAERI 1250 (1977).

8) Takano H., et al.: to be published.

9) Tsuchihashi K., et al.:" SRAC: JAERI Thermal Reactor Standard Code System for Reactor Design and Analysis,"JAERI 1285 (1983), and "Revised SRAC Code System", JAERI 1302 (1986).

10) Garrison G.D. and Roos B.W.: Nucl. Sci. Eng., 12, 115 (1962).

Table 1   One hundred fission product nuclides of JENDL-2

Ag107	Ag109	Ba134	Ba135	Ba136	Ba137	Ba138	Cd110
Cd111	Cd112	Cd113	Cd114	Cd116	Ce140	Ce142	Ce144
Cs133	Cs135	Cs137	Eu151	Eu152	Eu153	Eu154	Eu155
Gd155	Gd156	Gd157	Gd158	Gd160	In115	I127	I129
Kr083	Kr084	Kr085	Kr086	La139	Mo092	Mo094	Mo095
Mo096	Mo097	Mo098	Mo100	Nb093	Nd142	Nd143	Nd144
Nd145	Nd146	Nd148	Nd150	Pd104	Pd105	Pd106	Pd107
Pd108	Pd110	Pm147	Pr141	Rb085	Rb087	Rh103	Ru100
Ru101	Ru102	Ru103	Ru104	Ru106	Sb121	Sb123	Sb124
Sm147	Sm148	Sm149	Sm150	Sm151	Sm152	Sm154	Sr086
Sr087	Sr088	Sr090	Tb159	Tc099	Te128	Xe131	Xe132
Xe133	Xe134	Xe135	Xe136	Y089	Zr090	Zr091	Zr092
Zr093	Zr094	Zr095	Zr096				

Table 2   Fiftyfive fission product nuclides taken from ENDF/B-V

As075	Ba140	Br081	Ce141	Ce143	Cs134	Cs136	Dy160
Dy161	Eu156	Ge073	Ge074	In113	I130	I131	I135
Kr082	La140	Mo099	Nb095	Nd147	Pm148	Pm148m	Pm149
Pr143	Rb086	Rh105	Sb125	Sb126	Se076	Se077	Se078
Se080	Se082	Sn117	Sn118	Sn119	Sn120	Sn122	Sn124
Sr089	Tb160	Te122	Te123	Te124	Te125	Te126	Te127m
Te129m	Te130	Te132	Xe128	Xe129	Xe130	Y091	

Table 3 Comparison of thermal capture cross sections
and capture resonance integrals (barns)

Nuclide		JENDL-2	ENDF/B-V	JEF-1
Ru-103	2200m/s	5.0	7.7	66.8
	R.I	92.0	70.0	595.0
Pd-108	2200m/s	8.5	12.2	7.4
	R.I	252.4	226.0	188.0
Eu-155	2200m/s	4046.0	4040.0	3647.0
	R.I	18840.0	1857.0	2178.0
Am-241	2200m/s	600.0	576.0	610.0
	R.I	1299.0	1424.0	1449.0
Cm-243	2200m/s	131.3	58.0	134.0
	R.I	404.5	248.4	429.0
Cm-244	2200m/s	14.4	10.4	14.4
	R.I	593.7	593.5	637.3

1 Se79 ⟶ Se80

2 Kr83 ⟶ Kr84 $\xrightarrow{0.552}$ Kr85m
$\searrow^{0.178}$ Kr85g ⟶ Kr86 ⟶ Kr87 ⟶ Kr88

3 Rb85 ⟶ Rb86 ⟶ Rb87 ⟶ Rb88

4 Y89 $\xrightarrow{0.001}$ Y90m
$\searrow_{0.999}$ Y90g

5 Sr90 ⟶ Sr91

6 Zr91 ⟶ Zr92 ⟶ Zr93 ⟶ Zr94 ⟶ Zr95

7 Mo95 ⟶ Mo96 ⟶ Mo97 ⟶ Mo98 ⟶ Mo99

8 Zr96 ⟶ Zr97

9 Mo100 ⟶ Mo101

10 Tc99 ⟶ Tc100

11 Ru100 ⟶ Ru101 ⟶ Ru102 ⟶ Ru103

12 Rh103 ⟶ Rh104

13 Ru104 ⟶ Ru105

14 Pd104 ⟶ Pd105 ⟶ Pd106 $\xrightarrow{0.116}$ Pd107m
$\searrow_{0.884}$ Pd107g ⟶ Pd108 $\xrightarrow{0.016}$ Pd109m
$\searrow_{0.984}$ Pd109g

15 Rh105 ⟶ Rh106

16 Ag109 $\xrightarrow{0.05}$ Ag110m
$\searrow_{0.95}$ Ag110g

Fig.1 Capture chains used in the DCHAIN code

17 Cd111 ⟶ Cd112 $\xrightarrow[1.0]{0.0}$ Cd113m

　　　　　　　　　Cd113g ⟶ Cd114 $\xrightarrow[0.882]{0.118}$ Cd115m

　　　　　　　　　　　　　　　　　　　　　Cd115g

18 In113 ⟶ In114

19 In115 ⟶ In116

20 Sb121 $\xrightarrow[0.991]{0.009}$ Sb122m

　　　　　　　　Sb122g

21 Te122 $\xrightarrow[0.607]{0.393}$ Te123m

　　　　　　　　Te123g

22 Sb123 ⟶ Sb124

23 Te125 ⟶ Te126

24 I127 ⟶ I128

25 I129 ⟶ I130

26 Xe130 $\xrightarrow[0.877]{0.123}$ Xe131m

　　　　　　　　Xe131g ⟶ Xe132

27 Cs133 ⟶ Cs134 ⟶ Cs135 ⟶ Cs136

28 Xe135 ⟶ Xe136

29 Ba138 ⟶ Ba139

30 La139 ⟶ La140

31 Ba140 ⟶ Ba141

Fig.1 (continued)

32　Ce140 ⟶ Ce141

33　Ce142 ⟶ Ce143

34　Ce141 ⟶ Ce142

35　Pr141 $\underset{0.658}{\overset{0.342}{\rightleftarrows}}$ Pr142m

　　　　　　　↘ Pr142g

36　Nd143 ⟶ Nd144 ⟶ Nd145 ⟶ Nd146 ⟶ Nd147

37　Ce144 ⟶ Ce145

38　Pr143 ⟶ Pr144g

39　Pm147 $\overset{0.47}{\rightarrow}$ Pm148m

　　　　　　　↘ Pm148g ⟶ Pm149 ⟶ Pm150

40　Sm147 ⟶ Sm148 ⟶ Sm149 ⟶ Sm150 ⟶ Sm151 ⟶ Sm152 ⟶ Sm153

41　Sm154 ⟶ Sm155

　　　　　　　↗ Eu152n

42　Eu151 $\leftarrow$ $\underset{0.6518}{\overset{0.3477}{\rightleftarrows}}$ Eu152m

　　　　　　　↘ Eu152g ⟶ Eu153 ⟶ Eu154g ⟶ Eu155 ⟶ Eu156 ⟶ Eu157

43　Gd155 ⟶ Gd156 ⟶ Gd157 ⟶ Gd158 ⟶ Gd159

44　Tb159 ⟶ Tb160

Fig.1 　(continued)

Fig.2 Burn-up time dependence of one-group capture cross sections
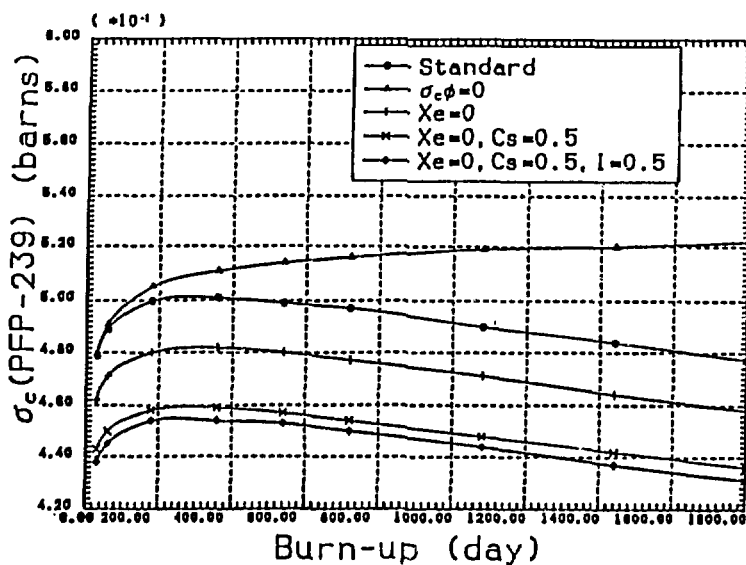
Fig.3 Comparison of burn-up dependence of one-group capture cross sections calculated with different chain models

Kr83 ⟶

Mo99
↓
Tc99 ⟶

Ru101 ⟶   Ru103   Ru105
            ↓   ↓
            Rh103 ⟶   Rh105
                         ↓
            Pd105 ⟶   Pd107 ⟶ Pd108 ⟶ ○
                                          ↓
                                  Ag109 ⟶

Cd113 ⟶

I131   I135
↓   ↓
Xe131 ⟶   Xe133   Xe135
           ↓   ↓
           Cs133 ⟶ Cs134 ⟶   Cs135 ⟶

Pr143
↓
Nd143 ⟶   Nd145 ⟶

Nd147 ⟋Pm148m⟍
↓   ⟋   ⟍
Pm147 ⟵Pm148g⟶ Pm149 ⟶ ○   Pm151
↓   ↓↓   ↓   ↓
Sm147 ⟶ Sm148 ⟶ Sm149 ⟶ Sm150 ⟶ Sm151 ⟶ Sm152 ⟶ ○
                                Eu153 ⟶ Eu154 ⟶ Eu155 ⟶ Eu156
                                ↓   ↓   ↓
                                Gd154 ⟶ Gd155 ⟶ Gd156 ⟶ Gd157 ⟶ Gd158 ⟶

pseudo ⟶
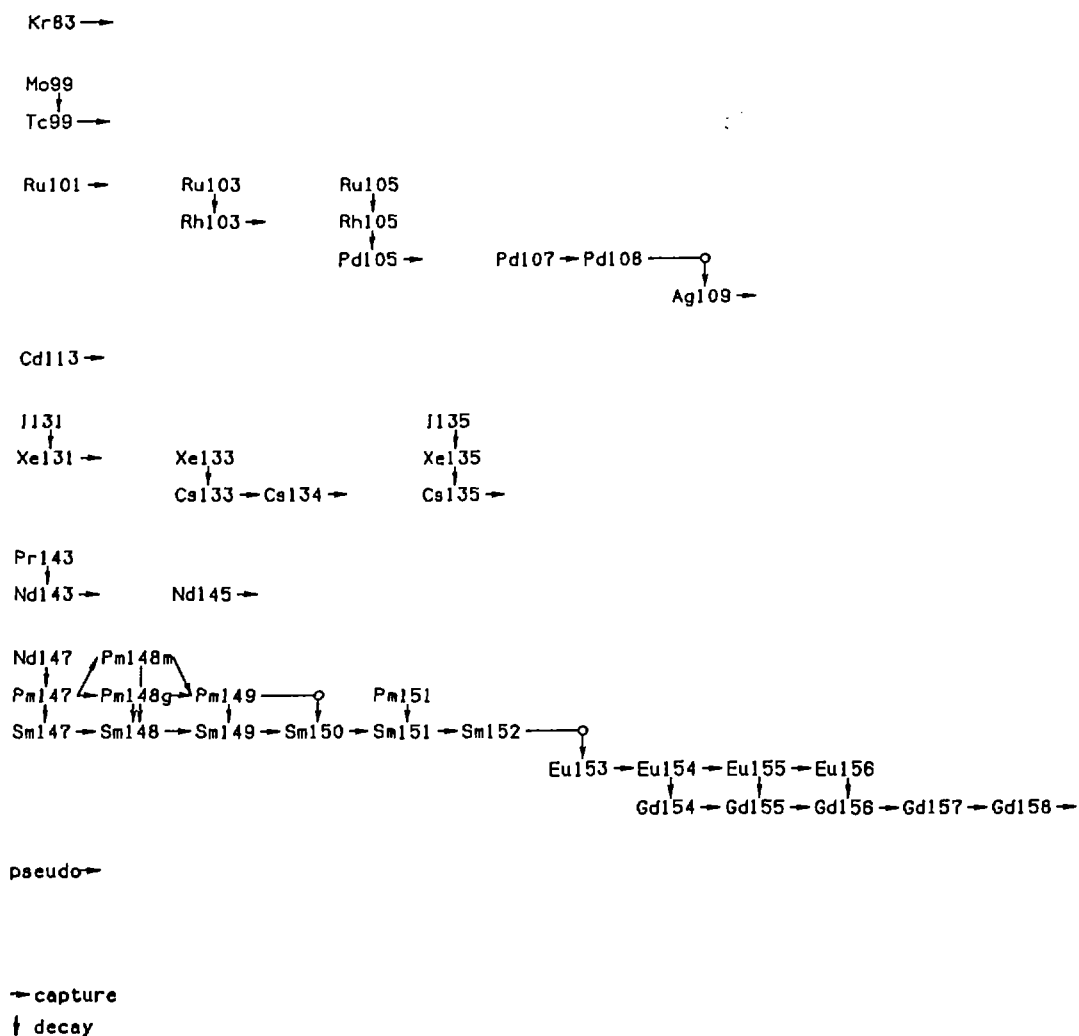
⟶ capture
↓ decay

Fig.4 The 45 fission product chain model proposed by Iijima et al.
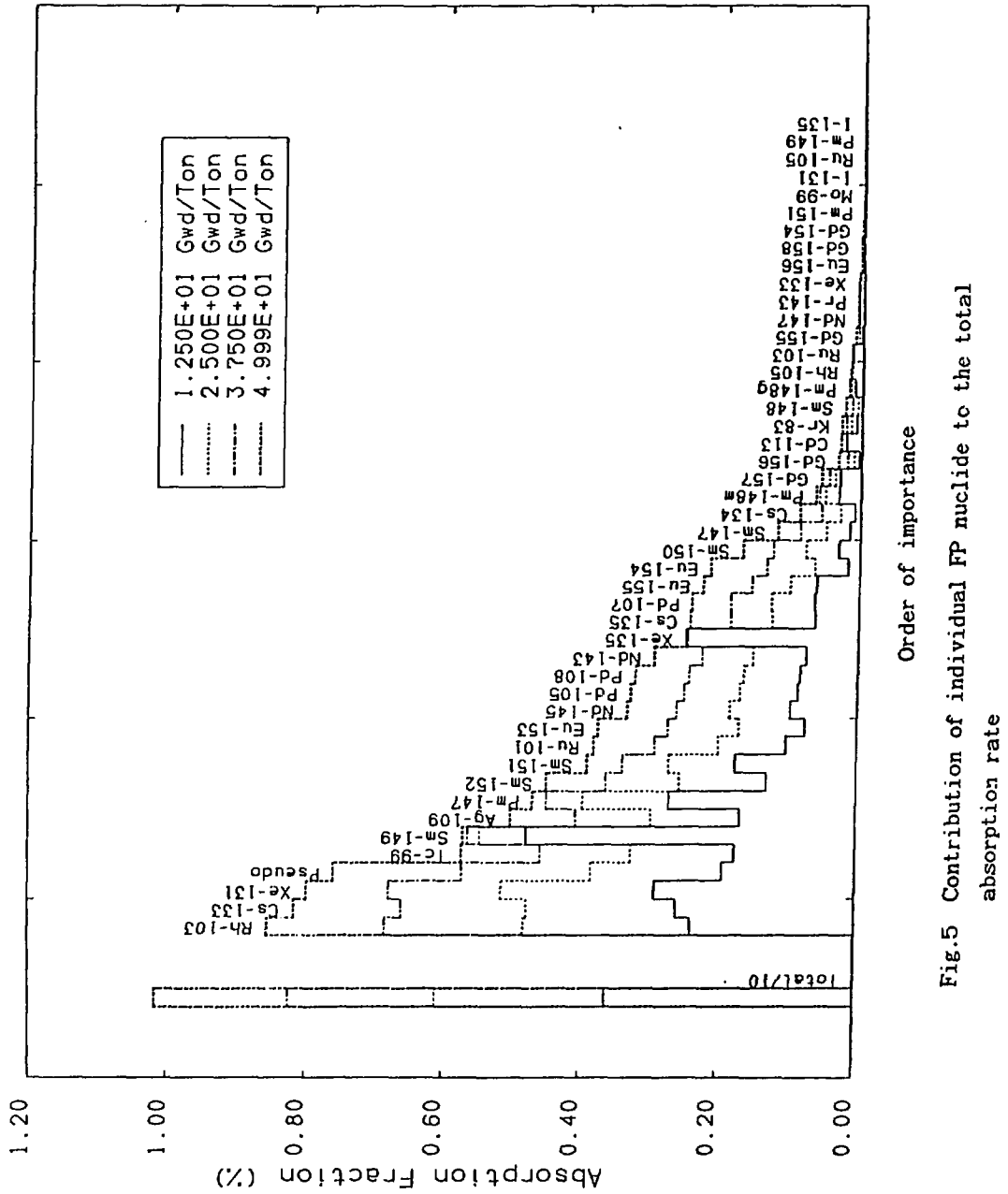
Fig.5 Contribution of individual FP nuclide to the total absorption rate
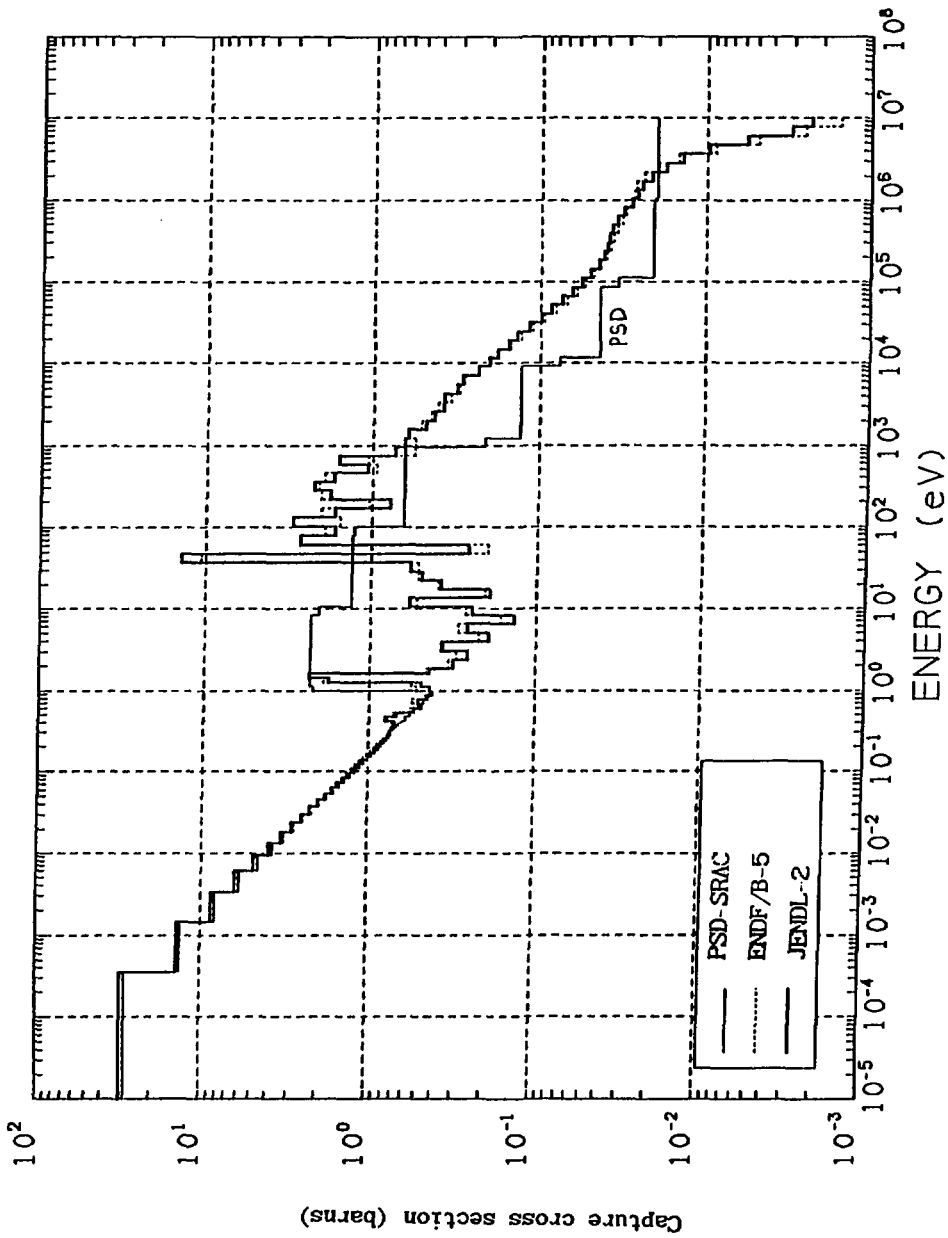
Fig.6 Comparison of the pseudo capture cross sections calculated
for the 45 FP chain model
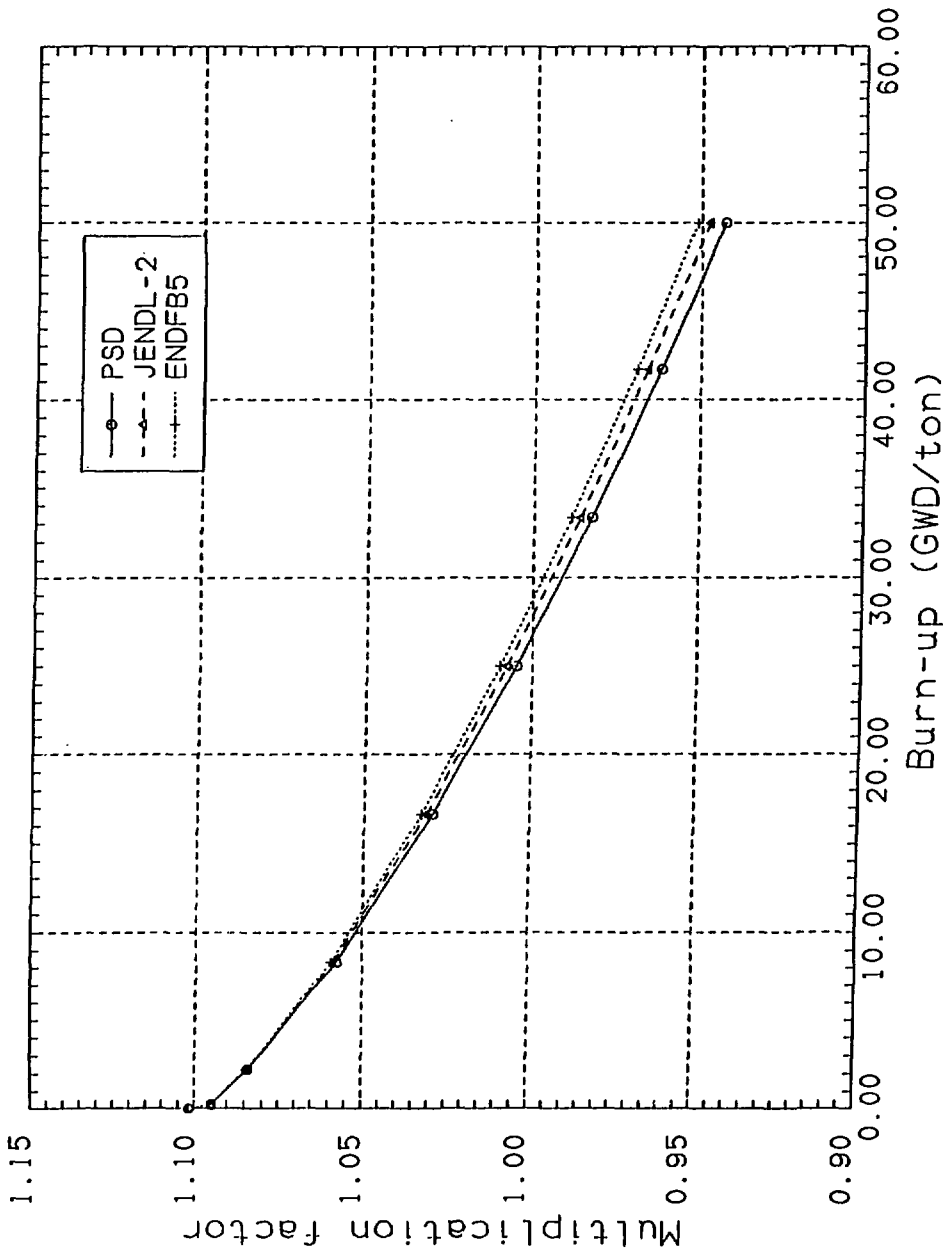
Fig. 7 Comparison of the reactivity changes calculated by using three different pseudo cross sections
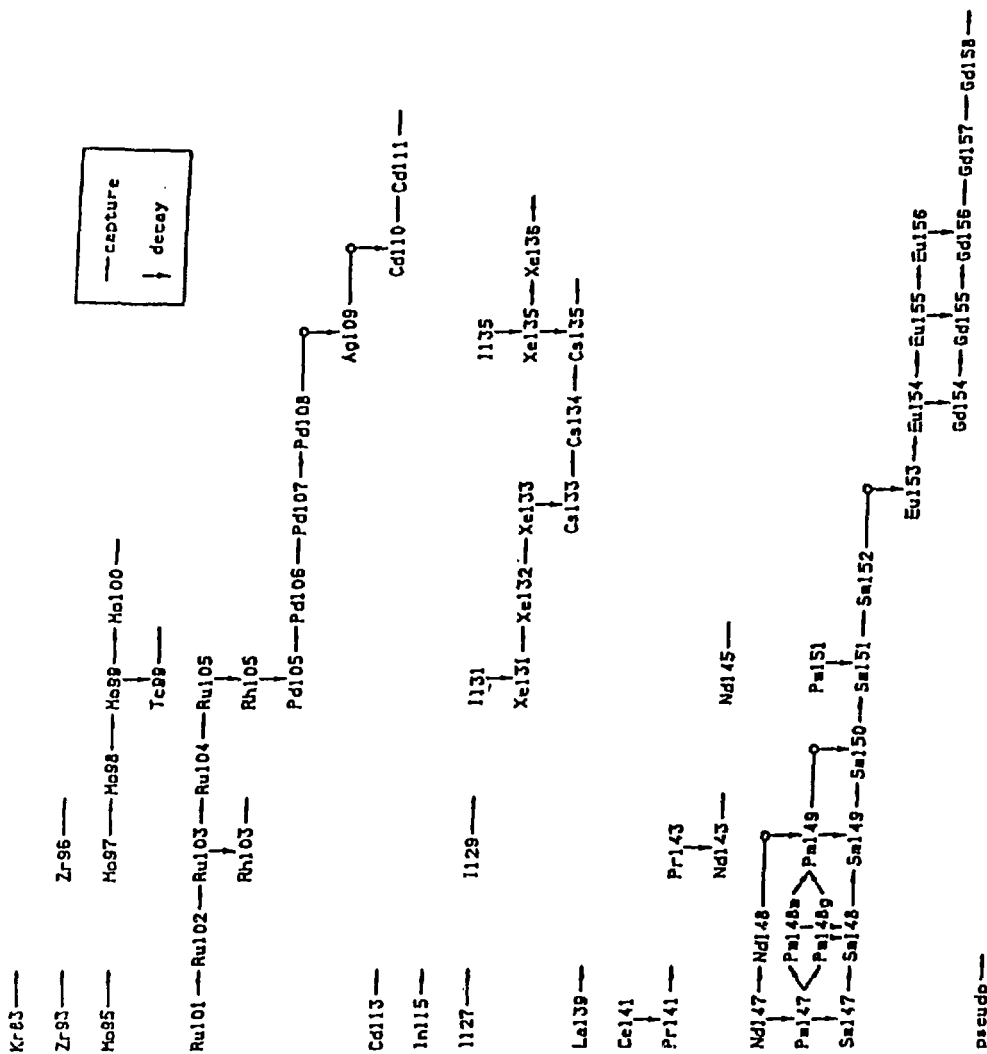
Fig.8 The 65 FP chain model derived for the HCLWR calculations
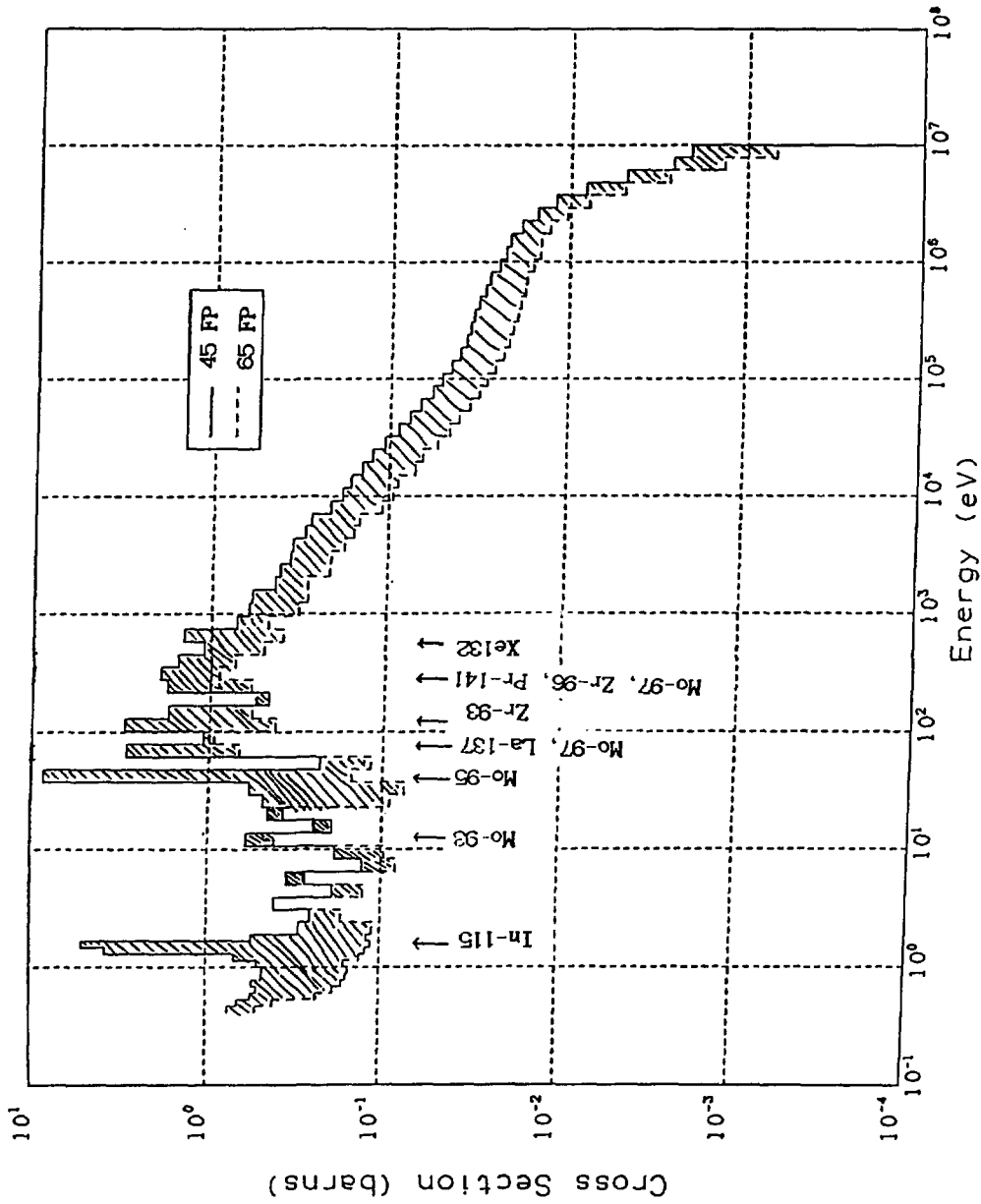
Fig.9 Comparison of the pseudo capture cross sections calculated for the 45 and 65 FP chain models
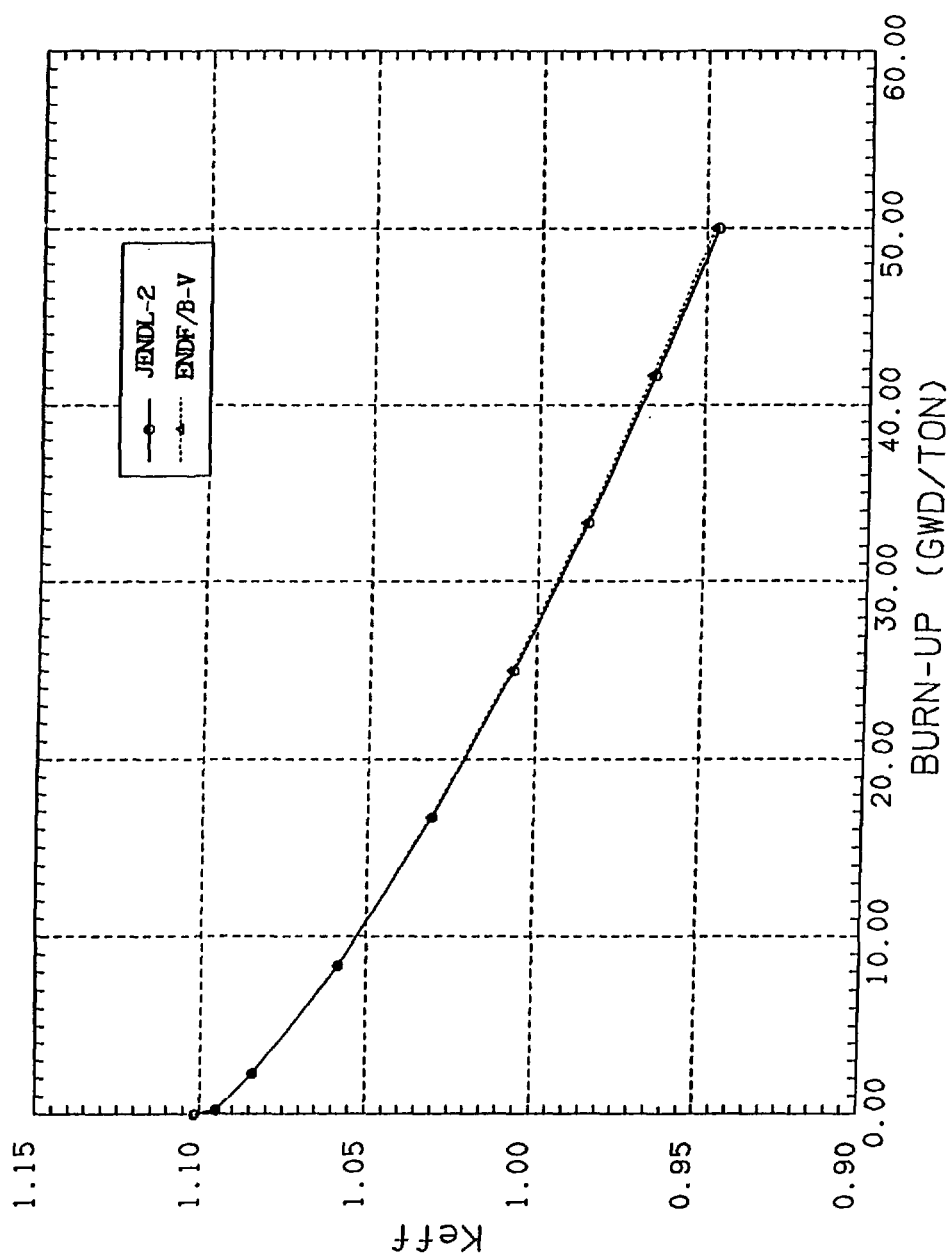
Fig.10 Comparison of the reactivity loss calculated with the
different pseudo cross sections for the 65 FP model
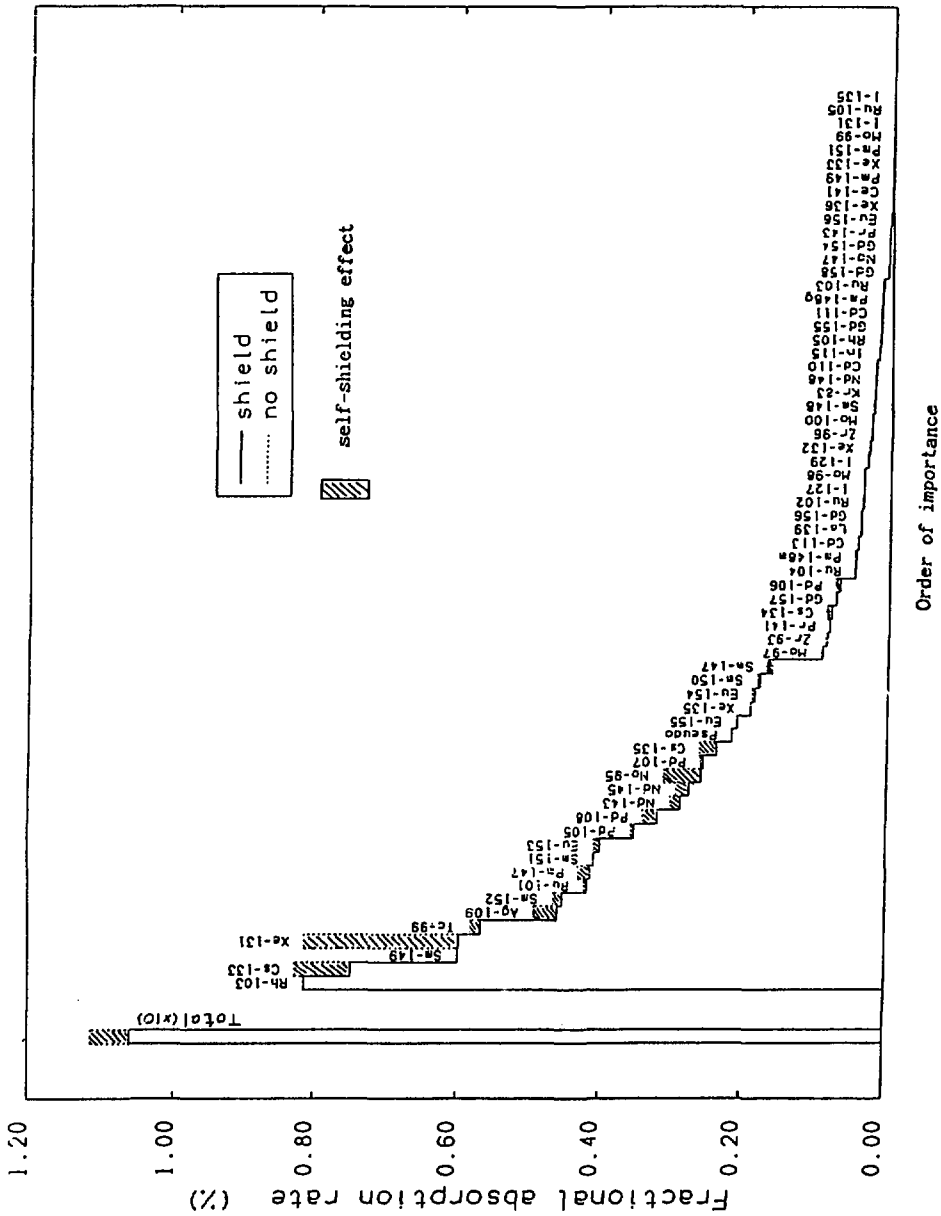
Fig.11 Comparison of the contributions of individual FP nuclide
to total absorption at the burnup stage of 50 GWD/t
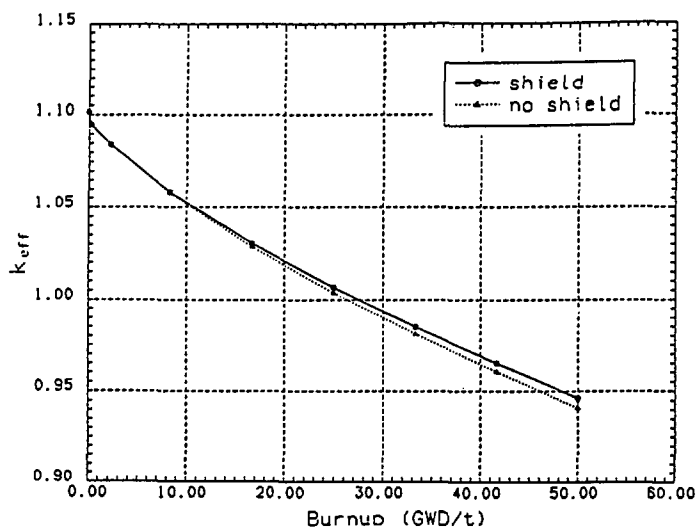
Fig.12   Comparison of reactivity loss calculated with and without
the self-shielding effects for fission products
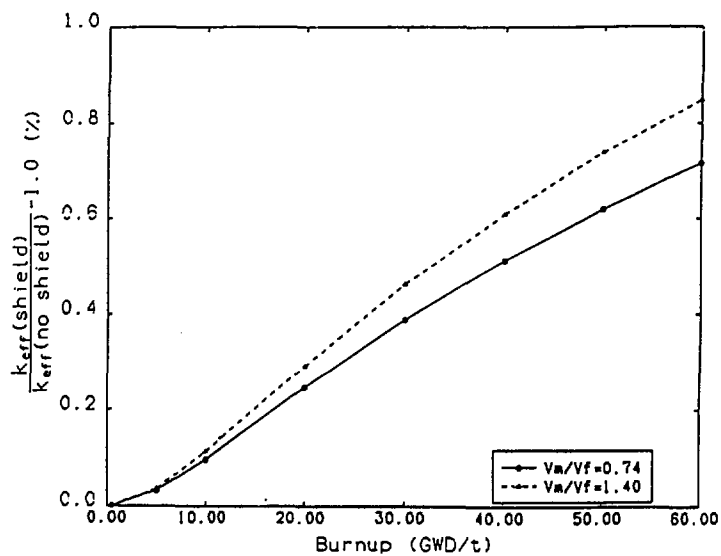
Fig.13 The effects of resonance self-shielding for fission products
on the multiplication factors calculated for the moderator
to fuel volume ratio of 0.74 and 1.4
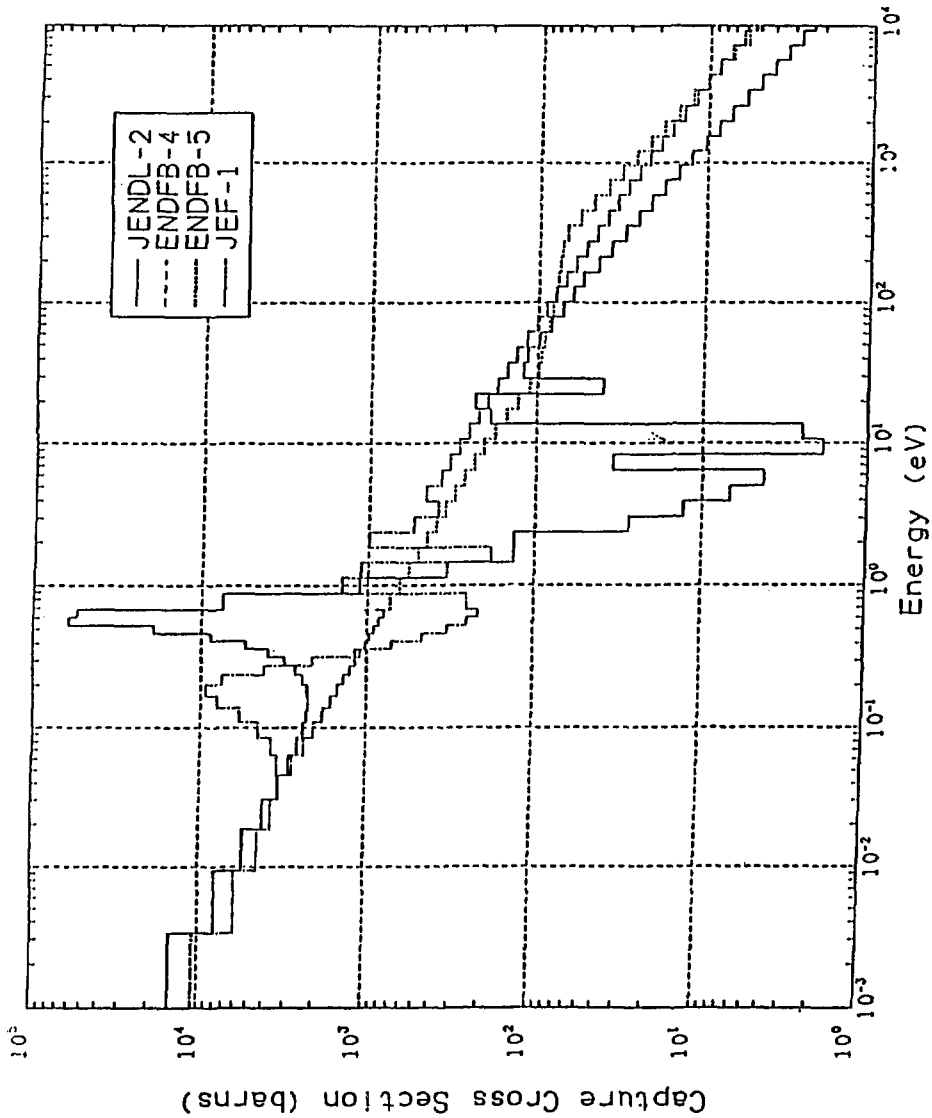
Fig.14 Comparison of capture cross sections of Eu-155
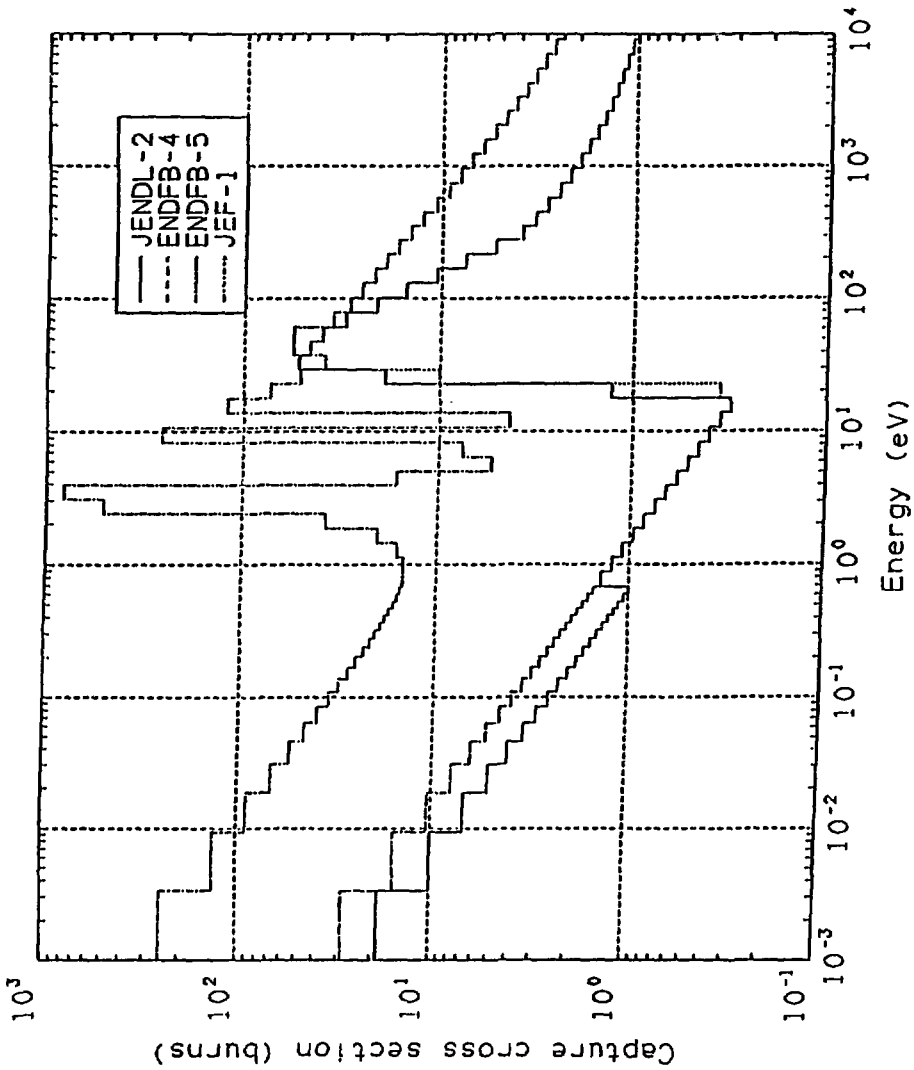
Fig.15 Comparison of capture cross sections of Ru-103 among the four nuclear data files
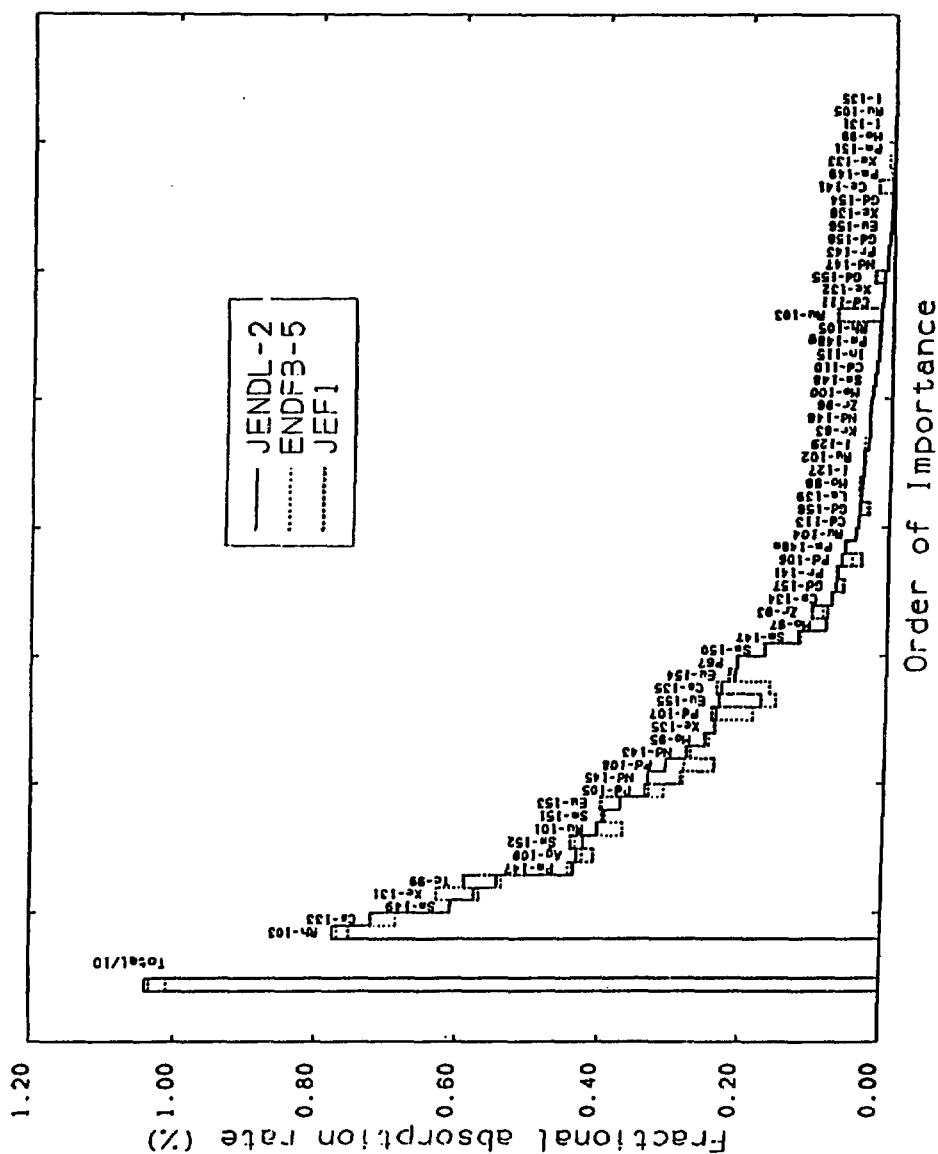
Fig.16 Comparison of the fractional absorption rates calculated with three different data of JENDL-2, ENDF/B-V and JEF-1. The nuclide p67 stands for the pseudo fission product.
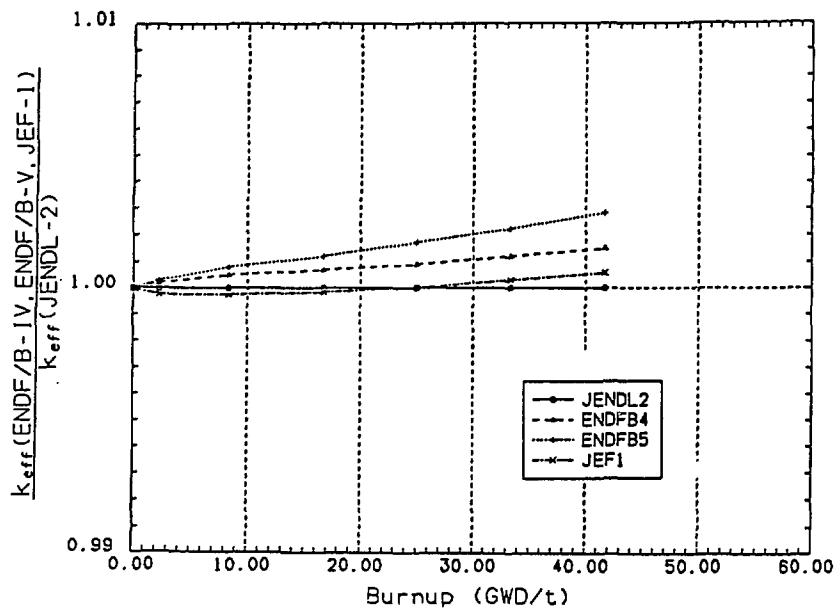
Fig.17 Burnup dependence of the ratios of the multiplication
factors calculated with the other files to those obtained
with JENDL-2
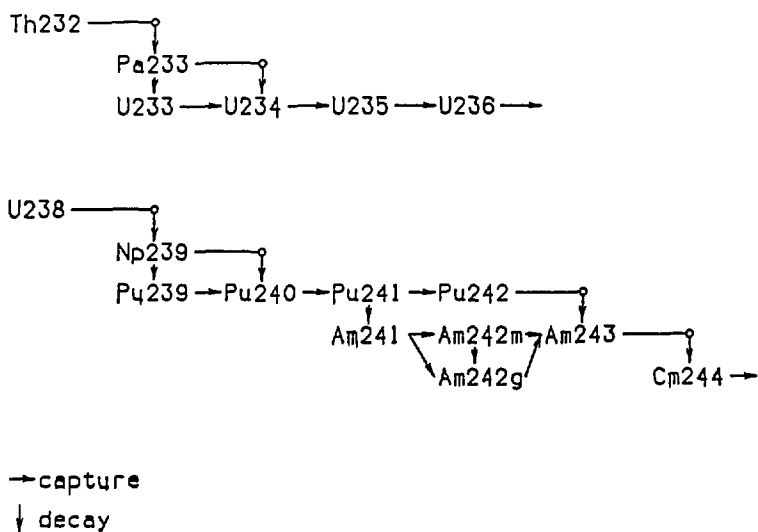
Fig.18 Actinide chain model used in the SRAC system
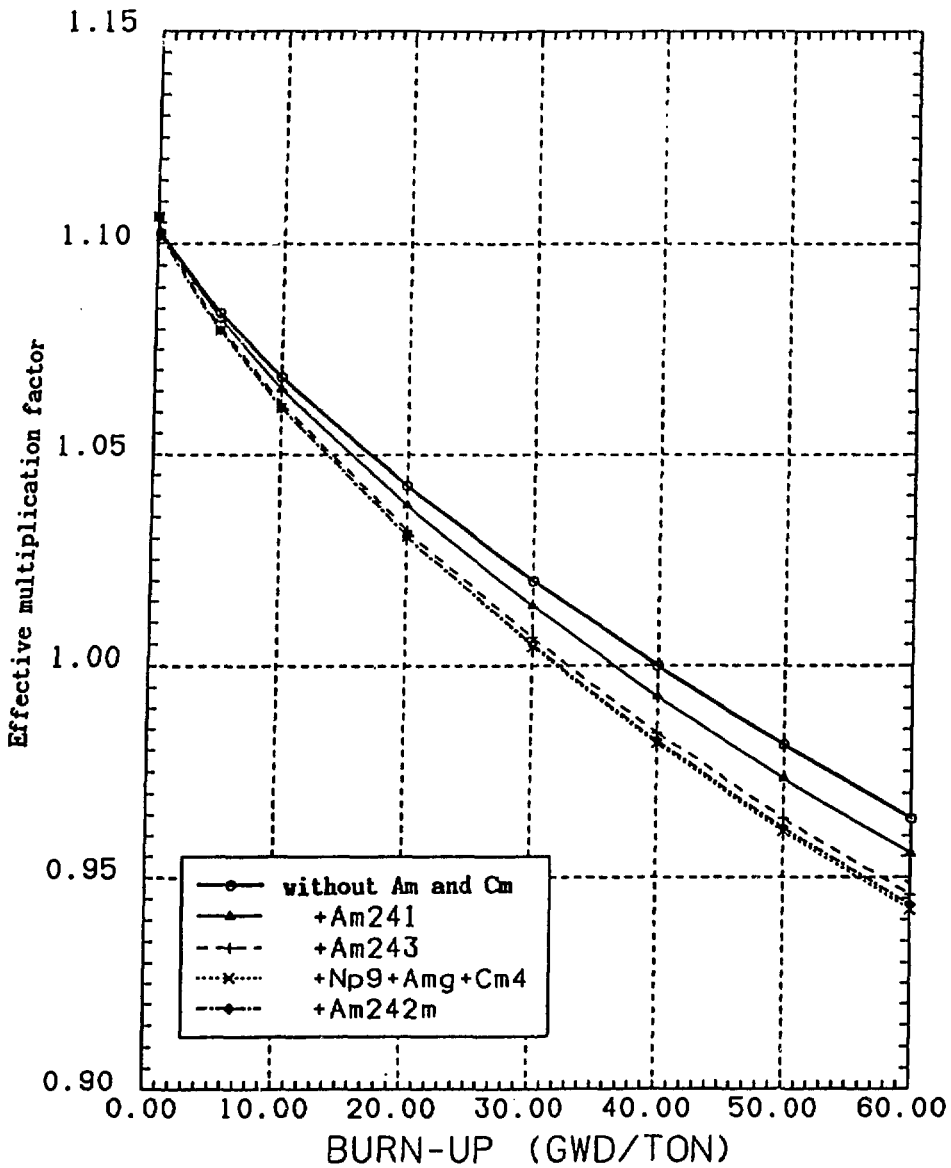
Fig.19 The effects of actinide nuclides on burnup reactivity loss
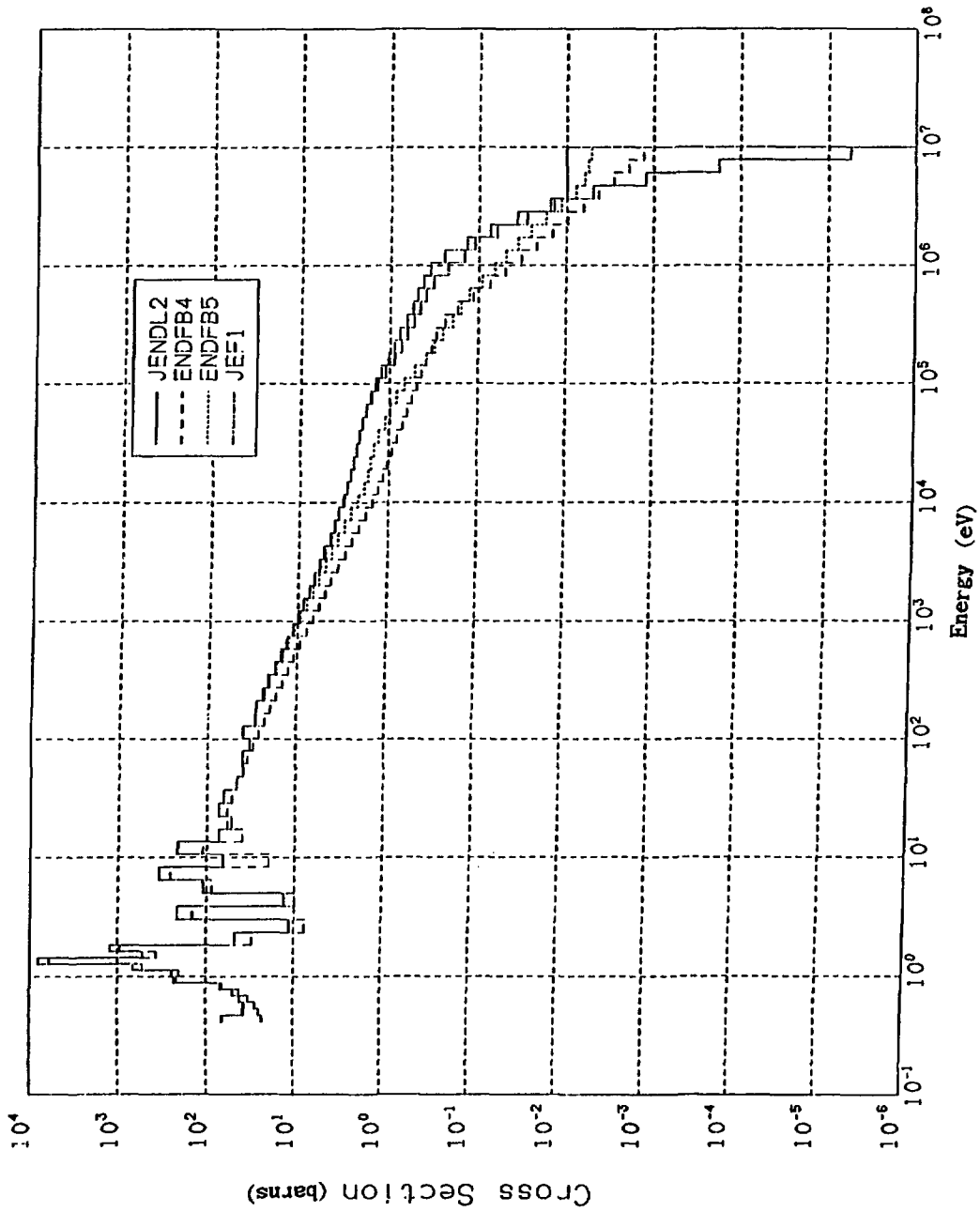
Fig.20 Comparison of capture cross sections of Am-243
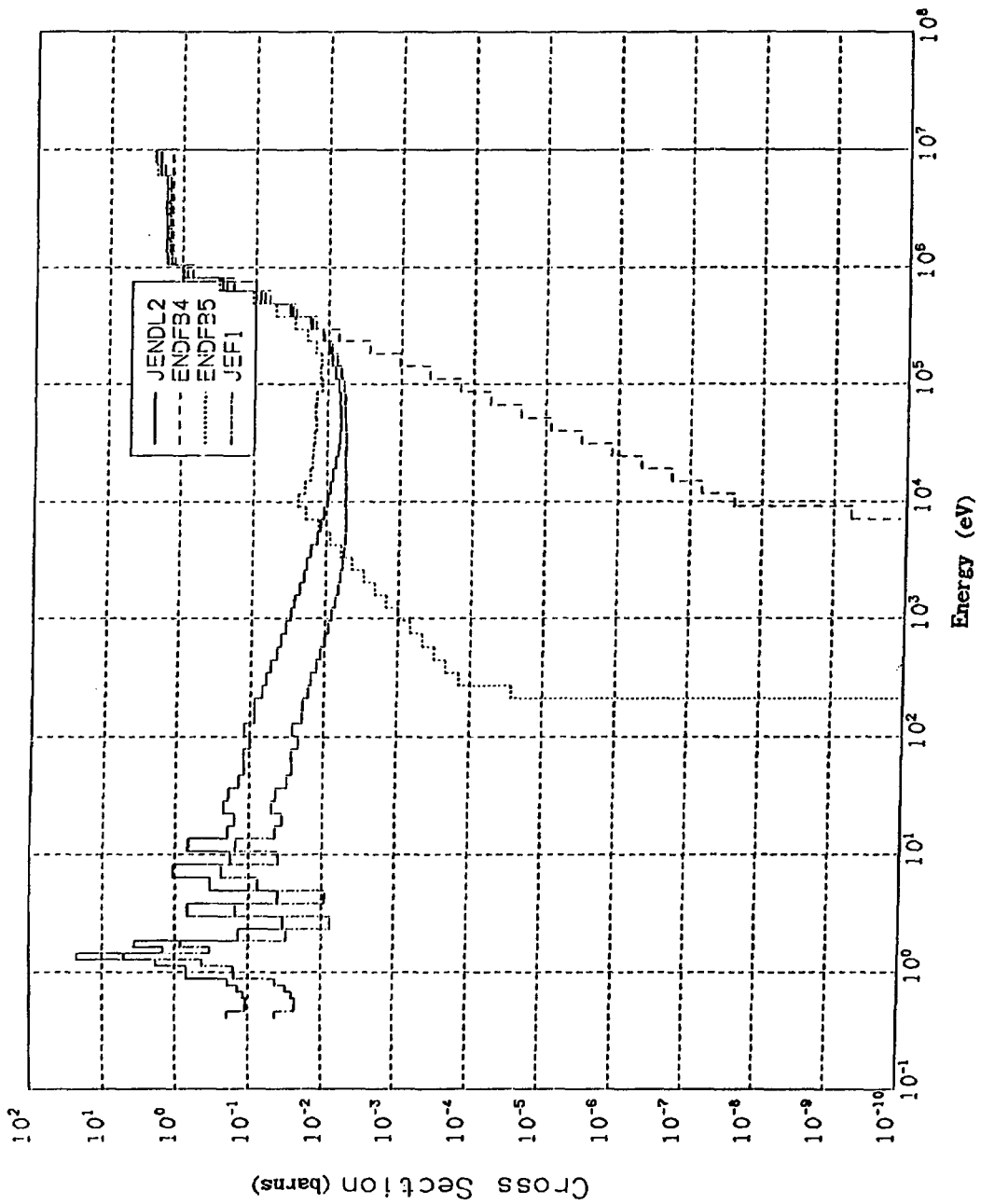
Fig.21 Comparison of fission cross sections of Am-243
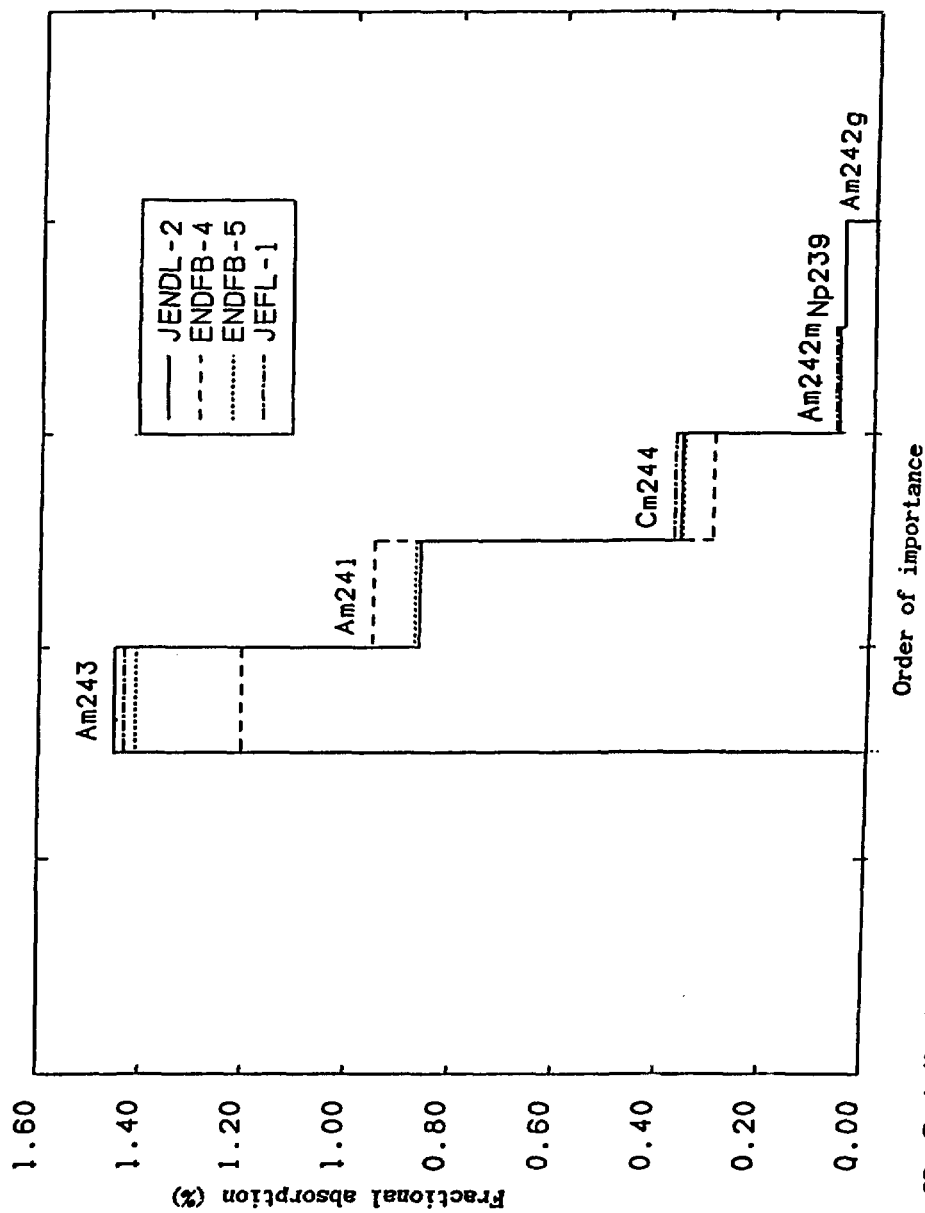
Fig.22 Contribution of individual actinide nuclides to total absorption

Fig.23   The effect of uncertainty of actinide cross sections
on burnup reactivity loss
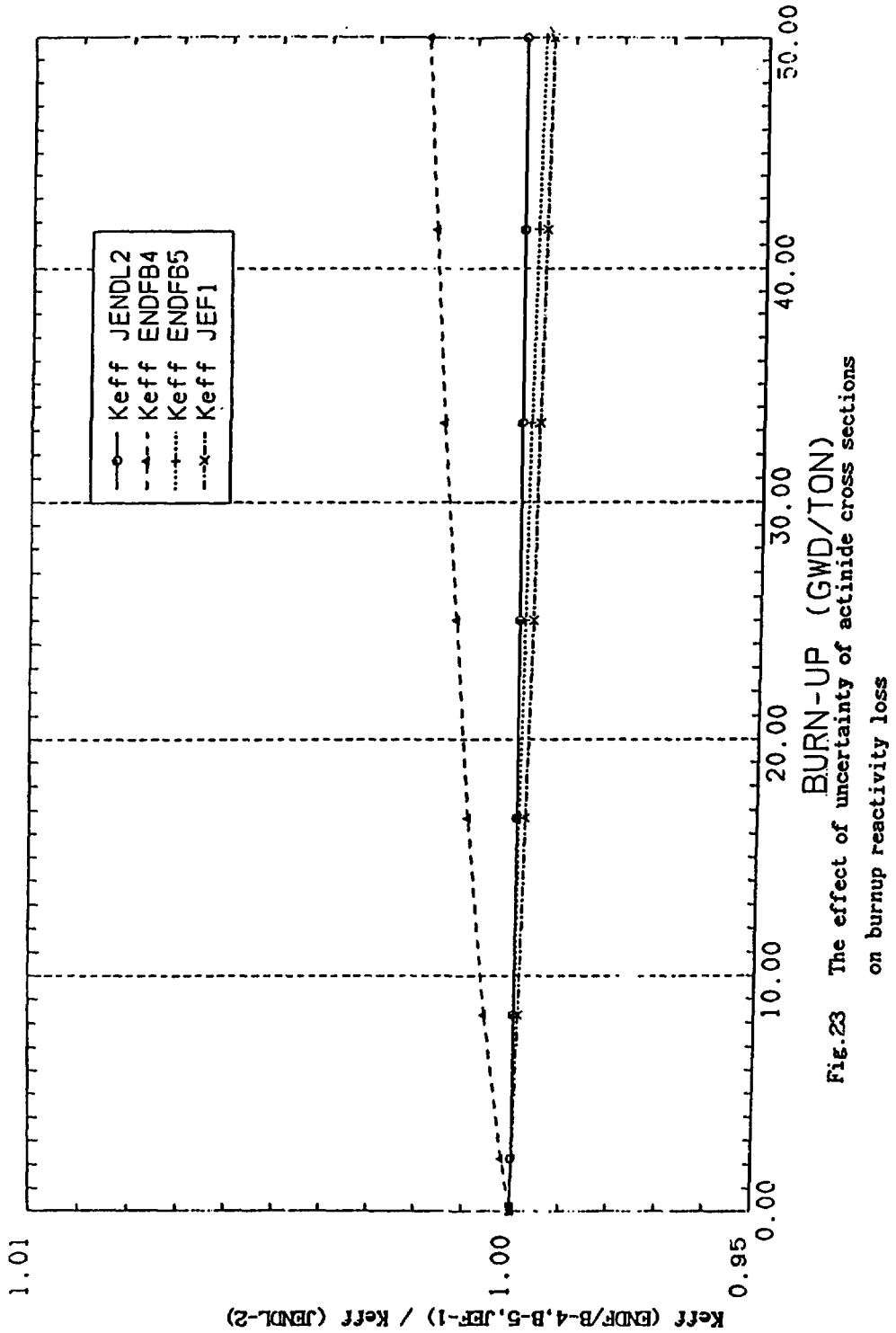
4.4 Sensitivity Analysis of HCLWR

Toshikazu TAKEDA

Department of Nuclear Engineering ,

Faculty of Engineering , Osaka University

Suita-shi , Osaka-fu

The sensitivity coefficients of neutronic performance parameters in high-conversion LWR cells have been calculated by means of the SAINT code. The difference between sensitivities was investigated for cells with different moderator to fuel volume ratios and different Pu enrichment. The burnup dependence of the sensitivities was also discussed with an emphasis on the effect of fission products on the cell parameters.

We have performed the sensitivity analysis for the PROTEUS core. The effect of the difference between the group cross sections obtained by SRAC code[1] from JENDL-2 and ENDF/B-IV on the cell parameters k_{eff}, reaction rate ratio and coolant void worth was estimated by considering the cross section changes in the resolved and unresolved resonances of main heavy nuclides, separately. This work was performed as the activity of Working Group on Integral Test for JENDL in JNDC.

1. INTRODUCTION

Much efforts are now being devoted to the design of the high-conversion light water reactors(HCLWR).[2][3] The neutronic performance parameters are, however, difficult to predict since the HCLWRs have intermediate neutron spectra, and the calculated results strongly depend on the utilized method and data. Therefore the sensitivity analysis is very useful to assess the accuracy of the utilized cross section data.

In this paper we first describe the specific features of the sensitivity coefficients in HCLWRs. The HCLWR cells differs from conventional LWR cells for its tight pitch and higher Pu enrichment. Therefore we discuss the effect of the change in moderator to fuel volume ratio (Vm/Vf) and Pu enrichment on the sensitivity coefficients, separately. The sensitivity coefficients are calculated by the SAINT code[4] which is based on generalized perturbation theory and can treat the cell performance parameters by means of the collision probability method. As sensitivity we concern here the cell parameters in HCLWR cores: k_{eff}, reaction rate ratio, and coolant void worth. The burnup dependence of the sensitivity coefficients was also investigated because some actinides and fission products play an important role in the prediction of the neutronic properties. Particularly the coolant void worth is very much dependent on burnup and this dependence is investigated using the sensitivity coefficients.

Next, we perform the sensitivity analysis in the PROTEUS cores[5]. To investigate the library difference between JENDL-2 and ENDF/B-IV we compare the group cross section obtained by the SRAC code from the two libraries. The effect of the group cross section difference on the cell parameters was discussed using sensitivity coefficients.

2. SENSITIVITY COEFFICIENTS

To see the features in HCLWR cells we compare the sensitivities in five cells, shown in Table 1 as cases 1~5 with different Vm/Vf ratios of 0.5,1.0 and 2.0 and different Pu fissile enrichment of 8.0,5.0 and 3.0%. We considered sensitivity coefficients of k_{eff}, conversion ratio defined by the ratio of ($^{238}U + {}^{240}Pu$) capture rates to ($^{235}U + {}^{239}Pu + {}^{241}Pu$) absorption rate, and coolant void worth. The sensitivity of coolant void worth strongly depends on the void fraction, then we considered two void patterns, one is the void fraction change from 0% to 90%, and the other is from 0% to 50%.

Table 2 lists the energy integrated sensitivity coefficients of k_{eff}. The k_{eff} sensitivity on the ^{238}U capture cross section in the HCLWR cell (case 1) is almost same as the conventional cell (case 3). However from the comparison of the cases 2 and 4 and the cases 1 and 4, it is seen that the tight pitching increases in negative sign the sensitivity because of the spectrum hardening and the

increace in the Pu enrichment decreases the sensitivity because of the decrease of the ^{238}U atomic number density. The small change in the sensitivities between the cases 1,2 and 3 is due to the cancellation of the above two effects. However, the energy dependence of the sensitivity is remarkably different for the cases 1 and 3 as shown in Fig.1. For the case 1 the sensitivity in the resonance energy range becomes larger. The sensitivity of k_{eff} is also large to the ν-value and fission cross sections of ^{239}Pu and ^{241}Pu. Table 3 lists the energy integrated sensitivity coefficients of conversion ratio. The ^{238}U capture, ^{239}Pu fission and capture and ^{241}Pu fission cross sections have large sensitivity in the HCLWR cells, while the ^{240}Pu capture cross section has large sensitivity in the conventional cell.

The energy-integrated sensitivity coefficients of the coolant void worth are listed in Table 4 and 5 for the two different void patterns. The void worth sensitivity is large to the ^{238}U capture, scattering, fission, ^{239}Pu capture, ν-value, fission, ^{240}Pu capture and fission, ^{241}Pu fission and ^{242}Pu capture cross sections. The sensitivity coefficients for the cases 2 and 3 do not show great variations for the two void patterns, while that of the case 1 differs remarkably. For instance the sensitivity to the ^{238}U capture cross section for the void pattern 1 is 2.4 times that of the void pattern 2, and this large difference is not seen for the case2 cell where the ratio of sensitivity coefficients for the two void patterns is 1.2. The large difference for the case 1 is caused by the small coolant void worth, and the absolute void worth variation due to the cross section change is almost the same for all the cases: The 1% increase in the

238_U capture cross section leads to the decrease of the void worth by 3.23×10^{-4} dk/kk' and 1.92×10^{-4} dk/kk' for the void patterns 1 and 2, respectively. The ratio of this absolute void worth change is 0.59 and it is almost the same for other cases (cases 2~5). The energy dependence of the sensitivity coefficient is shown in Fig. 2 to the 238_U capture cross section. For the case 1 the sensitivity is negative below about 100eV. This is because the neutron spectrum is harder and the cross section change below 100eV has only small effect on k_{eff} when coolant is voided (see Fig 3), and when coolant is nonvoided k_{eff} dereases by the increase of the cross section. Therefore, the difference, k_{eff} (voided)-k_{eff}(nonvoided),increases by the cross section change. The coolant void worth is negative, then the sesitivity becomes negative below 100eV.For other cases (cases 2 ~ 5), the sensitivity is positive because spectrum becomes larger above about 1eV when coolant is voided.   Next we consider the burnup dependence of the sensitivity coefficients. Table 6 lists the sensitivities of k_{eff} and coolant void worth at 0 and 50 GWD/t, respectively. With the void worth we considered the void pattern 2. As the burnup the sensitivities to the $238_U, 239_{Pu}$ and 240_{Pu} capture cross sections decrease and those to the fission products such as 131_{Xe}, 101_{Ru}, 103_{Rh}, 133_{Cs}, 149_{Sm} increase though in negative sign.

The sensitivity coefficients of coolant void worth change in sign with burnup   because   the   void worth is negative at 0 GWD/t but positive at 30 and 50 GWD/t. Using the sensitivity we interpret the increase of the coolant void worth. With the burnup (0-50GWD/T) 238_U, 239_{Pu} and 242_{Pu} number densities decrease by 5.8, 12.2 and 18.8% and 240_{Pu}

and ^{241}Pu number densities increase by 3.7 and 5.0% respectively. The total sensitivity coefficients of ^{238}U, ^{239}Pu, ^{240}Pu, ^{241}Pu and ^{242}Pu at 0 GWD/t are 4.53, -0.23, -4.47, -0.73 and -0.80, respectively. Thus the burnup of these heavy nuclides increase the void worth by 1.42×10^{-3} dk/kk'. Furthermore, the sum of sensitivity coefficients of fission products is about 2.0. Therefore the void worth is increased by 11.8×10^{-3} dk/kk'. As a result the coolant void worth increase by 13.2×10^{-3} dk/kk' from 0 to 50 GWD/t which shows a good agreement of the real void worth change of 10.9×10^{-3} dk/kk'. Thus, the fission products have a large effect on the coolant void worth change with burnup.

Lastly we consider the sensitivities to ^{239}Np, ^{241}Am, ^{242}Am, ^{243}Am and ^{244}Cm, which were added recently to the SRAC burnup chain. The sensitivity coefficients are listed for the case 1 in Table 7. The capture cross sections have a larger sensitivity than fission cross sections: ^{243}Am and ^{241}Am have a large sensitivity of -0.009 and -0.006 for k_{eff}, respectively. If these nuclides are neglected in the burnup calculation, the k_{eff} at 50GWD/T is over-estimated by 1.5%. This reveals that the accurate treatment of these actinides is required for the evaluation of the burnup properties in the HCLWR cell.

3. SENSITIVITY ANALYSIS IN PROTEUS CORE

In this section we estimate the effect of the group constants on the cell parameters of the PROTEUS core using

the sensitivity coefficients.

We calculated the group constant in 86 groups using the SRAC code from JENDL-2 and ENDF/B-IV. Figures 4 and 5 show the comparison of the ^{238}U capture and the ^{239}Pu fission cross sections obtained from the two libraries. Table 8 shows the effect of the difference on the k_∞, ^{238}U capture to ^{239}Pu fission rate ratio (28c/49f), and coolant void worth. As the void worth, we considered the void franction change from 0 to 42.5%. Table 9 shows that the effect becomes large for the ^{238}U capture and ^{239}Pu fission cross sections. The difference in the ^{238}U capture has a large effect mainly in the resolved resonance range and this effect is almost same for the 0 and 42.5% coolant voiding core. For ^{239}Pu fission, however, the effect becomes large for the 42.5% voiding core, especially in unresolved resonance range. This produces the large change in the void worth due to the difference of the ^{239}Pu fission cross section. The sum of both effects produces the 0.8~1.0% change in k_∞, 2.5~2.8% in 28c/49f and 6% in void worth.

4. CONCLUSION

Sensitivity coefficients of cell parameters in fuel cells with the different V_m/V_f ration and different Pu enrichment. It revealed that the tight-pitch cell with a small V_m/V_f has a large sensitivity, especially for the coolant void worth. The burnup dependence of the sensitivity coefficients was also discussed, and the increase of the coolant void worth with burnup was interpreted using the

sensitivity coefficients to fission products. Sensitivity coefficients of the coolant void worth varied remarkably with burnup.

Using the sensitivity coefficients we discussed the effect of cross section difference between JENDL-2 and ENDF/B-IV on the cell parameters of the PROTEUS core. The ^{238}U capture and ^{239}Pu fission cross sections have large effects on cell parameters.

REFERENCES

1) TSUCHIHASHI,K. et ai. : "SRAC: JAERI Thermal Reactor Standard Code System for Reactor Design and Analysis", JAERI-1285 (1983).

2) BROEDERS,C.H.M. and DONNE,M.D.:Nucl.Technol.,71,82 (1985).

3) BROEDERS,C.H.M.:Nucl.Technol.,71,96 (1985).

4) TAKEDA,T. and NAKANO,M.:J.Nucl.Sci.Technol.,23,681 (1986).

5) CHAWLA,R. et al.:"Comparison of Calculated and Mesured Parameters for a Pu-Fueled LWHCR Lattice", Proc. ANS Topical Meeting on Advances in Reactor Physics and Core Thermal Hydraulic, Kiamesha Lake, N.Y., NUREG/CP-0034,902 (1982).

Table 1   Cells used in the sensitivity calculation

Case No.	V_m/V_f	Pu enrichment(%)*
1	0.5	8.0
2	1.0	5.0
3	2.0	3.0
4	0.5	5.0
5	2.0	5.0

* Plutonium fissile enrichment

Table 2   Energy-integrated sensitivity coefficients of k_{eff}

Case		1	2	3	4	5
Vm/Vf		0.5	1.0	2.0	0.5	2.0
Pu-enrichment(%)		8.0	5.0	3.0	5.0	5.0
k_{eff}		1.0902	1.0401	1.1505	0.9648	1.1731
^{238}U	c*	-0.259	-0.259	-0.219	-0.312	-0.192
	s	-0.045	-0.024	-0.008	-0.049	-0.009
	f	0.074	0.066	0.041	0.095	0.038
^{235}U	c	-0.003	-0.004	-0.004	-0.004	-0.003
	s	-0.000	-0.000	-0.000	-0.000	-0.000
	f	0.008	0.009	0.009	0.012	0.006
^{239}Pu	c	-0.143	-0.195	-0.230	-0.150	-0.229
	ν	0.635	0.691	0.748	0.630	0.746
	s	-0.001	-0.000	-0.000	-0.001	-0.000
	f	0.383	0.353	0.333	0.375	0.336
^{240}Pu	c	-0.077	-0.116	-0.119	-0.088	-0.123
	s	-0.001	-0.000	-0.000	-0.001	-0.000
	f	0.020	0.010	0.003	0.015	0.005
^{241}Pu	c	-0.021	-0.024	-0.027	-0.020	-0.028
	ν	0.186	0.166	0.151	0.172	0.160
	s	-0.000	-0.000	-0.000	-0.000	-0.000
	f	0.116	0.092	0.071	0.108	0.077
^{242}Pu	c	-0.017	-0.021	-0.015	-0.018	-0.018
	s	-0.000	-0.000	-0.000	-0.000	-0.000
	f	0.003	0.002	0.001	0.003	0.001

* c:capture   ν: ν-value s:scattering   f:fission

Table 3 Energy-integrated sensitivity coefficients of conversion ratio

Case	1	2	3	4	5
Vm/Vf	0.5	1.0	2.0	0.5	2.0
Pu-enrichment(%)	8.0	5.0	3.0	5.0	5.0
Conversion ratio	0.8683	0.8700	0.6335	1.1082	0.6061
^{238}U c*	0.725	0.667	0.633	0.772	0.574
s	0.014	0.005	0.001	0.009	-0.009
f	0.001	0.000	0.000	0.001	-0.038
^{235}U c	-0.006	-0.006	-0.004	-0.008	-0.003
s	0.000	0.000	0.000	0.000	0.000
f	-0.012	-0.011	-0.011	-0.016	-0.008
^{239}Pu c	-0.222	-0.155	-0.113	-0.199	-0.123
ν	-0.000	-0.000	-0.000	-0.000	-0.000
s	-0.000	-0.000	-0.000	0.000	0.000
f	-0.395	-0.262	-0.203	-0.337	-0.218
^{240}Pu c	0.210	0.288	0.336	0.208	0.355
s	0.000	0.000	0.000	0.000	0.000
f	0.000	0.000	0.000	0.000	-0.000
^{241}Pu c	-0.034	-0.023	-0.015	-0.029	-0.018
ν	-0.000	-0.000	-0.000	-0.000	-0.000
s	0.000	0.000	-0.000	0.000	0.000
f	-0.124	-0.078	-0.049	-0.104	-0.058
^{242}Pu c	0.003	0.009	0.008	0.007	0.008
s	0.000	0.000	0.000	0.000	0.000
f	0.000	0.000	0.000	0.000	0.000

* c:capture ν:ν-value s:scattering f:fission

Table 4 Energy-integrated sensitivity coefficients of coolant void worth (void pattern 1 :0->90%)

Case		1	2	3	4	5
Vm/Vf		0.5	1.0	2.0	0.5	2.0
Pu-enrichment(%)		8.0	5.0	3.0	5.0	5.0
Void worth*		-2.011E-2	-1.423E-1	-1.734E-1	-8.420E-2	-1.575E-1
^{238}U	c**	1.607	0.658	0.608	0.853	0.551
	s	0.935	0.141	0.032	0.361	0.038
	f	-0.862	-0.310	-0.200	-0.475	-0.193
^{235}U	c	0.010	0.008	0.008	0.008	0.007
	s	0.002	0.000	0.000	0.001	0.000
	f	-0.083	-0.034	-0.019	-0.058	-0.017
^{239}Pu	c	-1.811	-0.185	0.139	-0.521	0.061
	ν	2.101	-0.083	-0.483	0.329	0.399
	s	0.030	0.003	0.000	0.007	0.001
	f	-0.685	-0.471	-0.316	-0.580	-0.375
^{240}Pu	c	-1.551	-0.061	0.180	-0.419	0.144
	s	0.016	0.001	0.000	0.003	0.001
	f	-0.341	-0.052	-0.017	-0.099	-0.028
^{241}Pu	c	-0.208	-0.008	0.014	-0.046	0.011
	ν	0.088	-0.213	-0.132	-0.181	-0.172
	s	0.006	0.001	0.000	0.001	0.000
	f	-0.331	-0.228	-0.095	-0.280	-0.141
^{242}Pu	c	-0.286	0.012	0.041	-0.061	0.041
	s	-0.004	0.000	0.000	0.001	0.000
	f	-0.054	-0.009	-0.003	-0.016	-0.005

* Void worth (1/k-1/k')
** c:capture ν:ν-value s:scattering f:fission

Table 5 Energy-integrated sensitivity coefficients of coolant void worth (void pattern 2:0->50%)

Case		1	2	3	4	5
Vm/Vf		0.5	1.0	2.0	0.5	2.0
Pu-enrichment(%)		8.0	5.0	3.0	5.0	5.0
Void worth*		-4.976E-3	-7.519E-2	-9.203E-2	-4.181E-2	-8.277E-2
^{238}U	c**	3.850	0.757	0.699	1.012	0.646
	s	2.541	0.188	0.058	0.474	0.066
	f	-1.855	-0.334	-0.213	-0.533	-0.207
^{235}U	c	0.016	0.008	0.008	0.008	0.007
	s	0.004	0.000	0.000	0.000	0.000
	f	-0.187	-0.037	-0.020	-0.066	-0.019
^{239}Pu	c	-4.353	-0.216	0.133	-0.626	0.051
	ν	5.398	-0.054	-0.468	0.451	0.386
	s	0.081	0.004	0.001	0.009	0.001
	f	-1.360	-0.508	-0.321	-0.647	-0.395
^{240}Pu	c	-3.701	-0.073	0.192	-0.499	0.153
	s	0.043	0.002	0.001	0.005	0.001
	f	-0.767	-0.057	-0.018	-0.114	-0.031
^{241}Pu	c	-0.515	0.012	0.013	-0.058	0.009
	ν	0.436	-0.219	-0.131	-0.184	-0.175
	s	0.017	-0.001	0.000	0.002	0.000
	f	-0.654	-0.245	-0.099	-0.313	-0.150
^{242}Pu	c	-0.679	0.017	0.049	-0.071	0.050
	s	-0.012	0.001	0.000	0.001	0.000
	f	-0.120	-0.010	-0.003	-0.018	-0.005

* Void worth (1/k-1/k')
** c:capture ν:ν-value s:scattering f:fission

Table 6 Sensitivity coefficients of k_{eff} and coolant void worth of case 1

Burnup (GWD/t)		k_{eff}			Coolant void worth*		
		0	30	50	0	30	50
		1.0902	1.0087	0.9724	-4.976E-3	4.069E-3	5.947E-3
238U **	c	-0.259	-0.240	-0.232	3.850	-4.251	-2.778
	s	-0.045	-0.049	-0.050	2.541	-3.417	-2.478
	f	0.074	0.082	0.085	-1.855	2.299	1.664
235U	c	-0.003	-0.002	-0.001	0.016	-0.008	-0.003
	f	0.008	0.006	0.004	-0.187	0.141	0.074
239Pu	c	-0.143	-0.125	-0.119	-4.353	5.343	3.776
	ν	0.635	0.617	0.608	5.398	-8.112	-5.849
	s	-0.001	-0.002	-0.002	0.081	-0.104	-0.074
	f	0.383	0.397	0.400	-1.360	-0.206	-0.293
240Pu	c	-0.077	-0.070	-0.068	-3.701	4.524	3.149
	f	0.020	0.024	0.025	-0.767	1.068	0.802
241Pu	c	-0.021	-0.020	-0.020	-0.515	0.706	0.525
	ν	0.186	0.198	0.205	0.436	-1.293	-1.057
	f	0.116	0.133	0.140	-0.654	0.161	0.033
242Pu	c	-0.017	-0.014	-0.013	-0.679	0.860	0.597
	f	0.003	0.003	0.003	-0.120	0.141	0.098
103Rh	c	0.	-0.003	-0.004	0.	0.196	0.205
107Ag	c	0.	-0.002	-0.003	0.	0.134	0.141
131Xe	c	0.	-0.005	-0.006	0.	0.091	0.096
135Xe	c	0.	-0.002	-0.002	0.	0.360	0.250
133Cs	c	0.	-0.004	-0.006	0.	0.097	0.095
147Pm	c	0.	-0.001	-0.002	0.	0.119	0.096
149Sm	c	0.	-0.006	-0.006	0.	0.987	0.742
151Sm	c	0.	-0.003	-0.003	0.	0.161	0.153
152Sm	c	0.	-0.002	-0.003	0.	0.088	0.097
155Eu	c	0.	-0.001	-0.001	0.	0.152	0.199

* VOID PATTERN 2 : 0->50%
** c:capture ν:ν-value s:scattering f:fission

Table 7   Sensitivity coefficients of higher actinides
(case 1 after 50GWD/t burnup)

		k_{eff}	Coolant void worth*
^{239}Np	c	-0.000	0.001
^{241}Am	c	-0.006	0.115
	f	0.001	0.011
^{242m}Am	c	-0.000	0.002
^{242g}Am	c	-0.000	0.000
^{243}Am	c	-0.009	-0.139
	f	0.001	0.013
^{244}Cm	c	-0.002	0.028

*   Void pattern 2 (dk/kk')

Table 8   Effect of difference between group constants
from ENDF/B-IV and JENDL-2   (%)

	k_{inf}		28C/49F		Void worth
	0%void	42.5%void	0%void	42.5%void	(0->42.5%void)
^{238}U capture					
Fast	-0.09	-0.10	0.28	0.16	0.08
Unresolved	-0.06	-0.11	0.27	0.25	1.02
Resolved	-0.38	-0.35	1.42	1.41	0.23
Thermal*	0.	0.	0.	0.	0.
Total	-0.53	-0.56	1.97	1.82	1.33
^{239}Pu fission					
Fast	-0.11	-0.18	0.21	0.31	1.06
Unresolved	-0.31	-0.45	0.57	0.84	3.25
Resolved	0.25	0.19	-0.36	-0.29	0.75
Thermal	-0.08	-0.05	0.10	0.09	-0.45
Total	-0.25	-0.49	0.52	0.95	4.61
^{239}Pu capture	0.04	0.01	-0.01	0.01	0.32
^{240}Pu capture	0.04	0.08	0.02	0.00	-0.69
Total	-0.70	-0.96	2.50	2.78	5.57

*   Same data is used for both library in this range.
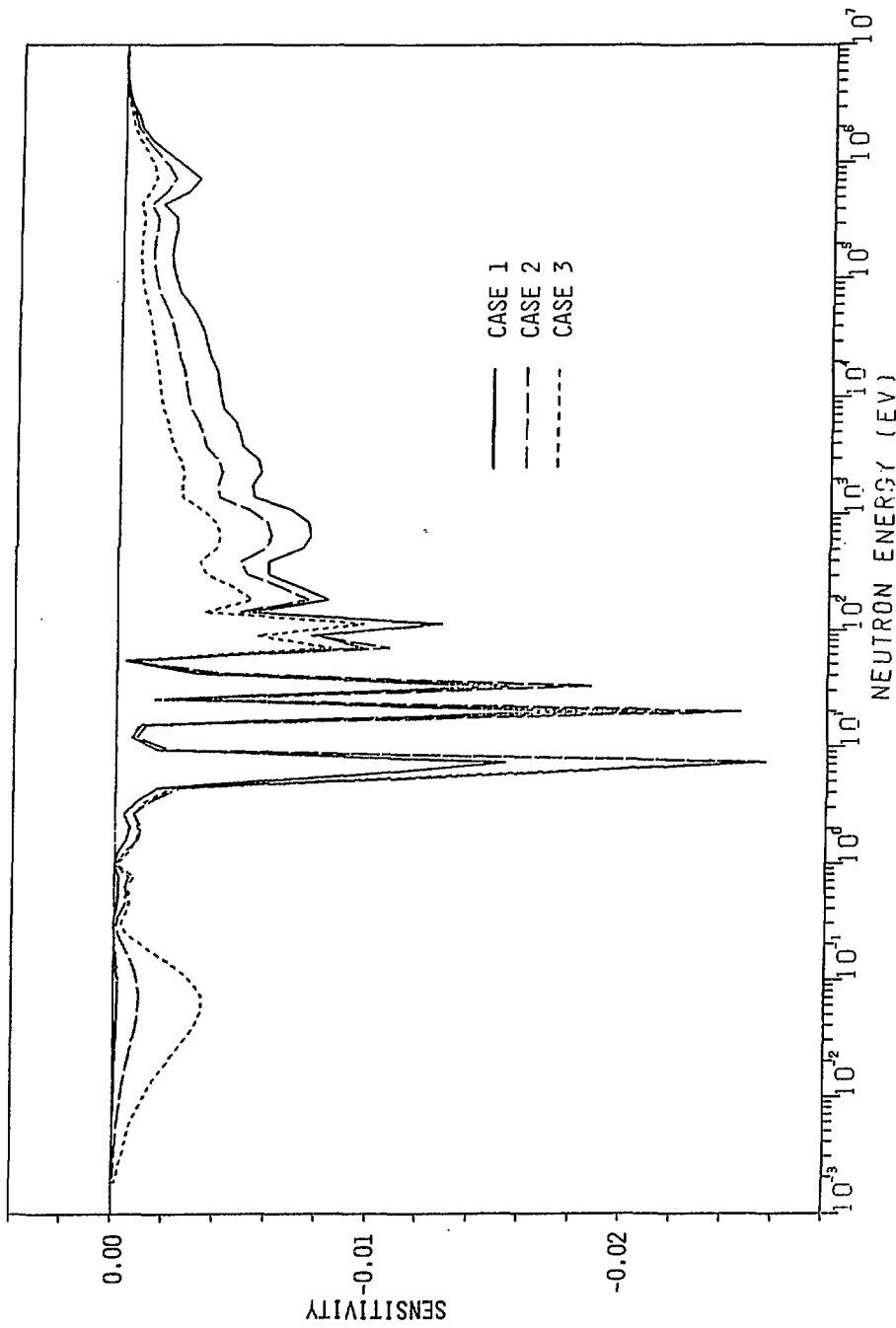
Fig. 1　Sensitivity coefficient of k_{eff}
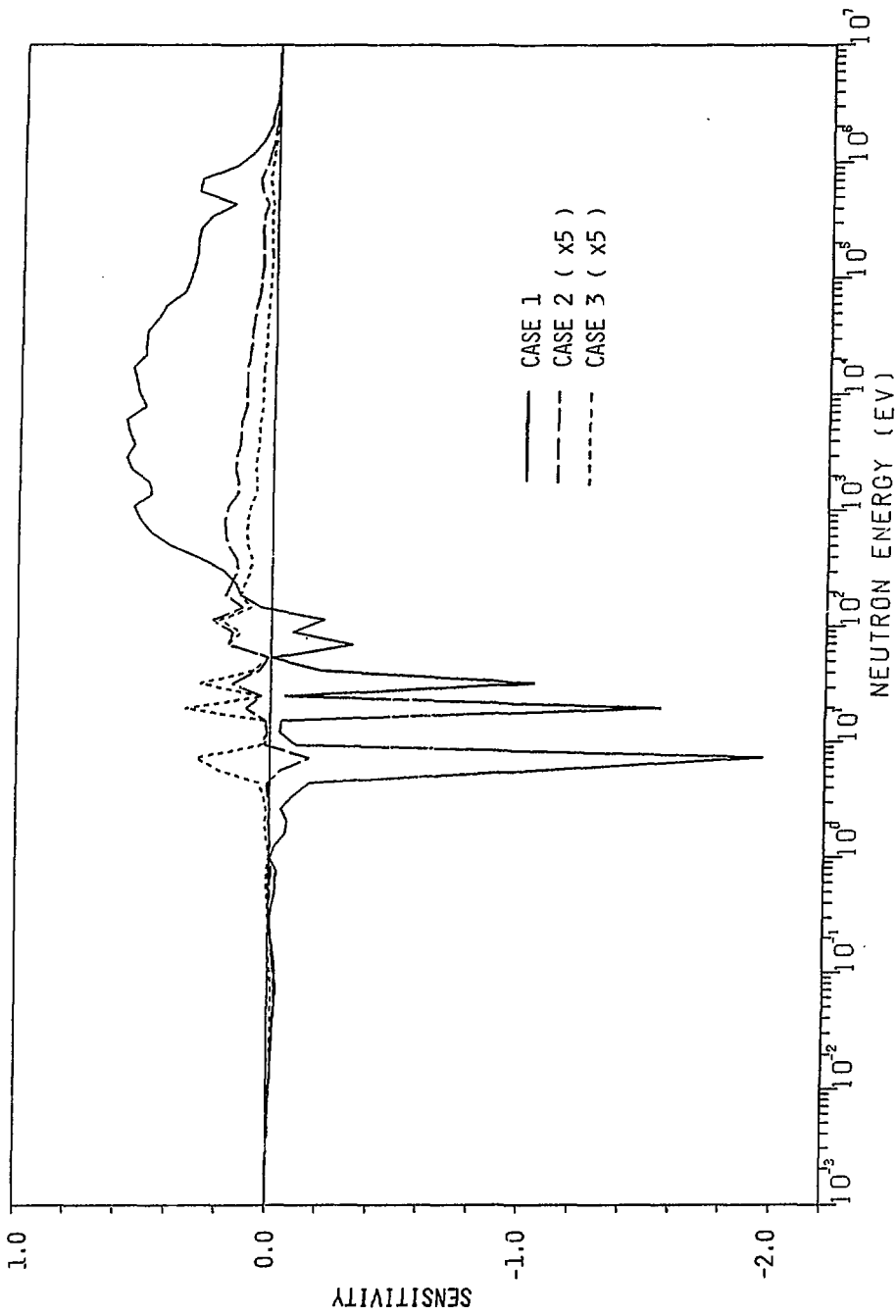to ^{238}U capture cross section

Fig. 2 Sensitivity coefficient of void worth
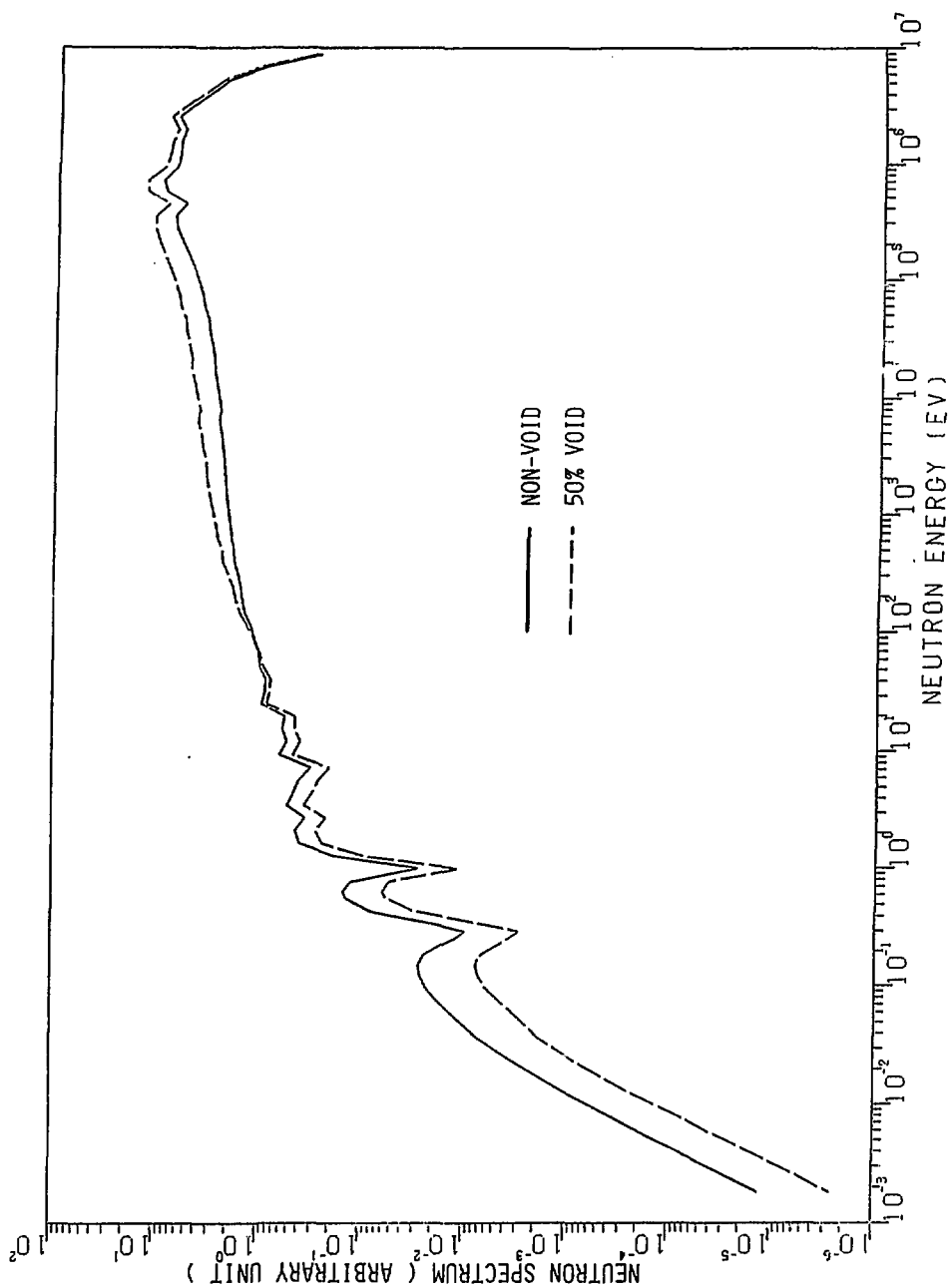to ^{238}U capture cross section

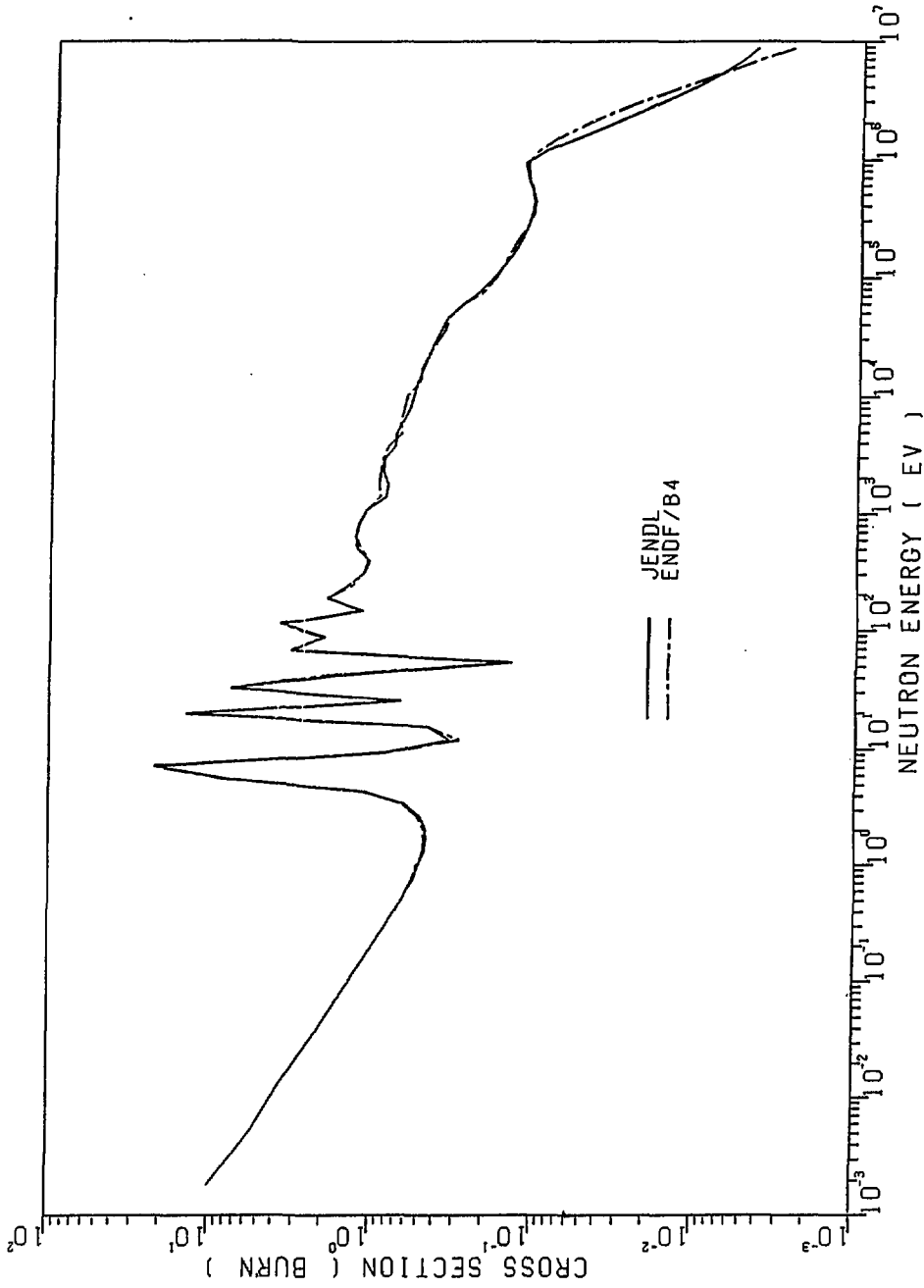Fig. 3   Neutron spectrum in fuel region of case 1 cell

Fig. 4 Comparison of ^{238}U capture cross section between JENDL-2 and ENDF/B-IV
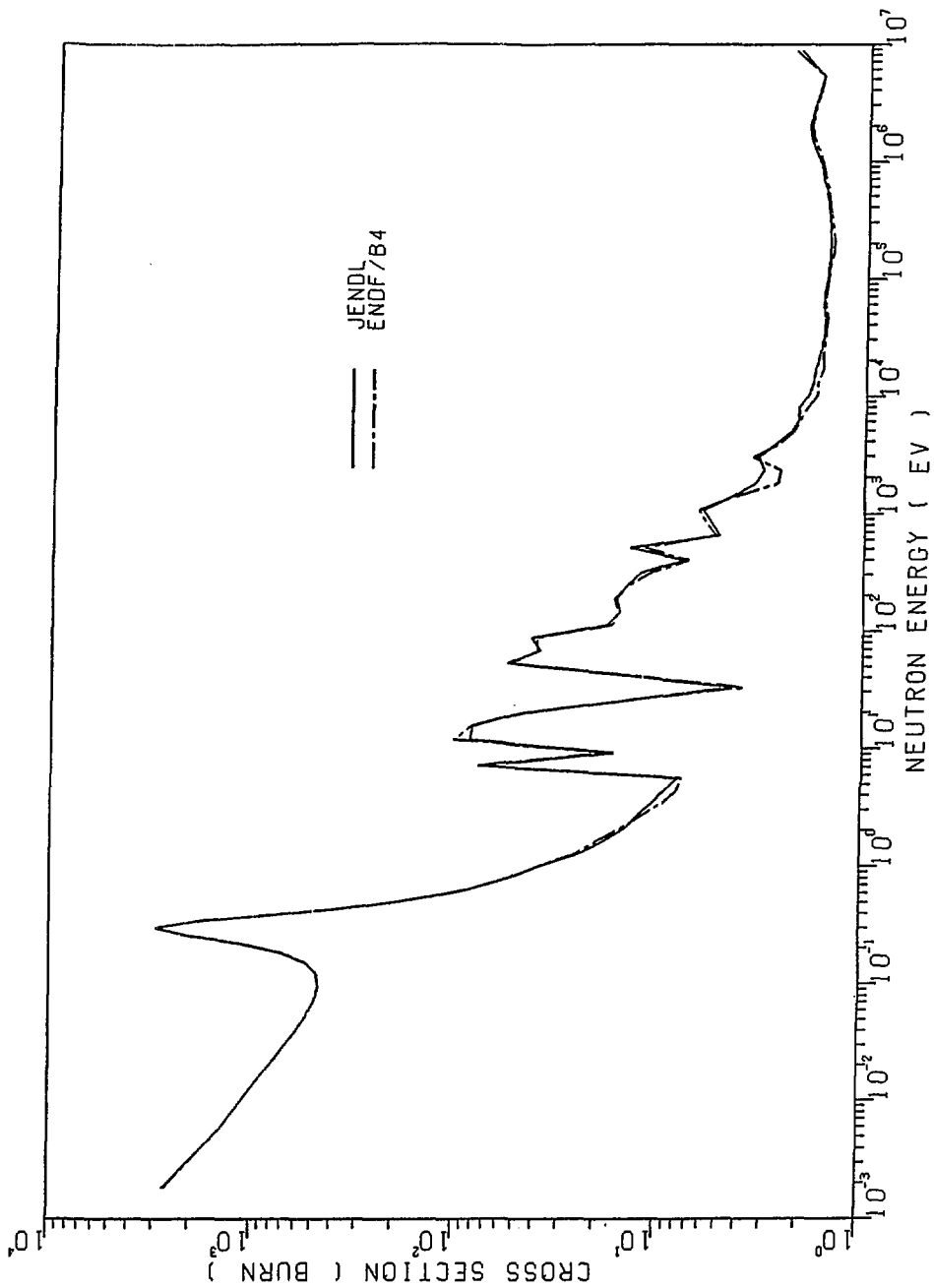
Fig.5   Comparison of ^{239}Pu fission cross section
between JENDL-2 and ENDF/B-IV

4.5 Comments from Nuclear Data Side

4.5.1 Resonance Parameters of ^{238}U

Tsuneo NAKAGAWA

Japan Atomic Energy Research Institute

Tokai-mura, Naka-gun, Ibaraki-ken

The present status of experimental and evaluated resonance parameters of ^{238}U are briefly reviewed. The parameters stored in JENDL-2 are accurate enough for low lying levels. At high energies, activities of NEANDC Task force on ^{238}U discrepancies are summarized. For JENDL-3, the resonance parameters will be evaluated up to 10 keV, if possible, by taking into account new values of parameters obtained by Olsen. Tentative calculation from the Olsen's parameters is shown.

1. Introduction

     The IAEA consultants' meeting on uranium and plutonium isotope resonance parameters was held at Vienna in 1981 and the following accuracy requirements[1] were confirmed.

 (1) For thermal reactors

        Radiative width   1 meV.

        Neutron width   2 % for the 6.67-eV resonance,

                               3 % for the 20.9-eV resonance,

                               5 % for the 36.7-eV resonance.

 (2) For fast reactors

        Average resonance parameters (S_0, S_1, D, $<\Gamma_\gamma>$) 5 %,

        Capture cross section (100 eV − 100 keV)   3 %.

These requirements seem to be achieved for thermal reactors and not to be satisfied for fast reactors. The evaluation of ^{238}U resonance parameters is in progress for JENDL-3. In the present evaluation, some modifications will be made to the resonance parameters evaluated for JENDL-2[2]. In the following, status of the resonance parameters are reviewed briefly.

2. Low Energy Region

In the energy region below 100 eV, the first three s-wave resonances are paticularly important for thermal reactors. Table 1 shows the relative absorption rate of low lying resonances to the total absorption by ^{238}U in PWR[3]. It is seen from the table that the contributions from the first three resonances is about 55 %. Therefore, accurate values of these resonance parameters are strongly required.

Figure 1 shows measured neutron and radiative widths of the 6.67-eV resonance. The accuracy requirement is drawn with dashed lines around the values evaluated for JENDL-2. The measured values of Γ_n have converged upon 1.5 meV since the measurement by 62Jackson+[4]. The accuracy of 2 % is satisfied for this resonance. On the radiative width, the accuracy requirement of 1 meV seems to be achieved since 1977, while the values by 77Liou+[5] and by 82Block+[6] are somewhat lower than JENDL-2 evaluation. In the case of the 20.9-eV resonance, the measured values satisfy the accuracy requirements since 1977, except the value of Γ_n by 82Block+[6]. From these figures, we may conclude that the low lying resonance parameters of JENDL-2 are accurate enough to fulfil the requirements from thermal reactor designers. However, it is needed to do further study on the discrepancy of Γ_n values among 82Block+ and others.

On the capture cross section at 0.0253 eV, Poenitz et al.[7] reported the new measured value of 2.680±0.019 barns which is about 1 % lower than ENDF/B-V and JENDL-2 evaluation of 2.7 barns. Another recent value is 2.721±0.016 barns by Bigham et al.[8] In the NEANDC-INDC Joint Discrepancy File, de Saussure[9] suggested that Bigham et al.'s value became 2.792 barns after renormalization with the new ^{235}U absorption cross section. Therefore, the discrepancy among recent measurements is rather large. This discrepancy should be resolved.

The most recently measured capture cross sections in the low neutron energy region are those by Liou and Chrien[5] at BNL. Figure 2 shows the comparison of JENDL-2 and the experimental data in the energy range from 1 to 25 eV. The solid curve calculated from the resonance parameters of JENDL-2 reproduces well the data of Liou and Chrien between 6.67-eV and 20.9-eV resonances. At energies below the 6.67-eV resonance, JENDL-2 is slightly larger than the experimental data.

The values of capture resonance integral are listed in Table 2. The measured data are scattered from 265 to 282 barns. Recently Kobayashi[10] reported the value of 277±12 barns, and Mughabghab[11] recommended that of 277±3 barns. The values of resonance integral calculated from ENDF/B-V and JENDL-2 are very consistent with these experimental values.

As for the elastic scattering cross section at 0.0253 eV, the following values are recommended in BNL-325[12] and by Mughabghab[11], respectively.

    BNL-325 (3rd) = 8.90 ± 0.16 barns

    Mughabghab   = 9.38 ± 0.09 barns.

The evaluations for ENDF/B-V and JENDL-2 are almost the same as the recommendation of BNL-325 (3rd). The subthreshold fission cross section was measured at 0.0253 eV by D'Hondt et al.[13] with the Grounoble High Flux Reactor. Their value of 11±2 μb is larger than JENDL-2 (2.3 μb) and ENDF/B-V (5.28 μb). The (n,α) cross section of 1.5 μb at 0.0253 eV was reported by Wagemans et al.[14] which is consistent with 1.3±0.6 μb measured by Asgher et al.[15] No evaluated data files store the (n,α) cross section at present.

From the above-mentioned status of JENDL-2 and experimental data, it is seen that the parameters in JENDL-2 are accurate enough and, if modification is needed, the elastic scattering and the subthreshold fission cross sections will be increased a little around the thermal neutron energy.

3. Resolved Resonance Region

    In the resolved resonance region, large systematic discrepancies have been found among neutron widths measured so far. Figure 4 shows the local s-wave strength functions calculated in the 500-eV intervals. Those obtained from JENDL-2 are written also in the figure. Below 1.5 keV, the discrepancies are relatively small. Above 1.5 keV, however, the large discrepancies are found. In order to satisfy the requirements from fast reactor designers, these discrepancies should be resolved.

    The NEANDC organized the task force on this problem at its 23rd meeting in Chalk River, Canada in September 1982. The activity of the task-force was reported by Nakajima[16] at the Nuclear Data Seminar in 1984, and by Sowerby[17] at the Santa Fe conference in 1985.

The NEANDC task force reanalysed transmission data measured at Geel[18], JAERI[19] and ORNL[20] with the shape analysis, because Derrien and Ribon[21] proposed that the shape analysis removed discrepancies among resonance parameters obtained with the area analysis. The reanalysis was performed in three energy intervals of 1460 to 1820 eV, 2470 to 2740 eV and 3820 to 4000 eV.

Figure 5 illustrates the results by Olsen[22] who did the reanalysis with the shape analysis code SIOB[23]. From Fig. 5, it is seen that discrepancies among new parameters are smaller than those among reported values, especially in Region 2. It is also evident that reanalysis gives neutron widths larger than originally reported ones in every energy region. The evaluated values in ENDF/B-V and JENDL-2 are also shown in Fig. 5, and they are smaller than the reanalysis.

It was found from the reanalysis that the main reason of the discrepancies was incorrect resolution functions assumed by experimenters, and that the correct resolution functions were wider and more complex than the assumed ones.

The task force decided reanalysis of the resonance parameters in wide energy region. The upper energy was selected to be 10 keV based on the recent requirements[24]. Olsen[25] has performed the reanalysis of ORNL transmission data with SIOB in the energy range from 1 to 10 keV. Moxon also did reanalysis of the same data with REFIT[26] in the energy range from 7.4 to 8.4 keV. Their reanalyses were completed just before the Santa Fe Conference. However, significant differences were found again in the large values of Γ_n, and they might be due to resolution function differences.

Sowerby concluded as follows in his report to the Santa Fe Conference;

1) Discrepancies are due to experimental resolution function.
2) Presently published Γ_n values are in error. Reanalysis is necessary.
3) All existing evaluations of resolved resonance parameters are in error. Ideally reevaluation must wait for the reanalysis to be completed.
4) Improvements are required to resonance analysis codes.
5) Etc.

However, the reevaluation for JENDL-3 will be done on the basis of these new data by Olsen[25]. Olsen obtained the parameters of 676 levels. Figure 6 shows a staircase plot of the number of resonances. The lower straight line is the number of s-wave resonances estimated from

D_0 = 20.9 eV. No levels were missed at least for s-wave resonances. On trial, pointwise cross sections were calculated from the Olsen's parameters, by assuming that all resonances were s-wave ones, the average radiative width 23.5 meV, the effective scattering radius 9.66 fm, and by using the multi-level Breit-Wigner formula. The pointwise cross sections were averaged in suitable energy intervals, and compared with JENDL-2.

Figure 7 is a comparison of the capture cross section. Olsen's parameters give the capture cross section smaller than JENDL-2 above about 2.5 keV. This underprediction is mainly due to level-missing of p-wave resonances. In the case of JENDL-2 evaluation, the level-missing of p-wave resonances was found also in the energy range from 1.5 to 4.0 keV as is shown in Fig. 8. Therefore, the background cross sections in Eq. 1 was given to compensate the p-wave level missing.

$$\Delta\sigma_{cap} = 0.0032\sqrt{E} - 4.8126 \frac{1}{\sqrt{E}}, \tag{1}$$

where E is neutron energy in eV. If this background cross section is adopted up to 10 keV, the modified capture cross section becomes very similar to JENDL-2. This result shows that the new parameters obtained by Olsen can be adopted up to 10 keV by correcting with the suitable background data. As for the total cross section, p-wave assignment is important. Therefore, the present calculation gave too large values at the higher neutron energies.

4. Conclusion

The present status of ^{238}U resonance parameters was reviewed briefly, and following conclusions were obtained for JENDL-3 evaluation.

1) The resonance parameters of low lying s-wave resonances can be taken from JENDL-2 after slight modification.

2) The energy region of resolved resonances should be extented up to 10 keV by adopting the parameters obtained by Olsen.

3) At high energies, the background correction due to p-wave
   level missing is necessary.

It is suggested frequently that large background correction should
be avoided, because they give unresonable shielding factors in the cases
of large potential cross sections. And, it was also pointed out that
if large number of p-wave resonances are missed Doppler effect cannot be
calculated properly. Detailed studies are required for these problems.

From the result of adjustment study of JENDL-2[28] data, it was
found that smaller capture cross section than JENDL-2 is preferable in
the resolved and unresolved resonance regions. On this point, however,
the present evaluation has not yet been completed for the resonance
parameters. More investigation is needed to get final results for
JENDL-3.

References

 1) Rowlands J.L. : "Proc. of IAEA Consultant Meeting on Uranium and
    Plutonium Isotope Resonance Parameters", INDC(NDS)-129/GJ, p.8
    (1982).

 2) Nakagawa T., et al. : "Evaluation of Resonance Parameters of ^{233}U,
    ^{235}U, ^{238}U, ^{239}Pu, ^{240}Pu, ^{241}Pu and ^{242}Pu", JAERI-M 9823 (1981).

 3) Tellier H. : "Proc. of IAEA Consultant Meeting on Uranium and
    Plutonium Isotope Resonance Parameters", INDC(NDS)-129/GJ, p.47
    (1982).

 4) Jackson H.E. and Lynn J.E. : Phys . Rev., 127, 461 (1962).

 5) Liou H.I. and Chrien R.E. : Nucl. Sci. Eng., 62, 463 (1977).

 6) Block R.C., et al. : Nucl. Sci. Eng., 80, 263 (1982).

 7) Poenitz W.P., et al. : Nucl. Sci. Eng., 78, 239 (1981).

 8) Bigham C.B., et al. : Can. J. Phys., 47, 1317 (1969).

 9) de Saussure G. : "Nuclear Data Discrepancies 1983", p.30 (1984).

10) Kobayashi K., et al. : private communication (1985).

11) Mughabghab S.F. : "Neutron Cross Sections, Vol.1, Neutron Resonance
    Parameters and Thermal Cross Sections, Part B: Z = 61-100", Academic
    Press (1984).

12) Mughabghab S.F. and Garber D.I. : "Neutron Cross Sections, Vol.1,
    Resonance Parameters", BNL 325, 3rd., Vol.1 (1973).

13) D'Hondt P., et al. : Ann. Nucl. Energy, 11, 485 (1984).

14) Wagemans C., et al. : Nucl. Phys., A362, 1 (1981).

15) Asgher M., et al. : Nucl. Phys., A259, 429 (1976).

16) Nakajima Y. : "Proc. of the 1984 Seminar on Nucl. Data", JAERI-M 85-035, p.196 (1985).

17) Sowerby M. : "Proc. of the International Conf. on Nucl. Data for Basic and Applied Science", Santa Fe, 13-17 May, 1985, Vol.2, p.1511 (1986).

18) Poortmans F., et al. : "Proc. IAEA Consultant Meeting on Uranium and Plutonium Isotope Resonance Parameters", INDC(NDS)-129/GJ, p.112 (1981).

19) Nakajima Y. : Ann. Nucl. Energy, 7, 25 (1980).

20) Olsen D.K., et al. : Nucl. Sci. Eng., 69, 202 (1979).

21) Derrien H. and Ribon P. : NEANDC(E)163U, p.63 (1975).

22) Olsen D.K. : "Report to the ^{238}U Discrepancy Task Force on SIOB Fits to the ORNL, CBNM and JAERI Transmission Data", ORNL/TM-9023 also ENDF-338 (1984).

23) de Sanssure G., Olsen D.K. and Perez R.B. : "SIOB : A Fortan Code for Least-Squares Shape Fitting Several Neutron Transmission Measurements Using the Breit-Wigner Multilevel Formula", ORNL/TM-6286 (1978).

24) Froehner F. : "Proc. of IAEA Consultant Meeting on Uranium and Plutonium Isotope Resonance Parameters", INDC(NDS)-129/GJ, p.15 (1982).

25) Olsen D.K. : Nucl. Sci. Eng., 94, 102 (1986).

26) Moxon M.C. : "Proc. of Specialists' Meeting on Neutron Data of Structural Materials for Fast Reactors", CBNM Geel, 5-8 Dec. 1977, p.644 (1977).

27) Takeda T., et al. : "Proc. of the 1985 Seminar on Nuclear Data", JAERI-M 86-080, p.228 (1986).

28) Grintakis E.M. and Kim J.I. : J. Radioanal. Chem., 42, 181, (1978).

Table 1

Absorption Rate in the First Resonances

of Uranium 238 Relatively to the Total Resonance Absorption

Resonance eV	6.67	20.9	36.7	66	80.7	102.6 116.4 189.6
Absorption %	27.7	15.2	11.9	5.2	2.8	6.7

(taken from Ref.3)

Table 2   Resonance integrals of ^{238}U

Reference			Values (barns)	
Macklin	JNE, 2, 243	(1956)	281	± 20
Hardy	NSE, 14,358	(1962)	282	± 8
Sampson	GA-3069	(1962)	265	
Baumann	DP-817	(1963)	281	
Steinnes	JIN, 34, 2699	(1972)	267	± 5
Linden	JRC, 20, 695	(1974)	265	± 21.8
Underhill	DA/B, 34, 6027	(1974)	269.4	± 5
Kobayashi[10]			277	± 12
Mughabghab[11]			277	± 3
ENDF/B-V			279.5	
JENDL-2			279.1	

This table was mainly based on Ref.28

6.67-eV Resonance
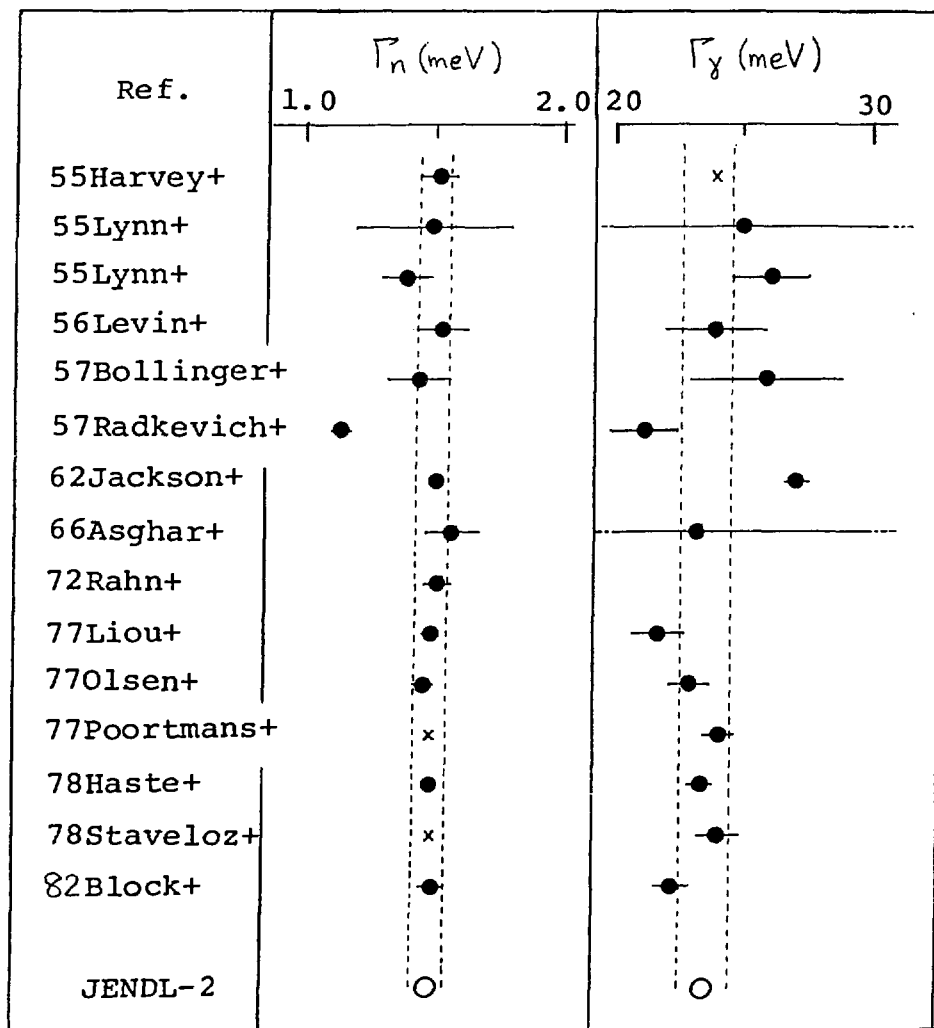
Fig.1. Comparison of Γ_n and Γ_γ values of the 6.67-eV resonance
The required accuracies are shown with dushed lines around the
evalualed values for JENDL-2.

20.9-eV resonance
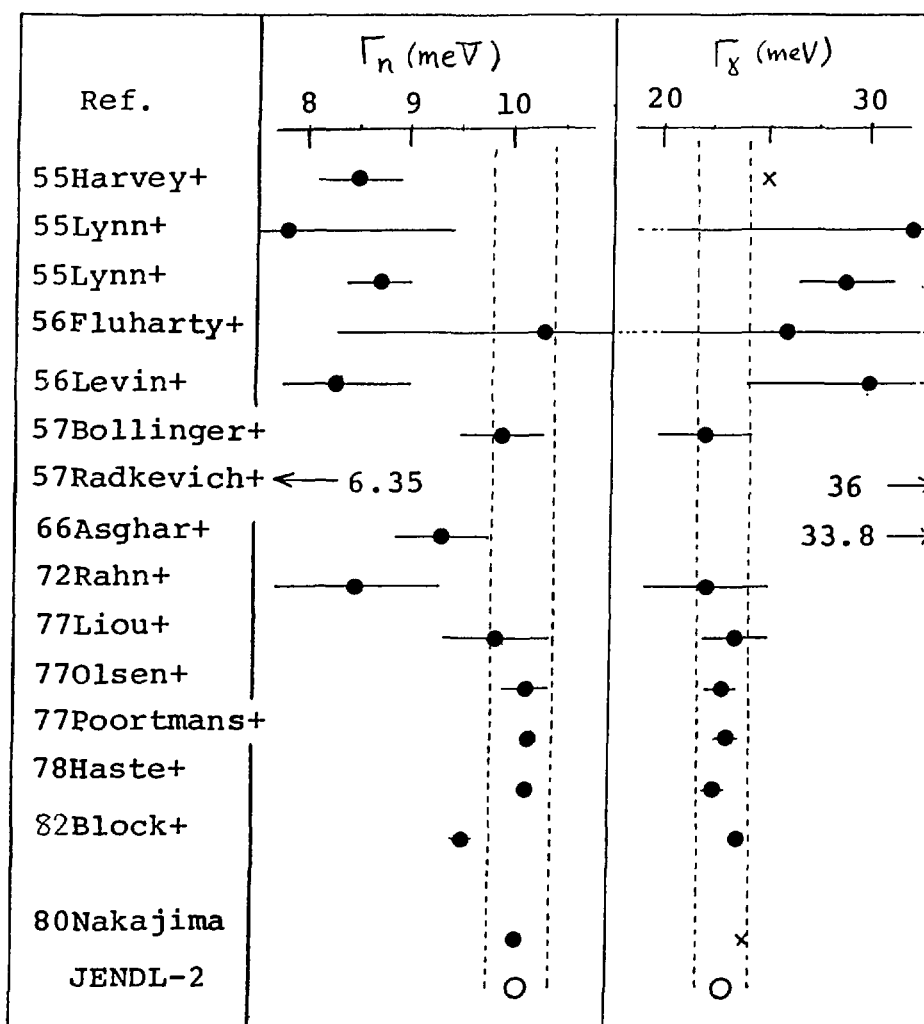
Fig.2. Comparison of Γ_n and Γ_γ values of the 20.9-eV resonance
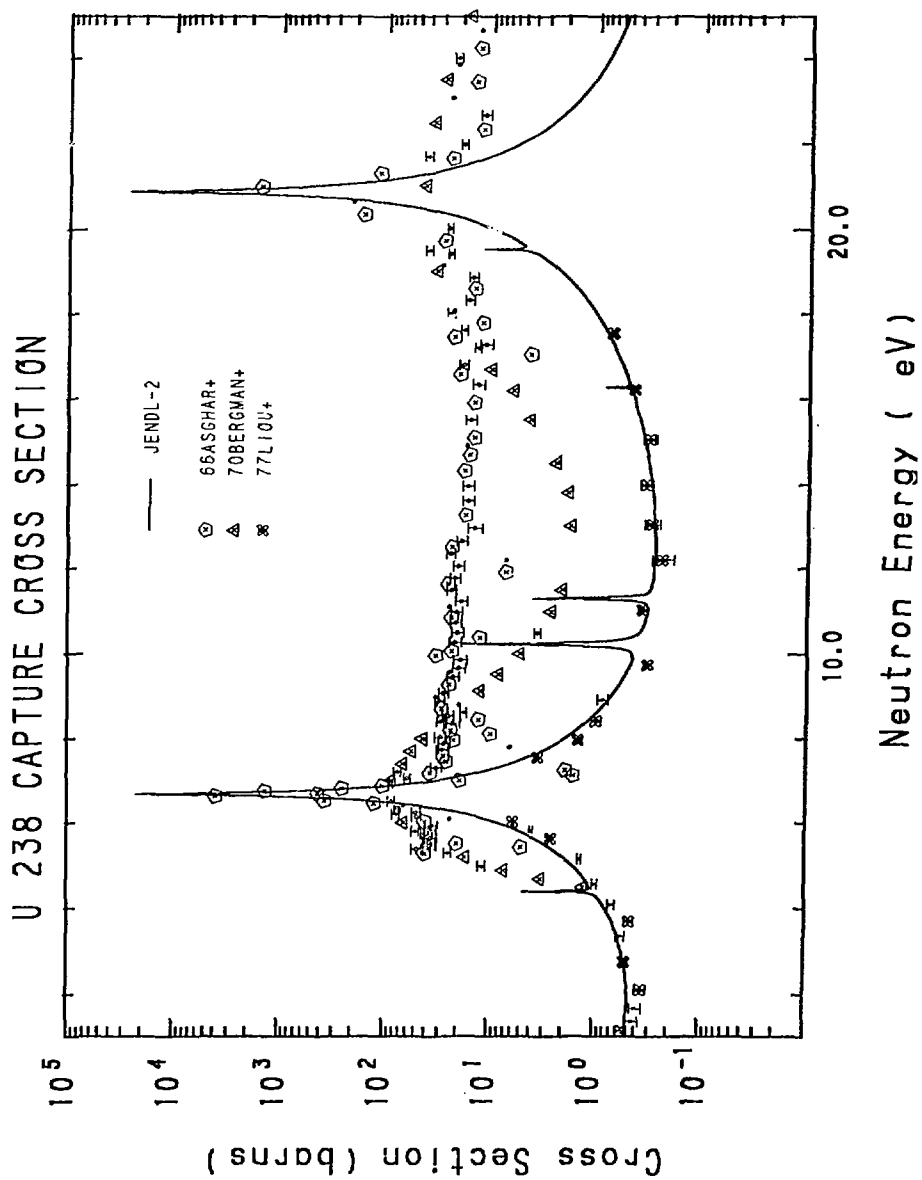
Fig.3. Capture cross section in the energy range from 1 to 25 eV
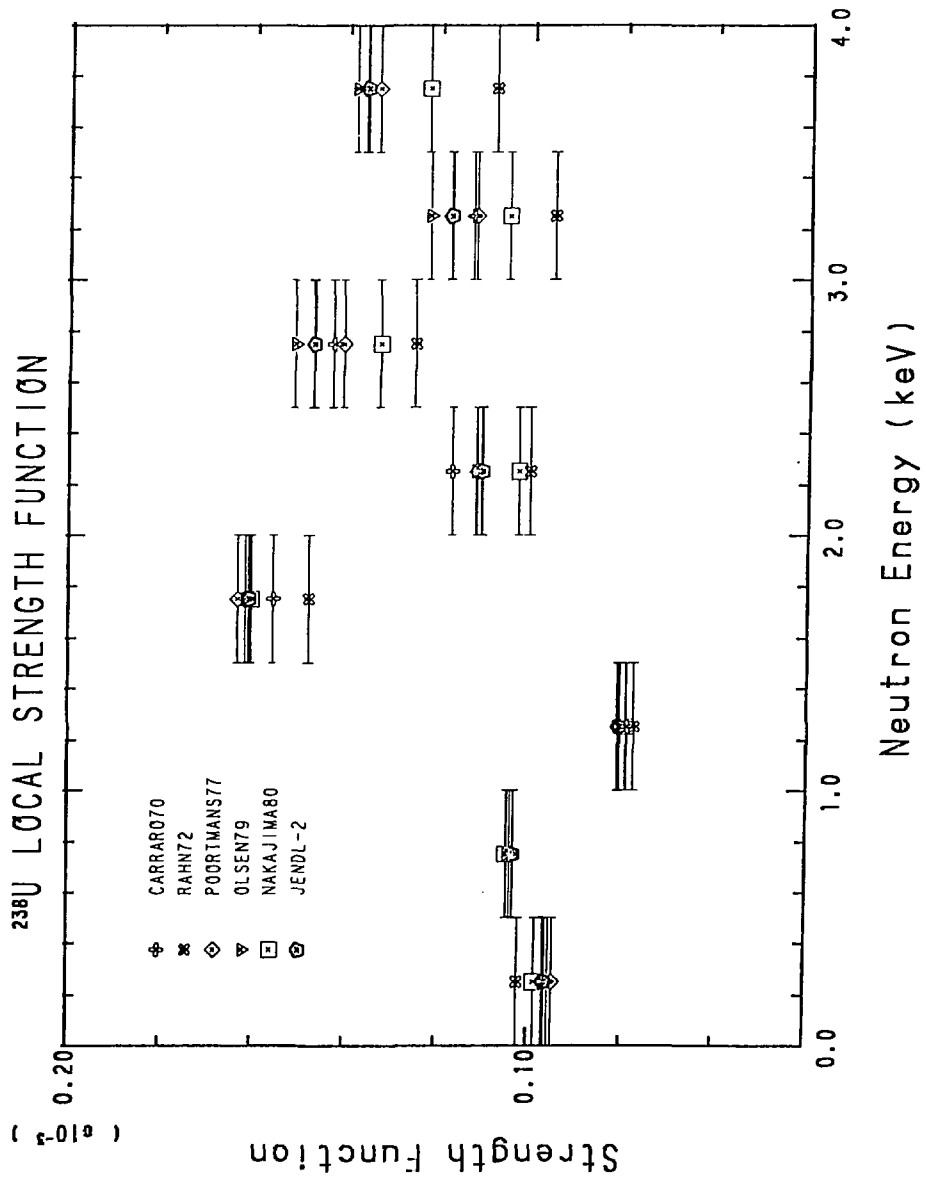
Fig.4. Comparison of local s-wave strength functions
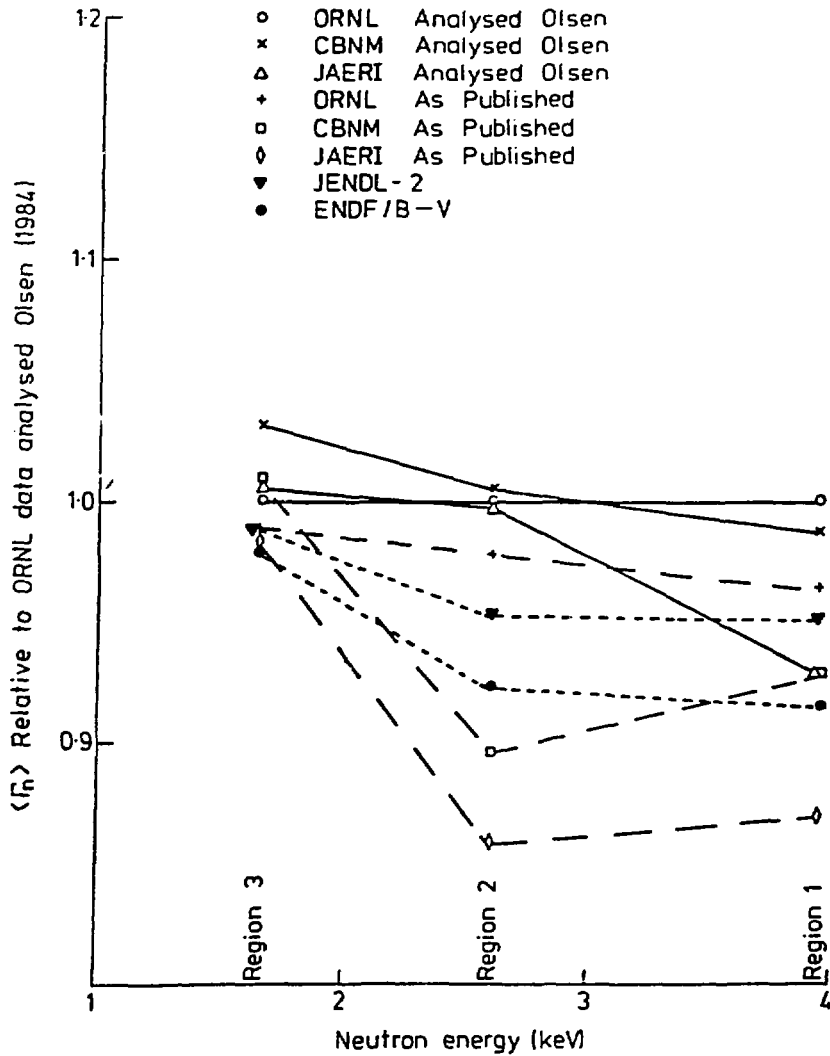
Fig.5. Results of reanalysis by Olsen[22]

Average values of Γ_n are shown as relative values to reanalysed ORNL data. Dushed lines connect the originally published values, solid lines the reanalysed ones and dotted lines the evaluated values for JENDL-2 and ENDF/B-V. This figure was taken from Ref.17.
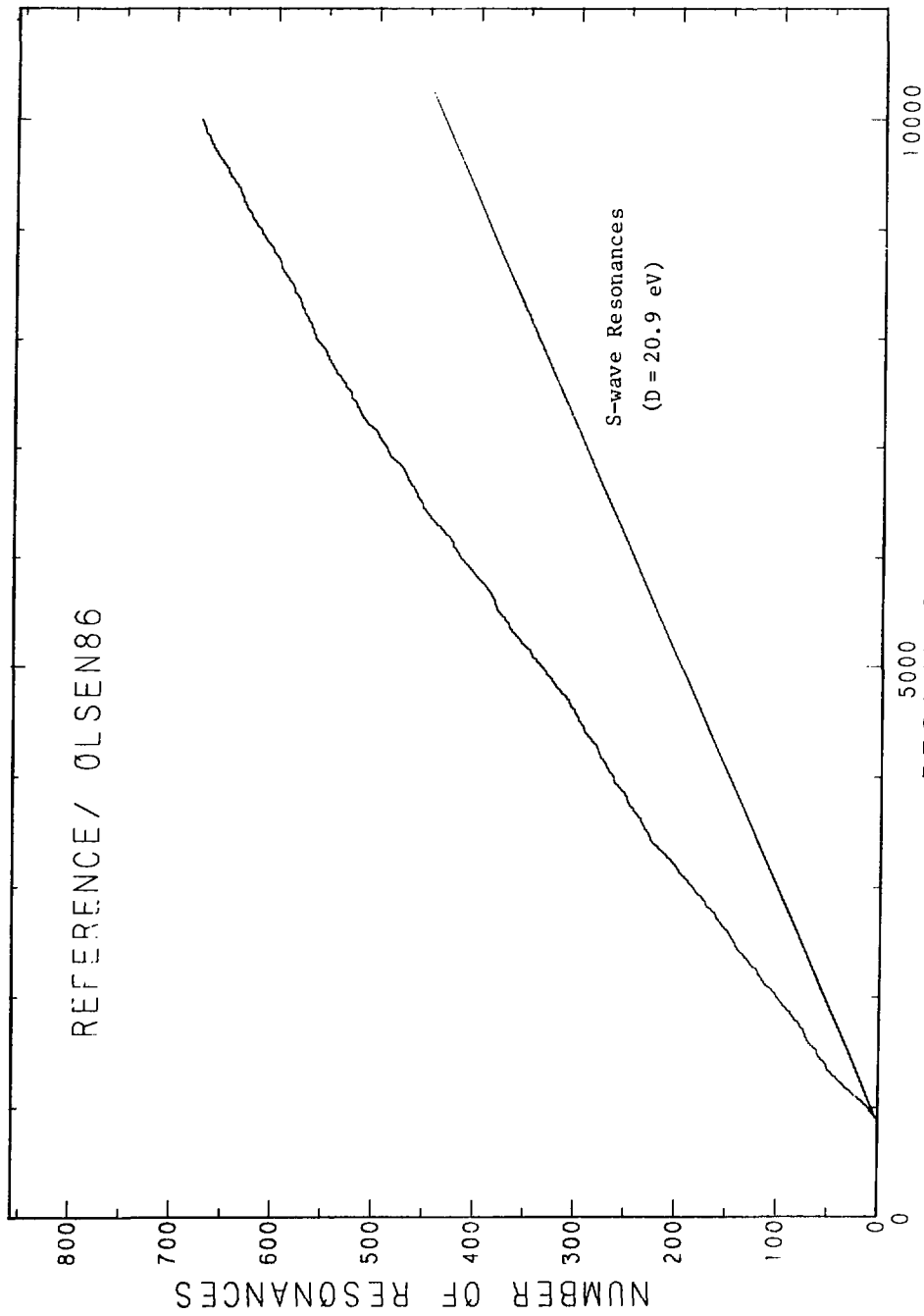
Fig.6. Staircase plot of number of resonances reanalysed by Olson. A lower solid line shows the expected number of s-wave resonance from D = 20.9 eV.
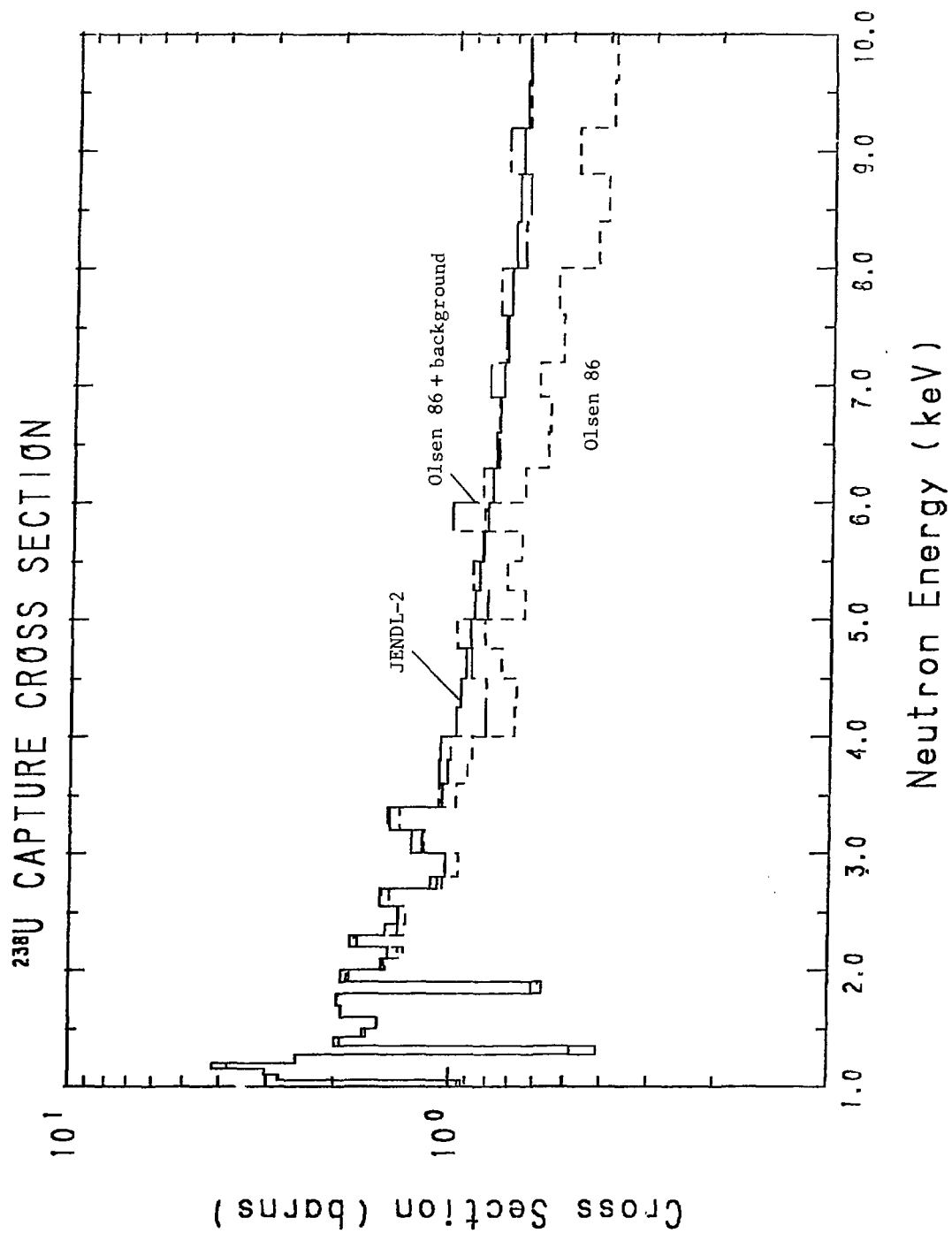
Fig.7. Capture cross section above 1 keV.
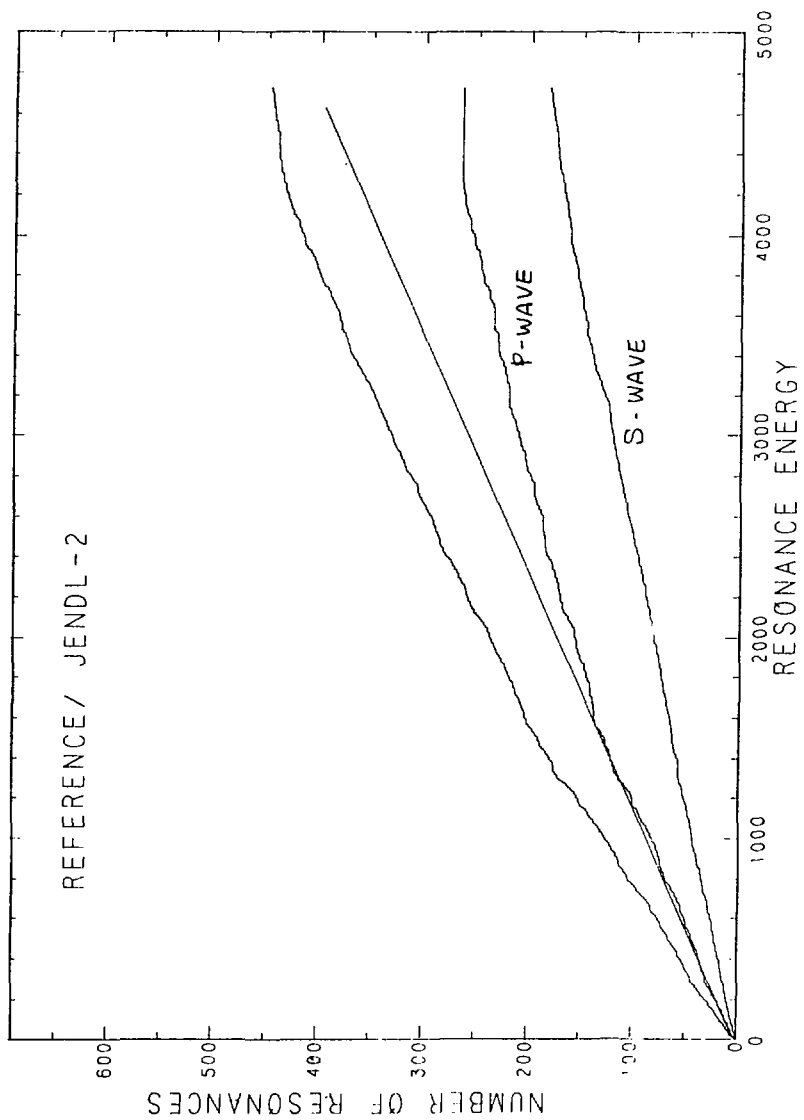
Fig.8. Number of resonances stored in JENDL-2.

4.5.2 Pu-239 Nuclear Data

M. Kawai

NAIG Nuclear Research Laboratory

Nippon Atomic Industry Group Co., Ltd.

Ukishima-cho, Kawasaki-ku, Kawasaki-shi

Some remarks on the nuclear data of Pu-239 are presented from viewpoint of HCLWR study. Resolved resonance parameters for JENDL-2 are on the basis of the data evaluated by Ribon, with the single level Breit-Wigner formulas. It is, however, pointed out that the interference effect between resonance levels upon the fission cross section is significant and multi-level formalism must be adopted to future evaluated data file. Recent experimental data for fission cross sections and multiplicities of prompt fission neutrons are also compared with the JENDL-2 data. The simultaneous evaluation of fission cross sections for main important actinides shows that Pu-239 fission cross sections in 50 keV - 1 MeV become smaller by 1 - 5 % than JENDL-2. This result may be discrepant with the requirement for JENDL-2 data modication, proposed from the integral test. The discrepancy between the differential and integral data may be reduced to some degree by slightly larger values of recently measured multiplicity of prompt fission neutrons below 100 keV.

1. Introduction

     For nuclear design of HCLWR (High Conversion Light Water Reactor), neutron cross sections of Pu-239, particularly the data in the resonance energy region, are more important than LWR. For example, Pu-239 fissions in the resonance energy region show large contributions to neutron balance in the case of HCBWR, while the fissions of LWR are determined by thermal fissions of U-235 and Pu-239.[1] After the JENDL-2 evaluation[2], several cross section measurements have been reported for Pu-239, and some discrepancies between the experimental data and JENDL-2 data become perceptible. In this report, the author gives some comments about the present status of Pu-239 nuclear data

such as resonance parameters, fission cross sections and prompt fission neutron numbers, which play the most important role to predict the HCLWR core characteristics, comparing the JENDL-2 data with the recent experimental data.

2. Resonance Parameters.

The resonance file (MF=2) of Pu-239 in JENDL-2 contains the resolved reonance parameters up tp 660 eV and unresolved resonance parameters in the energy range from 660 eV to 30 keV. The former is expressed with the Breit-Wigner's single level formula and based on the analysis of Ribon and LeCoq[3]. It is accompanied by smooth background cross sections in the file 3 (MF=3), so as to reproduce Blon's fission cross section data[4] at energies off resonances by adding them to the resonace cross sections calculated from the resonace parameyters. Unresolved resonance parameters are energy-dependent and were determined by the ASREP code[5], by fitting to the total, fission and capture cross sections.

However, there are following problems in the resonance parameters on the basis of the single level formula:

a) Single level formalism is unsatisfactory to correctly describe the fission cross sections which are influenced by interference effect between the levels having the same spin.[6]

b) The smooth background cross section given in the file is independent to temerature. It brings about misaccount of the Doppler effect, in reactor calculations.

Multilevel formalism due to R-matrix theory is a key to solve the problems mentione above. However, available data before 1985 were limited in the energy range; the maximum energy was 214 ev at the highest. Recently, Derrien et al.[7] have made resonace analysis with the Reich-Moore's multilevel formula. In the analysis, recent experimental data of fission cross section and transmission data were used, and the parameters for 375 levels were determined as a result.

Figure 1 compares the fission cross sections calculated from their parameters, denoted by ORNL86 with the JENDL-2 and the experimental data. Derrien's result shows better agrrement with the experimental data even at off-resonance energies than JENDL-2. Table 1 and Fig. 2 also compares the energy average fission cross sections over the 10- to

1000-eV energy range and ratios to JENDL-2 data. JENDL-2 deviates from the recent experimental data of Weston-Todd[8] and Wageman et al.[9]; this means that JENDL-2 data must be modified anyhow. On the other hand, the result by Derrien et al. agrees with the experimental data up to 1 keV, which is the highest analyzed for Pu-239 resolved resonances. Accordingly, it can be said that the multilevel parameters of Derrien et al. is the most useful for new evaluation of Pu-239. However, the following problems let the evaluator hesitate to adopt them. First, it is a question whether he accepts the Reich-Moore's multilevel formula for his reactor analysis code system, since reactor analyst is used to employ the Breit-Wigner's (single- or multi-level) or Adler-Adler's (multilevel) formulas for convenience of calculation of resonance self-shielded effective cross sections. Second, it is a problem that Reich-Moore's formula is not prepared in the ENDF/B-IV and -V format.

3. Fission Cross Sections

JENDL-2 data were evaluated on the basis of the experimental data before 1979. In the evaluation, mainly adopted were the ratio data of Carlson-Behrens[10], the absolute measurement by Gwin et al.[11] and the shape measurement by Gayther et al.[12] The shape measurement data were renormalized to the Gwins' data, with consideration of the requirement to fission cross section, proposed from from the integral test[13], so as to reproduce the criticality and fission rate ratios in the fast critical assemblies. As a result, JENDL-2 fission cross sections were determined to be considerably higher than JENDL-1.

Table 2 gives a list of new measurements for Pu-239 fission cross section, reported after the JENDL-2 evaluation. Figure 2 shows that the expermental data agree with each other up to 1 keV, but that discrepancy between different measurements becomes prominient above 1 keV. Compared with the recent experimental data in 1980 years, overpredicting trend of JENDL-2 is obvious and some modification is needed. Weston-Todd's data[8] are generally the lowest in the high resolution experiments above 1 keV. It is, however, questionable if their data, which were adopted in the resonance analysis by Derrien et al.[7], is the most reliable. Judging data reliability may be made by simultaneous evaluation of fission cross sections and ratio to U-235 fission cross section, because agreement of ratio data between different measurements

is better than that of absolute data.

Aboｖe 50 keV, simultaneius evaluations of fission and capture cross sections for heavy isotopes important to fission reactors were preliminarily made[14] for JENDL-3. It was based on the least squares method, taking account of covariance matrices of the experimental data. Covariance matrixces were obtained using the partial errors and the estimated correlation coefficients. Evaluated quantities are as follows: fission cross sections for U-235, U-238, Pu-239, Pu-240 and Pu-241; ratio to U-235 fission cross sections for U-238, Pu-239, Pu-240 and Pu-241 fission and forU-238 capture; capture cross sections for Au197, U238 and Pu240; and ratio to Au-197 capture cross sections for U-238 and Pu-240 capture. The results for Pu-239 are shown in Figs. 3 and 4. The evaluated ratio of Pu-239 to U-235 fission cross section is in good accordance with the experimental data, as shown in Fig. 3. Evaluated fission cross section is smaller by 0 - 10 % than JENDL-2 below 1 MeV, although it is larger than Westons' data which were not considered in the evaluation. Above 1 MeV, evaluated data generally agree with Kari's data[15], except for the energies above 7 MeV.

Finally, it is summarized that the recent data of Pu-239 fission cross section are several percent smaller than JENDL-2. The ratio is as follows:

10 eV to 1000 eV	:	0.87 to 1.02,
1 keV to 100 keV	:	0.89 to 1.04,
100 keV to 1 MeV	:	0.92 to 1.00,
1 MeV to 20 MeV	:	0.98 to 1.06.

The smaller fission cross section will decrease neutron multiplication of HCLWR with some degree. The effect may be severer for fast breeder reactor than HCLWR, because small ratios in the energy range below 1 keV are mainly observed at the energy intervals where fission cross section is small. Below 50 keV, further investigation by means of simultaneous evaluation method is needed. However, the result that will gives smaller values than JENDL-2 may still remain and produce a severe discrepancy with the requirement from the reactor analysts on the basis of the integral test of JENDL[13,16,17].

4. Multiplicity of Prompt Fission Neutrons.

JENDL-2 data are essentially same as JENDL-1[18], except for standard values of Cf-252 spontaneous fission numbers (3.756 for JENDL-1 and 3.757 for JENDL-2). Accordingly, the base data used for JENDL-1 evaluation are those measured before 1974. Table 3 lists new data after JENDL-1 evaluation. Figures 5 and 6 compares JENDL-2 and new experimental data. The recent data of Gwin et al.[19,20] and the revised data of Soleilhac et al.[21] show a significant difference from JENDL-2 data. The following points are noted about the experimetal data:

   0.1 eV to 50 eV: The experimental data are about 0.6 % lower than JENDL-2.

   50 eV to 100 keV: The experimental data show unaccountable structure and are slightly larger than JENDL-2 at the energies between 50 eV – 300 eV and 1 keV – 3 keV.

   Above 1.5 MeV: Experimental data are within 3 % lower than JENDL-2 in the energy range 1.5 and 8 MeV.

Gwin's experiment is only one which reported the structure of Pu-239 fission multiplicity in the energy range below 100 keV, and the value larger than JENDL-2 may give one of the lights to solve the discrepancy between the differential and integral data, which is described in the preceding section.

5. Concluding Remarks

The data status of resolved resonance parameters, fission cross sections and multiplicity of prompt fission neutrons, which play important roles to predict nuclear characteristics of HCLWR is surveyed in the present work. The following results are made clear.

a) For resolved resonance parameters, multilevel formalism is required for describing correctly fission cross sections. At present time, the parameters analyzed by Derrien et al.[7] with Reich-Moore's formula are the most useful. However, it is a question whether reactor analyst will use the Reich-Moore's formula, which should be treated in a different manner as that for Breit-Wigner's formula for calculation of resonance self-shielding effect.

b) The recent data of Pu-239 fission cross section show good agreement with the old data below 1 keV, but large discrepancy in the energy range between 1 keV and 50 keV. They are several percent smaller than JENDL-2. Cross section reduction amounts to about 10% in maximum. The smaller fission cross sections preliminarily derived by the simultaneous evaluation[14] must be contradictory to the requirement from the reactor analyst on the basis of the integral tests, because they will decrease neutron multiplication of reactor with some degree. These discrepancies are problems to be solved hereafter.

c) As for fission neutrons, Gwin's data are within 2 % smaller than JENDL-2 in the MeV energy, while they are slightly larger in the whole energy below 100 keV where some unaccountable structures are observed. The change of evaluated data due to these data may bring about some significant effects on the HCLWR characteristics: it may act on reduction of the dicrepancy between the differential and the integral data, to some degree.

Reference:

1) Mizuta, H.: private communication.

2) Kikuchi, Y., Nakagawa, T., Asami, T., Kawai, M., Matsunobu, H., and Kanda, Y., J. Nucl. Sci. Technol., 22, 593   (1985).

3) Ribon, P. and LeCoq, G.: "Evaluation des donnees neutroniques de ^{239}Pu," CEAA-N-1484 (1971).

4) Blons, J.:   Nucl. Sci. Eng., 51, 130   (1973)

5) Kikuch, Y.: private communication.

6) Derrien, H., "Status of Nuclear Data for the ^{239}Pu Resonance Region," Proc. of Int. Conf. on Nuclear Data for Basic and Applied Science, Santa Fe, 1983, GOrdon and Breach Science Pub., Vol. 1, p. 459 (1985).

7) Dereien, H., de Saussure, G., Perez, R.B., Larson, N.M., and Macjlin, R.L.: "R-Matrix Analysis of the ^{239}Pu Cross Sections up to 1 keV", ORNL-TM-10098 (1986).

8) Weston, L.W., and Todd, J.H.: Nucl. Sci. Eng. 88, 567 (1984).

9) Wageman, C., Coddens, G., Weigman, H., and Barthelemy, R.: Ann. Nucl. Energy, 7, 495 (1980).

10) Carson, G.W., and Behrens, J.W.: Nucl. Sci. Eng., 66, 205 (1978).

11) Gwin , R., Silver, E.G., Ingle, R.W., and Weaver, H: Nucl. Sci. Eng., 59, 79 (1976)

12) Gayther, D.B., "Measurement of the ^{239}Pu Fission Cross Section and Its Ratio to the ^{235}U Fission Cross-Section in the Energy Range from 1 keV to 1 MeV," Proc. of Int. Conf. on Nuclear Cross Sections and Technology, Washington D.C., 1975, NBS Spec. Publ. 425, Vol. II, p. 564 (1975).

13) Kikuchi, Y., Hasegawa, A., Hojuyama, T., Sasaki, M., Seki, Y., Kamei, T., and Otake, I.: "Benchmark Tests of Japanese Evaluated Nuclear Data Library (JENDL)," Proc. of Int Conf. on Nuclear Cross Sections for Technology, Knoxville, 1979, NBS Special Pub. 594, p. 581 (1980).

14) Nakagawa, T.: "Nuclear Data Evaluation for Heavy Nuclides," JAERI-M 86-080, p. 213 (1986).

15) Kari, K.: "Messung der Spartquerschnitte von ^{239}Pu und ^{240}Pu relativ zum Spaltquesschnitt von ^{235}U und Streuquerschnitt H(n,p) in dem Neutronenenergiebereich zwischen 0.5 - 20 MeV," KFK 2673 (1978).

16) Takeda, T., Nishigori, T.., Aoyama, T., and Suzuki, T.: "Integral Test for Heavy Nuclides," JAERI-M 86-080, p. 228 (1986).

17) Takeda, T., "Sensitivity Analysis of HCLWR," presented at this seminar, session 4.4. (1986).

18) Kikuchi, Y., Nakagawa, T., Matsunobu, H., Kanda, Y., Kawai, M., and Murata, T.: "Neutron Nuclear Data of ^{235}U, ^{238}U, ^{239}Pu, ^{240}Pu and ^{241}Pu Adopted in JENDL-1 -Preliminary Results-," JAERI-M 6996 (1977).

19) Gwin, R., Spencer, R.R., and Ingle, R.W., Nucl. Sci. Eng., 87, 381 (1984).

20) Gwin, R., Spencer, R.R., and Ingle, R.W., Nucl. Sci. Eng., 94, 365 (1986).

21) Solelhac M., and Frehaut, J., private communications to EXFOR, Accession No. 20490 3 and 20568 4. (1980)

Table 1 Comparison of average fission cross section values
over the 10- to 1000-eV energy range.

En (eV)	JENDL-2[a]	Derrien+ (Reich-Moore)	Weston and Todd (1984)	Blons (1973)	Gwin et al. (1976)	Wagemans et al. (1980)
10 - 20	98.5	98.8 (1.00[b])	100.6(1.02)	-	105.1(1.07)	103.8(1.05)
20 - 30	31.8	31.4 (0.99)	31.5 (0.99)	-	31.6 (0.99)	32.2 (1.01)
30 - 40	4.05	3.09 (0.76)	3.05 (0.75)	-	3.09 (0.76)	2.58 (0.63)
40 - 50	28.5	24.7 (0.87)	25.6 (0.90)	28.6 (1.00)	25.7 (0.90)	25.4 (0.89)
50 - 60	79.2	72.0 (0.91)	72.8 (0.92)	76.8 (0.97)	71.1 (0.90)	73.5 (0.93)
60 - 80	59.3	58.6 (0.99)	57.6 (0.97)	60.5 (1.02)	59.3 (1.00)	60.1 (1.01)
80 - 100	51.5	46.5 (0.90)	47.4 (0.92)	49.7 (0.97)	46.6 (0.90)	48.8 (0.95)
100 - 200	18.7	17.95(0.96)	17.98(0.96)	18.93(1.01)	17.96(0.96)	18.31(0.98)
200 - 300	17.2	17.37(1.01)	17.23(1.00)	17.79(1.03)	17.90(1.04)	17.67(1.03)
300 - 400	9.09	7.91 (0.87)	8.06 (0.89)	8.91 (0.98)	8.48 (0.93)	8.56 (0.94)
400 - 500	9.65	9.19 (0.95)	9.25 (0.96)	9.71 (1.01)	9.40 (0.97)	9.60 (0.99)
500 - 600	15.70	15.00(0.96)	15.04(0.96)	15.51(0.99)	15.46(0.98)	15.14(0.96)
600 - 800	5.48	4.65 (0.85)	4.76 (0.87)	5.29 (0.97)	4.95 (0.90)	4.88 (0.89)
800 -1000	6.37	6.34 (1.00)	6.43 (1.01)	6.84 (1.07)	6.47 (1.02)	6.45 (1.01)

N.B. a) JENDL-2 data below 660 eV are on the basis of Breit-Wigner's single level
parameters analyzed by Ribon-LeCoq, together with background cross sections so as
to reproduce the fission cross sections measured by Blons (1973) at the off-
resonance energies.

b) The value in parenthesis are a ratio to JENDL-2.

Table 2 Fission cross section measurements
after JENDL-2 Evaluations

Category	Author	Energy
Absolute measurement	Weston-Todd (1984)	up to 100 keV.
	Wageman et al. (1980)	up to 30 keV.
	Gwin et al. (1984)	up to 30 eV.
	Meadows et al. (1983)	100 keV to 10 MeV.
	Adamov et al (1979)	14.7 MeV.
	Art et al. (1979)	14.7 MeV.
	Li et al. (1982)	14.7 MeV.
	Zhou et al (1982)	1.0 to 5.4 MeV.
Ratio to U-235 fissions	Varnagy et al (1982)	13.5 to 14.8 MeV.
	Garlea et al. (1983)	14.8 MeV.

Table 3 Measurement of multiplicity of promt fissionneutrons
after JENDL-1 evaluation.

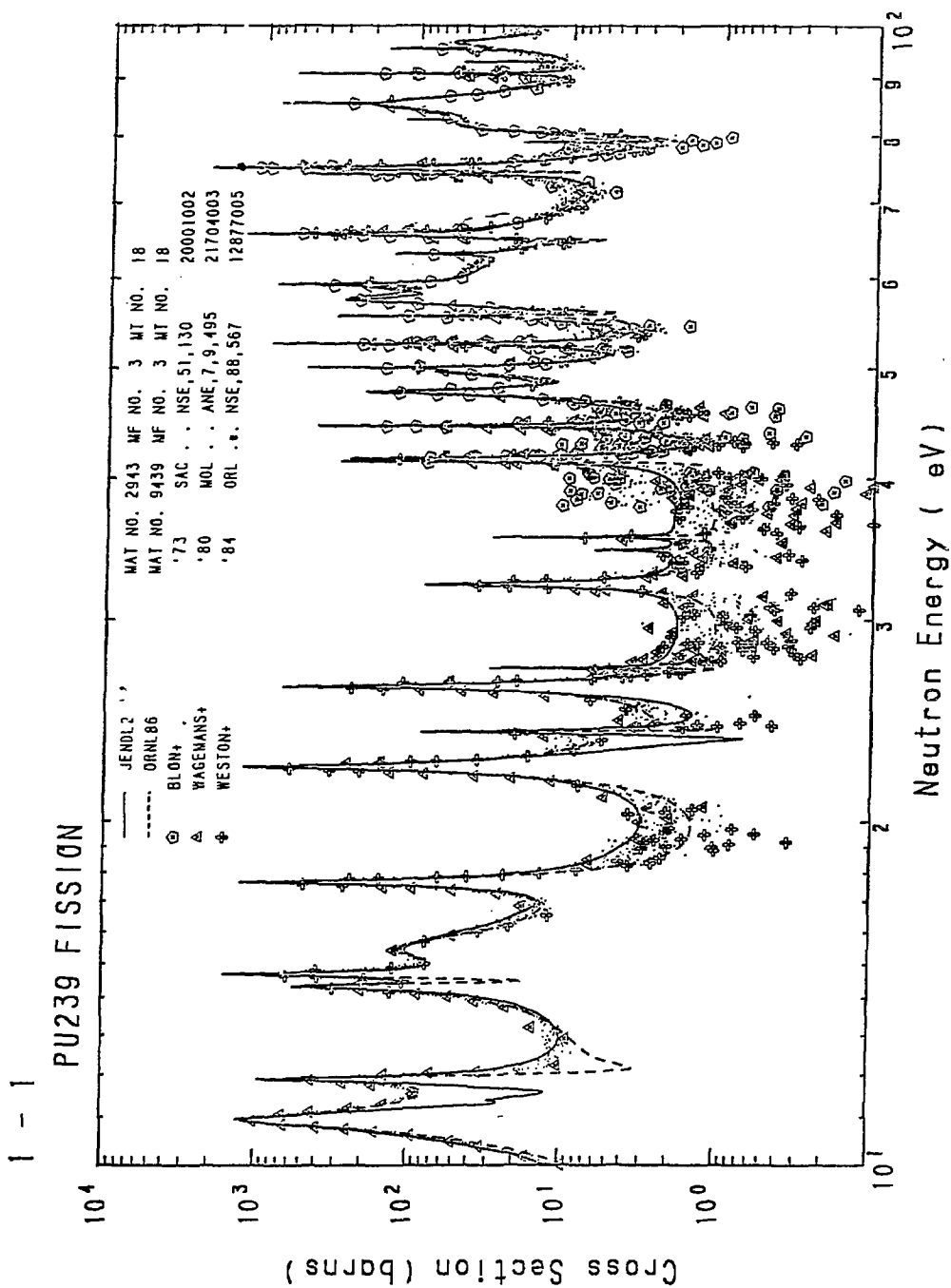| Author	Energy range measured
Nurpeikov et al. (1975)	Thermal to 4.9 MeV.
Khokhlov et al. (1976)	1.1 and 1.8 MeV.
Soleilhac et al. (1980)	0.3 to 1.4 MeV (revision for data in 1970)
Soleilhac et al. (1980)	1.5 to 15 MeV (revision for data in 1969)
Freaut (1980)	22.8 to 28.8 MeV.
Zhang et al. (1980)	0.19 to 1.44 MeV.
Gwin et al. (1984)	0.005 ev to 10 eV.
Gwin et al. (1986)	up to 10 MeV.

Fig. 1 Comparison of Pu-239 fission cross sections in the energy range between 10 eV and 100 eV.
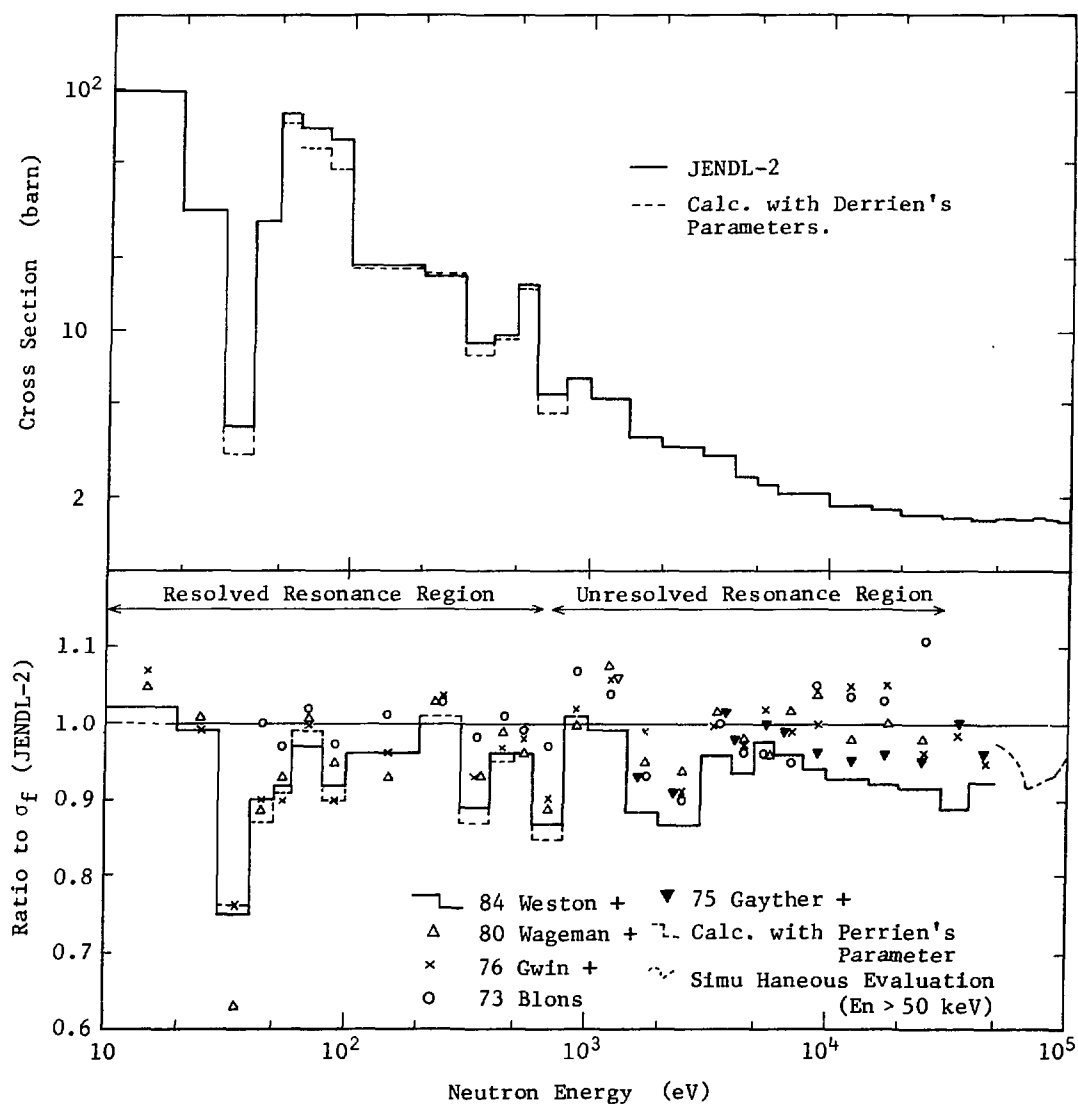
Fig. 2 Comparison of Pu-239 fission cross section calculated from
Derriens' resonance parameters with JENDL-2, and ratio of
measured fission cross sections to JENDL-2 data.

1 - 1 ^{239}Pu FISSION TO ^{235}U FISSION

		MAT NO. 9439		KFK .	NSE, 40,375
		MAT NO. 2943		ANL .	NSE, 40,383
PRESENT		'70	KFK .		NSE, 40,375
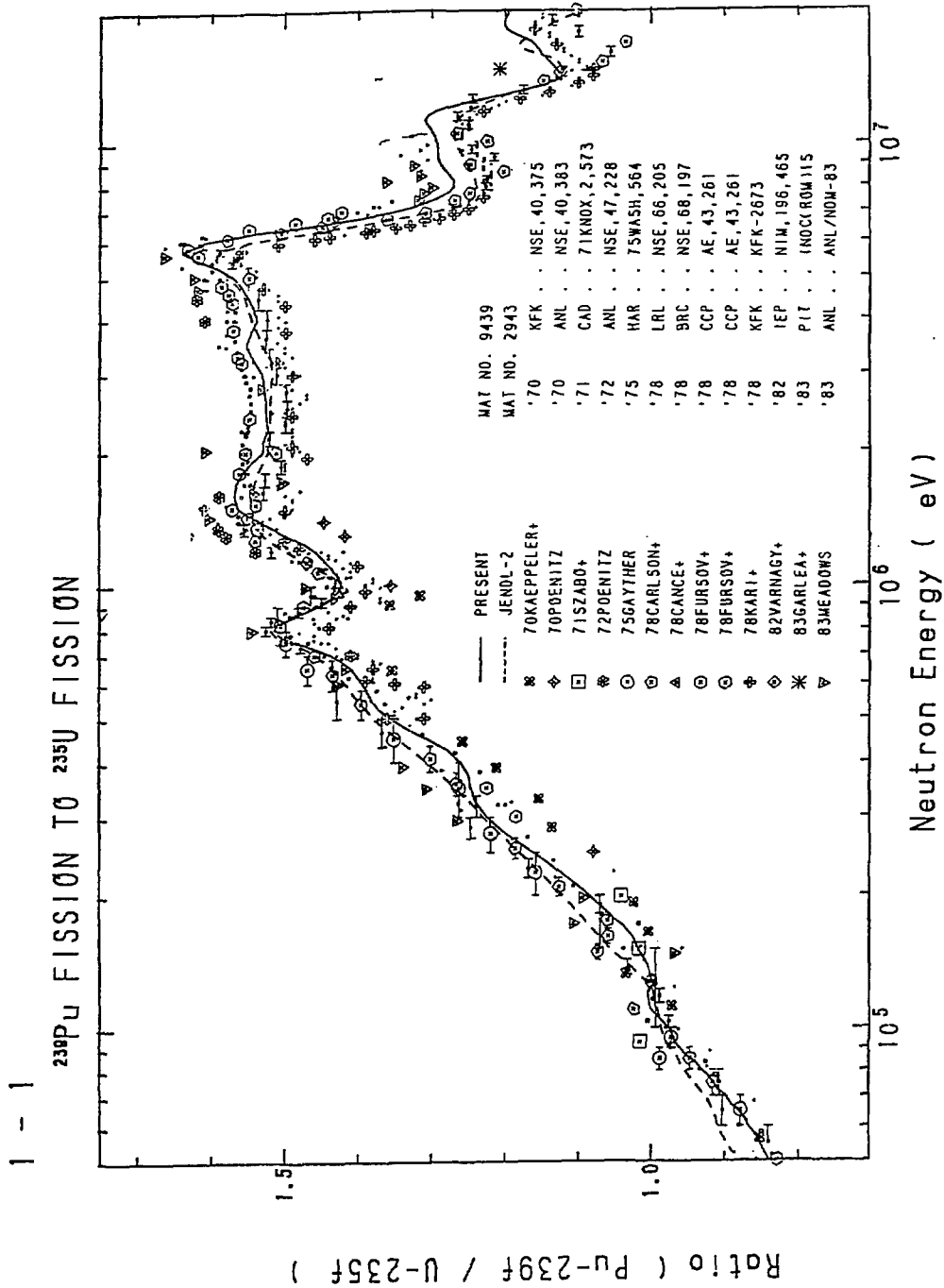
Fig. 3 Comparison of evaluated fission cross section ratio for Pu-239 to U-235 with measured data.

3 – 1

²³⁹Pu FISSION

Fig. 4 Comparison of Pu-239 fission cross section evaluated
simultaneously and measured data in the energy range between 50
keV and 1 MeV.

Fig. 5 Comparison of multiplicity of prompt fission neutrons for Pu—239 in the energy range 10 eV to 100 keV.

Fig. 6 Comparison of multiplicity of prompt fission neutrons for Pu-
239 in the energy range 1.5MeV to 15 MeV.

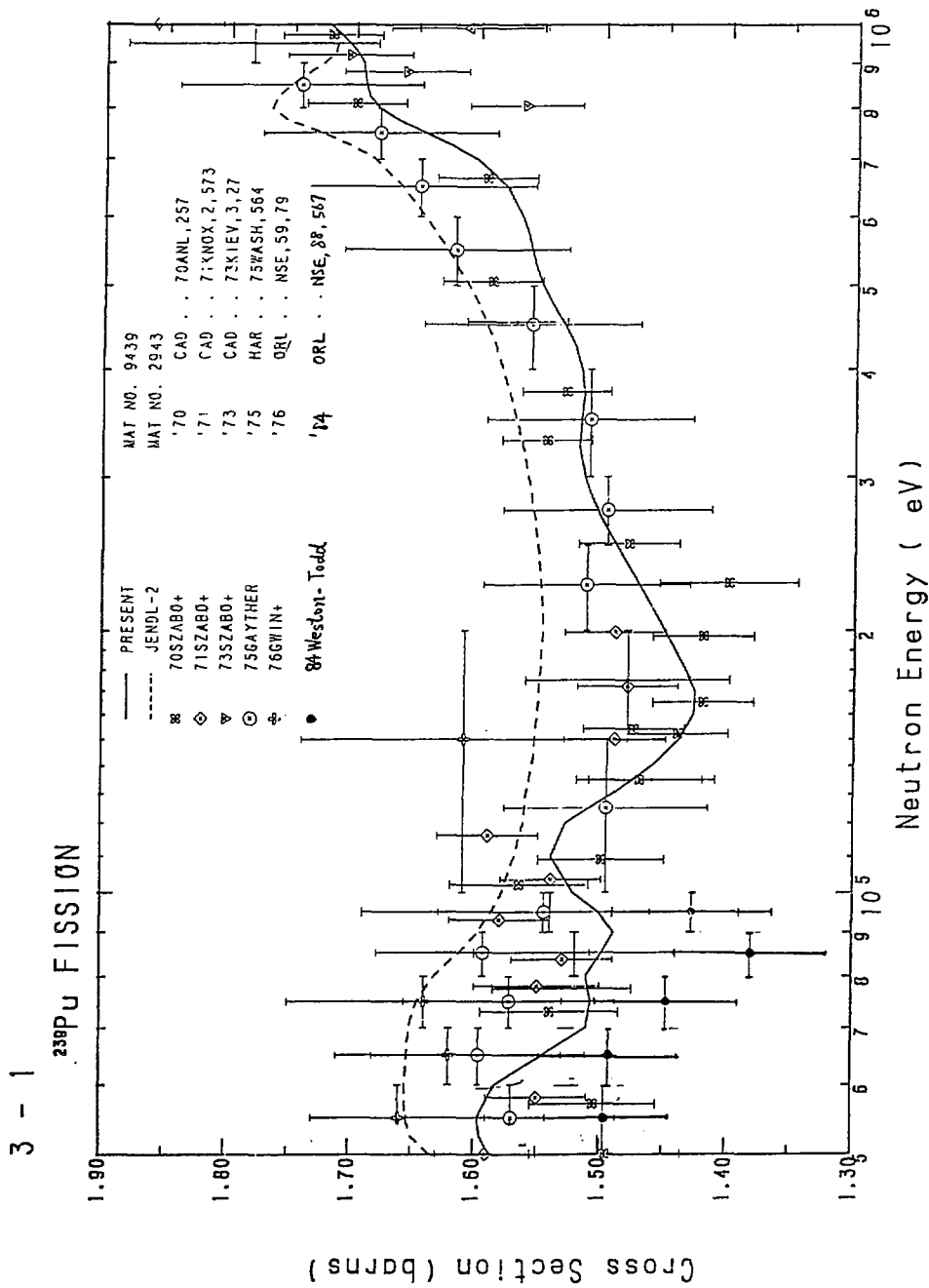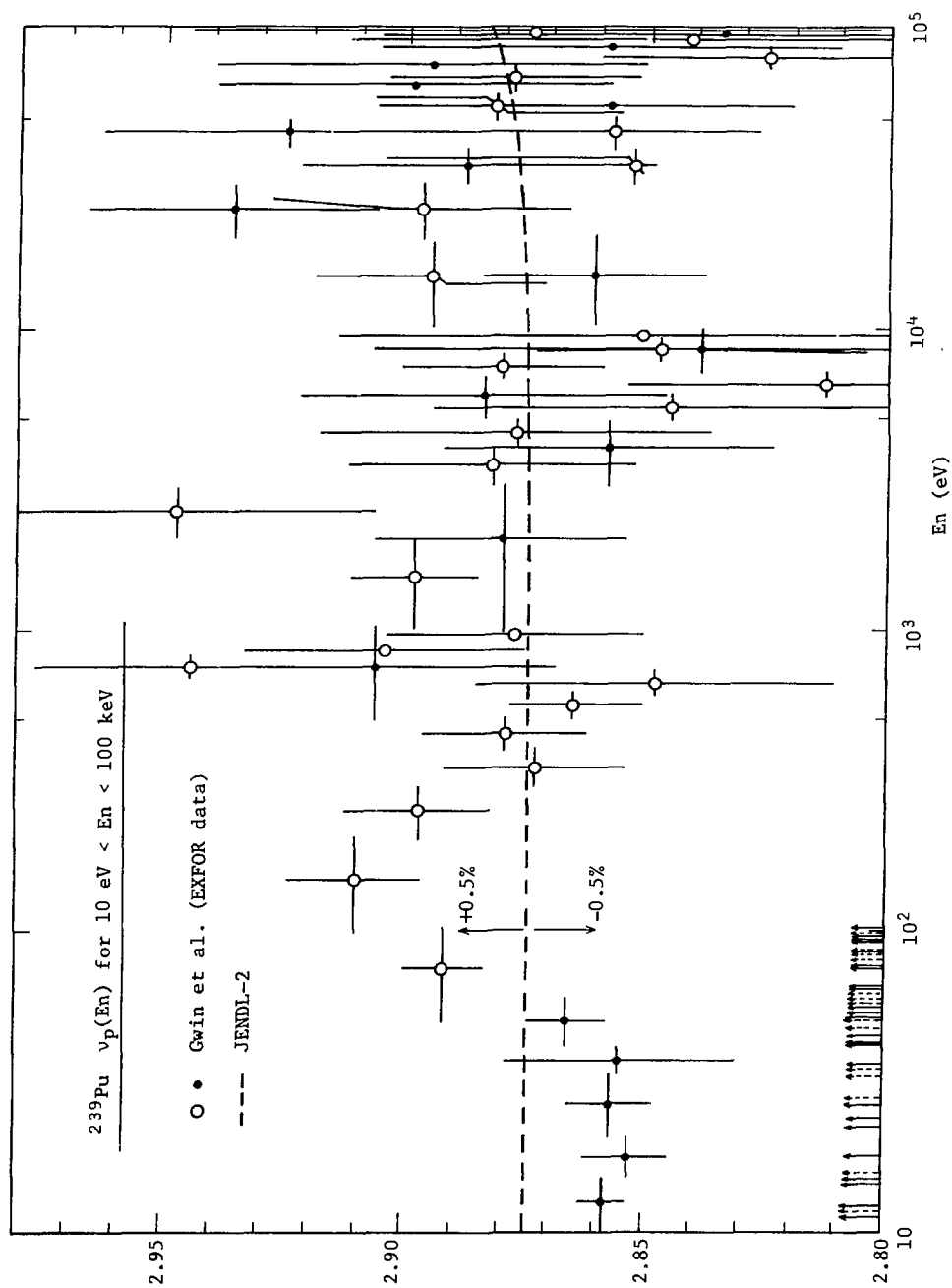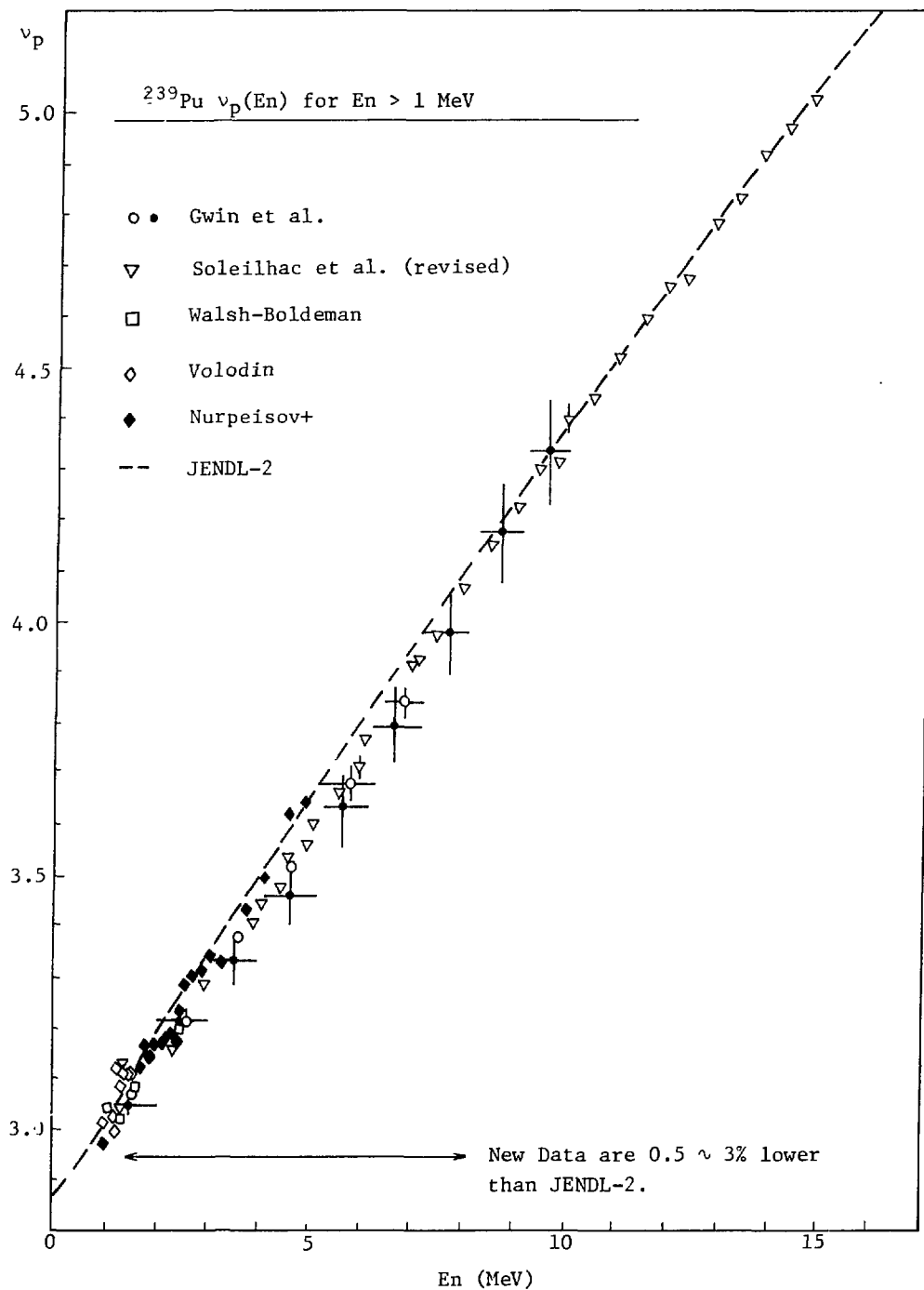### 4.5.3 Plans for JENDL-3 Fission Product Data File

JNDC Fission-Product Cross Section Evaluation W.G.

Presented by Shungo IIJIMA

NAIG Nuclear Research Laboratory

Nippon Atomic Industry Group Co., Ltd.

The scope of the ongoing evaluation of fission-product neutron cross sections for JENDL-3 is presented. The number of nuclides is extended to 170 compared to 100 in JENDL-2. New featrures of evaluation are presented.

JENDL-2 fisssion product data file[1] was completed in 1984 with primary emphasis on the application to fast rectors. It contains just 100 nuclides ranging from Kr to Gd. Evaluation was made taking account of recent neutron capture data up to 1984. Integral test and the cross section adjustment based on integral data are underway especially for nuclides for which differential cature data are not available or are very discrepant. These are Xe-132, 134, Pm-147, Eu-152 and 154.

The evaluation for the fission-product data file of JENDL-3 has recently started. New features are as follows.

(1) Number of nuclides is extended to 170 in all, ranging from As to Gd. It was aimed that the file should be applicable to thermal and epi-thermal reactors as well as fast reactors, and also to other possible general applications. Nuclide list is given in Table 1.

(2) Recent data for capture and resonance parameters since 1984 are taken into account when possible. Integral test results on JENDL-2 file would be reflected on JENDL-3.

(3) Direct and semi-direct capture cross sections will be included, using the formula of Benzi and Reffo.

(4) For imporatant neutron scattering nuclides, the direct inelastic scattering cross sections will be incorporated using DWBA calculation.

(5) Also for important nuclides, the preequilibrium and multi-step evaporation theory will be used to generate the neutron emission spectra, (n,p),(n,alpha) and (n,2n) cross sections. PEGASUS[2] code will be used for this calculation.

References :

1) JENDL-2 Fission-Product Data File, edited by T. Nakagawa (1984)
2) Presented at the poster session of this seminar.

Table 1. List of Nuclides of JENDL-3 Fission-Product Cross Section File

Nuclides marked with asterisk are those included newly in JENDL-3.

33 As		*75										
34 Se	*74		*76	*77	*78	*79	*80		*82			
35 Br						*79	*81					
36 Kr	*78		*80		*82	83	84		86			
37 Rb								85		87		
38 Sr	86	87	88	*89	90							
39 Y				89		*91						
40 Zr					90	91	92	93	94	95	96	
41 Nb								93	*94	*95		
42 Mo	92		94	95	96	97	98	*99	100			
43 Tc								99				
44 Ru	*96		*98	*99	100	101	102	103	104		106	
45 Rh								103		*105		
46 Pd	*102		104	105	106	107	108		110			
47 Ag						107		109	*110m			
48 Cd	*106		*108		110	111	112	113	114		116	
49 In								*113		115		
50 Sn	*112		*114	*115	*116	*117	*118	*119	*120		*122	*123
	*124		*126									
51 Sb		121		123	124	*125						
52 Te	*120		*122	*123	*124	*125	*126	*127m	128	*129m	*130	
53 I								127		129		*131
54 Xe	*124	*126		*128	*129	*130	131	132	133	134	135	136
55 Cs				133	*134	135	*136	137				
56 Ba	*130		*132		134	135	136	137	138		*140	
57 La								*138	139			

Table 1.   (cont'd)

58Ce	140	*141	142		144							
59Pr		141		*143								
60Nd			142	143	144	145	146	*147	148		150		
61Pm								147	*148^m_g	*149			
62Sm	147	148	149	150	151	152	*153	154					
63Eu	151	152	153	154	155	*156							
64Gd		*152		*154	155	156	157	158		160			
65Tb								159					

5. Concluding Remarks

Yuji SEKI

関　雄次

FBR Engineering Co., Ltd.

高速炉エンジニアリング株式会社

The two main themes of this seminar, "Post-JENDL-3 activity" and "Sensitivity analysis", attracted both nuclear data evaluators and users; There was a large attendance of 78 yesterday and 63 today, who took part in active discussions.

In his presentation on "Post-JENDL-3 activity program", Nakazawa stressed that nuclear data activities be coordinated with national development projects and he noted that key elements for the success in the past development of JENDL-1 and 2 were "good timing ", "need ", and "feedbacks" between the JENDL activity and the JUPITER project. I would like to add a remark. The JASPER project, FBR shielding experiments started last year, now provides a good opportunity to start to promote mutual feedbacks between JENDL and FBR shielding activities.　We encourage JASPER people to use the JENDL file in their analysis and succeeding FBR designs.

Sensitivity analysis is now playing a role of a bridge between reactor designers and nuclear evaluators, providing very important information for both of them; It tells the uncertainty of nuclear characteristics to reactor analysts and gives suggestions to evaluators how to improve nuclear data. The audience enjoyed very vivid discussions, sometimes an exchange of bluff, between reactor analysts and evaluators.

1.　はじめに

　私は，ＦＢＲ核設計分野でのＪＥＮＤＬの一利用者ですので，今日のレビューもこの方面に偏ることがあるかとは思いますが，御了承戴き度いと思います。

　今回の核データ研究会の二つのテーマ，「ＪＥＮＤＬ－３以後」と「炉定数と感度解析」は，利用者を引き付け易いテーマであったこともあり，出席者も多く盛会であったと思います。昨日が78人（原研内34人，外部44人），本日は63人（原研内27人，外部36人）の多数の方の御出席を戴き，活発な討論が行われました。本日は，討論時間も充分

でしたが、昨日は講演者の方々が熱心のあまり時間をオーバーしてしまい、討論時間がやや少なくなったのは、多少残念な気がいたします。

2. JENDL-3以後の活動計画

まず浅見さんから、JENDL-1、-2の評価の歴史的経緯も含めてJENDL-3の概要とその特長についてお話し戴きました。つづいて中沢さんより"JENDL-3以後の核データ活動を如何に行うか"についての検討委員会報告が行われました。JENDL-1、-2の開発が、何故こんなにもうまく進んで来たのかを、過去に遡って考察し、また、関連分野の将来の動向を予想し、核データへの希望を調査するなど巾広い検討を行っています。この仕事は原子力委員会の長期計画を作るような大変な作業であったかとは思いますが、非常に明快に、あざやかにまとめられました。今後この報告がシグマ委員会活動の指針として活用されますよう、期待したいと思います。

中沢さんの報告の後、6人の方からコメントを戴きました。利用者側から燃料サイクルの内藤さん、軽水炉の栃原さん、核融合炉の中村さん、評価者兼利用者で、椙山先生の御紹介によれば、評論家でもある瑞慶覧さん、高エネルギー実験側から馬場さん、最後にFBRの利用者で検討委のメンバーでもある長谷川さんからコメントを戴いたわけですが、これらをここで要約していますと、昨日と同じぐらいの時間を要しますので、特に印象に残った事柄についてお話ししてみたいと思います。

(1) 開発プロジェクトとの時間的な整合性について

JENDL-3以後には、核燃料サイクル及び核融合炉のための核データ活動、特に、特殊目的ファイルの作成を今後進めていくわけですが、中沢さんは国の開発プロジェクトと整合性を持った発展が必要である事を強調されました。特に、①タイミング、②ニーズ、③フィードバックの3つが重要であると言われたのが印象的でした。またコメンターの何人かの方からもJENDL利用の促進のためには"標準群定数の整備・提供が不可欠である"との発言がありました。

JUPITERとJENDLとの関係で考えてみますと、これらのことは誠にもっともな事であることが判ります。即ち、昨日瑞慶覧さんもコメントされましたが、私共のモーツアルト解析の頃、各メーカー毎に異なる炉定数を用いて解析していたのですが、このため混乱というか色々無駄な苦労をしたわけです。従いまして、当時、モーツアルトの次のJUPITERの解析では、始めから共通の核定数で出発しようという機運とニーズが高まっていました。また、これがJENDL-1、-2の開発時期とうまくタイミングが合っていた。更に、種々の積分ベンチマークテストの結果がJENDL-1から2へ向けての核データ改良に適切にフィードバックされたと思うわけです。

現在、FBR実証炉の炉心設計には国内各社共、JENDL処理の標準群定数セットが用いられており、JENDLは大型FBRの炉心設計に完全に定着していると言

えます。

しかし，残念ながら，FBRの遮蔽設計におきましては事情は異なっております。JENDLは使われておりませんで，ENDF/Bが用いられています。

しかしながら，遮蔽設計についても，現在，非常にタイミングの良い時期に差しかかって来ていると思われます。と言いますのは，昨年10月からPNCと米国DOEとの間で大型炉遮蔽実験に関する日米共同計画JASPERが始まっておりまして，実験データが日本に送られ始めています。また国内の解析作業が間もなく開始されようとしています。JENDL利用を開始する非常に良いタイミングになっていると思います。しかし，問題が無い訳ではありません。遮蔽設計者からは今まで3年間行って来た設計計算をやり直さなくてはならないので抵抗が出てくるでしょう。

本日は，幸いなことに，岡先生はじめJASPERに関係しておられる方が何人か出席しておられます。是非ともJENDLが，JASPER解析，ひいては大型FBRの遮蔽設計の標準核データファイルとして定着して行くよう，お働きかけをお願いしたいと思うのでございます。

(2)　核データセンターのサービスについて

これについては昨日，厳しい批評家でもある瑞慶覧さんからも"極めて良い"との太鼓判を押されました（但し，"マニュアル整備は，なっちょらん"と注がつきましたが）。私，今日ここにシグマ2年報の最新号（58，59年度の作業報告，原子力学会誌No.12，1985）を持ってきております。第IV章「核データ普及のために」の部分を読み上げますと「JENDL等の評価済み核データ，FPのJNDCライブラリー，その他を利用したいときには，原研の核データセンター（TEL 0292-82-5481）へ申し込めば提供を受けられる。」と書いてあります。極めてuser-oriented な核データセンターになって来ているわけです。

これで憶い出しますのは，これの更に2年前の56，57年度の2年報の執筆担当を仰せつかりまして，当時，やはり核データセンターのPRが必要ではないかと感じまして，「核データに関するお問い合わせは原研・核データセンターまで（TEL○○○-○○○○）」と書いて原稿を提出しておきましたら，（個人名を出して申し訳ありませんが）菊池さんから，「こんなこと書いて，もし電話が1日に10本も20本もかかって来たら，関さん，どうしてくれる?!」

(3)　JENDLの利用促進について

高速炉以外に軽水炉でも，従来からの設計手法の比較検証のためにJENDLが一部併用され始めています。しかしながら臨界安全性や核融合Activation等，肝心のお膝元の原研プロジェクトにおいて，JENDLがまだ使用されていないのは誠に遺憾なことであります。

これは原研内部の問題ですから，身内の努力でなんとか改善の糸口をつかんで戴くようお願いしたいと思います。

3. JENDL-3以後の核データ

まず，核燃料サイクルの核データとして，（α，n）反応：村田さん，アクチニド：吉田さんの発表がありました。（α，n）反応断面積評価値の精度は数十％乃至ファクター2弱と見受けられます。吉田さんは，再処理等の際"嫌がられる核種"（^{232}Th, ^{237}Np, ^{238}Pu 等）を紹介し，これらが単純パスではなく，複雑なチェインを経て生成されること，従ってチェインに現れる多数の核種のデータが必要であり，また（n，2n）のような，しきい値反応が多いが，現状では100％もの不確かさがあることを説明されました。

高エネルギー核データ関して，トピックス3件の発表がありました。山内さんからは高速中性子散乱実験の現状を紹介戴きましたが，Optical modelを用いた計算値は実験値を驚く程良く再現できています。水本さんからは，加速器の最近の利用分野が拡がっており，高エネルギー核データのニーズの高まりが核データ関係者をstimulateしていると話され，各国の核データ測定施設も紹介されました。原研100MeVリニアックでの誘導放射能には^{24}Na, ^{60}Co, ^{54}Mn 等が生じるとのお話でしたが，生成の過程は全く異なるのですが，FBRの1次冷却系Na配管と同じ放射性核種が生じているのは私には興味深く思われました。橋爪さんからは，荷電粒子による核反応断面積測定にはスタンダードクロスセクションが必要であるとのお話で，C，Al, Cu 等の断面積測定値の現状を紹介戴きました。測定値の不確かさは5～6％とのことです。

4. 炉定数と感度解析

第2日目は，炉定数と感度解析について，核融合炉輸送計算から岡さん，同じく群定数から橋倉さん，FBR&LWRの燃焼計算から高野さん，HCLWRから竹田さんの4件の発表のあと，核データ側からのコメントとして^{238}U：中川さん，^{239}Pu：川合さん，FP：飯島さんから発表がありました。本日の講演については，まだ皆様のご記憶に新しいところと思いますので，個々のレビューは省かせて戴いて，特に印象に残った点についてお話ししてみます。

(1) 遮蔽解析用標準群定数について

橋倉さんの講演のあと，活発な議論が沸き出たのですが，飯島さんが最後にコメントされたように，「何群の標準群定数が良いと結論する前に，まず群定数処理法（重み関数の選び方）の標準化について検討する必要がある」と思われます。会場の皆さんも同じ印象を持たれたことと思います。

(2) 感度解析について

感度解析手法が炉解析と核データとの橋渡し役として有効な情報を提供しつつあると感じました。即ち，炉解析者には，炉特性値の不確かさ巾を教え，一方，核データ

評価者には，adjustmentの結果から核データの見直しの方向を示唆することができる。「今回の研究会は核データ評価者と利用者との議論がうまく噛み合って来た」と，今朝がた山室先生がおっしゃっておられましたが，誠にその通りと感じます。

　2，3年前と較べますと，感度解析をやっている人達は自分達の結果に自信を持っている。遂には飯島さんのように「今，核データを見直さないと，30年，後悔し続けるぞ！」と脅迫めいた発言も出て来た。

　一方，核データ評価側の川合さんの方も「現在の核データ値から見て，上げろ，下げろの要求には応じられない！」との発言です。

　こういう公式の場では譲歩はお互いに難しいでしょうが，マァ，裏取引には応じて戴いて，"業務命令"は避けて戴くよう願いたいと思います。

(3)　FPデータファイル

　JENDL－3に向けてのFPデータファイル構想について，飯島さんより紹介がありました。FPデータファイルについては，JENDL－2の段階で既に世界的な定評を得ているわけですが，今後ますます充実されることを皆さんと共に期待したいと思います。

5.　ポスターセッション

　JENDLの利用について3件，断面積の測定・計算について10件の発表がありましたが，講演内容を補足・充実するテーマの発表が多かったため，判り易かったと思います。蛍光カラーペンや写真等も活用され，視覚に訴える工夫がされていました。どのパネルでも熱心な質疑応答が続いて，このセッションも成功だったと思います。

6.　おわりに

　この核データ研究会の企画をして戴いたプログラム・コミティーの方々，また，研究会の運営，ならびに懇親会の広い会場と，おいしい御馳走を用意して戴きました核データセンターの方々に感謝いたします。

　2年後には核データ国際シンポジウムが開催されますが，これに向けて，核データ研究会がますます充実・発展されますよう祈念しまして，Concluding Remarksを終わらせて戴きます。どうもありがとうございました。

（当日の雰囲気を伝えるため，速記録に近い口語体のままとし，数多くの個人名をそのまま残させて戴きました。御迷惑がかかるかも知れませんが御容赦下さい。）

Poster Session

P.1 Usage of Nuclear Data Library and Proposal to JENDL

M. Sasaki[1], S. Iijima[2], Y. Kawai[2]
H. Matsunobu[3], and A. Zukeran[4]

ABSTRACT

A usage status of nuclear data libraries and proposals to the JENDL library are briefly reviewed.

1) Data bases used in plant design and fuel cycle design fields are summarized. JNDC evaluated data and JENDL   are not utilized so much than expected in these fields.

2) Performances between JENDL-2 and ENDF/B-IV are compared in the FBR nuclear design field. JENDL-2 shows good characteristics.

3) Usages of JENDL-2 are shown in the LWR nuclear design field. JENDL-2 isn't always superior to the licensing library.

4) Usages of JENDL-2 are shown in the FBR shielding R&D field. JENDL-2 underestimates measured spectra in case of the deep penetration experiment.

5) Based on the above usage status of JENDL-2,   proposals to future JENDL and Nuclear Data Center are tabulated.

(1) MAPI, 4-1, Shibakouen 2-chome, Minato-ku, Tokyo
(2) NAIG, 4-1 Ukishima-cho, Kawasaki-ku, Kawasaki-shi, Kanagawa
(3) SAIG, 6-1, Kajicho 2-chome, Chiyoda-ku, Tokyo
(4) HERL, 1168 Moriyama-cho, Hitachi-shi, Ibaraki

1. General View of Usage Status of Nuclear Data Libraries

Usage status of nuclear data libraries in a plant design field is shown in Table 1. In this table the mark O means that a library is used for a licensing design, and the mark Δ means that a library is used only for a R&D calculation and so on.

JENDL-2 and JNDC decay data and so on are not always used in a LWR core design field. The licensing libraries based on ENDF/B are principally used for convensional plants, and JENDL-2 was only used to make benchmark calculation for HCR (high conversion reactor) as mentioned below. JENDL-2 is neither used in the ATR nor the fusion design fields. In these fields, the licensing libraries and ENDF/B are adopted. JENDL-1 and -2 are used only for R&D calculations and plant design studies of DFBR (demonstration fast breeder reactor) from 1977 in the FBR design field.

Usage status of nuclear data libraries in a fuel cycle design field is shown in Table 2. As shown in this Table, foreign data libraries are especially used in this design field. To our deep regret, JENDL and other JNDC evaluation data are hardly used in this field. So, we hope usage of data based on JENDL in the future of this design field.

2. Usage Status in FBR Nuclear Design

JENDL-2 was released in time for starting of the JUPITER (Japanese-USA Program of Integral Tests and Experimental Researches) experimental analysis, because there is strong motive power for standarization of data base in the Japanese DFBR (Demonstration FBR) nuclear design field. Hence, JENDL-2 is greatly utilized in the JUPITER experimental analysis and the DFBR nuclear design study by the Japanese makers, PNC and JAERI.

Core compositions of the JUPITER-I and II mockup experiment analysed with JENDL-2 are shown in Fig. 1. JUPITER-I was planded to a homogeneous DFBR core design and JUPITER-II was planed to a radially heterogeneous one.

Fig. 2 shows comparison of performance on keff between JENDL-2 and ENDF/B-IV. The keffs calculated with JENDL-2 show good agreement with the measured values for all core configurations, different from the calculated one with ENDF/B-IV by ANL. The C/E values with JENDL-2 hold especially a stable position in the both core configurations.

Fig. 3 shows comparison of C/E values between JENDL-2 and ENDF /B-IV for ^{235}U fission reaction rates on the ZPPR-13A assembly, as an example. A performance (discrepancy between measured and calculated reaction rates, radial dependency of C/E values and so on) of JENDL-2 on reaction rate calculations is nearly equal to that of ENDF/B.

Fig. 4 shows comparison of C/E values between JENDL-2 and ENDF /B-IV for control rod worths on the ZPPR-13 assemblies. Japan and ANL use different B_{eff} value, respectively. Kinetic parameters as B_{eff} are not evaluated by JNDC. The B_{eff} value used in the calculation with JENDL-2 was evaluated by Tuttle's yield data[2] and Saphier's delayed neutron spectra[3], and the B_{eff} value used in the calculation with ENDF/B-IV was evaluated by the delayed neutron data contained in ENDF/B-IV. The use of these two values causes about 5% difference into calculated values on the control rod worth. In either case, JENDL-2 makes underestimation on the control rod worths, comparing with ENDF/B-IV. Table 2 shows present accuracies obtained with JENDL-2 and required ones for cost reduction (on DFBR core design calculation). From this table, JENDL is required more better performance on DFBR core design.

As shown above, JENDL-2 has good performances, comparing with ENDF/B-IV. However, JENDL is only used in DFBR core design field, to our deep regret.

3. Usage Status in FBR Shielding Design

JENDL has never been used in FBR shielding design field, only used for benchmark calculations.

The banehmark experiment for neutron transport in thick sodium[6] as shown in Fig. 5 was performed in ORNL Tower Shielding Facility (TFS). DOT-3.5 calculations with JENDL-2 100 group P5-S48 approximation gives good C/E values, comparing with ENDF/B-IV, as show in Fig. 6.[7]

The axial shielding mockup experiment for CRBR was performed in ORNT TFS[8] as shown in Fig. 7. Comparing with ENDF/B-IV calculations with JENDL-2 give good C/E values as far as 30cm depth in the carbon steel region, where epithermal neutron flux has main contribution.[7][9] The result of this analysis proves a good evaluation of F_e total cross section. However, beyond the above depth, calculations with JENDL-2 make underestimation due to the misevaluation of fast neutron flux in the sodium region.

4. Usage Status in LWR core design

Fig. 10 shows an example of keff tracking of operating LWR with the revised licensing library in which data of some isotopes are substituted by JENDL-2. The uncertainty of this library is less than 0.2%Δk and has good performance.

Fig. 11 shows the C/E values of the U or UO_2 benchmark thermal criticals[10] with the library in which some main isotopes are substituted with JENDL-2. From this results, it is guessed the performance of JENDL-2 is better than ENDF/B-IV, and is not superior to the licensing library.

Fig. 12 shows comparison of keff and conversion ratio (C.R.) of HCLWR (Vm/Vp = 0.8) between JENDL-2 and UKNDL.[11] JENDL-2 gives keff by 2.3% Δk and C.R. by 0.025 larger than UKNDL for the clearn core.

5. Conclusion and Proposal to JENDL

JENDL-2 and JNDC data are used only in the R&D calculation and the design studies for DFBR core, as mentioned above. In other design field, these data are not used in a general way, *because*

o   group constants made from these data are not prepared.
o   performances of these data are not so good compared the licensing data.
o   these data are not authorized and published.

and so on.

If it will be hoped JENDL and JNDC data are widely used, the following are proposed to the future JENDL.

(1) Perfection of JENDL ; o Extension of isotopes, reactions
                            o Preparation of covariance data
                              and so on.

(2) Data evaluation for
     usage of accelerator; o high energy neutron data
                            o proton data
                            o photo-reaction data

(3) Accomplishment of COMRAD system

(4) Authorization of JNDC data and JENDL

(5) Publication and
     announcement   ; o one-group cross section
                              o group cross section
                              o $\nu(E)$ and $\nu d(E)$ or β
                              o $\chi(E)$ and $\chi d(E)$
                              o K_f
                              o σ_f^{25} (E)
                              o decay-heat data

and so on.

(6) Production service of group constants

(7) Standardization of nuclear data evaluation method

(8) Preparation of code system for integral test and data base
     (including with measured and calculated data)

(9) Perfection of computer network and consalting services

Reference

(1) Kikuchi Y. and Hasegawa A. et al., "Benchmark Test of Japanese Evalu-
     ated Nuclear Data Library (JENDL)", Int. Conf. on Neutron Cross
     Sections for Technology, Univ. of Tenesse (Kmoxvill), 1979.

(2) Yamamoto M. and Nishi H. et al., "Analysis of Large Convensional
     LMFBR Core Critical Experiments and Their Implication to Design
     Methods", Topical Mtg. on Reactor Physics and Shielding, Chicago,
     1984

(3) Shirakata K. and Suzuki S. et al., "Studies of Large Radially Hetero-
     geneous LMFBR Critical Experiments Analysis", ibid.

(4) Tuttle. R. J. "Delayed-Neutron Yields in Nuclear Fission", Consult-
     ant's Mtg. on Delayed Neutron Properties, IAEA, Vienna, 1979

(5) Saphier D. and Ilberg D. et al., "Evaluated Delayed Neutron Spectra
     and their Importance in Reactor Calculations", NSE vol. 62, p 660,
     1979.

(6) Maerker R. E. and Muckenthaler F. J. et al., "Final Report on a
     Benchmark experiment for Neutron Transport in Thick Sodium", ORNL-
     4880, 1974

(7) Kawai M. "Shielding Benchmark Test with sodium cross section of
     JENDL-2", Kaku-deta-nyusu No.25, 1986 (in Japanese)

(8) Maerker R. E. and Muckenthaler F. J., "Final Report on a Benchmark
     Experiment f~r Neutron Transport Through Iron and Stainless Steel",
     ORNL-4892, 1974

(9) Tsunoda H. and Ohtani N. , "Analysis of Neutron Transmissions
     Through Iron and Sodium Layers", 1986 Fall Mtg. of the AESJ B1
     (in Japanese)

(10) Strawbridge L. E. and Barry R. F. "Critical Calculations for Uniform
     Water-Moderated Lattices", NSE vol. 23, P. 58, 1965

(11) Suzuki K. and Saji E. et al., "Benchmark Calculation of Nuclear
     Design Code for HCLWR", JAERI-M86-178, p 2, 1986

Table 1   Usage of Nuclear Data Libraries in Plant Design Field

○ Reference Calcu., △ R&D Calcu.

Design Field	Items	Data Base	LWR (conv.)	LWR (HCR)	FBR	ATR	Fusion
Nuclear	K_{eff}	Licensing Data	○	△	—	○*	—
		JENDL	—	△	○	—	△**
		ENDF/B	—	△	—	—	○
		WIMS	—	△	—	—	—
Thermal-Hydraulic	$\phi n, \phi \gamma$(nuclear)	Licensing Data	○	△	—	○*	—
		JENDL	△	△	○	—	—
		ENDF/B	△	△	—	—	○
Structure	$\phi n, \phi \gamma$(shielding)	Licensing Data	○		—	—	—
		JENDL	—		○	—	—
		ENDF/B	○		○	○	○
Shielding	Activation Production	ORIGEN	○		○	—	—
		FPGS-3	—		○	—	—
		Maker's Data	○		○	○	—
		THIDA	—		—	—	○
Safety	Decay Heat	JNDC	△		○	—	—
		ANS 5.1	△		—	○	—
		THIDA	—		—	—	○
Fuel	Kinetic Parameters (β_{eff}, λ)	Keepin, Tuttle, Tomlinson	○		○		○
Maintenance						○	

* WIMS-ATR, ** Tritium-Breeder

Table 2   Usage of Nuclear Data Libraries in Fuel Cycle Design Field

Design Field	Items	Using Data Base	Proposal to Near Future
Thermal / Shielding	K_{eff}	Licensing Data, Hansen-Roach, MGCL, SCALE, WIMS	Standardization with JENDL Data Base
	Radioactive Inventry	ORIGEN-2 (FPGS-3)	Standardization with JENDL Data Base, o Apply to Advanced Reactor
Critical Safety	Radiation Source (γ, n)	ORIGEN (FPGS-3)	Standardization with JENDL Data Base, o Apply to Advanced Reactor
Waste Disposal	Decay Heat	ANS 5.1 (JNDC)	Standardization with JNDC (Decay Heat) Data Base, o autholization, o error file
	Kinetic Parameters (β_{eff}, λ)	Keepin, Tuttle Tomlinson	JNDC (β_{eff}, λ) Evaluation and Standadization with JNDC Data Base

Table 3 Present and Required Design Accuracies
on DFBR Core

(2σ reliability)

Items	Present Accuracy	Required Accuracy	Needs of Resalution
1. Multiplication Factor (keff)	±0.75%Δk/k	±0.30%Δk/k	
2. Burn-up Reactivity	−	±10%Δk/k	data is unavailable by mock-up experiment, so confirmation with data obtained from preceding reactors is required.
3. Power Distribution (P)			
core	±8%	±5%	radial dependency
blanket	±13%	±10%	of C/E values
C/R	−	±15%	
4. Control Rod Worth			
total worth	±12%	±7%∿ I 10%	radial dependency
backup rod			of C/E values
differential worth			
5. Sodium-void Reactivity Worth	±50%	±30%	
6. Doppler Reactivity Worth	±30%	±20%	
7. Material Sample Worth			
fuel	±20%	±10%∿ 20%	
structure	±20%∿ 30%	±10%∿ 40%	
coolant	±50%	±30%∿ 40%	

Table 4 Analysis of Shielding Benchmark with JENDL-2

System	C/E Values
Fe (1m Thickness)	0.6 ∼ 1.3
Na (3m Thickness)	0.8 ∼ 1.4 → Fig. 6
Carbon (50cm Thickness)	0.7 ∼ 1.0
Na/Fe Multi-layer	0.12∼ 0.8 → Fig. 8

(1) JUPITER- I : Mockup experiment for hemogeneous DFBR

ZPPR-19A & 19B
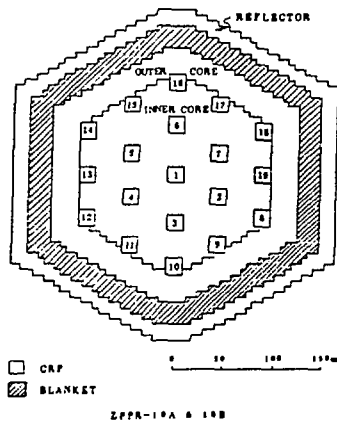
(2) JUPITER- II : Mockup expriment for radially heterogeneous DFBR

ZPPR-13 A
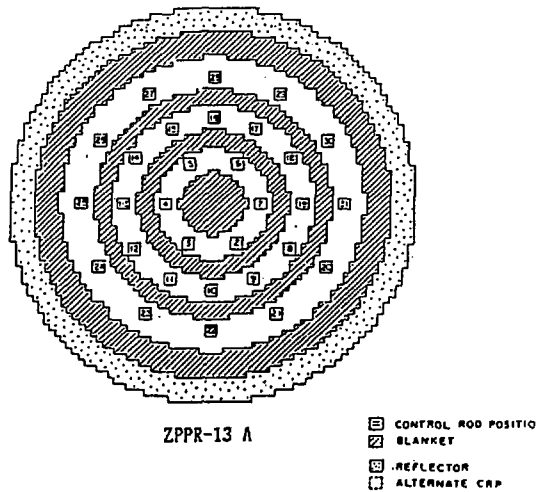
Fig. 1   Core Configuration of JUPITER Experiment
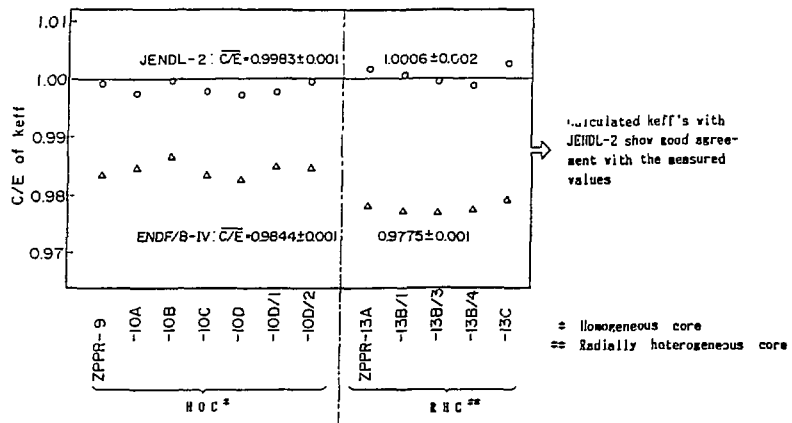
Fig. 2   Comparison of Criticality between JENDL-2 and ENDF/B-IV
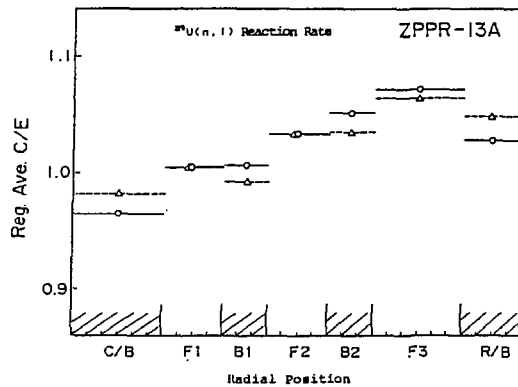
Fig. 3   Comparison of C/E Values between JENDL-2 and ENDF/B-IV
          for ^{230}U Fission Reaction Rates
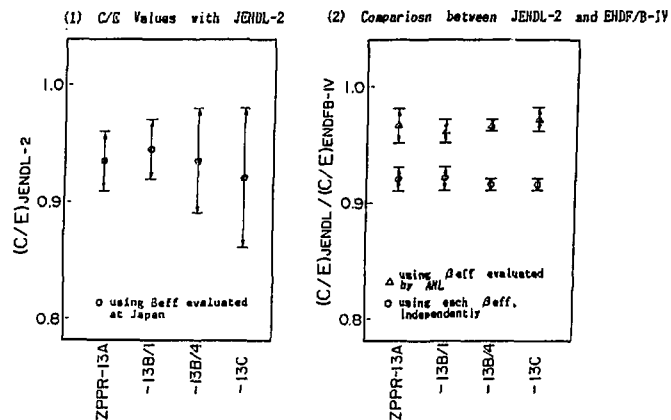
Fig. 4   Comparison of C/E Values between JENDL-2 and ENDF/B-IV
          for Control Rod Worths

Fig. 6　C/E Values of Sodium Deep Penetration Experiment on TFS
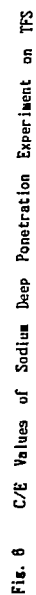
Fig. 5　Side-View of Reactor and Sodium Shield Geometry on TFS
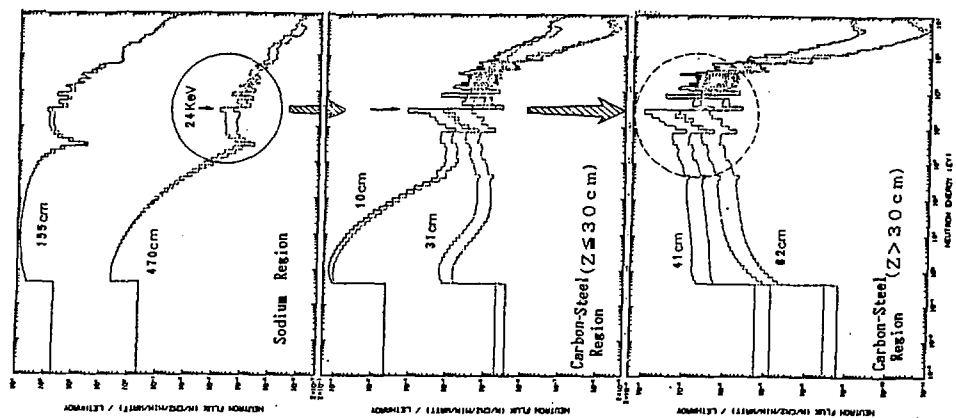
Fig. 9   Neutron Spectra
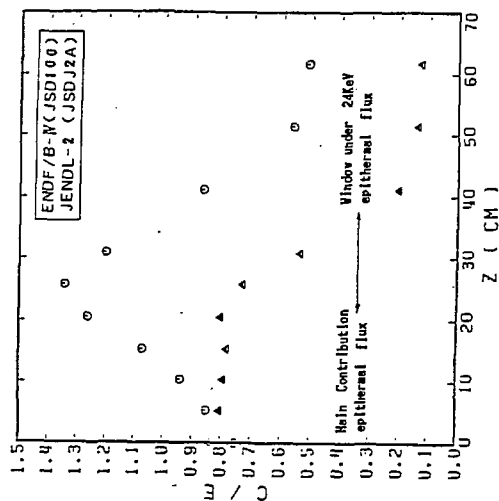
Fig. 5   C/E Value In Carbon-Steel Region
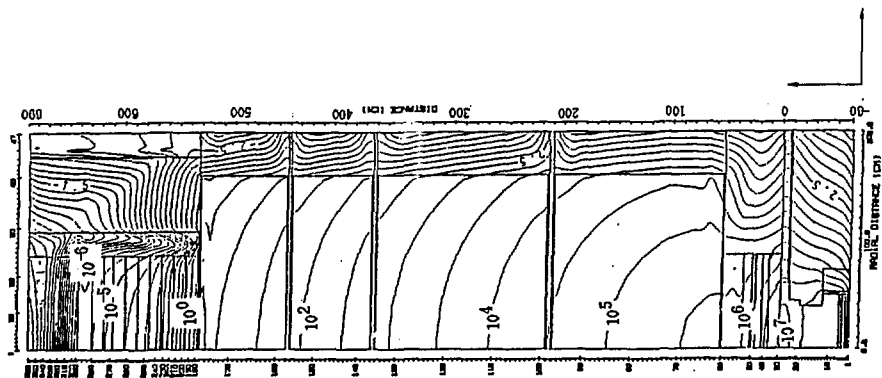
Fig. 7   Count Rate with 4" Bonner-Ball Counter
In Axial Shielding Mockup Experiment
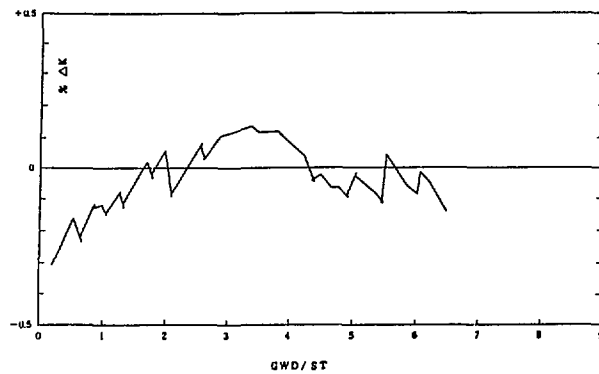
Fig. 10   Example of Keff Tracking of Operating LWR
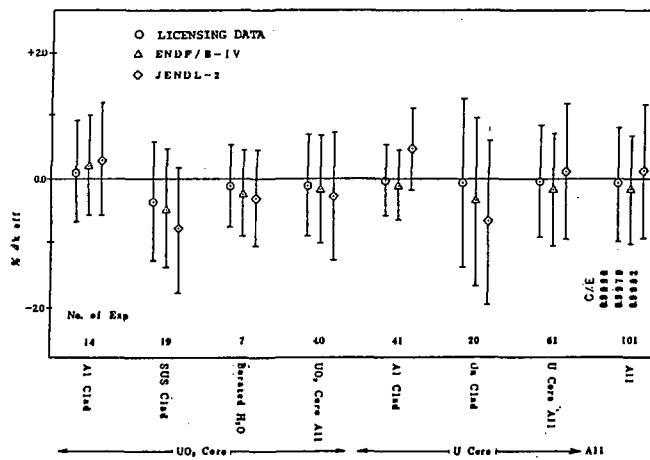
Fig. 11   Calculated Keff for U or UO_2 Benchmark Thermal Criticals
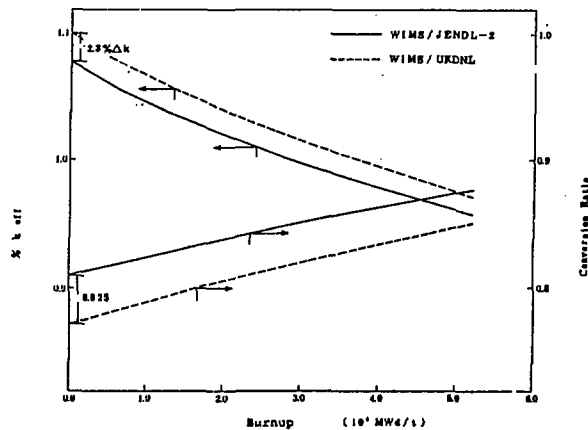
Fig. 12   Comparison of Keff & C.R. of HCLWR (Vm/Vf=0.8)
between JENDL-2 and UKDHL

P.2   JENDL Special Purpose Data Files

S. Iijima (NAIG), J. Katakura (JAERI), M. Nakazawa (Tokyo Univ.),

M. Kawai (NAIG), T. Asami (JAERI), and T. Nakagawa (JAERI)

JNDC Ad-hoc Committee on Special Purpose Data File

An ad-hoc JNDC committee on special purpose data file discussed
the general and specific features of the JENDL Special Purpose Data
Files.   And several special purpose data files were proposed.   Brief
sketch of the proposed files and the status of the some selected data
are described.

1.Introduction

JENDL has been directed to the so-called "general purpose files",
which should contain complete cross section set. However, there have
been increasing requirements for "special purpose data files" which
contain only specific nuclear data of interest to the evaluation of
fuel cycle, radiation damage, radioactivities, etc. It is known that
these special purpose data files are defined in ENDF/B.

An ad-hoc JNDC committee was setup in spring, 1985 to discuss the
general and specific features of the JENDL Special Purpose Data Files.
A rough scope of the files was designed, and the questionaires were
sent to the JNDC members as well as to the experts of related fields
concerning the applications of interest, the data source currently
used, the quantities to be included in the planned files, and the
possibility for participation to the file-making activity. Based on
the answers recieved and the further discussions, the committee
reached to the conclusion that the plan is feasible, and the scope of
the special purpose data file was finalized. The report was published

as JAERI-memo for internal use of JNDC.

In the present paper, brief sketch of the proposed files and the status of the some selected data are described. For details the readers are requested to refer to the JAERI-memo report.

2.Contents of the Special Purpose Data Files

The following nine categories are considered as the JENDL Special Purpose Data Files.

(A) Activation cross section and decay data file

(B) Actinide cross section and decay data file

(C) Decay data file (not included in files (A) and (B))

(D) Dosimetry cross section file

(E) Gas production cross section file

(F) Kerma factor and DPA cross section file

(G) (α,n) cross section file (including thick target yields)

(H) Photo-reaction data file

(I) Standard data file

The point wise total cross section data will be included in Files (A) and (D) to facilitate the calculation of the self-shielding factors. The data for natural elements, concrete and alloys of practical interest will be included. Detailed list of the data types to be included in the files is given in JAERI-memo, through these should be further examined and elaborated by the responsible working groups when the work starts. A general rule was proposed that the data of Special Purpose Data File must be identical with that of General Purpose File if the MAT number and the reaction number MT are the same.

The contents of each file is briefly described below.

(A) Activation cross section and decay data file

This file contains the nuclear data needed for estimation of residual radioactivity in reactor and for activation detectors except for actinides and fission-product nuclides. It is planed to include the decay data of 191 nuclides and the neutron induced reaction data of 138 nuclides. The number of the reactions amounts to 369. About 60 percent of the reactions are covered with JENDL3 file. To facilitate

the calculation of the self-shielding factors, the pointwise total cross sections will be stored at the same time for nuclides having strong resonances.

(B) Actinide cross section and decay data file

This file contains neutron cross sections and decay data relating to the nuclide generation and depletion of actinide nuclides from Tl to Fm. The reactions to be included in this file are neutron capture, (n,2n) and fission. The reaction data of ^{232}Th, ^{233}U, ^{235}U, ^{238}U, ^{239}Pu, ^{240}Pu and ^{241}Pu are not included because the self-shielding factors are needed for these nuclides.

The number of nuclides are planed to be 127 for decay data and 73 for reaction data. The total number of the reactions is 219. The JENDL3 file covers 50 percent of the reactions.

(C) Decay data file

This file contains the decay data of the nuclides produced by neutron induced reactions from stable nuclides. The number of nuclides amounts to 562.

(D) Dosimetry cross section file

The purpose of this file is to be used for neutron dosimetry of reactor and acceralator. The nuclear data in this file include total cross section to be able to calculate the self-shielding factors. The number of nuclides is 44 and the total number of reactions amounts 56. The JENDL3 file covers about 80 percent of the reactions.

(E) Gas production cross section file

This file contains the cross section data of the neutron reactions resulting in radiation damage by gas production. The number of nuclides needed for this purpose is 27 and that of reactions 66. The JENDL3 covers about 80 percent of the reactions.

(F) Kerma factor and DPA cross section file

The purpose of this file is to prepare the basic data needed for

calculating Kerma factor and DPA cross section. The number of nuclides in this file is 49, but that of total reactions amounts over 700.

(G) (α,n) reaction data file

This file contains the data to estimate the neutron production rate by (α,n) reaction. Natural elements such as Li, Be, B, C and so on are beeing planed.

(H) Photo reaction data file

The reaction data induced by photons are included in this file. The reaction types considered now are (γ,xn), (γ,f), (γ,γ') and (γ,p)

(I) Standard data file

This file contains the standard data which are used as basic data for measurement and evaluation of nuclear data. They are planed to be limited to the reactions reported in IAEA Technical Reports Series No. 227 (1983) and that of ENDF/B-V standard data file.

3.Examples of the special purpose nuclear data

3.1.Actinide cross section and decay data

Figure 1 shows the main actinide chains leading to the production and deplation of strong α emitters and γ-ray emitters which are important for fuel cycle evaluation and waste disposal considerations. The threshold reactions like (n,2n) and (n,3n) become important for estimating the nuclide generation and depletion. In this case, the data at the energy region near the threshold must be evaluated carefully because of the little overlap between the reaction range and the neutron spectrum. A reaction branching ratio to the metastable state and the ground state, for example, ^{241}Am(n,γ)^{242m}Am and ^{241}Am(n,γ)^{242}Am, is also important and must be evaluated carefully.

The examples of the evaluated reaction data are shown in Figs.2 and 3 for ^{237}Np(n,2n) and ^{241}Am(n,γ), respectively.

3.2.(α,n) reaction data

The quantities of interest are the thick target (α,n) neutron yields (n/α-particle) and the neutron spectrum. Figure 4 shows the calculated neutron yields in various light element materials per atom as a function of the initial α-particle energy. In case of oxide fuel, the calculated neutron yield is shown in Fig. 5 together with experimental data of West and Bair and the evaluated data of Liskien and the old and new evaluations by Bell. The neutron spectra are shown in Fig. 6. For details of the calculation readers are referred to the paper by T. Murata presented at this seminar.

3.3.Kerma factor and DPA cross section

The Kerma factor and the DPA cross section are defined by :

$$KF(E_n) = \int dE_x d\Omega \; \sigma_{n,x}(E_n,E_x,\Omega)(T+E_x),$$

$$\sigma_{DPA}(E_n) = \int dE_x d\Omega \; \sigma_{n,x}(E_n,E_x,\Omega)\nu(T).$$

Here, $\sigma_{n,x}$: the double differential (n,x) cross section,

     $T=T(E_n,E_x,\Omega)$: primary knock-on atom (PKA) kinetic energy,

     $\nu(T)$: displacement per PKA.

The calculated DPA cross section for natural iron using JENDL-3PR1 and ENDF/B-IV are shown Fig. 7. Figure 8 shows the DPA cross section for natural nickel and its reaction components calculated with JENDL-2 file. It is noted that the (n,p) and (n,α) reactions contribute significantly to the total DPA cross section in the case of nickel. All calculations were made by using TENJIN-1 code developed by T. Ariga, JAERI. The evaporation spectra were assumed for the proton and α-particle spectra in the code since these spectra have not been defined in JENDL nor ENDF/B-IV. The charged particle spectrum data and the double differential neutron spectrum data are to be incorporated in JENDL-3 for important structural materials. Therefore, there are much work to be done concerning this file when JENDL-3 is completed.
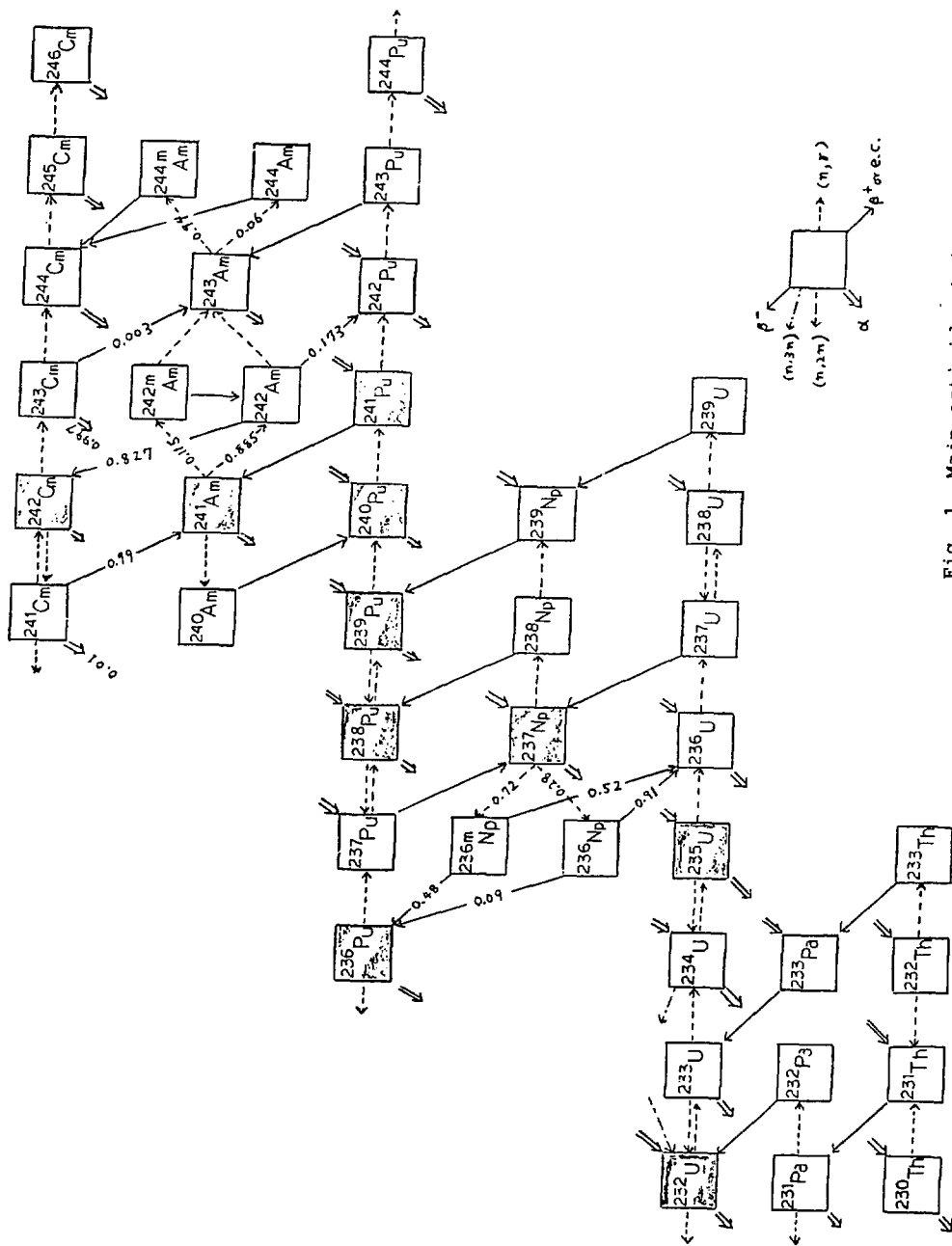
Fig. 1 Main actinide chains.
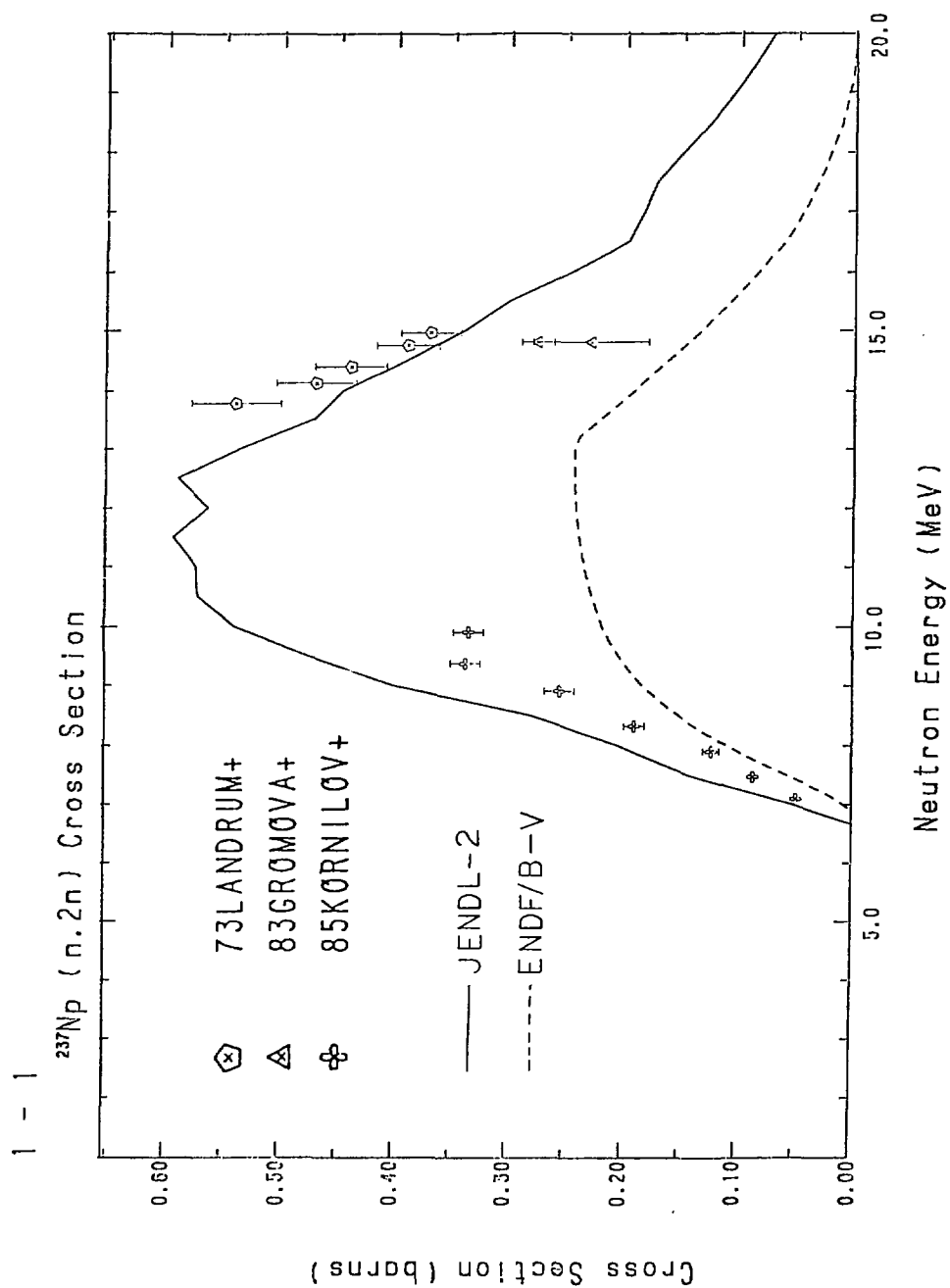
Fig. 2 ^{237}Np(n,2n) cross section.
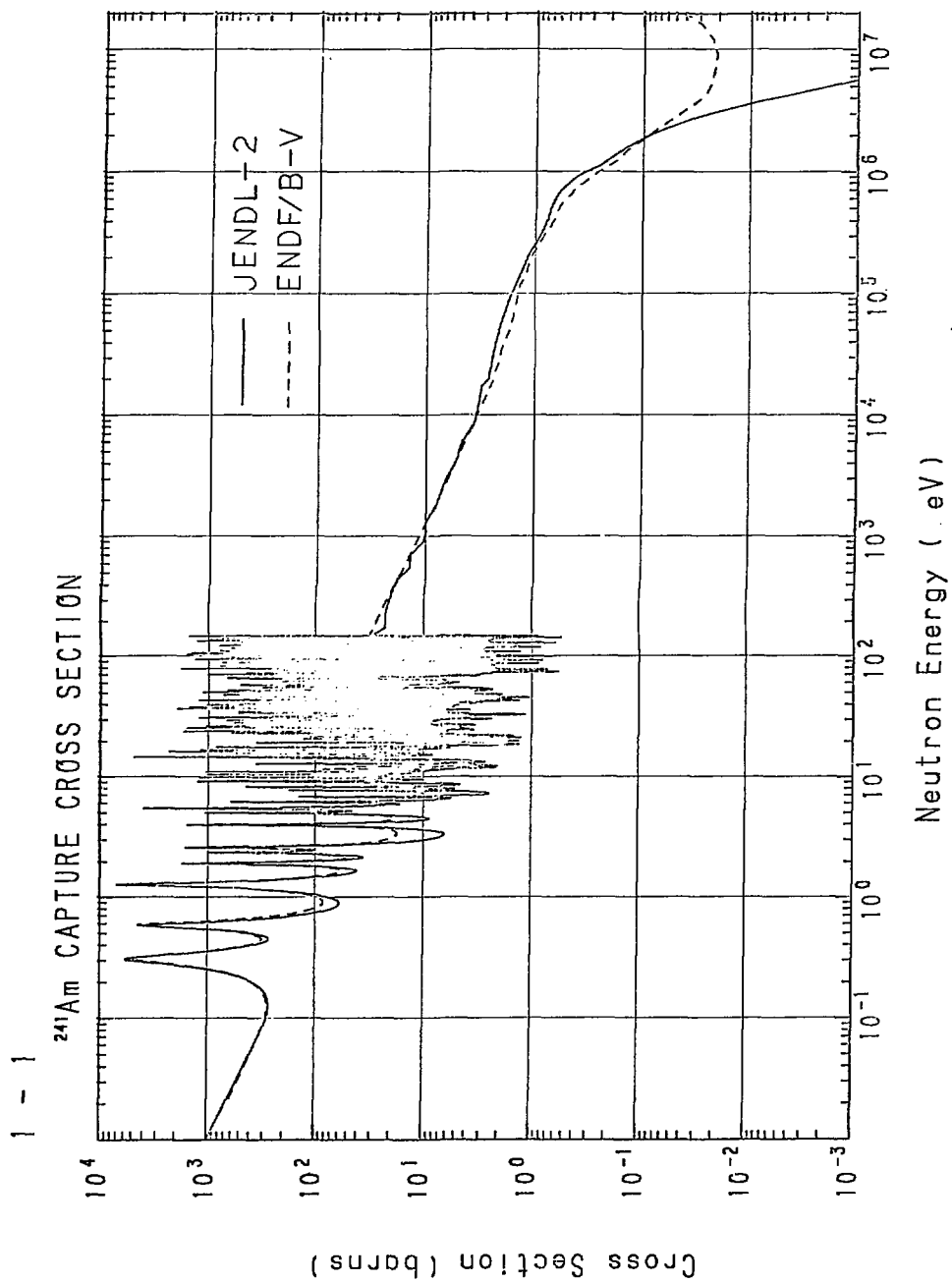
Fig. 3 ^{241}Am(n,γ) cross section.
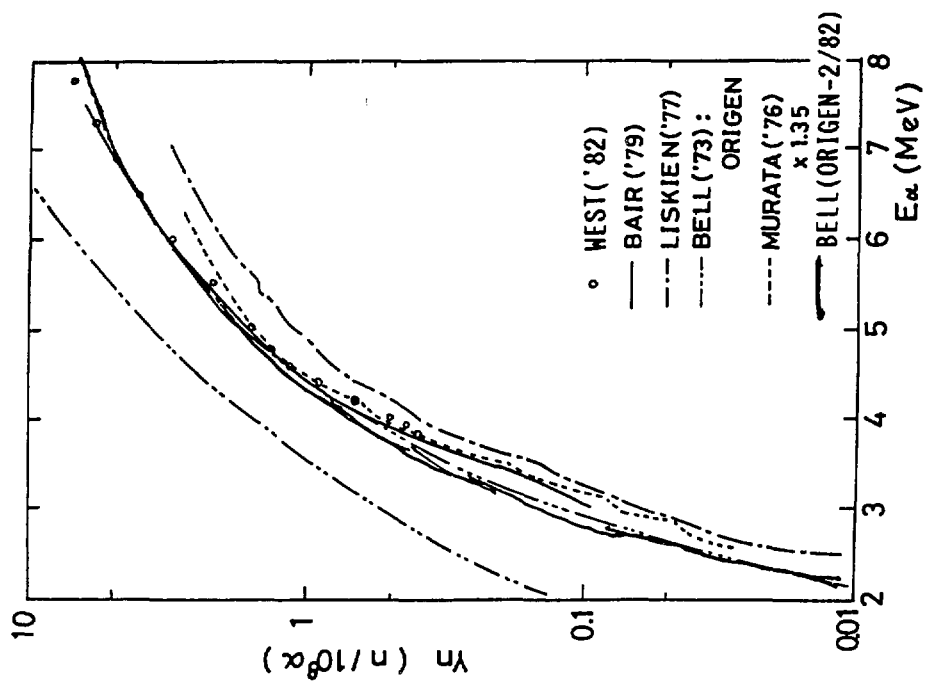
Fig. 5 Calculated thick target (α, n) yield in UO_2. Comparison of the calculation with the experimental and the evaluated data.
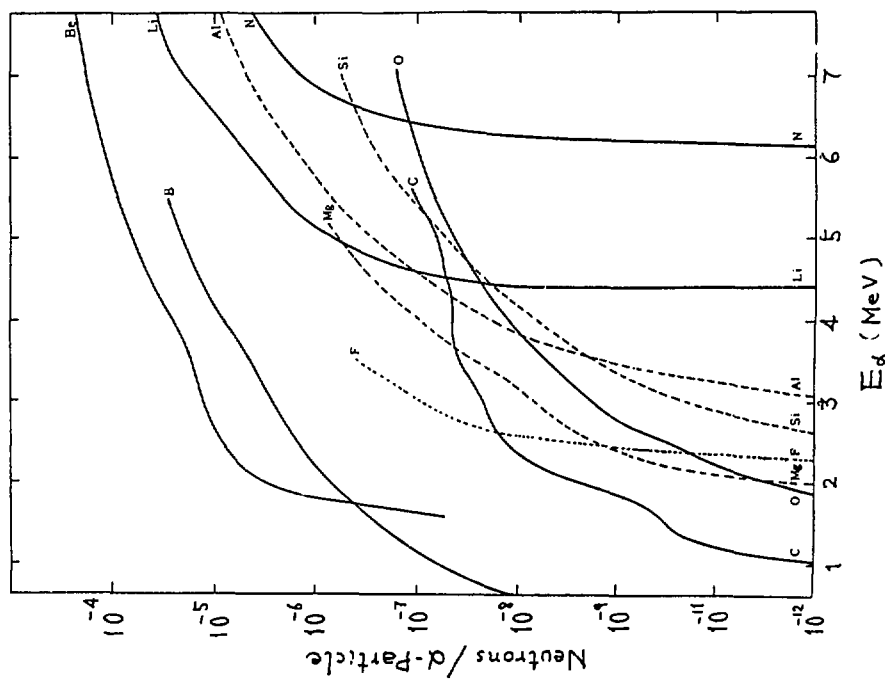

Fig. 4 Calculated thick target (α, n) yields in light element materials. (reproduced from R. Nakasima, JAERI−M 82-117 (1982))
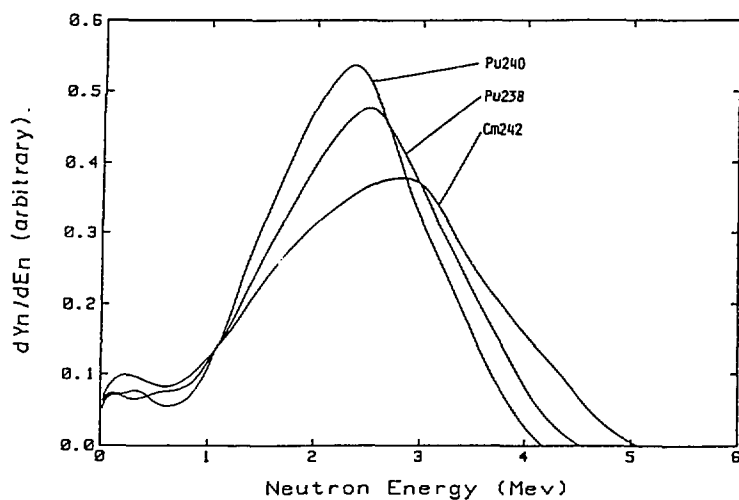
Fig. 6 Calculated (α,n) neutron spectra in oxide fuel for α-particle
emission from ^{240}Pu, ^{238}Pu and ^{242}Cm.
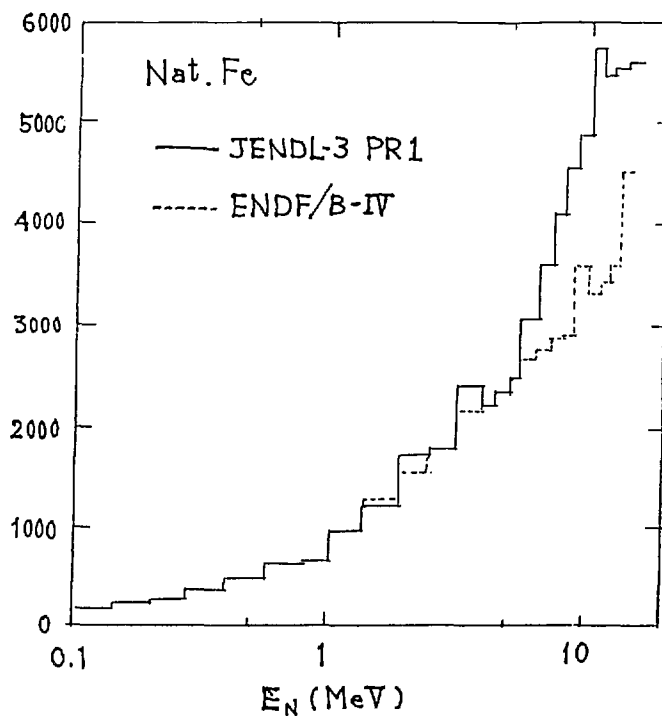
Fig. 7 Calculated DPA cross sections for natural iron using
JENDL-3PR1 and ENDF/B-IV. Calculation was made with TENJIN1
code of T. Ariga, JAERI (1984, priv. comm.).
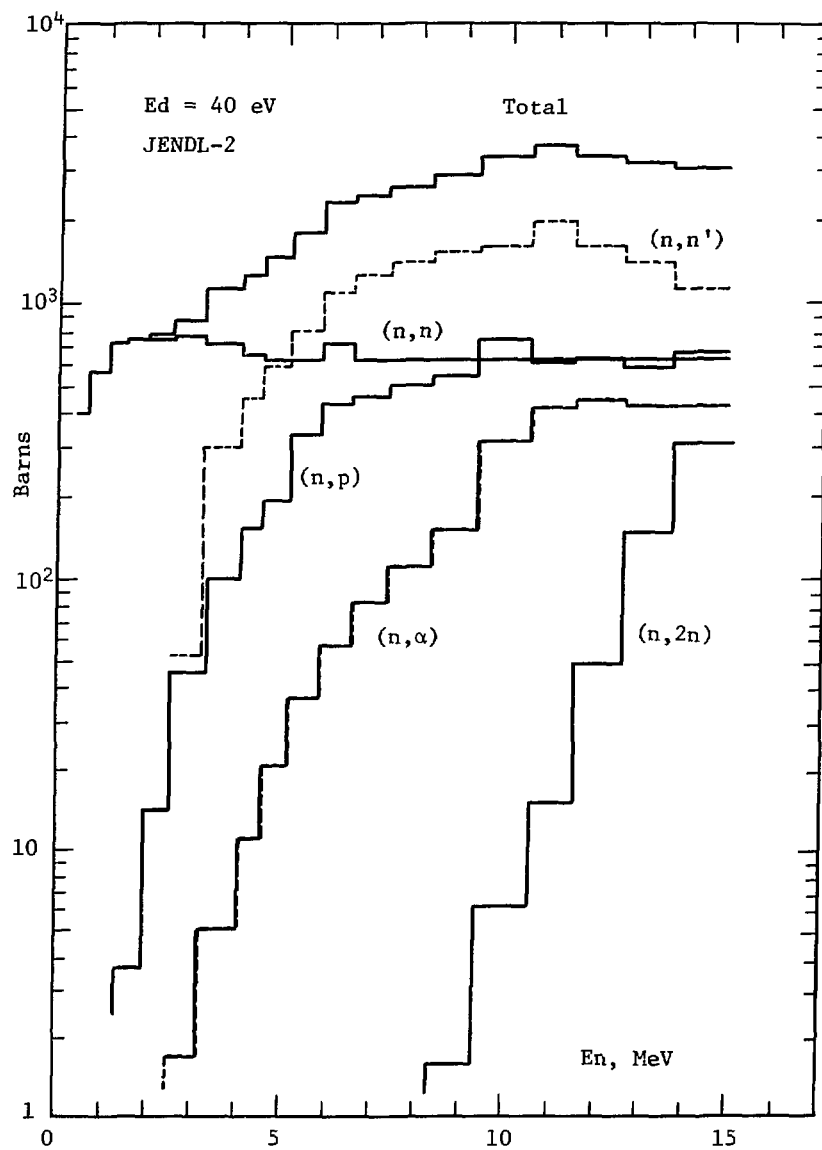
Fig. 8 Calculated DPA cross section for natural nickel and its reactionwise components using JENDL-2.

P.3   A Plan for Post-JENDL-3 Project

Tsuneo NAKAGAWA, Tadashi YOSHIDA[1], Akira HASEGAWA,

Masaharu NAKAZAWA[1], Motoharu MIZUMOTO, Jun-ichi KATAKURA

Working Group on Post-JENDL-3 Activity Program
Japan Atomic Energy Research Institute

JENDL-3 project is in progress, and will be completed by the end
of this fiscal year. Japanese Nuclear Data Committee has investigated
the various possibilities of nuclear data activities by organizing *ad
hoc* committee on the post JENDL-3 project. Conclusion obtained by the
ad hoc committee was reported as an internal report, and also presented
in the oral session[1] and in the poster session at this Nuclear Data
Seminar. In the poster session, the stress was put on the standard
group constants and data books made from JENDL-3. Because Hasegawa[2]
gave the comment on the standard group constants, only the outline of a
plan for making data books is given below.

The wide range and long term activities of the JNDC have almost
completed the evaluated neutron data file JENDL 3 and the JNDC FP Decay
Data File version 2. These comprehensive files are expected to be uti-
lized widely for nuclear calculations in the form of the computer data-
base. These files, however, contains enormous pieces of valuable
information useful not only for the computers but also for individual
nuclear scientists and engineers if they are supplied in an appropriate
form. An effective means is to edit good data books from these data
files. One example is JEARI-M 9715[3] which carries yield and decay data
of more than 1000 fission-product nuclides. Because of extensiveness of
the data and clearness of display, this data book is widely used in
laboratories and industries in and out of Japan. Here we try to list
necessary conditions of good data books on nuclear data for application
purpose.

1) Completeness: A data book should cover all the quantities belonging to the category treated there. Lacking information should be filled up by theoretical means, for example.

2) Clearness: It is desirable that tables and graphs therein are self-explaining. Or, at least, the meaning of the quantities contained there should be understood with minimum reading explanations.

3) Well processing: Detailed data are not always required. Engineers and scientists often want processed data for specific purposes such as averaged one-group cross sections, resonance integral values, or rough idea on energy released by one fission or one decay.

The following are the data books which seem to be useful and can be easily made from JENDL-3 and the JNDC FP Decay Data File Version 2.

1) One group cross-section book: Comprehensive tables of one-group cross sections for as many as possible. Selection of appropriate averaging spectrum (FBR, LWR, LCLWR and so on) may be a key issue. Resonance integrals and the 2200-m/s values should be included.

2) FP decay and yield data book: Lives, averaged energies, fission yields (both independent and cummulative) should be included as well as illastrative display of decay chains.

3) Actinide data book: A comprehensive collection of actinide nuclear data may be worthy making. Effective cross sections, decay chains, lives and branching ratios, released energy associated with decay or fission should be included.

The above are only three of possible candidates of data book. A small task-force is planned to be formed to steer activity toward publication of data books on the basis of JENDL-3 and JNDC FP Decay Data File.

References

1) Nakazawa M., et al.:"Proposals on Post-JENDL-3 Activity Programme for Japanese Nuclear Data Committee", presented at this meeting.
2) Hasegawa A.:"For the Enhancement of the Utilization of Nuclear Data Prepared by JNDC", presented at this meeting.
3) Ihara H., et al.:"JNDC FP Decay and Yield Data", JAERI-M 9715 (1981)

P.4 A Program of Activation Cross Section Measurements on Fusion Reactor

Structural Components for 14 MeV Neutrons Using FNS Facility

Y. Ikeda, C. Konno, K. Oishi[*], K. Kawade[**], H. Yamamoto[**],

H. Miyade[**], T. Yamada[**], T. Katoh[**] and T. Nakamura

Japan Atomic Energy Research Institute Tokai-mura, Naka-gun, Ibaraki-ken

More than one hundred neutron activation cross sections on the fusion
reactor structural components have been measured for the energy range from
13.3 to 14.9 MeV utilizing the FNS facility in order to meet the nuclear data
needs in the fusion applications. To achieve the high quality experimental
data in terms of accuracy, reproducibility and reliability, considerable
cares have been taken into the data taking and their process by introducing
the sophisticated measuring technique to reduce significantly the overall
experimental time. The data measured showed much improvement in the accuracy
in comparison with previous data. The new compilation based on the present
data will be helpful for the new evaluation of the activation and the
dosimetry files.

1. Introduction

In recent years, there have been strong needs for activation cross
section data in terms of the induced activity and safety design analysis of
the D-T fusion reactor. A plenty of experimented data around 14 MeV have
been previously reported and great effort were taken place on their
compilation and evaluations. However, we often meet the severe discrepancy
among those data and difference between the evaluations for almost all
reaction cross sections. As for a user, it is a very serious problem that
which data is reliable to be used to estimate the quantity associated with
the activation in the fusion reactor. It is expected that the main source of
the discrepancy in the experimental data may arise from the difference of the
experimental conditions (the neutron field characterization, radiation
measuring technique, neutron monitor and standard data) and nuclear data used

---

* Shimizu Construction Company

** Nagoya University

to deduce the final data.

Recently, Bernard[1] has reported the compilation and evaluation of 14 MeV neutron activation cross sections on the selected reactions to solve the problem and showed the useful method to confirm the range of the accuracy of the available data. However, if we concern the more wide data assessement, more systematic experimental approach is required.

On this point of view, a program of activation cross section measurements on fusion reactor structural components for 14 MeV neutron has been conducted using the FNS [2] facility since 1983. In this experimental program, first of all we intended to measure the cross sections as many as possible and a emphasis was placed on the systematics and consistency in all data measured.

To achieve the systematic measurements on many reactions in the short time range, we introduced the new sophisticated γ-ray measuring technique employing multiple Ge detectors. And great concern was put on the source characteristic for the irradiation, which was very important to determine the incident neutron energy.

In this report, we describe the present status of the program. First, the categorization of the half-life of the activity is presented regarding with measuring conditions. Secondly, the irradiation field and its characteristics is given. And a brief note of the experimental configuration is described. Finally, some results are shown together with the previously reported data

2. Category of Activity

The radioactivities produced by the activation reactions are categorized in accordance with length of their half-lives regarding the measurement technique of radiation. The summarized categories are given in table 1 with associated impacts of these activities on the reactor parameters. In order to measure the activities with half-lives shorter than a minute, it is expected that there is some difficulty in the sample transportation in short time and the accuracy in the sample positioning during irradiation. Another difficulty arises in the category 4 where the long lived activity with half-life longer than years are concerned, because the activity level can not be expected to be enough to get satisfactory statistics of radiation. Thus, in this program, we focused on the reactions in the category 2 and 3. The activities in the category 3 can be measured by adapting the ordinary procedure : there is enough time to transport the sample manually to be

measured. On the other hand, in the category 2, we employed the pneumatic
sample transfer apparatus because of the rather short half-lives of the
activities.

3. Irradiation field and sample preparation

The D-T neutrons were generated at the tritium target mounted on the
target assembly at the end of the 80° beam line. The target assembly, as
shown in Fig. 1.1, was newly fabricated for the purpose of the cross section
measurement designing to keep the structural material around the target as
small as possible and to be able to measure the sample at 165° with respect
to incident d^+ beam direction. The incident d^+ ion energy and nominal
intensity were 330 keV and 1.5 mA, respectively. The neutron yield was about
2×10^{11} n/s at the target. Irradiation time ranged 2 min to 6 hr depending
on the half-lives of the activities.

Basically, we used the separated isotopes to measure the independent
reaction cross section in order to identify the contribution from the
competing reactions which occured in the adjacent isotopes. The samples were
deployed around the D-T target at the distance of 10 cm centered the target.
The angles of the samples with respect to the d^+ beam direction covered 0° to
165° so that the neutron energies ranged 13.3 to 14.9 MeV. Usually, the
samples were placed at the nine positions of angles 2.8°, 45°, 60°, 80°,
100°, 115°, 135°, and 165°. When the irradiation materials were powder, the
samples were prepared by wrappng them of about 50 mg in a cartridge paper,
the effective area being 1 cm². As the neutron flux monitor, we employed the
reaction of $^{93}Nb(n,2n)^{92m}Nb$ because the reaction has properly high and
constant cross sections around 14 MeV neutron energy region and the product
of ^{92m}Nb has the considerably long half-life which enables rather lengthy
γ-ray measurements of them. For the measurements of the category 3
activities, two niobium foils of 10 x 10 x 0.1 mm were attached to the front
and rear surfaces of the samples. The samples were supported by the holder
made of foam styrene shown in Fig. 1.2.

For the measurements of the category 2 activities, a pneumatic sample
transport system shown in Fig. 1.3 was introduced. The system enabled the
measurement of γ-rays so efficient in a short time getting enough counting
statistics. The angles of the irradiation position to the d^+ beam were 5°,
45°, 65°, 95°, 135° and 165°. The samples were put in the sample holders
(outer dia. 18 mm, length 40 mm) shown in Fig. 1.4 and were sent to the other
end of the pneumatic tube through the thick shielding wall between the target

room and the work room at the FNS facility. The neutron flux at the sample
position was determined with use of the associated α-particle counting, the
relation to which was obtained from the flux value measured absolutely by the
$^{27}Al(n,\alpha)^{24}Na$ activation. Thus there was no need to measure the monitor
activity.

4. γ-ray measurement and data analysis

   After the irradiation, gamma-rays emitted from the produced activities
were measured by Ge detectors. In this series experiment, we employed five
Ge detectors two of which served as standard detectors, the others of which
played as the relative detectors. This detection system made the overall
measuring time short. Consequently, we could manage the many different
measurements so efficiently. The irradiated samples were placed just in
front of the relative detector head and the γ-rays were measured one by one.
The short distance between the source to the detector made the detection
efficiency higher by a factor of about 10 to 20 than that at the usual
position of the source at several cm. One more sample with the same form as
the other samples was irradiated with rather strong neutron flux. This sample
was used in the calibration between the standard and relative detectors.

   This procedure also showed its efficiency in the measurement of the
monitor foils of Nb. Regarding the large number of Nb to be measured, the
two Nb monitor foils for one sample were measured simultaneously with one
relative detector. Moreover, we adopted the total counts of the γ-ray from
the Nb foils as the relative counts because there is no interference activity
except ^{92m}Nb produced by the monitor reactions. This method could signifi-
cantly reduce the over-all measuring time. In the case of the category 2,
the samples were measured as soon as possible after they were returned to the
outside through the pneumatic tubes. The source for the detector calibration
was prepared by irradiating the sample using a special pneumatic channel end
of which located near the target.

   All cross section values were obtained as the ratio to the standard
reaction cross sections of $^{27}Al(n,\alpha)^{24}Na$ or $^{93}Nb(n,2n)^{92m}Nb$. The reaction
rate was deduced from the measured activity by performing appropriate
corrections which included the time of irradiation, cooling and measuring,
the sample weight, the counting loss due to the sum peak, the self-absorption
of the γ-ray in the sample, the difference of the effective sample position
due to the finite thickness of the sample from the position of the calibra-
tion sample and the neutron flux fluctuation during irradiation. The

absolute γ-ray detection efficiencies of the standard detectors were obtained
by using the standard calibration sources. The terms to deduce the reaction
. rate are shown in Table 2 together with their estimated errors. The main
error sources were due to the detector efficiency and the counting statis-
tics.

The reaction rate is given as the integrated products with the incident
neutron flux and cross section over the sensitive energy range. The incident
neutron usually has the energy spectrum and the neutron energy spreads below
14 MeV whenever any target assembly is used to support the target. In other
words, the neutron spectrum is not monoenergetic. The kinematics of the
$^3T(d,n)^4He$ in the target layer also yield somewhat distributed energy
spectrum of the emitted neutron.

On the other hand, almost all reactions have their threshold energies
and react with the neutrons above the thresholds. A difficulty is expected
in the determination of the mean reaction neutron energy from the integrated
reaction rate. In order to solve this problem, we calculated the neutron
spectra emitted from the target with the Monte Carlo code, MORSE simulating
the structure of the target assembly precisely. The neutron spectra for
corresponded angles of the sample position with respect to the incident d^+
beam direction are show in Fig. 2. In order to estimate the contribution of
the low energy neutrons to the reaction rate, the fractional reaction rates
due to neutrons below 10 MeV were calculated by using the neutron spectra and
well known reaction cross sections as a function of their Q values. By using
these results the contribution of neutron lower then 10 MeV was subtracted
from the measured reaction rate regarding its Q value. Fortunately, all
neutron spectra have deep valley around 10 MeV. We assume the 10 MeV as the
cut off energy to analyze the mean neutron energy.

5. Results and Summary

The list of reaction types measured are shown in Table 3 with associated
nuclear data used. Some of the results are shown in Fig. 3.1 to 3.4 together
with data previously reported and evaluated. As shown, the present data as a
whole cover the wide energy range and show the smaller experimental errors in
comparison with other data. The systematics among the present multiple data
indicates the reliability of the measurements. We are now compiling all of
data in a report including all informations about experimental conditions.
We hope the present experimental data to be helpful in the new evaluation of
the activation and the dosimetry files.

References

1. Evain, B. P., Smith, D. L and Lucches, P., ANL/NDM-89 (1985)

2. Nakamura, T., JAERI-M-86-080 (1986) PP290

Table 1 Categories of the activities and their impacts on the reactor
parameters

Category	Range of Half-Life	Associated impact
1	T1/2 $\lesssim$ min	accident gas production
2	min. < T1/2 $\leq$ hr.	maintenance
3	hr. < T1/2 $\lesssim$ year	waste
4	year < T1/2	transmutation

Table 2 Items needed to deduce the reaction rate and the cross section

Items	Estimated error (%)
1. Statistics of γ-ray counts	0.3 $\sim$ 5
2. Detector efficiency	2.0 $\sim$ 3.0
3. Sample weight	< 0.1
4. Time for irradiation, cooling and measuring	< 0.1
5. Self-absorption of γ-ray in the sample	< 0.5
6. Half-life (decay constant)	0.1 $\sim$ 2
7. γ-ray emission probability	0.5 $\sim$ 2
8. Correction factor about mean source position	$\sim$ 0.5
9. Fluctuation of neutron flux during irradiation	< 0.1
10. Counting loss due to sum peak of γ-rays	< 0.1
11. Monitor reaction cross section	$\sim$ 3.

Table 3 List of the reaction types measured and associated nuclear data

No.1

Target Nucleus	Reaction	Product	Half-life	Gamma-ray Energy [keV]	Branching Ratio[%]
^{19}F	(n,2n)	^{18}F	109.72 m	511.0	193.8
^{23}Na	(n,2n)	^{22}Na	2.602 y	1274.55	99.93
^{24}Mg	(n,p)	^{24}Na	15.03 h	1368.6	100
^{25}Mg *	(n,np)	^{24}Na	15.03 h	1368.6	100
^{27}Al	(n,p)	^{27}Mg	9.462 m	843.76	73.1
^{28}Si	(n,p)	^{28}Al	2.24 m	1778.7	100.0
^{29}Si *	(n,p)	^{29}Al	6.56 m	1273.2	89.1
	(n,np)	^{28}Al	2.24 m	1778.7	100.0
^{30}Si	(n,α)	^{27}Mg	9.462 m	843.76	73
^{35}Cl	(n,2n)	^{34m}Cl	31.99 m	2127.65	42
^{39}K	(n,2n)	^{38}K	7.613 m	2167.5	99.8
^{41}K	(n,p)	^{41}Ar	1.827 h	1293.64	99.16
	(n,α)	^{38}Cl	37.29 m	1642.16	31
^{42}Ca *	(n,p)	^{42}K	12.36 h	1524.3	18.8
^{43}Ca	(n,p)	^{43}K	22.2 h	617.8	64.8
^{44}Ca *	(n,p)	^{44}K	22.15 m	1157.0	58
	(n,np)	^{43}K	22.2 h	617.8	64.8
	(n,α)	^{41}Ar	1.827 h	1293.64	99.16
^{48}Ca *	(n,2n)	^{47}Ca	4.54 d	1297.0	77
^{45}Sc	(n,2n)	^{44m}Sc	2.442 d	271.24	86.6
	(n,2n)	^{44g}Sc	3.927 h	1157.0	99.89
	(n,α)	^{42}K	12.361 h	1524.6	18.8
^{46}Ti *	(n,2n)	^{45}Ti	3.08 h	511.0	170.0
	(n,p)	^{46}Sc	83.8 d	889.25	100.0
^{47}Ti *	(n,p)	^{47}Sc	3.422 d	159.38	68.5
	(n,np)	^{46}Sc	83.8 d	889.25	100.0
^{48}Ti *	(n,p)	^{48}Sc	43.67 h	983.5	100.0
	(n,np)	^{47}Sc	3.422 d	159.38	68.5
^{49}Ti *	(n,np)	^{48}Sc	43.67 h	983.5	100.0
^{50}Ti *	(n,p)	^{50}Sc	1.71 m	1553.71	100.0

Table 3 (Continued)

Target Nucleus	Reaction	Product	Half-life	Gamma-ray Energy [keV]	Branching Ratio[%]
	(n,α)	^{47}Ca	4.54 d	1297.03	77.0
^{51}V	(n,p)	^{51}Ti	5.8 m	319.7	93.4
	(n,α)	^{48}Sc	43.67 h	983.5	100.0
^{50}Cr *	$(n,2n)$	^{49}Cr	41.9 m	152.93	29.07
^{52}Cr *	$(n,2n)$	^{51}Cr	27.701 d	320.08	10.2
	(n,p)	^{52}V	3.746 m	1434.06	100.0
^{55}Mn	$(n,2n)$	^{54}Mn	312.2 d	834.83	100.0
^{54}Fe *	(n,p)	^{54}Mn	312.2 d	834.83	100.0
	(n,α)	^{51}Cr	27.701 d	320.03	10.2
^{56}Fe	(n,p)	^{56}Mn	2.5785 h	846.75	98.87
^{57}Fe *	(n,np)	^{56}Mn	2.5785 h	846.75	98.87
^{59}Co	$(n,2n)$	^{58}Co	70.78 d	810.76	99.44
	(n,p)	^{59}Fe	44.56 d	1099.22	56.5
	(n,α)	^{56}Mn	2.579 h	846.75	98.87
^{58}Ni	$(n,2n)$	^{57}Ni	35.99 h	1377.59	77.6
	(n,p)	$^{58m+g}$Co	70.78 d	810.76	99.44
	(n,np)	^{57}Co	271.65 d	122.06	85.6
^{63}Cu	$(n,2n)$	^{62}Cu	9.730 m	511.0	195.6
^{65}Cu	$(n,2n)$	^{64}Cu	12.699 h	511.0	38.6
	(n,p)	^{65}Ni	2.52 h	1115.84	15.134
^{90}Zr *	$(n,2n)$	^{89m}Zr	4.18 m	587.8	89.5
	$(n,2n)$	$^{89m+g}$Zr	78.43 h	909.2	99.01
	(n,p)	^{90m}Y	3.19 h	479.51	91.0
	(n,α)	^{87m}Sr	2.805 h	388.4	87.0
^{91}Zr *	(n,p)	^{91m}Y	49.71 m	555.57	94.9
	(n,np)	^{90m}Y	3.19 h	479.51	91.0
^{92}Zr *	(n,p)	^{92}Y	3.54 h	934.5	13.9
	(n,np)	^{91m}Y	49.71 m	555.57	94.9
^{94}Zr *	(n,p)	^{94}Y	18.7 m	918.8	56.0
	(n,α)	^{91}Sr	9.48 h	1024.3	33.0

Table 3   (Continued)

Target Nucleus	Reaction	Product	Half-life	Gamma-ray Energy [keV]	Branching Ratio[%]
	(n,np)	^{93}Y	10.25 h	266.9	6.8
^{96}Zr *	(n,2n)	^{95}Zr	63.98 d	756.72	54.6
^{93}Nb	(n,2n)	^{92m}Nb	10.14 d	934.51	99.2
	(n,α)	^{90m}Y	3.19 h	202.53	98.0
^{92}Mo *	(n,2n)	^{91m}Mo	64 s	652.9	48.1
	(n,p)	^{92m}Nb	10.14 d	934.51	99.2
	(n,α)	^{89m}Zr	4.18 m	587.8	89.5
	(n,α)	$^{89m+g}Zr$	78.43 h	909.2	99.01
^{94}Mo *	(n,2n)	^{93m}Mo	6.95 h	263.06	56.72
	(n,p)	^{94m}Nb	6.26 m	871.0	0.47
^{95}Mo *	(n,p)	^{95m}Nb	86.6 h	235.69	25.54
	(n,p)	^{95g}Nb	34.97 d	765.78	99.82
^{96}Mo *	(n,p)	^{96}Nb	23.55 h	778.22	96.8
	(n,np)	^{95m}Nb	86.6 h	235.69	25.54
	(n,np)	^{95g}Nb	34.97 d	765.78	99.82
^{97}Mo *	(n,p)	^{97m}Nb	60 s	747.0	97.9
	(n,p)	$^{97m+g}Nb$	72.1 m	657.92	98.2
	(n,np)	^{96}Nb	23.55 h	778.22	96.8
^{98}Mo *	(n,p)	^{98m}Nb	51.3 m	787.36	93.2
	(n,np)	^{97m}Nb	60 s	747.0	97.9
	(n,np)	$^{97m+g}Nb$	72.1 m	657.92	98.2
^{100}Mo *	(n,2n)	^{99}Mo	66.02 h	739.4	12.6
	(n,α)	^{97}Zr	16.9 h	743.36	92.8
^{112}Sn *	(n,2n)	^{111}Sn	35.0 m	761.2	0.66
	(n,np)	^{111}In	2.83 d	172.1	87.6
^{114}Sn *	(n,2n)	^{113}Sn	115.07 d	255.06	1.82
	(n,p)	^{114m}In	49.51 d	190.24	15.6
^{116}Sn *	(n,p)	^{116m}In	54.12 m	416.86	27.8
^{117}Sn *	(n,p)	^{117m}In	1.93 h	315.3	16.9
	(n,p)	^{117g}In	42.3 m	552.9	99.7
	(n,np)	^{116m}In	54.12 m	416.86	27.8

Table 3 (Continued)

Target Nucleus	Reaction	Product	Half-life	Gamma-ray Energy [keV]	Branching Ratio[%]
^{118}Sn *	(n,2n)	^{117m}Sn	14.0 d	158.6	86.4
^{120}Sn *	(n,α)	^{117m}Cd	3.31 h	564.4	15.2
	(n,α)	^{117g}Cd	2.42 h	273.28	29.0
^{124}Sn *	(n,2n)	^{123m}Sn	40.08 m	160.33	85.5
^{134}Ba	(n,2n)	^{133m}Ba	38.9 h	275.6	17.5
^{135}Ba *	(n,p)	^{135m}Cs	53 m	781	99.7
^{136}Ba *	(n,2n)	^{135m}Ba	28.7 h	268.24	16
	(n,p)	^{136}Cs	13.0 d	818.5	99.7
^{137}Ba *	(n,np)	^{136}Cs	13.0 d	818.5	99.7
^{138}Ba *	(n,2n)	^{137m}Ba	2.5513 m	661.65	89.9
	(n,p)	$^{138m+g}$Cs	32.2 m	1435.86	75
	(n,α)	$^{135m+g}$Xe	9.104 h	249.79	90
^{181}Ta	(n,2n)	^{180m}Ta	8.0 h	93.0	5.0
^{180}W *	(n,2n)	$^{179m+g}$W	37.5 m	133.9	0.106
^{184}W *	(n,p)	^{184m}Ta	8.7 h	111.19	24.3
^{186}W	(n,α)	^{183}Hf	64 m	783.73	65.0
^{197}Au	(n,2n)	^{196m}Au	9.70 h	188.23	37.84
	(n,2n)	^{196g}Au	6.183 d	355.65	87.6
^{204}Pb	(n,2n)	^{203}Pb	52.02 h	279.18	81.0

* Separated isotope
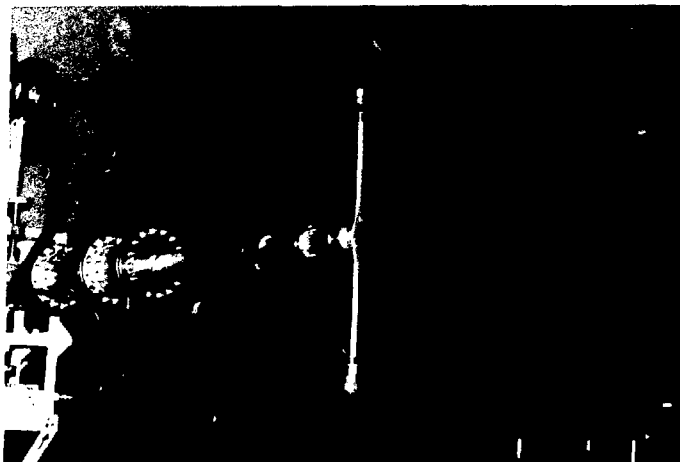
Fig. 1.1 Photograph of the target assembly specially fabricated for the
purpose of this activation cross section measurement program
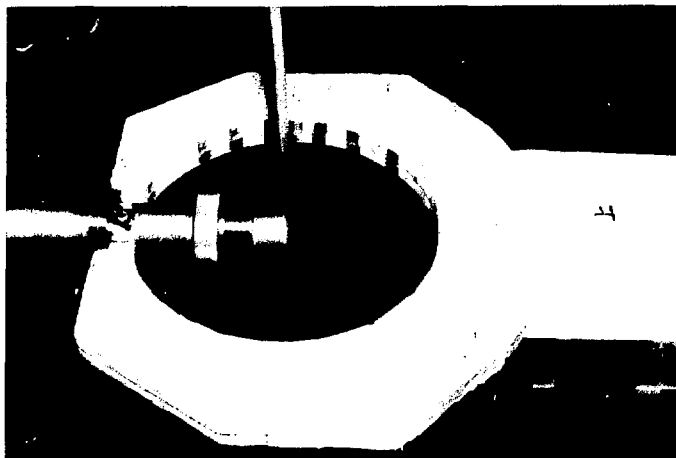
Fig. 1.2 Photograph of the sample holder to support the samples around the
target
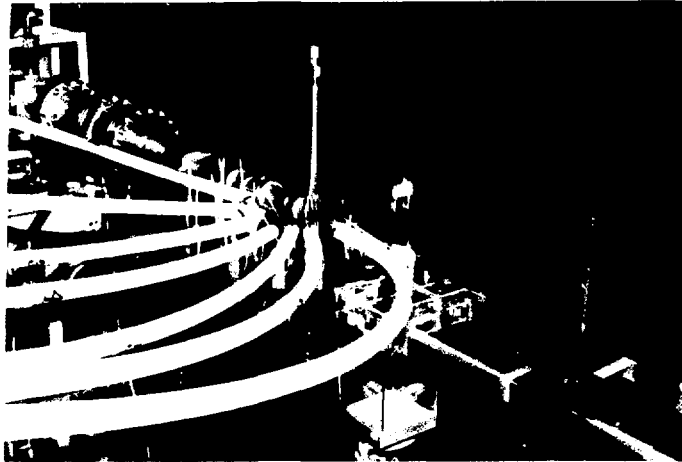
Fig. 1.3 Photograph of the pneumatic sample transfer system for the activity
of the category 2
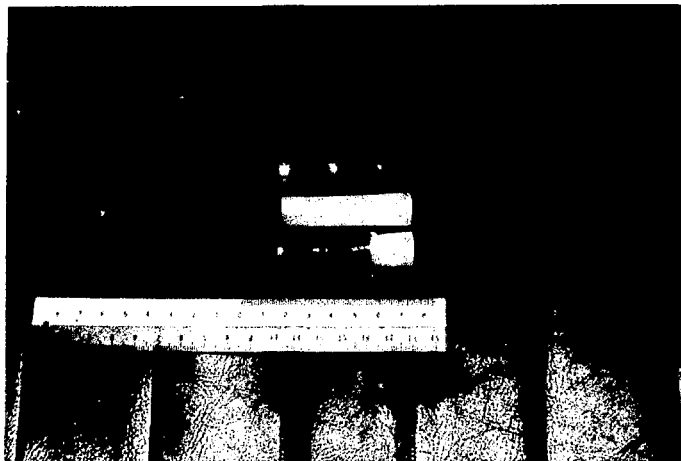
Fig. 1.4 Photograph of the sample holder for the pneumatic system
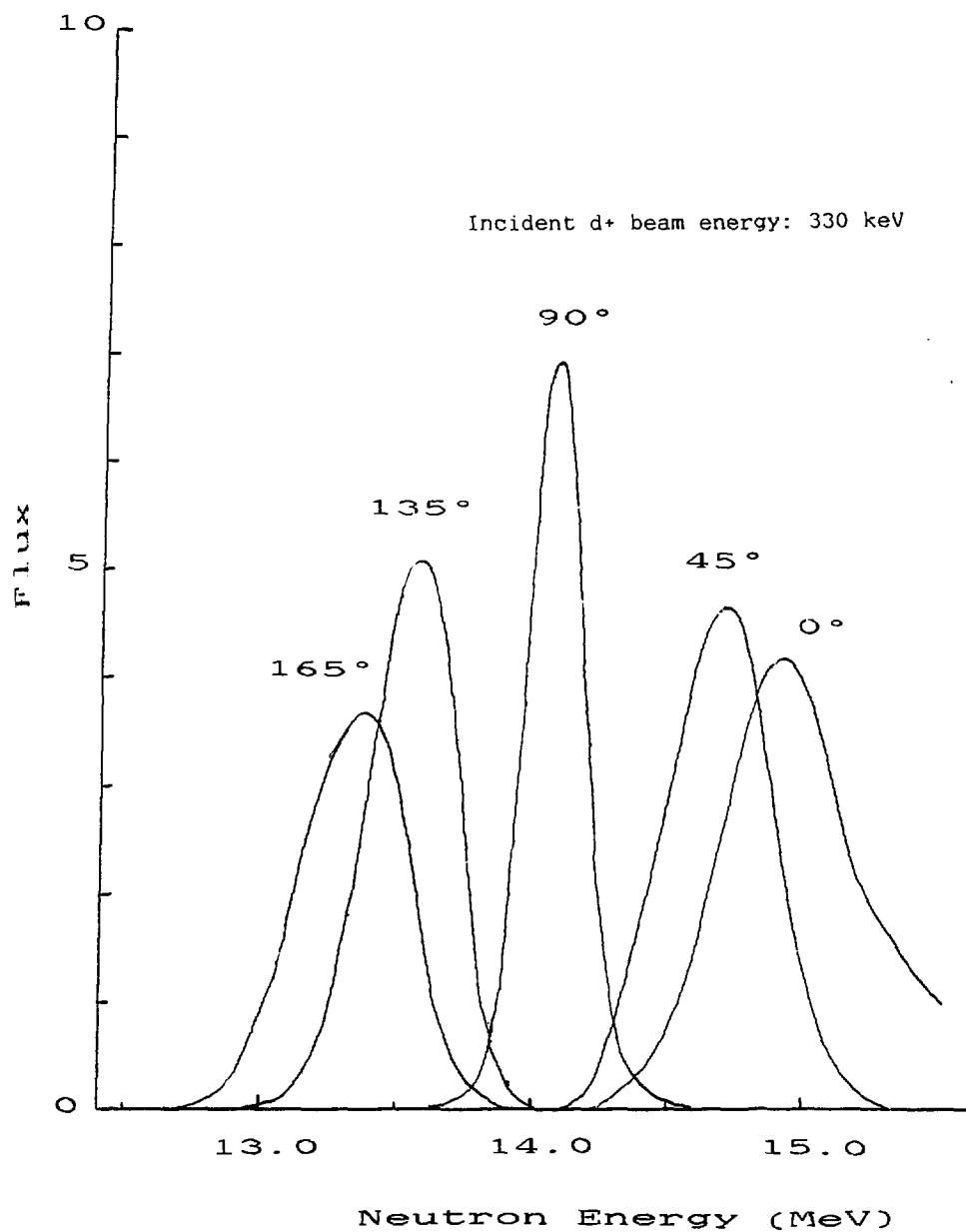
Fig. 2   Source neutron spectra calculated with the Monte Carlo code MORSE
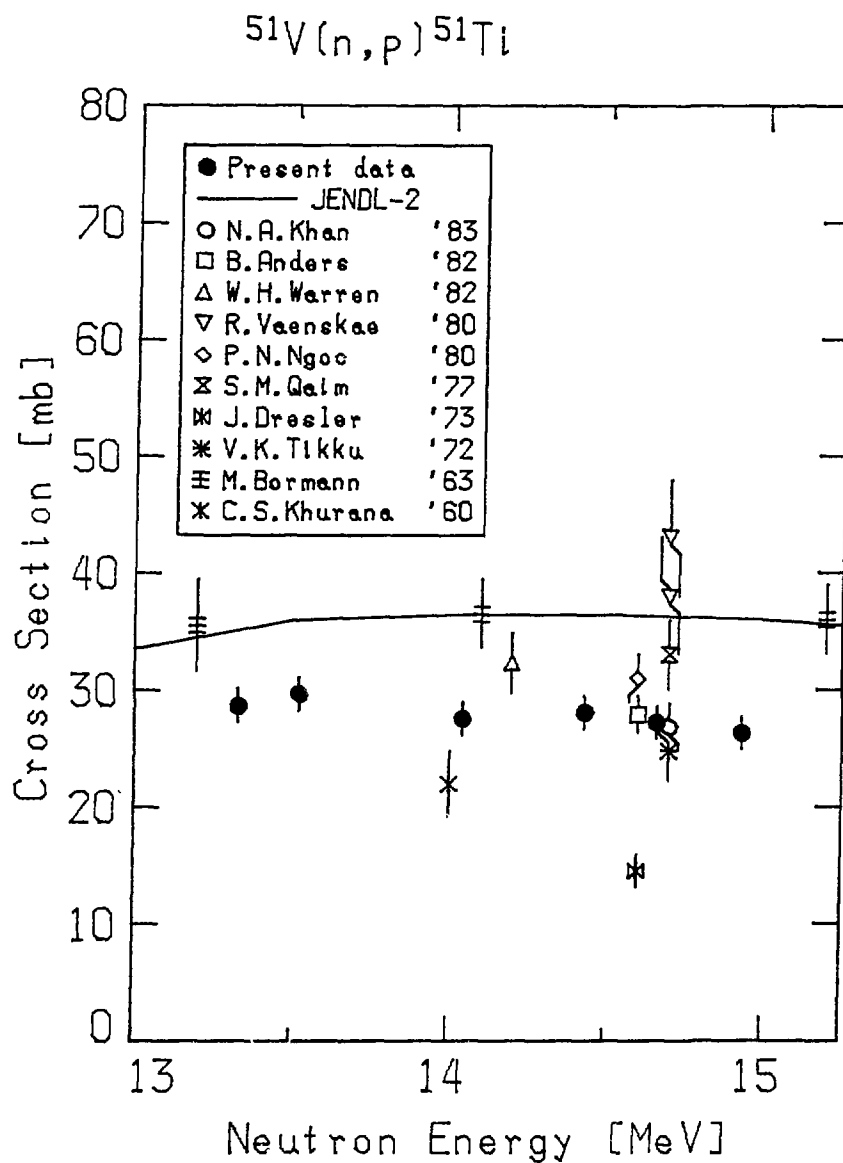
$$^{51}V(n,p)^{51}Ti$$

Fig. 3.1 Cross section data of $^{51}V(n,p)^{51}Ti$
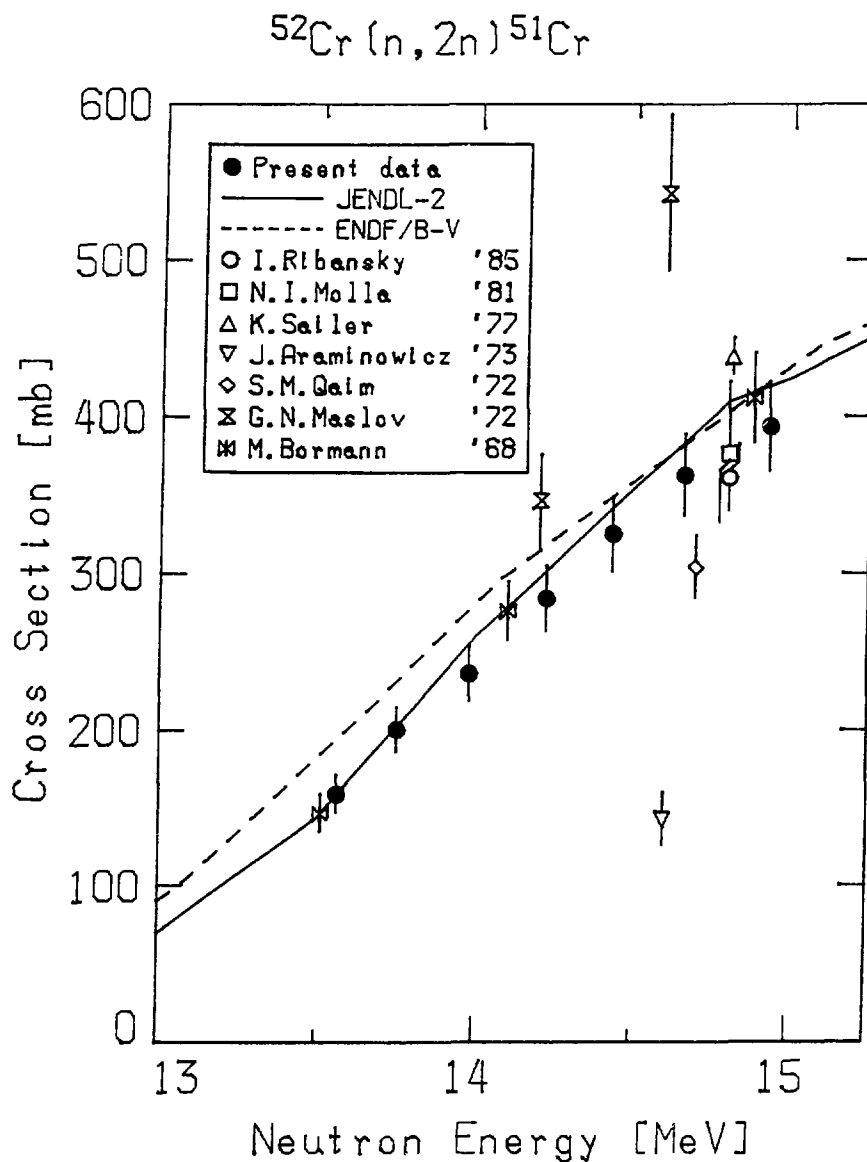
Fig. 3.3   Cross section data of $^{52}Cr(n,2n)^{51}Cr$
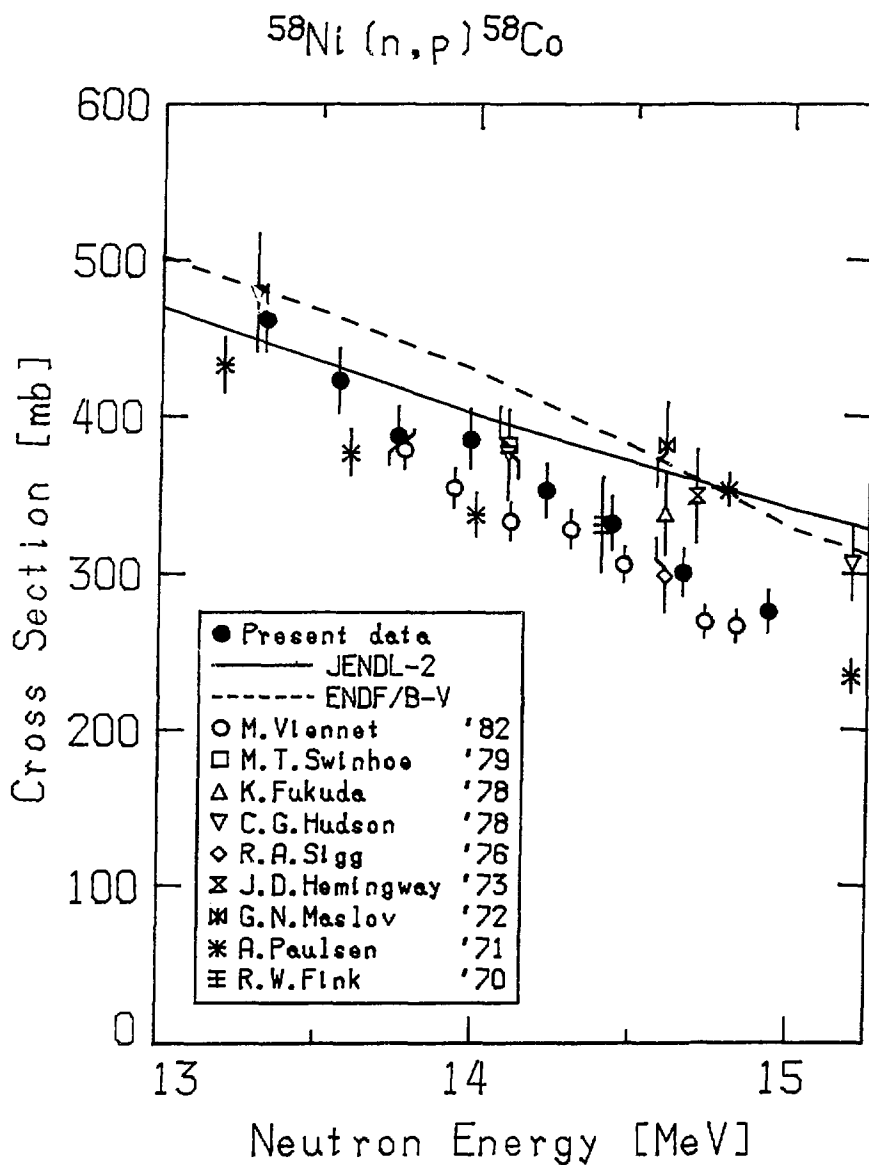
$$^{58}\text{Ni}\,(\text{n},\text{p})\,^{58}\text{Co}$$

Fig. 3.3   Cross section data of $^{58}\text{Ni}(\text{n},\text{p})^{58}\text{Co}$
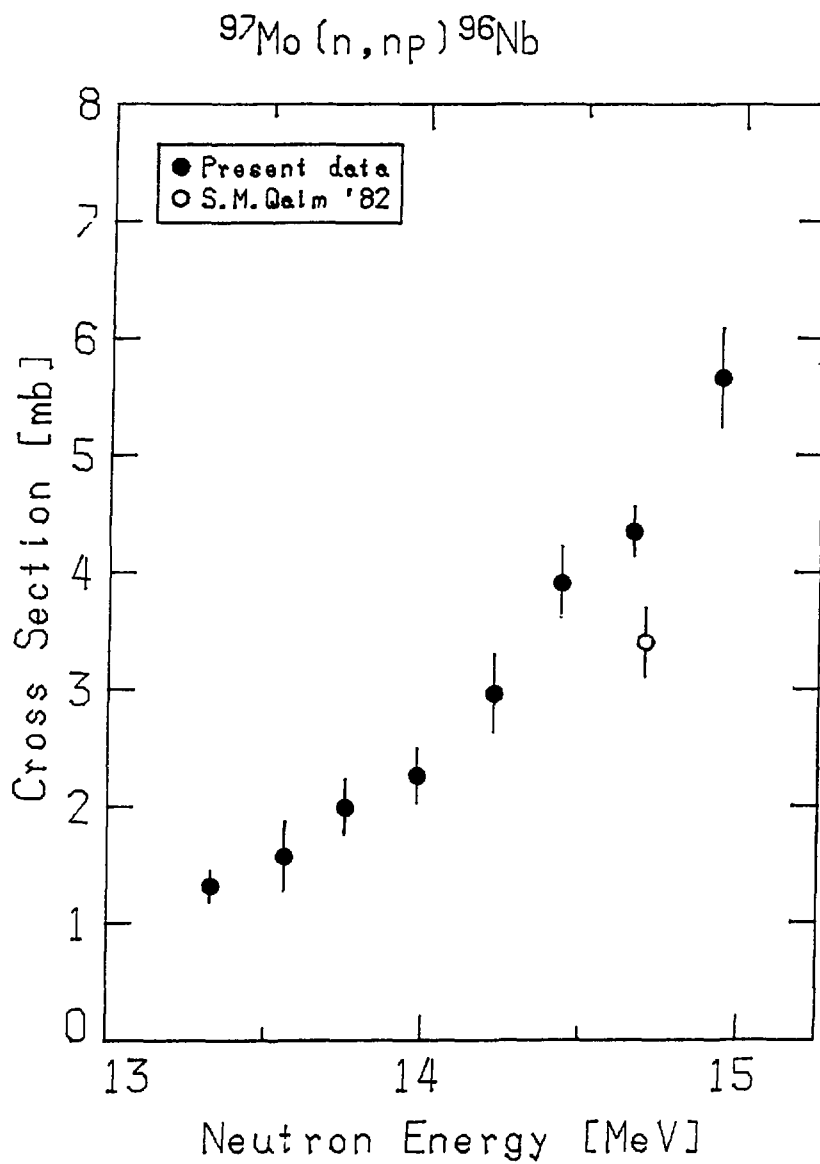
^{97}Mo (n, np) ^{96}Nb

Fig. 3.4 Cross section data of ^{97}Mo(n,np)^{96}Nb

P.5   Measurement of the fast neutron cross sections
at the JAERI tandem accelerator facility

S. Chiba, Y. Yamanouti, M. Mizumoto, M. Sugimoto,
M. Hyakutake*, S. Iwasaki** and Y. Kawarasaki

Japan Atomic Ene: zy Research Institute,
Tokai-mura, Naka-gun, Ibaraki-ken

The fast neutron time-of-flight and (n,xγ) spectrometers installed
at the JAERI tandem accelerator can provide the neutron nuclear data
between En = 5 and around 30 MeV region.   This paper presents an over-
view of the facility and methods of the fast neutron cross section
measurements there.   Some preliminary results of the recent experiments
are also described.

1. Introduction
     The JAERI tandem accelerator can provide 2.5 to 35 MeV proton and
deuteron beams. With the aid of these beams and the D(d,n) and ^{7}Li(p,n)
reactions, neutrons of about 5 to 30 MeV can be utilized in the neutron
nuclear data measurements. Except around 14 MeV, the neutron nuclear
data of this energy range are very poor, because there are no suitable
neutron sources with small accelerators. The neutron scattering cross
sections and neutron induced gamma-ray spectra of some isotopes have
been measured using the fast neutron time-of-flight (tof) spectrometer
and (n,xγ) spectrometer installed in the neutron target room of the
tandem accelerator facility. In the following sections, simple
descriptions of these spectrometers and some preliminary results
measured with them will be presented.

2. Fast neutron time-of-flight spectrometer
     A schematic layout of the fast neutron time-of-flight spectrometer
is shown in Fig. 1. This spectrometer was designed so as to measure the

----

 * : Faculty of Engineering, Kyushu University
** : Faculty of Engineering, Tohoku University

neutron scattering cross sections between En = 5 and 40 MeV.

A proton or deuteron beam bombards the neutron producing target. The charged particles can be extracted from both of the negative ion source (tandem mode) and in-terminal ion source (single Van de Graaff mode). Because the measurement is based on the time-of-flight method, these beams are usually chopped and bunched to produce pulsed beams. The pulse duration is typically about 1 ns at FWHM. The beam current is as much as 2 μA at a repetition rate of 2 MHz.

The $D(d,n)^3He$ reaction with gaseous D_2 target and the $^7Li(p,n)$ reaction with metallic lithium target are used as the neutron sources. The latter is used in the energy region of 30 MeV, because in this energy range it produces nearly monoenergetic neutrons.

Fig. 1 shows a setup with the $D(d,n)$ neutron source. The D_2 gas target is contained in a gas-cell of 3 cm in length and 1 cm in diameter, with a pressure of 2 atm. The scatterer is located at about 12cm from the center of the gas target.

Scattered neutrons are detected by an array of four VLD (very large detector) style NE213 liquid scintillation detectors. They are similar to that developed at OHIO university[1] except their sizes. However, the time-compensation can be done by both of the hardware and software method[2]. The flight path is about 8 m long. Angular range covered with this normal setup is 15 to 140°. But with a modified setup, the scattering angle is extended up to 160°.

Two monitor detectors view the neutron generating target directly for run-to-run normalization. Each monitor detector is a 5 cm diameter and 1.3 cm thick NE213 scintillator.

With this setup, we have measured the neutron scattering cross sections of ^{28}Si and ^{27}Al at En = 13.0 MeV, ^{118}Sn at En = 14.9 and 18.0 MeV, ^7Li at En = 11.0 and 13.0 MeV and ^{208}Pb at En = 12.0 MeV.

3. Measurement of the neutron scattering cross sections of ^{118}Sn
   at En = 14.9 and 18.0 MeV

As an example of the data measured at the fast neutron tof spectrometer, the results with ^{118}Sn target is presented. The scattering sample was loaned from the isotope division of Oak Ridge National Laboratory.

Typical tof spectra, after background subtraction, are shown in fig. 2. They were obtained at angles of 60° with 14.9 MeV and 70° with 18.0 MeV neutrons, respectively. Three prominent peaks can be noticed in this figure. The peaks corresponding to elastically scattered neutrons and inelastically scattered ones to the first 2^+ state (Q=-1.23 MeV) can be assigned undoubtedly, as seen in this figure. The remaining one contains contributions from many higher levels. But at most of the angles it is excited more strongly than the first 2^+ state which is a quadrupole one phonon vibrational state. Hence we temporally assigned $J^\pi = 3^-$ level (Q=-2.32 MeV, octupole vibrational state) to this peak.

Yields of these peaks were determined by fitting skewed gaussian functions to these spectra. After applying detector efficiency and absolute normalization, effects of the finite sample size were corrected by the Monte-Carlo method.

In figs. 3, 4 and 5 shown are the presently measured angular distributions. Solid lines show results of theoretical calculations.

Fig. 3 shows the angular distributions of elastically scattered neutrons. The solid lines represent the results of the spherical optical model (SOM) calculation. They were calculated by the code ECIS79. The optical model parameters were adjusted to reproduce the presently measured values. Agreement between the measured and calculated results is very good.

Figs. 4 and 5 show that the differential cross sections of the inelastically scattered neutrons are very strongly forward peaked. Thus the direct reaction process is dominant in these reactions. This is verified by a Hauser-Feshbach (H-F) calculation made by the code ELIESE-3. Contributions of the H-F process was found to be less than 0.1 % of the total yield of each level. Because ^{118}Sn is an even-even nucleus of medium weight, an incoming nucleon will strongly excite nuclear surface oscillation. Hence we performed a DWBA calculation assuming vibrational model with the same optical potential parameters as fig. 3. The DWUCK-4 code was used for this purpose. The solid lines in figs. 4 and 5 show the results of this calculation. The present calculation reproduces the measured data very well. Deduced quadrupole deformation length (deformation parameter times the real part radius)

agrees with that of Finlay et al.[3] but systematically lower than the
(p,p')[4,5] results. This difference shows the extent to which the
closed proton core is inhibited from vibration.

4. Measurement of the emitted gamma-ray spectrum of Al at En = 8.0 MeV

Using the (n,xγ) spectrometer, spectrum of the emitted gamma-rays
from Al at the incident neutron energy of 8 MeV was measured. Fig. 6
shows the schematic layout of the spectrometer. Source neutrons were
generated by the D(d,n)^{3}He reaction with a gas target. The main detec-
tor was a NaI(Tl) scintillator of 7.6 cm in diameter and 15.0 cm in
length. An annular NaI(Tl) scintillator surrounded the main detector to
suppress the Compton background. A 5 cm diameter by 1.3 cm thick NE213
scintillator was used as a neutron flux monitor. The pulse height
spectrum was converted to the gamma-ray energy spectrum by the FERDO
code.

Circles in fig.7 show the presently measured results. The trian-
gles show the data measured by Morgan et al. at ORELA[6]. Though the
present results are only preliminary, the resolution of them is superior
to those of Morgan et al's.

5. Conclusion

Using the JAERI tandem fast neutron tof facility, the fast neutron
scattering cross sections have been measured in the energy range of 10
to 20 MeV. We have also measured the spectrum of emitted gamma-rays
from Al at En = 8.0 MeV. The neutron nuclear data of this energy range
are very important for fusion reactor development. They are also very
important to study the reaction mechanisms and nuclear structures
through the optical model potentials and deformation parameters, etc.

References
1)J. D. Carlson et al.: Nucl. Instr. Methods 147(1977)353
2)M. Sugimoto: to bu published in Nucl. Instr. Methods
3)R. W. Finlay et al.: Nucl. Phys. A338(1980)45
4)O. Beer et al.: Nucl. Phys. A147(1970)326
5)W. Makofske et al.: Phys. Rev. 174(1968)1429
6)G. L. Morgan and F. G. Perey: ORNL/TM-5241 (1976)
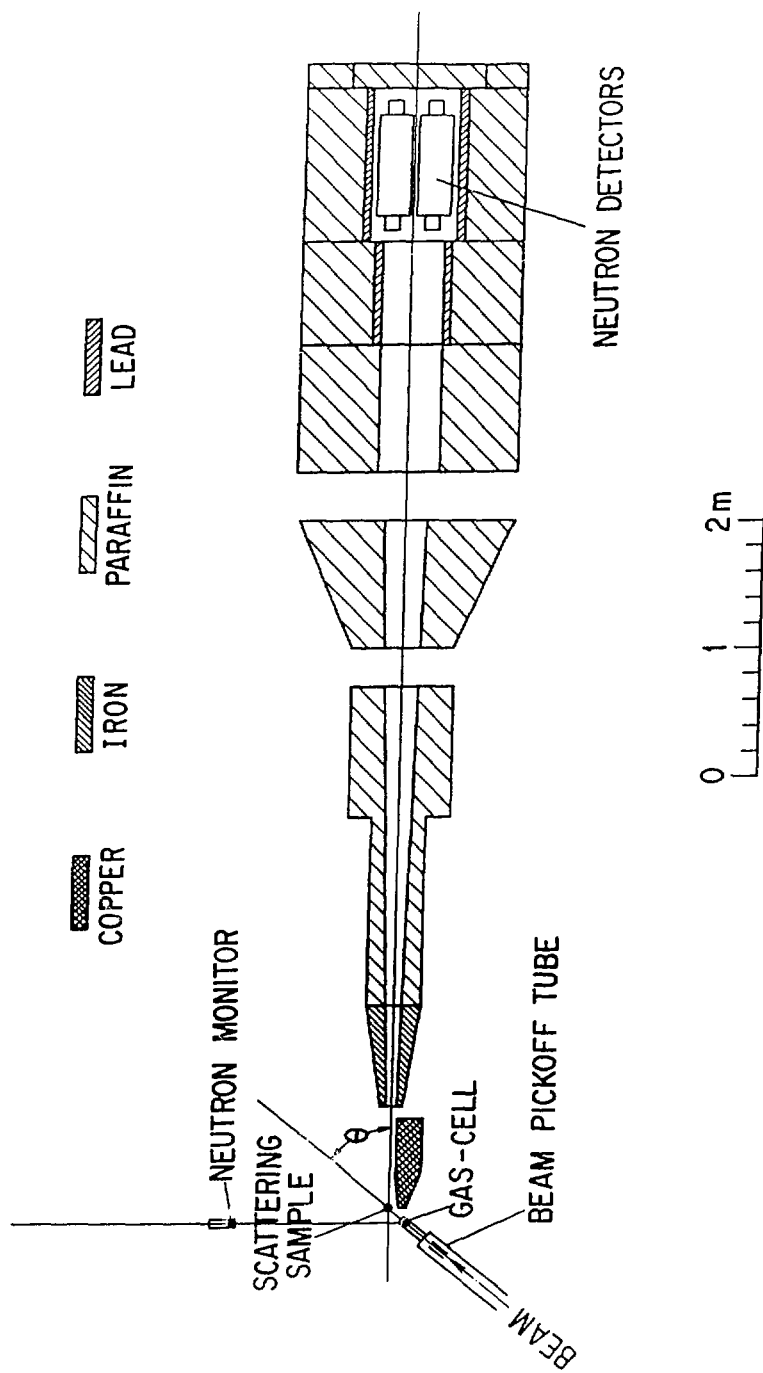
Figure 1   Experimental setup of the fast neutron time-of-flight
spectrometer
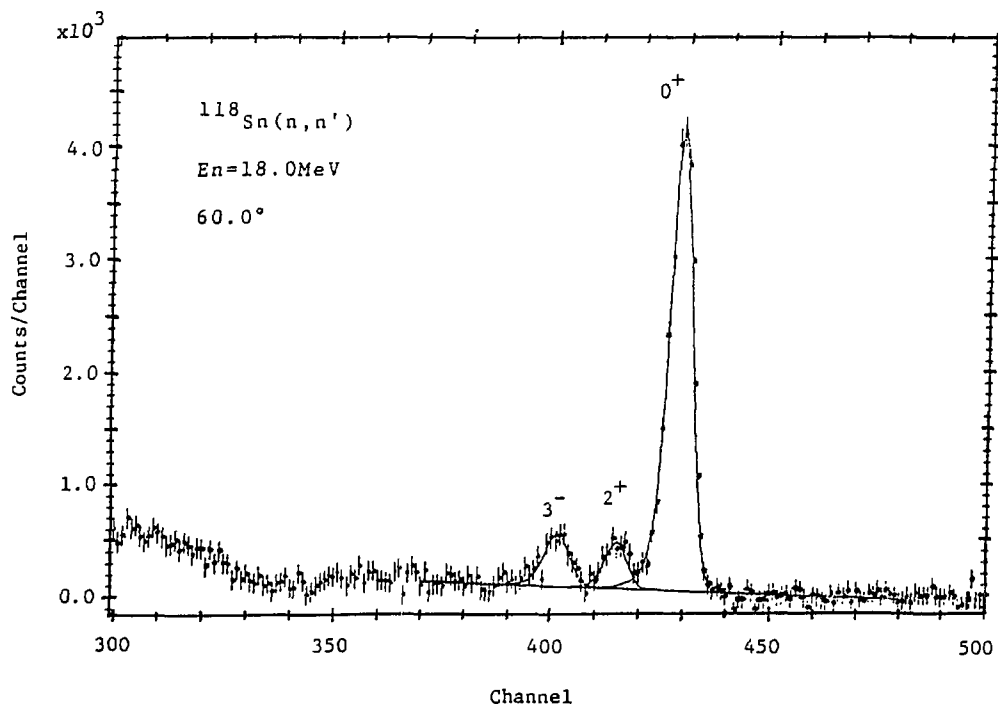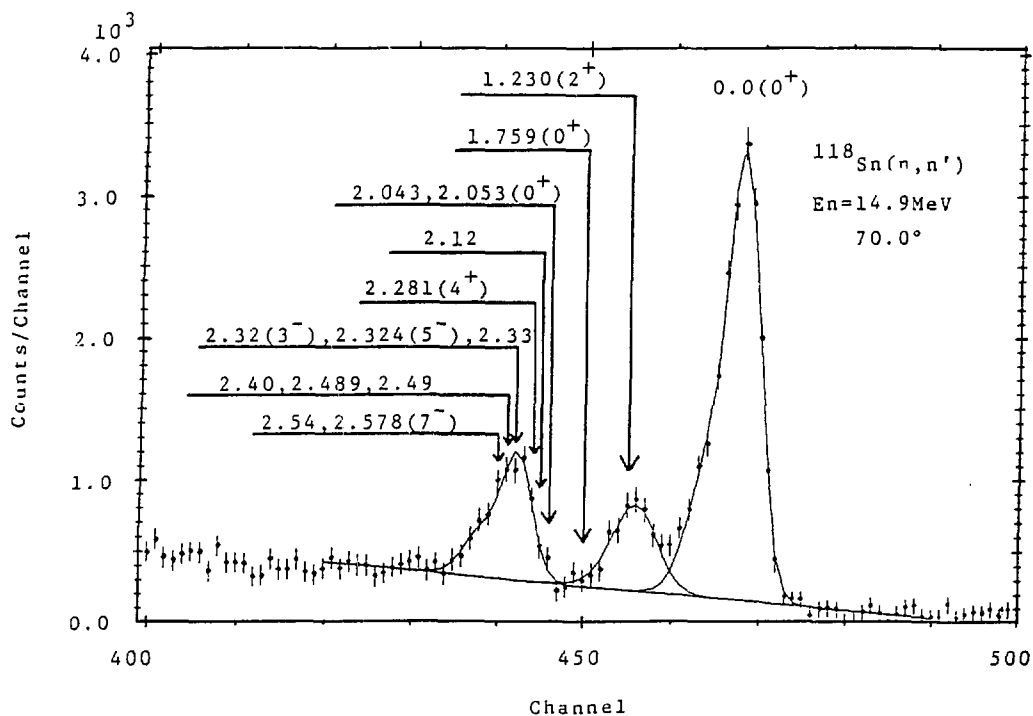
Figure 2   Typical time-of-flight spectra measured with (a) 14.9 and
(b) 18.0 MeV neutrons on ^{118}Sn
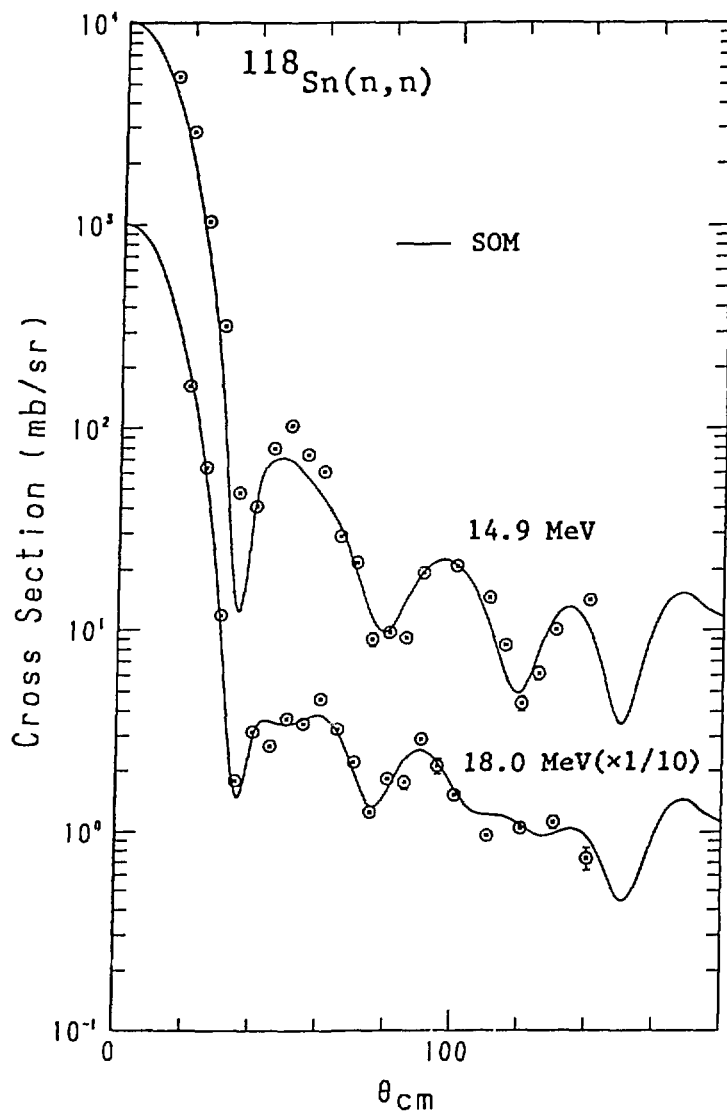
Figure 3 Angular distributions of the elastically scattered neutrons
from ^{118}Sn
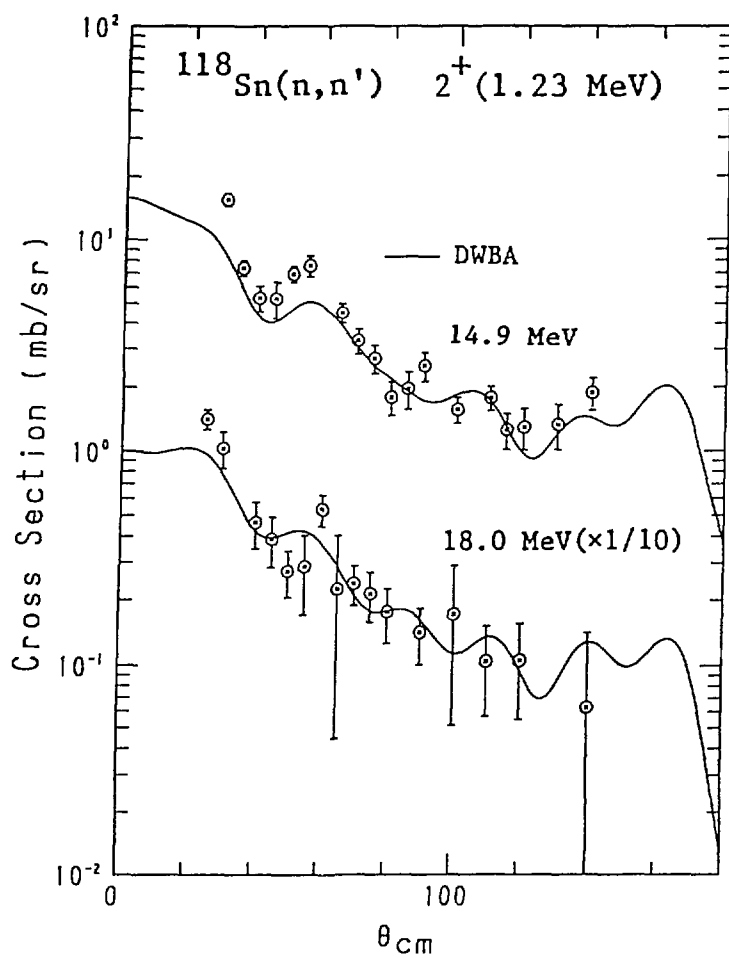
Figure 4 The ^{118}Sn(n,n') (Q = -1.23 MeV) angular distributions
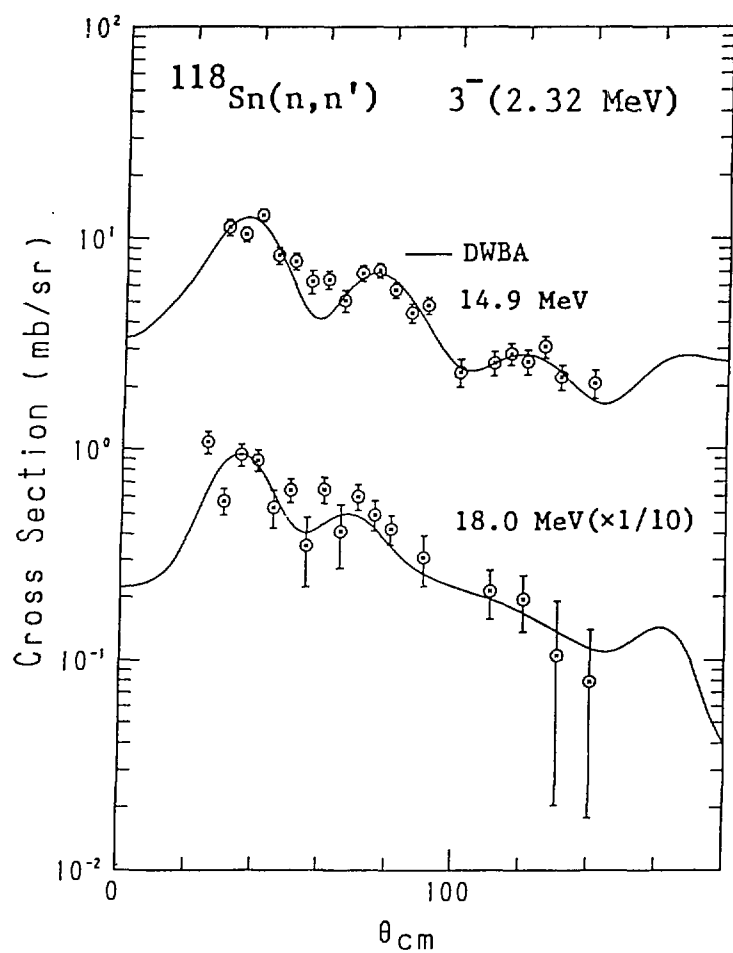
Figure 5 The ^{118}Sn(n,n') (Q = -2.32 MeV) angular distributions
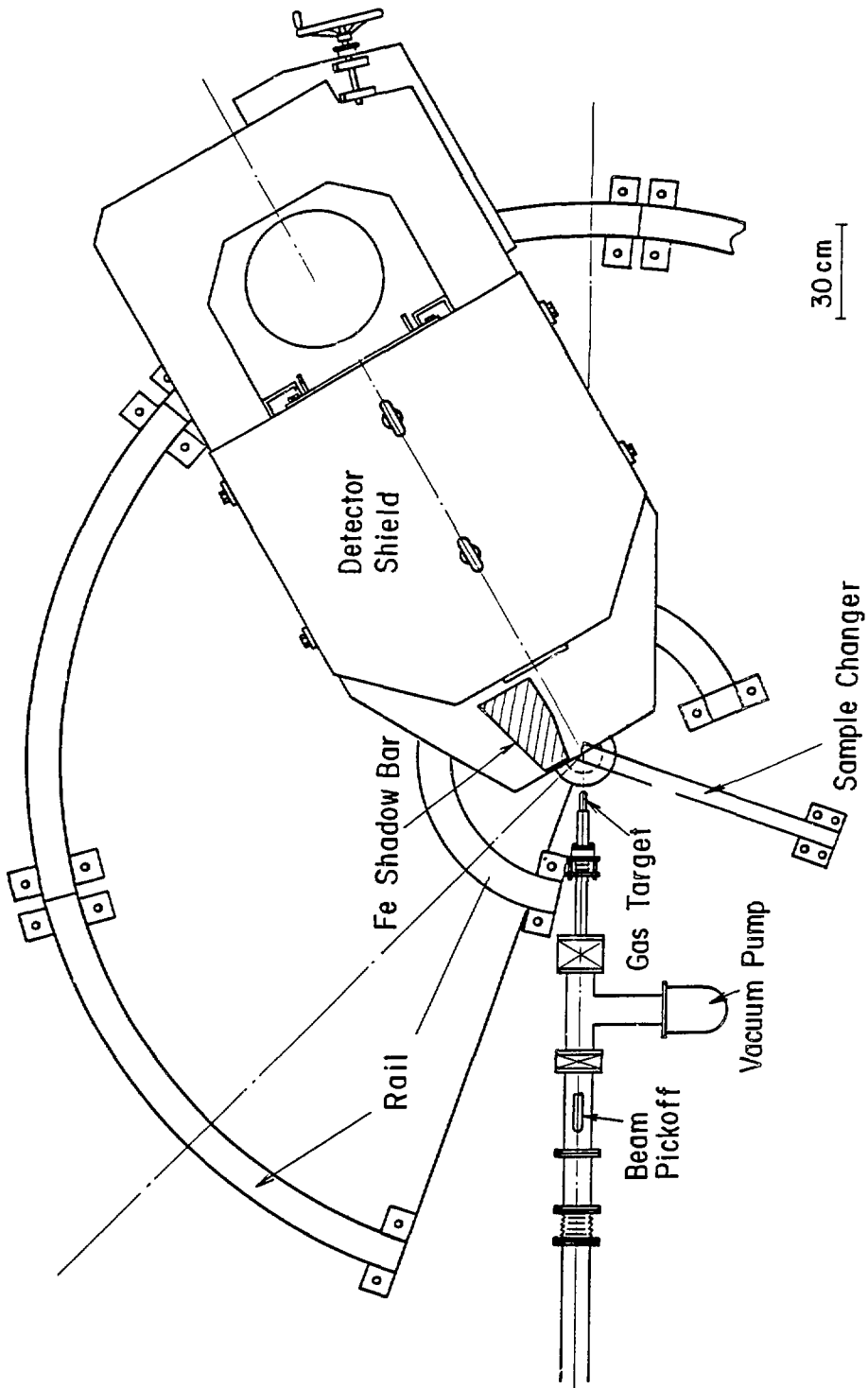
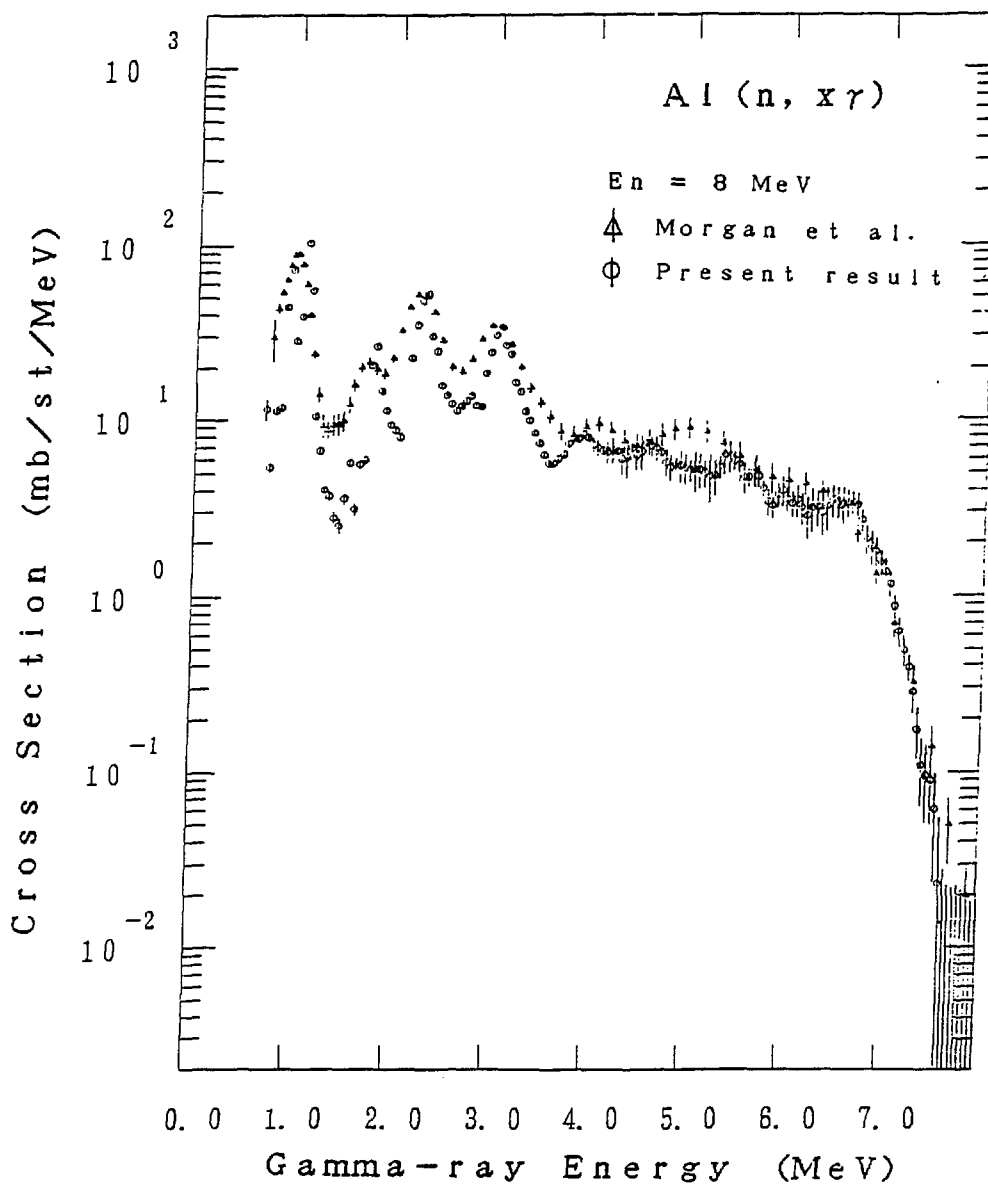Figure 6　Schematic layout of the (n,xγ) experimental arrangement

Figure 7   Spectrum of the emitted gamma-rays from Aluminum at En = 8.0
MeV

P.6 Measurements of Fast Neutron Inelastic-Scattering and Fission Cross Sections

S. Itagaki, M. Baba, T. Iwasaki, N. Hirakawa

and K. Sugiyama

Department of Nuclear Engineering, Tohoku University

Aoba, Aramaki, Sendai

Recent experiments performed at Tohoku University 4.5-MV Dynamitron accelerator are described briefly:

(1) measurements of double-differential neutron emission cross sections of Ti, Fe, Ni, Cu and Zr,

(2) measurements of inelastic scattering cross sections determined from $Cr(n,n'\gamma)$ reaction, and

(3) measurements of fission cross section ratio of actinide nuclei, and absolute value of ^{235}U.

The results obtained are compared with experimental results of others and evaluated data in JENDL-2, -3PR and ENDF/B-IV.

1. Introduction

The fast neutron cross section for inelastic-scattering plays an important role for neutronic calculation of fusion and fission reactors[1,2]. In previous measurements, however, the agreements among the experimental data are insufficient.
In order to improve the data reliability, more experimental data with definite experimental conditions are required. Fast neutron cross sections of stainless-steel is of special importance for the fusion and fast reactor design.

At higher neutron energies than several MeV, the slowing-down cross sections of structual materials are required to be improved[3]. Chromium is the second constituent of stainless steel. For this reason, the behaviors of fast-neutron inelastic scattering cross sections of this element is of interest. Finally, accurate data of fast neutron induced fission cross sections are required for the reactor calculation and radio-active waste management including actinide burning fast reactor.

The present report explains each of these experiments and discusses the results of these experiments.

2. Double-Differential Emission Cross Sections

A series of double-differential neutron emission cross sections(DDX) measurements have been continued. Experimental details and previous results have been described elsewhere[2,4-6]. Recently we have obtained the results for

   1) iron and nickel at 18 MeV incident energy[6], and

   2) copper, titanium, zirconium and carbon at 14.1 MeV.

The measurements at 18 MeV are thought to be useful beccause no DDX data are practically available at neutron energies other than $\sim$ 14 MeV. Figure 1, 2 illustrates the 18 MeV results for iron and nickel together with the evaluated values. The experimental spectra show strong angle dependence and marked disagreement with the evaluation, especially at backward angles. The JENDL-3PR1 data for iron, while it reproduces the 14 MeV data fairly well, looks to over emphasize the pre-compound components of continuum neutrons at higher incident energy.

The 14.1 MeV DDX data for copper at 45° is shown in Fig.3. The present values are in good agreement with those at OKTAVIAN[7] while they show apparent discrepancy with those by Hermsdorf et al[8]. The evaluation by ENDF/B-IV largely underpredicts the pre-equilibrium part of the neutron continuum. Recent theoretical calculation by Yamamuro[9] using the code GNASH and DWUCK, provided consistent interpretation of spectra and cross sections of emission particles. As shown in Fig.4, the present angle-integrated neutron emission spectrum is nicely traced by the calculation.

The DDX results for titanium are shown in Fig.5 together with those of Hermsdorf et al.[8] and ENDF/B-IV. While the agreement between the experiments is not good enough, the evaluated values show marked disagreement with the experiments. The results of zirconium and carbon will be reported later.

The DDX measurements will be continued as well in coming years. The 18 MeV measurements with better energy resolution and counting statistics will be interesting to obtain new information not available from the existing data.

3. Inelastic Scattering Cross Sections Determined from Cr(n,n'γ) Reaction

Neutron inelastic scattering from individual levels in the region $E_n \leq 4$ MeV has been studied by a number of investigators using either fast-neutron spectrometers or the (n,n'γ) techniques[10]. At higher neutron energies than 4 MeV, the cross sections of (n,n'γ) reaction are not well known.

Having used a natural chromium sample, we therefore report

here inelastic neutron excitation functions inferred from our
(n,n'γ) gamma-ray production measurements at incident energy
intervals of 200 KeV from 4.4 to 5.1 MeV.   The sample was
a 3.5-cm-high x 2.0-cm-diam. cylinder of high purity metallic
(99.98%) chromium. The particular apparatuses and details of
the methods are described elsewhere[11].
Typical uncertainties can be summarized as 3 % for the HP- Ge
detection efficiency, 6 % for the absolute neutron flux, 3% for
the finite sample corrections, and 2% for the calculated conver-
sion factors.   In addition, statistical and background uncer-
tainties arise in the extraction of gamma-ray peaks, and these
are often the dominant uncertainty for weak lines. For inferred
neutron cross sections, the uncertainty is estimated by taking
all the above effects into account and adding effects due to
feeding transitions, summed gamma-ray decays, and branching
ratio uncertainties.   The estimated accuracies of the resulting
cross sections were generally 10 to 20 %.
The level schemes in Fig.6 is based on the present experimental
results obtained by using the Ritz combination principle and on
the previous studies[12].   Absolute total inelastic neutron
scattering cross sections for excited states in ^{52}Cr are listed
in Table 1.   Some typical results are shown in Figs.7 and 8,
together with the results obtained Karatzas et al.[10] for $E_n \leq 4$
MeV (open circle) and JENDL-3PR cross sections (solid curve).
The 1434-KeV(2^+) level cross section is in good agreementt with
JENDL-3PR, except for the region near E_n = 5 MeV.
Our results for the 2370-KeV(4^+) state are considerably low
relative to those of JENDL-3PR, which are consistent with those

.

of Karatzas et al. for $E_n \leq 4$ MeV. At higher energies, the level schemea shown in Fig. 6 is more complicated in comparison with those of "Table of Isotopes (7th,ed.)[13]"used in the evaluation of JENDL-3PR. As a consequence, it is suggested that the above discrepancy in the cross section is probably due, in part, to the difference between those level schemes.

For the 2768-, 2965- and 3162-KeV state, disagreement between the experiment and the JENDL-3PR values should be marked in the region 3.5 MeV $\leq E_n \leq$ 5.2 MeV.

The results of ^{53}Cr will be reported later.

4.   Neutron Induced Fission Cross Sections

        Measurements of fission cross section ratio relative to ^{235}U are continued; the experimental method and previous data have been reported elsewhere[14,15]. In addition, a study of ^{235}U absolute fission cross section measurement was initiated. Recent results of the ratio measurements are the following;

  1) ^{236}U (0.99 - 6.99, $\sim$14 MeV), 2) ^{237}Np(0.7 - 6.99, $\sim$14 MeV),

  3) ^{243}Am(1.06 - 6.83, $\sim$14 MeV), and

  4) ^{232}Th, ^{233}U, ^{234}U, ^{238}U and ^{242}Pu(13.4 - 14.9 MeV).

The present data are generally in reasonable agreement with other experiments and the evaluation. However appreciable differences were found for ^{243}Am, ^{242}Pu and ^{237}Np. As shown in Fig.9, the present ^{243}Am data differ by 10 to 20 % from those by Behrens & Brown and JENDL-2. The present results are in better agreement with recent experiments by Knitter & Budze-Jorgensen[18] and Fursov et al.[19]. The present ^{242}Pu values around $\sim$14 MeV are larger by $\sim$10 % than JENDL-2 but agree well

with ENDF/B-IV.

For absolute fission cross section measurement, a proton-recoil counter-telescope backed with a fission chamber (Fig. 11) was fabricated and tested using the time-correlated associated particle technique. A preliminary results of ^{235}U fission cross sections around 14 MeV are illustrated in Fig. 12. The measurements will be extended to lower neutron energy.

Concluding remarks

Thus, several nuclear data have been newly obtained, and they will be useful in judging and improving the adequacy of evaluated data.

References:

1. Takahashi, A.: JAERI-M86-029 p.99 (1986),

2. Baba, M.: ibid. P.119,

3. Maki, K.: ibid. p. 57,

4. Chiba, S.et al.: J. Nucl. Sci. Technol. 22 771 (1985),

5. Baba, M. et al.: Radiation Effects 92-96 223 (1986),

6. Yabuta, N. et al.: NETU-47 p. 10
(Dep. Nucl. Eng., Tohoku Univ.)

7. Takahashi, A. et al.: OKTAVIAN report A-83-01 Osaka Univ.

8. Hermsdorf, D. et al.: Zfk - 277 (1975),

9. Yamamuro, N.: Internal Report
and private communication,

10. Karatzas, P. et al.: Nucl. Sci. and Eng. 67 34 (1978),

11. Yoshida, M. et al.: NETU-47 p.24 (1986),

12. Beene, R.J.: compilers, Nucl. Data Sheets 25 235 (1978),

References (continued)

13. Lederer, C.M. et al.: " Table of Isotopes " 7 th ed.(1978),

14. Kanda, K. et al.: JAERI-M85-035 p.220 (1984),

15. Kanda, K. et al.: Radiation Effects <u>92-96</u> 569 (1986),

16. Teɪayama, H. et al.: NETU-47 p.53 (1986),

17. Manabe, F.: et al.: ibid., p.61(1986),

18. Knitter, H.H. & Budtz-Jorgensen:
                    Radiation Effects <u>92-96</u> 413 (1986),

19. Fursov, B. et al.: ibid., p.641.
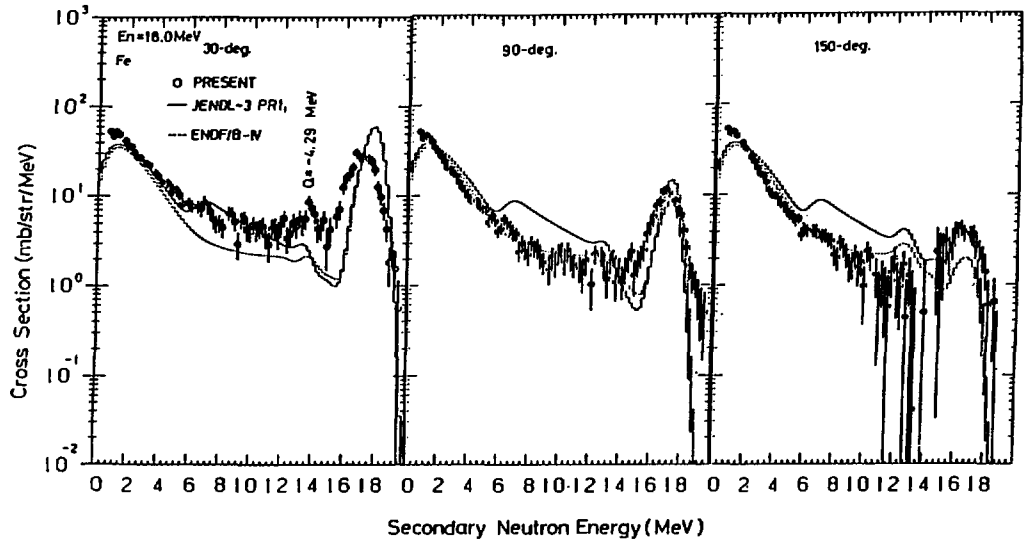
Fig.1   DDX of iron at the incident energy of 18 MeV.
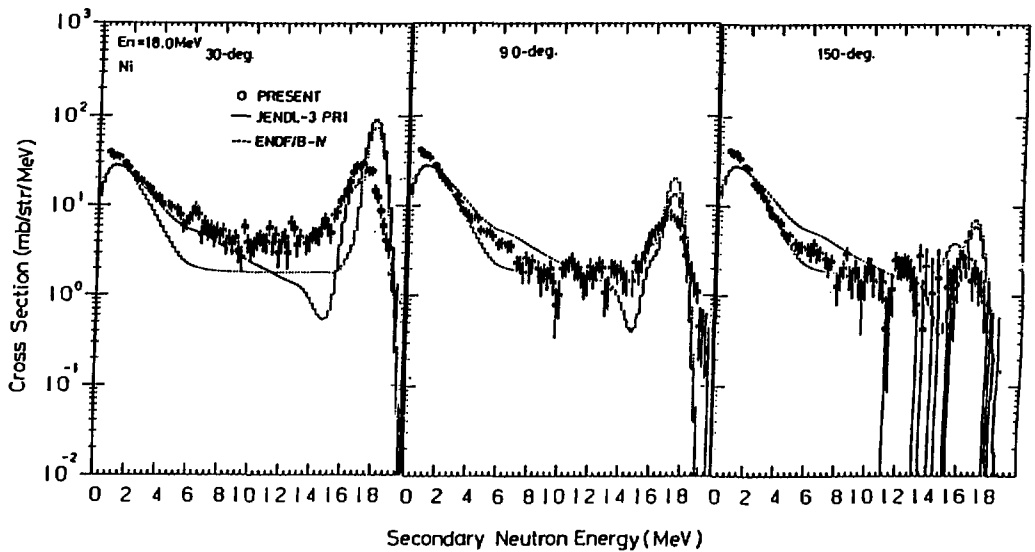
Fig.2   DDX of nickel at the incident energy of 18 MeV.
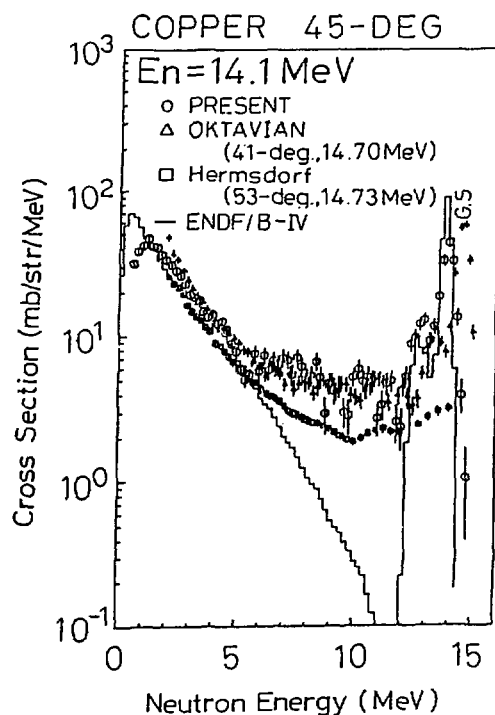
Fig.3 DDX of copper at 14.1 MeV.
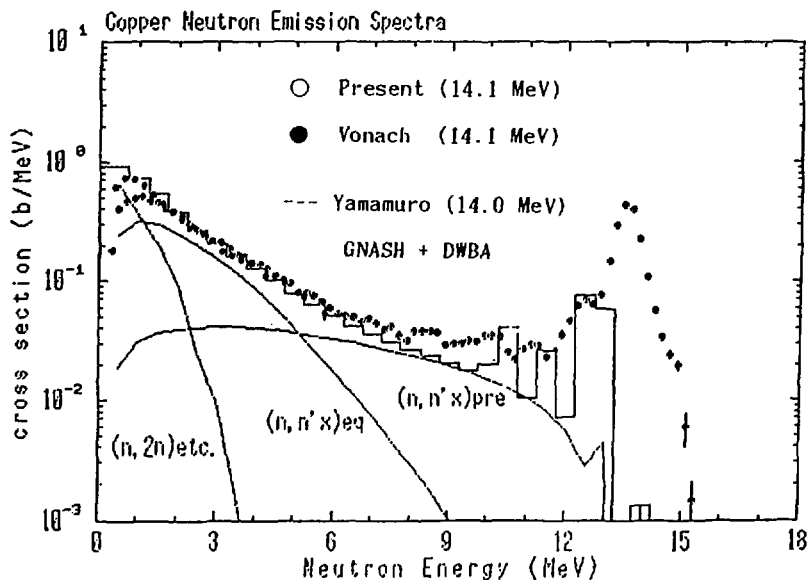
Fig.4 Angle-integrated neutron emission spectra of copper

at the incident energy of 14.1 MeV.
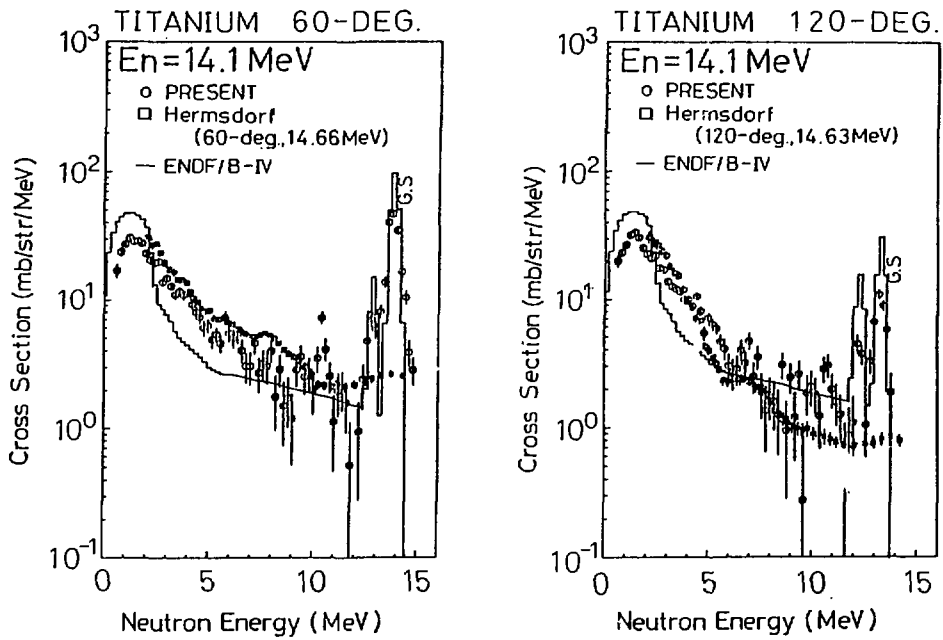
Fig.5 DDX of titanium at the incident energy of 14.1 MeV.
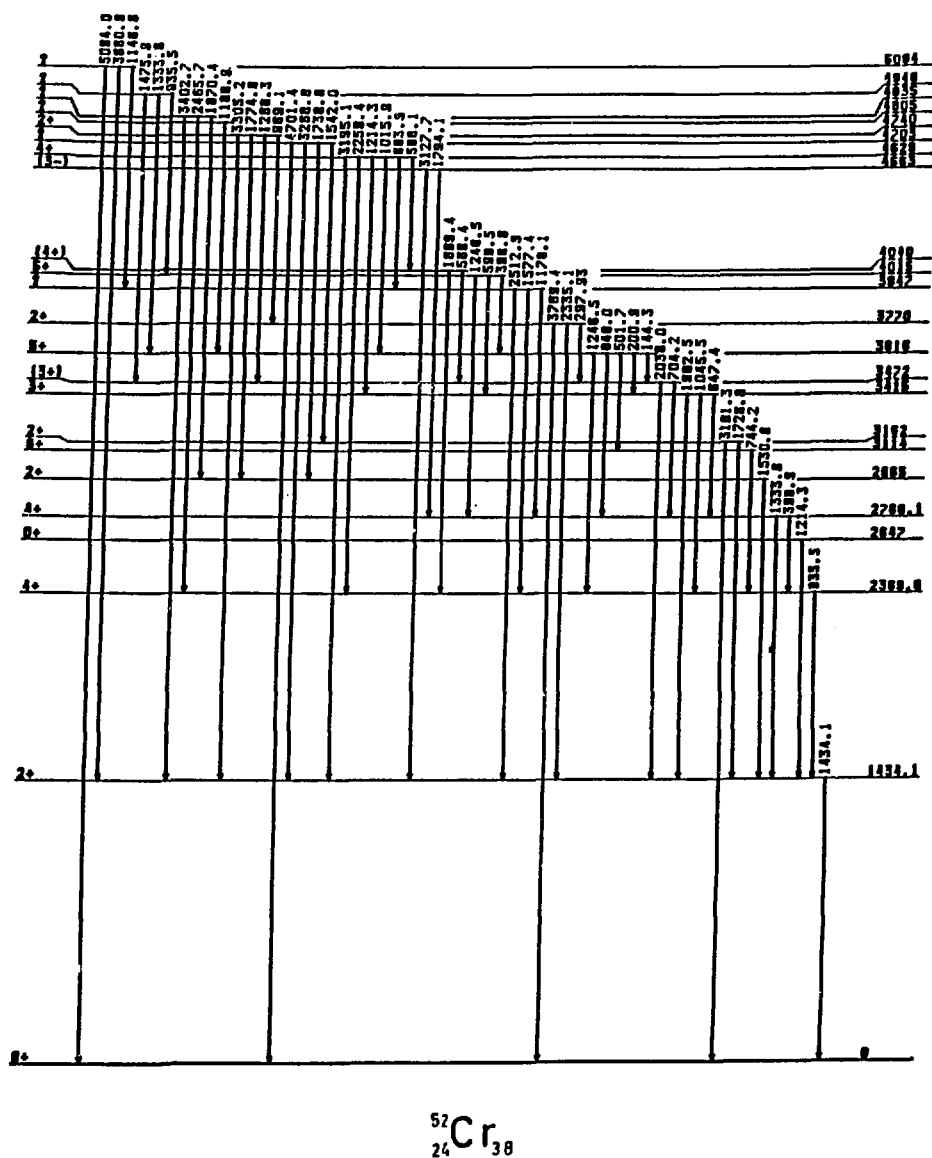
Fig. 6.   Chromium energy-level and decay schemes
          below 5.1 MeV (Energy is KeV).

Table 1. Natural chromium cross sections
of levels in ^{52}Cr (barn)

E_n (KeV)	J^π	4.41 (MeV)	4.64	4.84	5.11
1434.1	2⁺	0.333 ±0.031	0.298 ±0.027	0.275 ±0.026	0.204 ±0.020
2369.8	4⁺	0.091 ±0.008	0.082 ±0.008	0.067 ±0.006	0.057 ±0.006
2647	0⁺	0.061 ±0.006	0.054 ±0.005	0.044 ±0.004	0.031 ±0.003
2768.1	4⁺	0.096 ±0.009	0.095 ±0.009	0.089 ±0.008	0.071 ±0.008
2965	2⁺	0.150 ±0.014	0.145 ±0.013	0.132 ±0.013	0.110 ±0.010
3114	6⁺	0.006 ±0.001	0.007 ±0.001	0.009 ±0.001	0.008 ±0.001
3162	2⁺	0.142 ±0.014	0.122 ±0.012	0.114 ±0.011	0.086 ±0.008
3415	3⁺	0.028 ±0.003	0.030 ±0.003	0.038 ±0.004	0.044 ±0.005
3472	(3⁺)	0.052 ±0.006	0.059 ±0.006	0.056 ±0.005	0.006 ±0.001
3616	5⁺	0.010 ±0.001	0.015 ±0.002	0.014 ±0.001	0.010 ±0.001
3770	2⁺	0.067 ±0.008	0.079 ±0.008	0.080 ±0.008	0.071 ±0.007
3947		0.009 ±0.001	0.019 ±0.002	0.023 ±0.002	0.027 ±0.003
4015	5⁺	0.010 ±0.001	0.008 ±0.001	0.007 ±0.001	0.006 ±0.001
4040	(4⁺)	0.016 ±0.002	0.021 ±0.002	0.024 ±0.002	0.031 ±0.003
4563	(3⁻)			0.033 ±0.003	0.045 ±0.004
4630	4⁺			0.011 ±0.001	0.023 ±0.002
4703				0.006 ±0.001	0.032 ±0.003
4740	2⁺				0.023 ±0.002
4837					0.009 ±0.001
4950					0.010 ±0.001
5049					0.011 ±0.001
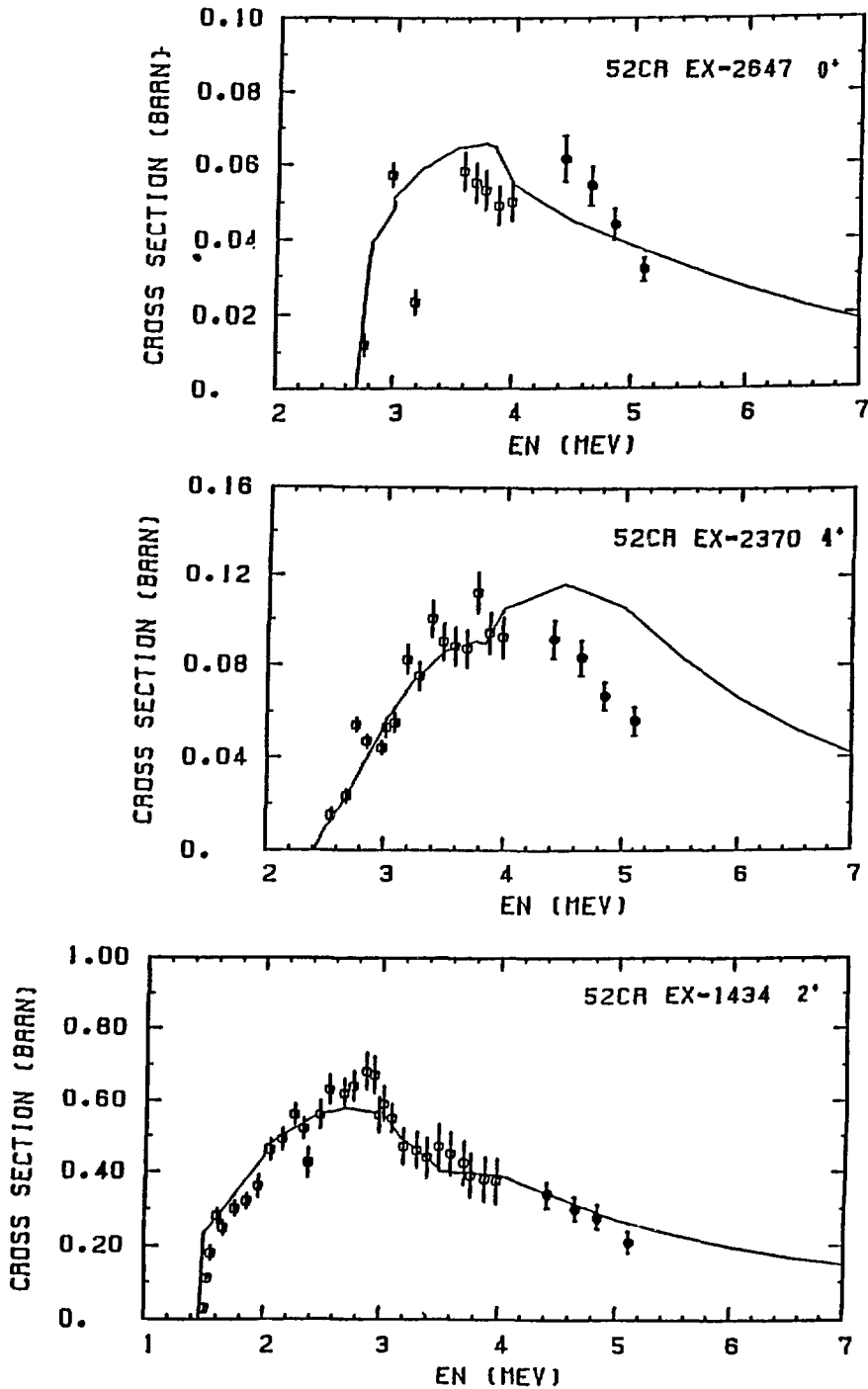
Fig. 7.   Natural chromium cross sections of levels in ^{52}Cr.
The solid lines are JENDL-3PR cross sections,
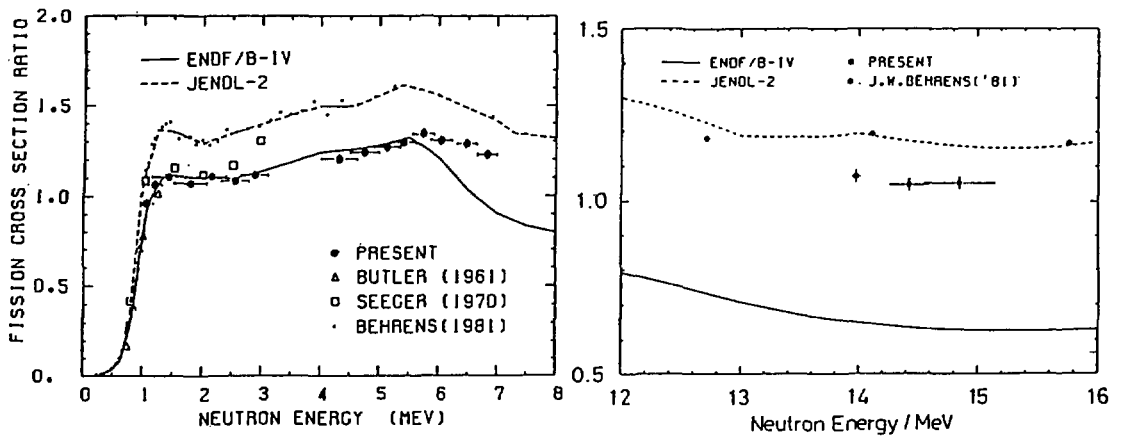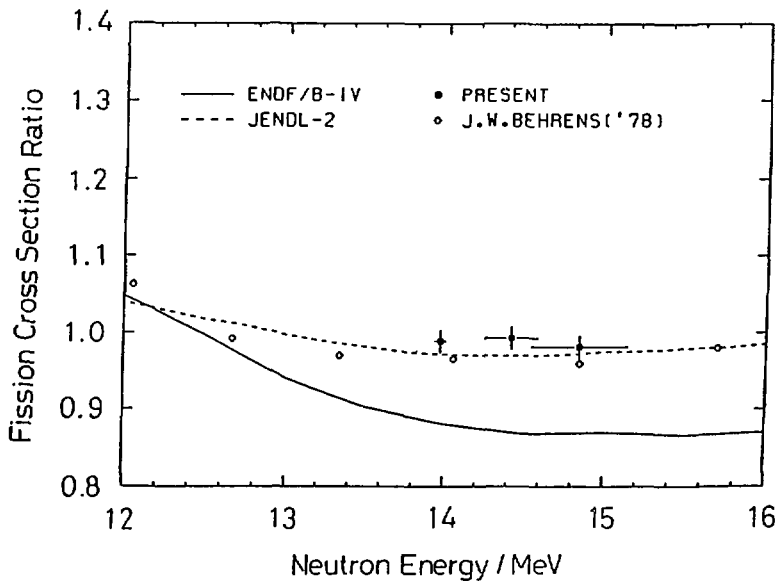Ø , P.T. Karatzas et al.: Nucl.Sci. and Eng.67 34('78).
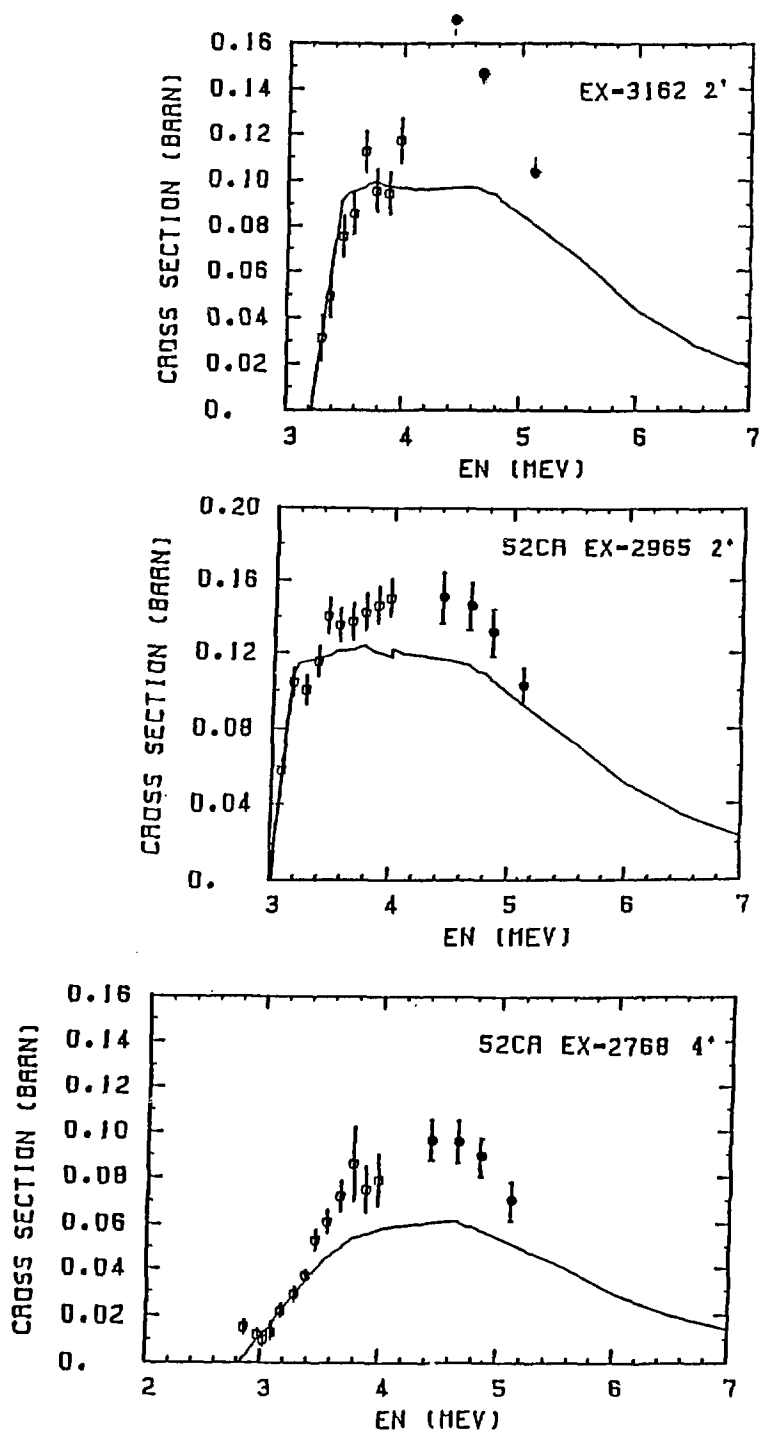
Fig. 8.   Natural *chromium* cross sections of levels in ^{52}Cr.

Fig.9 Fission cross section ratio of ²⁴³Am to ²³⁵U.
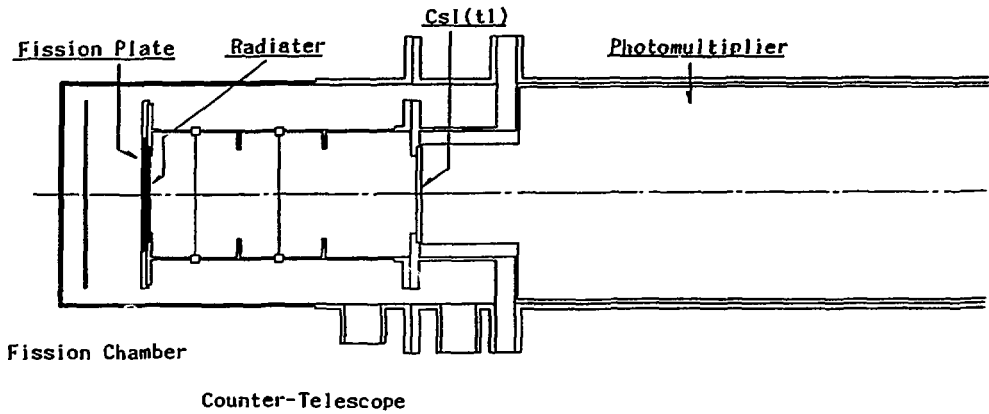

Fig.10 Fission cross section ratio of ²⁴²Pu to ²³⁵U.

Fig.11 Back-to-back fission-chamber and proton-recoil telescope
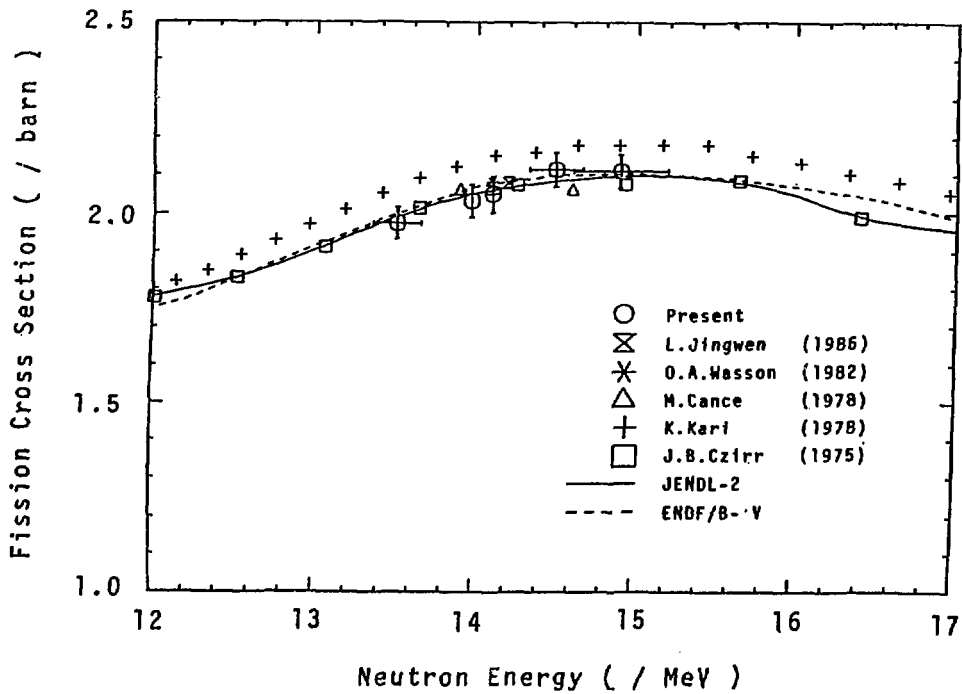for absolute fission cross section measurement.

Fig.12 Fission cross section of ^{235}U.

P.7 Study on Capture Gamma-Ray Spectra

in the keV-Neutron Region

H. Kitazawa and M. Igashira

Research Laboratory for Nuclear Reactors
Tokyo Institute of Technology
2-12-1 O-okayama, Meguro-ku, Tokyo 152, Japan

Capture gamma-ray spectra of O-16, Si-28 and S-32 have been measured to investigate the mechanism of the neutron capture on s- and p-wave resonances with large reduced neutron width. For heavy nuclei with the neutron number N=50-126, characteristic features of the pygmy E1 resonance were obtained to disclose the physical origin of the resonance. Moreover, resonance-averaged capture gamma-ray spectra of Fe-56 have been measured at the neutron energies of 20-600 keV, which will be utilized as photon-production data of the japanese evaluated nuclear data library JENDL-3.

1. Valence transitions in 434-keV p3/2-wave neutron capture by O-16

Capture gamma-ray spectra of O-16 have been observed in our expectation that the high single-particle nature of the ground state (5/2+;0.0 MeV) and the first excited state (1/2+;0.87 MeV) of O-17 would facilitate the E1 valence transitions from the 434-keV p3/2-wave resonance (fig. 1). The results demonstrate that the Lane-Mughabghab valence capture model produces successfully the observed partial radiative widths for these transitions (table 1). They will furnish typical evidence of the valence neutron capture in light nuclei.

2. Gamma-ray transitions following p-wave neutron resonance capture and off-resonance capture by Si-28[1]

Observations were made for gamma rays from the 565-keV and 806-keV p3/2-wave neutron resonance captures by Si-28 and from the off-resonance capture at the 485-keV neutron energy. The p-wave resonance capture is followed by strong gamma-ray transitions to a small number of low-lying states of Si-29. The valence capture model reasonably accounts for the

ground-state (1/2+;0.0 MeV) and second-excited-state (5/2+;2.03 MeV) transitions from both p-wave resonances, while the transitions to the first (3/2+;1.27 MeV), third (3/2+;2.43 MeV) and fourth (5/2+;3.07 MeV) excited states cannot be understood by this model. Moreover, the off-resonance capture is successfully explained by the direct capture model in the phenomenological DWBA formalism rather than by the potential capture model.

3. Particle-vibrator coupling model calculation of partial radiative widths for p3/2-wave neutron resonance on Si-28[2)]

A particle-vibrator coupling model was applied to the calculation of partial radiative widths for the Si-28 p3/2-wave neutron resonance. The calculation assumed a neutron excitation coupled to one-phonon vibrational states of Si-28 and neglected the continuum nature of the resonance state wave function in the nuclear external region. As a result, we found that the core excitation is quite essential to explain the observed partial radiative widths and that these transitions are completely decoupled from the giant electric dipole resonance.

4. Final state correlation in gamma-ray transitions from 188-keV s-wave neutron resonance on Si-28

Pronounced final state correlation between spectroscopic strengths and reduced partial radiative widths has been observed for gamma-ray transitions from the 188-keV s-wave neutron resonance on Si-28 (fig. 2). Special interest was aroused by the enhanced M1 transitions to the ground state and the first excited state of Si-29 and by the prominent E1 transition to the higher excited state (3/2-;4.93 MeV). The results show that the valence capture model taking the neutron effective charge -Ze/A produces the partial E1 radiative width in reasonable agreement with the observed one, while the ground-state transition is well understood by the valence model extended to the M1 transition, using the renormalized single-particle g-factor which takes into account the core polarization due to the excitation of the isovector giant M1 resonance. The l-forbidden M1 transition to the first excited state was described in terms of the tensor component of the magnetic dipole operator (table 2).

These results manifest the core-excitation mechanism and the physical

nature of the coupling of the single-particle E1(M1) transition to the giant electric(magnetic) dipole resonance.

5. Core-excitation in 202-keV p1/2-wave neutron resonance capture by S-32

The effect of the core excitation in the neutron capture by S-32 was investigated with measurements of gamma rays from the 202-keV p1/2-wave neutron resonance. Strong E1 gamma rays have been observed for the ground-state (3/2+;0.0 MeV) and first-excited-state (1/2+;0.84 MeV) transitions (fig. 3). The observed partial radiative widths are in remarkable disagreement with the predictions of the valence capture model: they suggest some contribution of the core excitation (fig. 4).

6. Resonance-averaged capture gamma-ray spectra from Fe-56[3),4)]

Resonance-averaged capture gamma-ray spectra, which include dominant contributions of p-wave neutron capture, have been measured at the neutron energies of 20-600 keV. Comparison was made between the observed gamma-ray spectra and the statistical model calculations based on the Hauser-Feshbach theory. Consequently, remarkable disagreement between theory and experiment was found, in particular, for gamma rays around 2 MeV and 8 MeV (fig. 5). The stressed, calculated gamma-rays at 2 MeV results from a breakdown of the statistical assumption of the nuclear level distribution, while the enhanced M1 transition from capture states to the ground state (1/2-;0.0 MeV) and/or first excited state (3/2-;0.014 MeV) might indicate the coupling of the single-particle transitions to the isovector M1 resonance.

7. Systematics of pygmy E1 resonance[5)]

Neutron capture gamma-ray spectra of Nb, Mo, Ag, In, Sn, Sb, I, Cs, Pr, Tb, Ho, Lu, Ta, and Au have been measured with an anti-Compton NaI(Tl) detector in the keV-neutron energy region, using a time-of-flight technique. All observed spectra except for Nb and Mo show the anomalous bump, so-called the pygmy resonance (fig. 6). The observed spectra were compared with the statistical model calculations which used the Brink-Axel E1 gamma-ray strength function with a pygmy E1 resonance. The pygmy E1 resonance parameters were extracted from these spectra by a spectrum fitting method,

and the systematics of the resonance energy and the E1 strength exhausted in the resonance were obtained as the functions of neutron number. Both the systematics show distinct shell effects at the neutron magic number of N=82 and at the proton magic number of Z=50 (fig. 7). Comparison with both shell model and hydrodynamical model predictions for the pygmy E1 resonance indicates that the observed pygmy E1 resonances, at least in the mass region of A=110-210, have a common physical origin, and that neutron-particle states decoupled from the giant E1 resonance would be responsible for these resonances.

References

1) Shimizu, M., Igashira, M., Terazu, K. and Kitazawa, H.: Nucl. Phys., A452, 205 (1986).

2) Kitazawa, H., Ohgo, M., Uchiyama, T. and Igashira, M.: to be published in Nuclear Physics A.

3) Komano, H., Igashira, M., Shimizu, M. and Kitazawa, H.: Phys. Rev., C29, 345 (1984).

4) Kitazawa, H., Komano, H., Igashira, M. and Shimizu, M.: Proc. 5th. Int. Symp. on Capture Gamma-Ray Spectroscopy and Related Topics, Knoxville, 1984, ed. S. Raman (American Institute of Physics, New York, 1985) p.520 (AIP Conference Proceedings No 125).

5) Igashira, M., Kitazawa, H., Shimizu, M., Komano, H. and Yamamuro, N.: Nucl. Phys., A457, 301 (1986).

6) Igarashi, S.: J. Nucl. Sci. Technol., 12, 67 (1975).

7) Allen, B. J. and Company, F. Z.: Proc. 5th. Int. Symp. on Capture Gamma-Ray Spectroscopy and Related Topics, Knoxville, 1984, ed. S. Raman (American Institute of Physics, New York, 1985) p.501 (AIP Conference Proceedings No 125).

Table 1 Experimental and theoretical partial radiative widths for the ground-state and first-excited-state transitions in the 434-keV p3/2-wave neutron resonance on O-16.

Ex (MeV)	Experiment (eV)	Valence Model (eV)
0.00(5/2+)	1.28 ± 0.24	1.76
0.87(1/2+)	1.86 ± 0.30	2.12

Table 2 Experimental and theoretical partial radiative widths of the 188-keV s1/2-wave neutron resonance on Si-28. The valence-model calculations use the renormalized g-factor (=6.9g_s) and the tensor component $\sqrt{3/4\pi}\ \kappa r^2 (Y_2 \otimes \sigma)$ (κ=0.8) for M1 transition and the effective charge of a unit charge for E2 transition.

Ex (MeV)	Experiment (eV)	Valence Model (eV)	
0.00(1/2+)	3.5 ± 0.7	3.55	(M1)
1.27(3/2+)	2.7 ± 0.7	2.84	(M1)
2.03(5/2+)		0.012	(E2)
2.43(3/2+)	0.45 ± 0.16	0.10	(M1)
3.07(5/2+)		0.005	(E2)
4.93(3/2-)	2.3 ± 0.6	1.64	(E1)
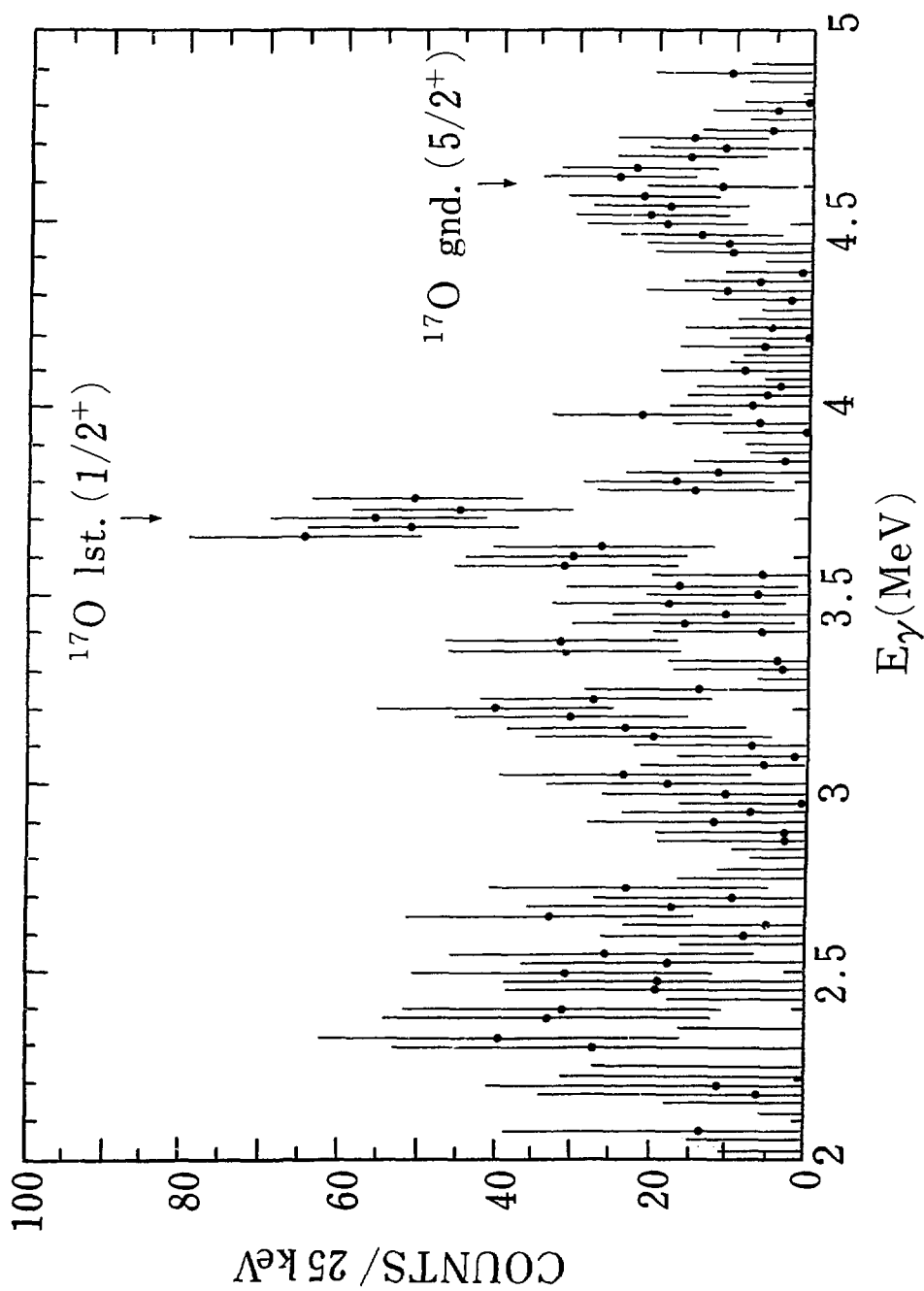
Fig. 1 Capture gamma rays from the 434-keV p3/2-wave neutron resonance on O-16.
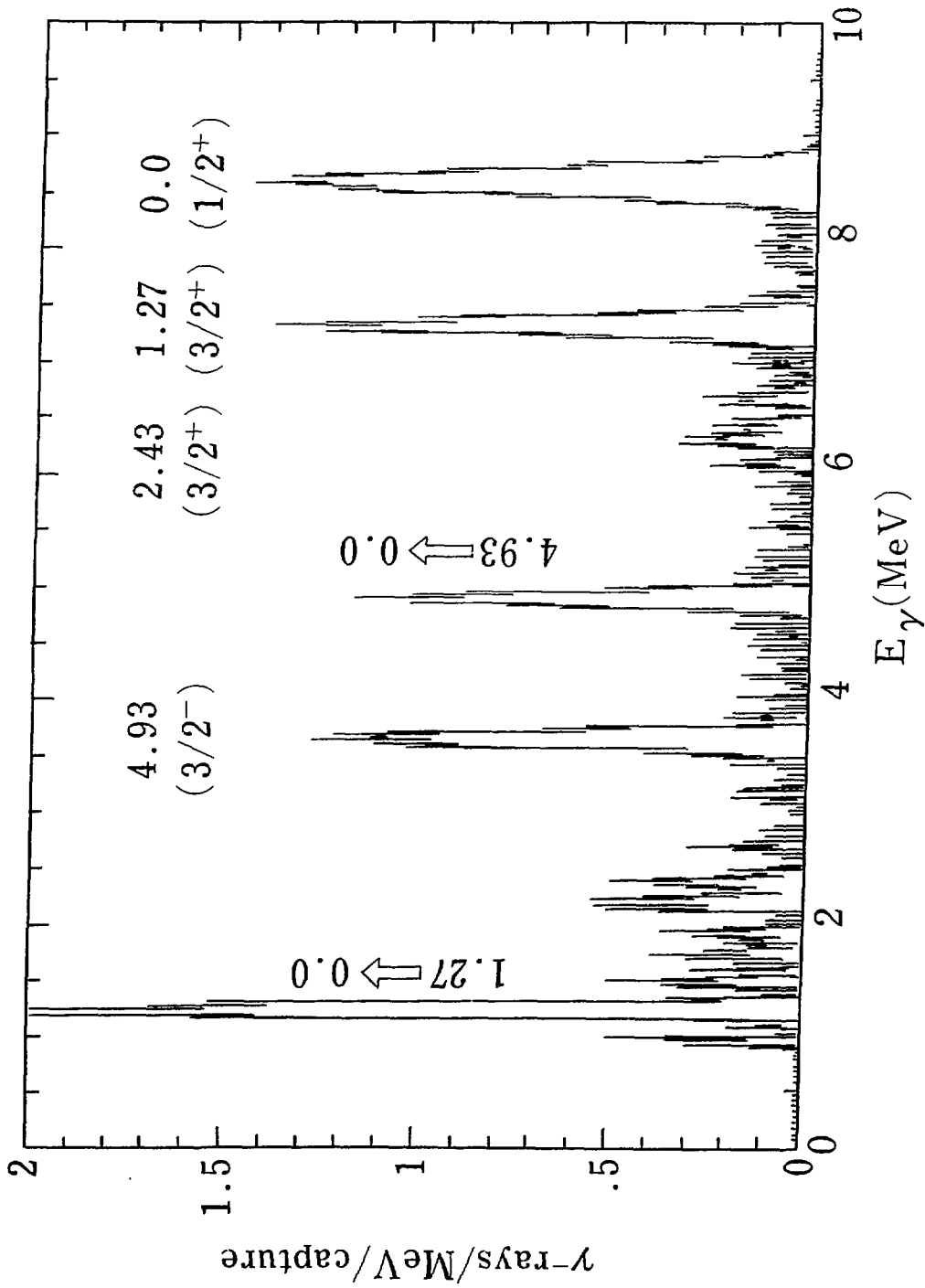
Fig. 2 Capture gamma rays from the 188-keV s1/2-wave neutron resonance on
Si-28.
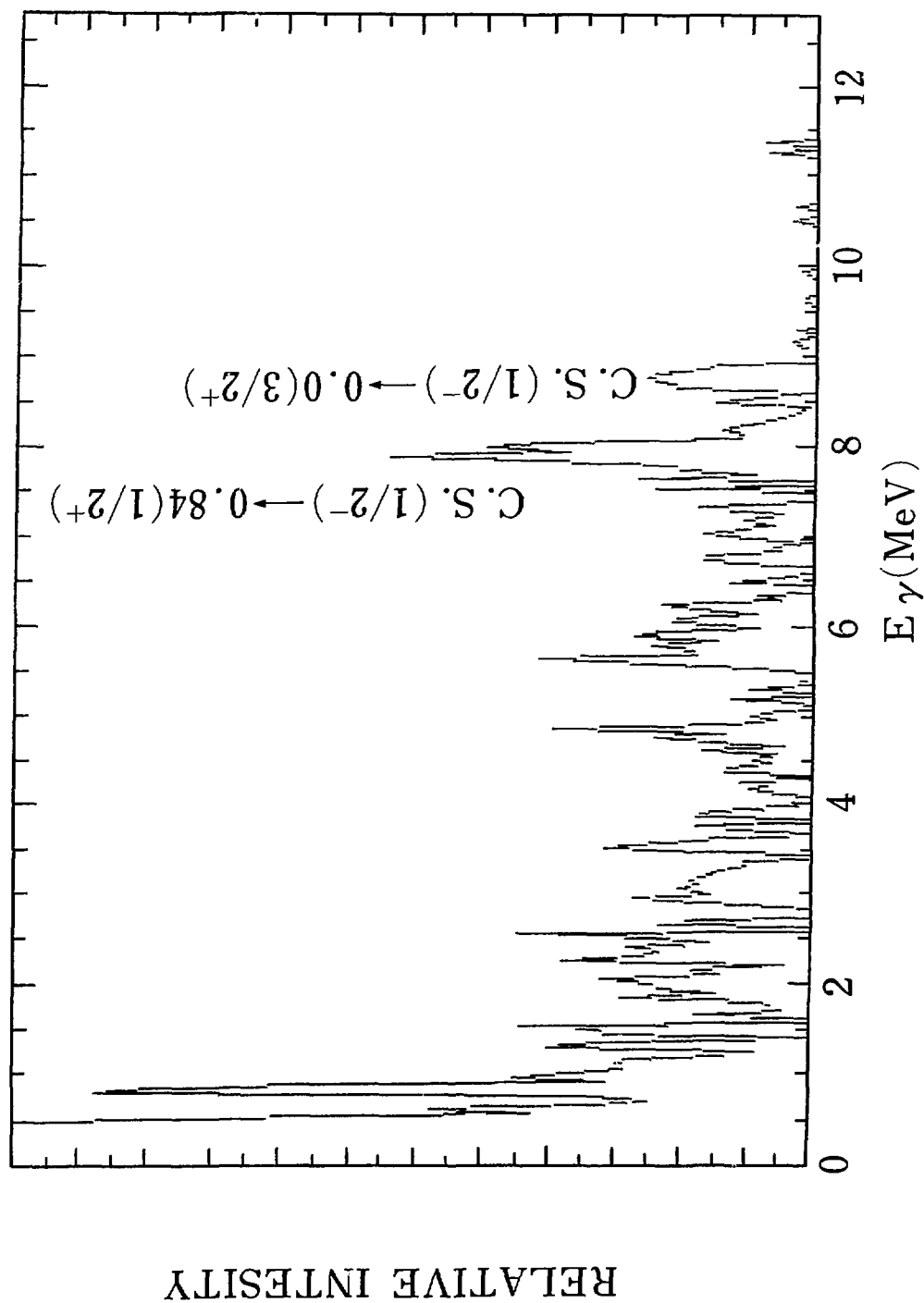
Fig. 3 Capture gamma rays from the 202-keV p1/2-wave neutron resonance on S-32.
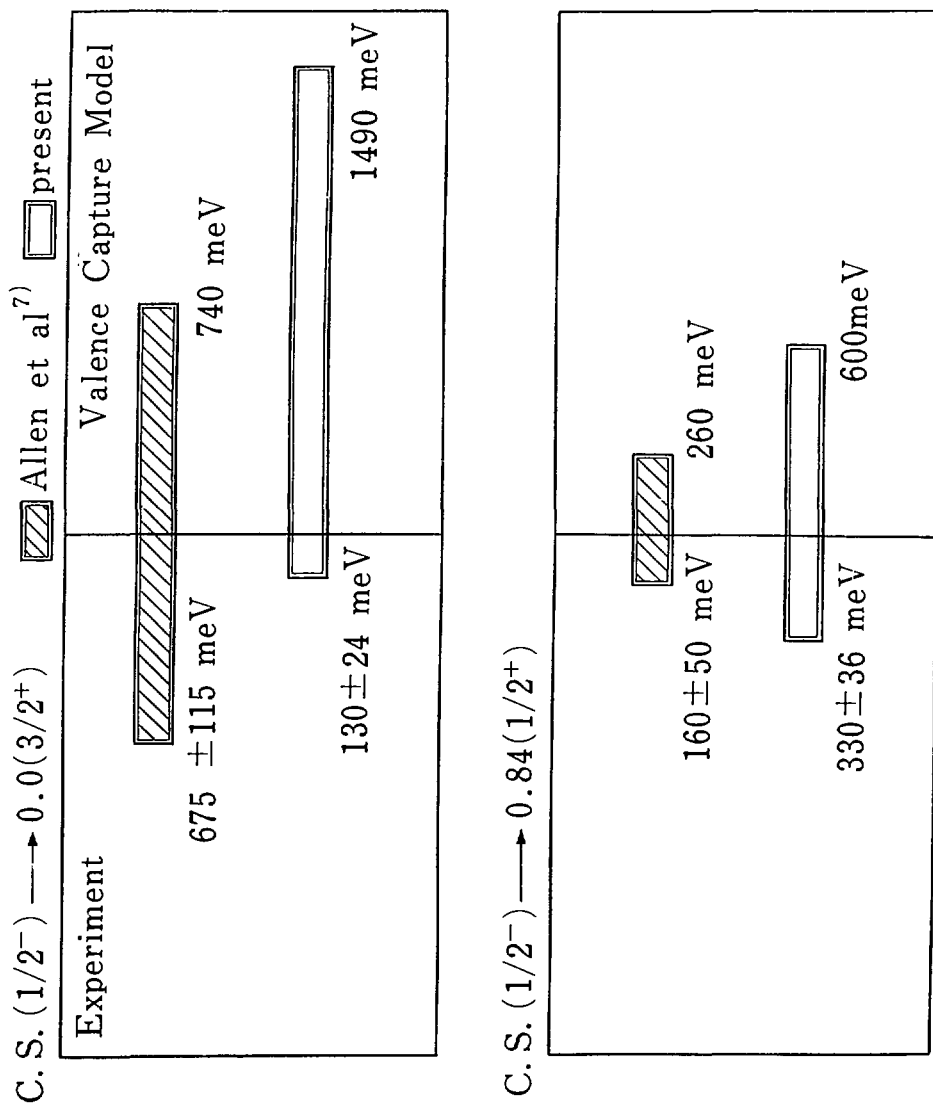
Fig. 4 Comparison between the observed partial radiative widths and the valence-model calculations for the ground-state and first-excited-state transitions in the 202-keV p1/2-wave neutron resonance capture by S-32.
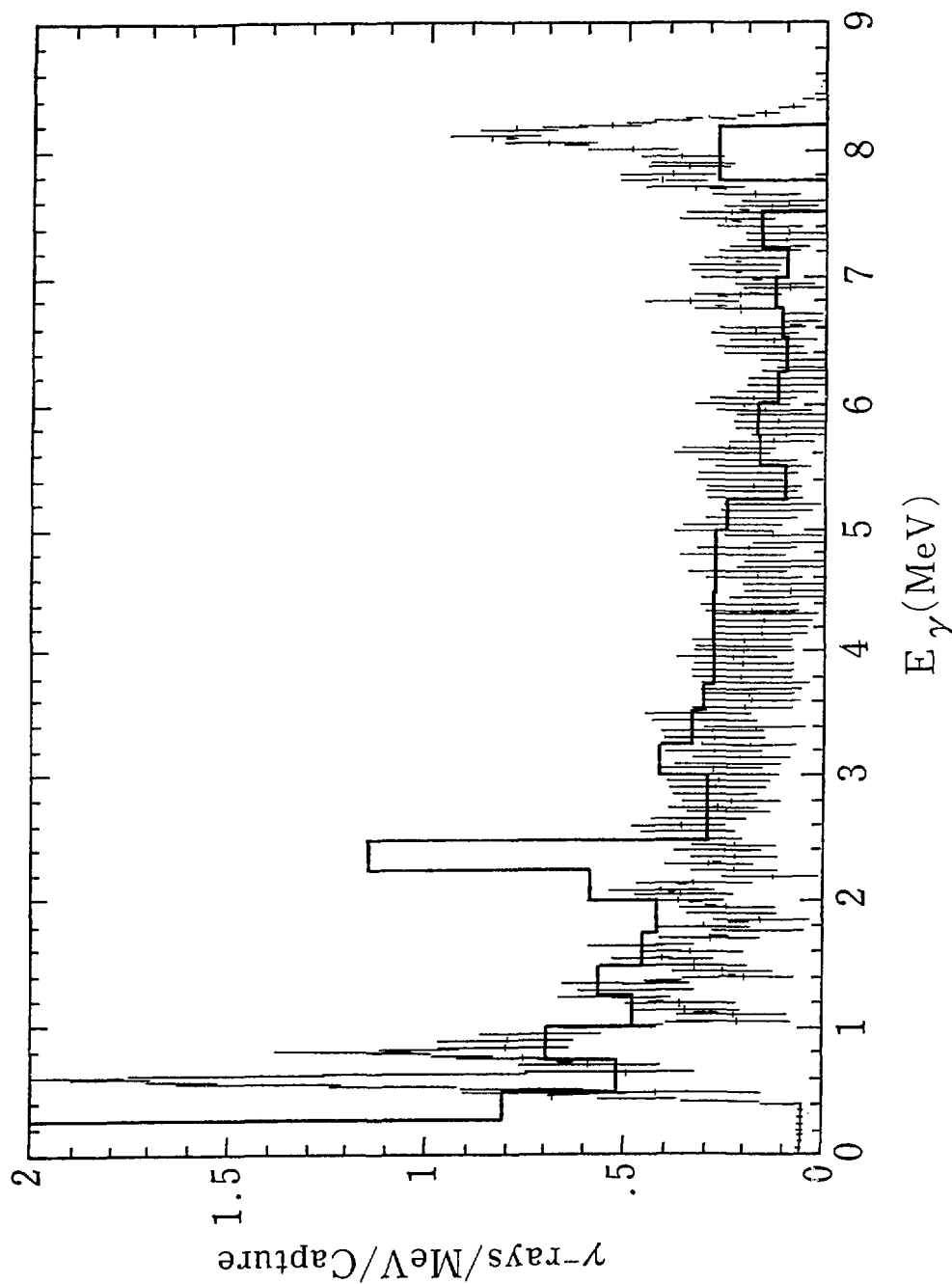
Fig. 5 Resonance-averaged capture gamma rays from Fe-56 at the neutron energy of 570 keV. The histogram shows the statistical model calculation using the computer program CASTHY[6].
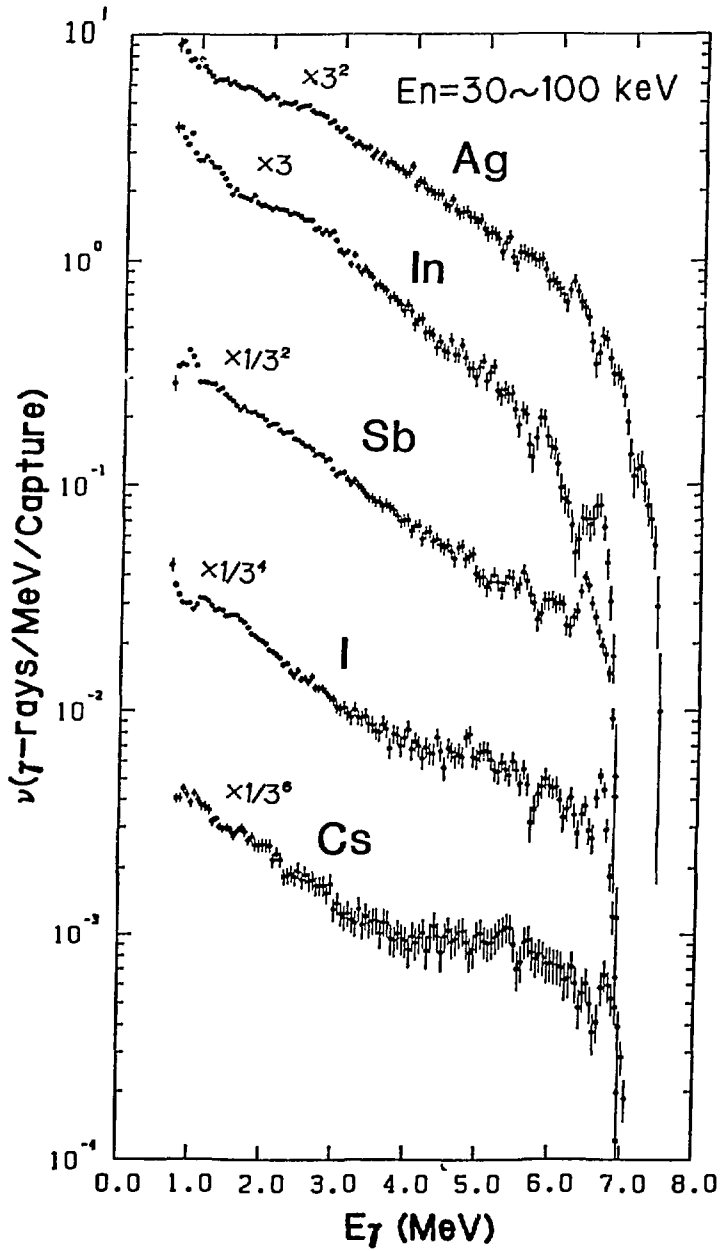
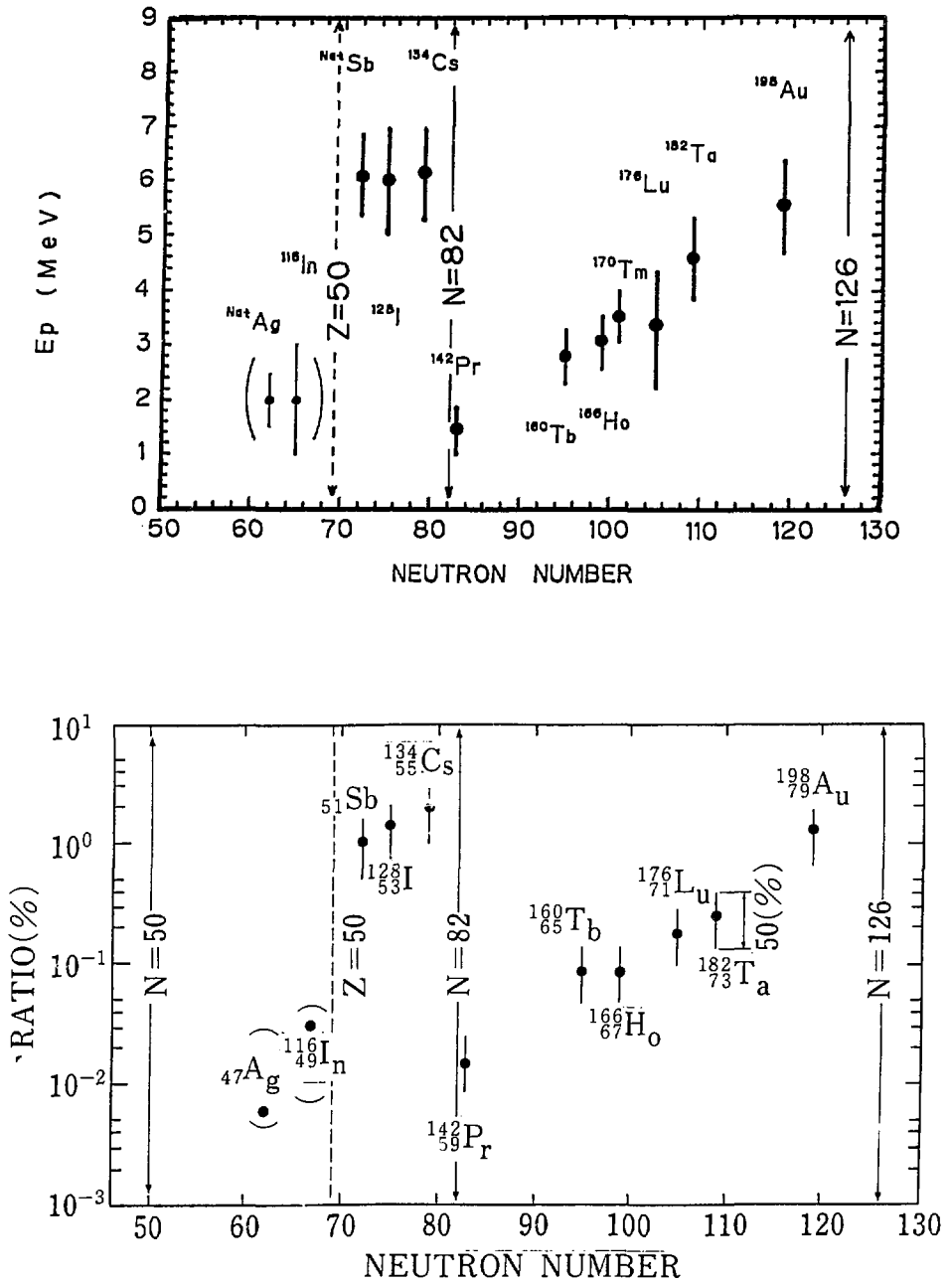Fig. 6 Neutron capture gamma rays from heavy nuclei in the unresolved
resonance region.
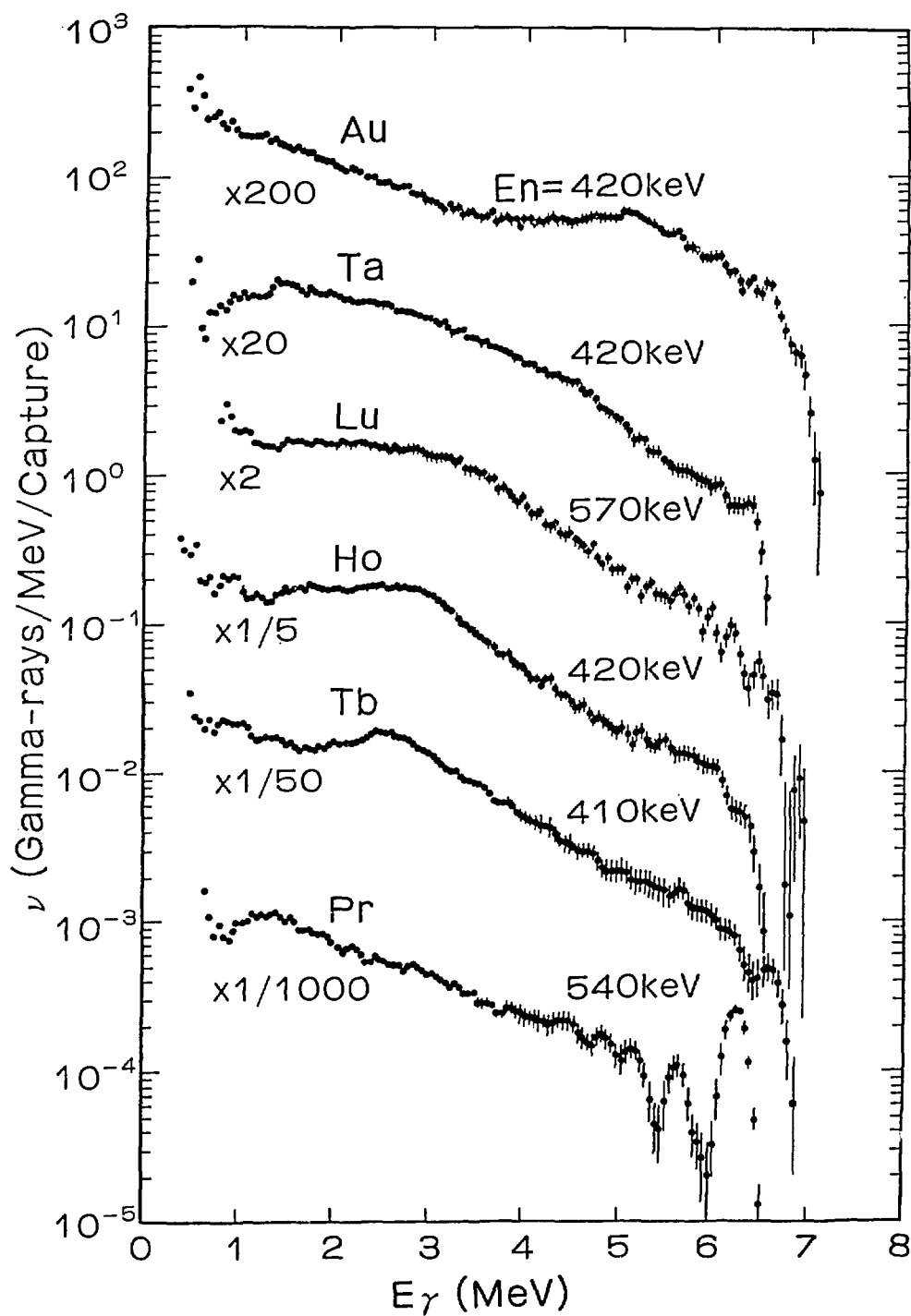
Fig. 6

Fig. 7 Systematics of the pygmy resonance parameters.

P.8 Recent Measurements of Neutron Cross Section with KURRI-Linac

Yoshiaki FUJITA, Katsuhei KOBAYASHI, Hiroyuki OIGAWA,
Shuji YAMAMOTO and Itsuro KIMURA

Research Reactor Institute, Kyoto University
Kumatori-cho, Sennan-gun, Osaka   590-04

At the Research Reactor Institute, Kyoto University(KURRI), the 46 MeV electron linear accelerator has been used as a powerful and useful tool to have (1) time-of-flight measurements, such as neutron cross section and neutron spectrum for reactor materials, (2) irradiation experiments for isotope production, (3) radiation damage studies in a liquid nitrogen temperature, and so on.   In this paper, in order to assess the evaluated nuclear data for ^{181}Ta or ^{232}Th in JENDL-2 and ENDF/B-IV, two studies are introduced from the recent results concerning (1) the experimental check of the self-shielding effects for ^{181}Ta, and (2) measurement of the ^{232}Th resonance parameters, and the integral check of the parameters by comparing with the resonance integral measured in the standard 1/E neutron spectrum field.

I.   Measurement of Self-Shielding Factor of the Neutron Capture Reaction for ^{181}Ta in Unresolved Resonance Region

The resonance parameters in the resolved region and the average resonance parameters in the unresolved region are the most important data for the calculation of nuclear reactors, such as High Conversion Light Water Reactors or Fast Breeder Reactors. These parameters directly give a large influence on the conversion ratio, reactivity worth and Doppler coefficients in the reactor calculation.   In recent years, there are several works[1]-[4] which pointed out inconsistencies between the energy

dependent capture cross section and the integral data for ^{238}U or ^{232}Th resonance self-shielding effects. Some of the problems are due to the fact that the average resonance parameters in the evaluated nuclear data files are taken from the data evaluated by lower energy resonances or from the infinite dilute capture cross sections measured with a wide energy width.

In this experiment, we have experimentally determined the self-shielding factor for the ^{181}Ta$(n,\gamma)^{182}$Ta reaction, and compared the result with the calculated values. The neutron transmission and self-indication ratio measurements for ^{181}Ta have been made by the time-of-flight(TOF) method using the 46 MeV electron linear accelerator(linac) at the Research Reactor Institute Kyoto University(KURRI). A water-cooled photoneutron target was made of Ta plates 5 x 5 cm square, and a small water tank 8 cm thick was put just beside the target to moderate the neutron energies. A Pb block 7 cm diam. and 10 cm long, was placed in the neutron flight path in front of the target to shield the neutron detector against the intense gamma-flash from the target. A Cd sheet 0.5 mm thick was also placed in the beam to remove thermal neutrons and to suppress the overlapping of neutrons.

The experimental conditions of the linac and Ta samples are summarized in Table 1. The transmission rate $T_g(N_i)$ and the self-indication ratio $R_g(N_i)$ are given as follows, respectively.

$$T_g(N_i) = \frac{\int_g \mathcal{E}(E)\,\emptyset(E)\,e^{-N_i\sigma_t(E)}\,dE}{\int_g \mathcal{E}(E)\,\emptyset(E)\,dE} \approx \frac{\int_g e^{-N_i\sigma_t(E)}\frac{1}{E}\,dE}{\int_g \frac{1}{E}\,dE} \quad (1)$$

$$R_g(N_i) = \frac{\int_g \mathcal{E}'(E)\,\emptyset(E)\,e^{-N_i\sigma_t(E)}\,n\,\sigma_\gamma(E)\,dE}{\int_g \mathcal{E}'(E)\,\emptyset(E)\,n\,\sigma_\gamma(E)\,dE}$$

$$\approx \frac{\int_g e^{-N_i\sigma_t(E)}\,\sigma_\gamma(E)\frac{1}{E}\,dE}{\int_g \sigma_\gamma(E)\frac{1}{E}\,dE} \quad (2)$$

where, $T_g(N_i)$: transmission rate as a function of transmission
          sample for the neutron energy group g,

   $R_g(N_i)$: self-indication ratio as a function of shield-
          ing sample thickness for the neutron energy group
          g.

   $\varepsilon(E)$: detection efficiency at neutron energy E,

   $\varepsilon'(E)$: detection efficiency at neutron energy E for
          neutron capture rate measurement,

   $\phi(E)$:   neutron flux at neutron energy E,

   $\sigma_t(E)$:   total cross section at neutron energy E,

   $\sigma_\gamma(E)$:   capture cross section at neutron energy E,

   n   :   thickness of capture sample(atom/barn).

Figure 1 shows the transmission rate $T_g(N_i)$ and the self-indica-
tion ratio $R_g(N_i)$ obtained from the Ta samples. A least squares
fitting was applied to these data points to get N-dependent
functions of $T_g(N)$ and $R_g(N)$. After the term of $\exp(-N\sigma_0)$ has
been multiplied to the $T_g(N)$ and $R_g(N)$, the following calcula-
tions have been performed to obtain integral values $T_g(\sigma_0)$ and
$R_g(\sigma_0)$.

$$T_g(\sigma_0) = \int_0^\infty T_g(N)\ e^{-N\sigma_0}\ dN\ = \frac{\int_g \frac{1}{\sigma_t(E)+\sigma_0}\frac{1}{E}dE}{\int_g \frac{1}{E}dE} \tag{3}$$

$$R_g(\sigma_0) = \int_0^\infty R_g(N)\ e^{-N\sigma_0}\ dN\ = \frac{\int_g \frac{1}{\sigma_t(E)+\sigma_0}\frac{1}{E}dE}{\int_g \sigma_\gamma(E)\frac{1}{E}dE} \tag{4}$$

The self-shieding factor from the present measurement is the
Bondarenko type[5], as defined by

$$f_g(\sigma_0) = \frac{\int_g \frac{\sigma_\gamma(E)}{\sigma_t(E)+\sigma_0}\frac{1}{E}dE}{\int_g \sigma_\gamma(E)\frac{1}{E}dE}\ \Big/ \ \frac{\int_g \frac{1}{\sigma_t(E)+\sigma_0}\frac{1}{E}dE}{\int_g \frac{1}{E}dE} \tag{5}$$

With the relation of eqs.(3) and (4), eq.(5) is easily rewritten

as

$$f_g(\sigma_0) = \frac{R_g(\sigma_0')}{T_g(\sigma_0')} \quad .$$

(6)

The self-shielding factors measured in the 0.2 to 22 keV energy region for ^{181}Ta are depicted in Fig. 2. Figure 3 shows the calculated self-shielding factors from JENDL-2, whose factors were obtained by using the processing code PROF-GRAUCH-G2/B[6] from JENDL-2. As seen in Figs. 2 and 3, there are large discrepancies between the measured and calculated results, especially in the unresolved resonance region from 1 to 50 keV. The calculated values illustrate more rapid decrease as the σ_0 becomes smaller, comparing with the measurement. The problem may be mainly derived from the fact that the total cross section of ^{181}Ta in JENDL-2 includes minus background cross sections. An additional investigation is necessary for the ^{181}Ta cross section, especially in the unresolved resonance energy region, in JENDL-2.

We are now doing self-shielding experiments for ^{232}Th and ^{238}U samples which have higher radioactive background.

II. Resonance Parameters and Resonance Integral of ^{232}Th

It is said that the first four s-wave resonances of ^{232}Th give about 70 % of the resonance integral for the ^{232}Th(n,γ) reaction. These resonance parameters play an important role in the safe and economical design of nuclear reactors utilizing thorium-based fuels. Nevertheless, marked discrepancies around 20 % can be seen among the existing data for the resonance parameters of ^{232}Th, especially in the lower energy region.

Transmission measurements of metallic Th-samples were made by the linac time-of-flight(TOF) method. The experimental method is similar to that in the previous work[7]. Neutron transmission rates from thorium samples (1.5, 2.9, 9.1, 18.4, 27.7 x 10^{-3} atom/barn) were measured, and the resonance para-

meters were deduced from the area analysis by the Hughes' method[8] and the shape analysis by the SIOB code[9]. The results obtained by the area analysis were also employed as the initial values used in the SIOB calculation.

The results obtained are shown in Table 2, where the evaluated resonance parameters in JENDL-2, ENDF/B-IV and ENDF/B-V are also given. The present results agree well with the recent works by Olsen[10] and Chrien[11], except Γ_γ at 69.2 eV for the area analysis. The 17 s-wave resonance parameters at energies from 113 to 401 eV have been also obtained by the shape analysis, and the results are shown in Table 3. Although the experimental uncertainties in some of the data are up to be about 50 %, the values are in general agreement with those in JENDL-2 and ENDF/B-IV.

In order to make an integral assessment of the resonance parameters of ^{232}Th, resonance integrals calculated by using the evaluated nuclear data files have been compared with that measured in the standard 1/E neutron spectrum field. The calculations of the resonance integral have been carried out with the code RESENDD[12], which generates resonance cross sections from the data file and followed by the code INTERN[13]. From the comparison of the results in Table 4, one can recognize that the ENDF/B-IV data show good agreement with the measurement, and that the difference of about 7.3 % can be, however, seen between the measurement and the JENDL-2 result. Additional integral checks were tried by partially exchanging the parameters in JENDL-2 or ENDF/B-IV for the present parameters' values. We have tested the following ten substitution cases;
1) first four s-wave parameters from the present measurement (shape analysis) and the others from JENDL-2,
2) first four s-wave parameters from the present measurement(area analysis) and the others from JENDL-2,
3) first four s-wave parameters from ENDF/B-IV and the others from JENDL-2,
4) first four s-wave parameters from ENDF/B-V and the others from JENDL-2,

5) first 21 s-wave parameters from the present measurement and the others from JENDL-2,

6) to 10) cases, in which ENDF/B-IV data, except the relevant parameters, were used instead of JENDL-2.

Resonance integrals from these substitution data are also given in Table 4. The resonance integrals from cases 1) to 5) are all higher than that from the JENDL-2 data, and the value from case 8) is obviously lower than those in 6),7),9) and 10). This means that the resonance parameters, especially first four s-wave parameters are smaller. The exchanged values for ENDF/B-IV or ENDF/B-V seem to be in good agreement with the measured resonance integral. The present 21 s-wave data show a satisfactory agreement with the measurement.

References

1) Sowerby,M.G., et al., INDC(NDS)-129/GJ (1981).

2) De Saussure,G., et al., Ann. nucl. Energy, 9, 79 (1982).

3) Ganesan,S., Ann. nucl. Energy, 9, 481 (1982).

4) Perez,R.B., et al., Trans. Am. Nucl. Sco., 44, 537 (1983).

5) Bondarenko,I.I.(ed.), "Group Constants for Nuclear Reactor Calculations", Consaltants Bureau, New York (1964).

6) Hasegawa,A., Private communication (1986).

7) Kobayashi,K., et al., Ann. nucl. Energy, 11, 315 (1984).

8) Hughes,D.J., J. Nucl. Energy, 1, 237 (1955).

9) De Saussure,G., et al., ORNL/TM-6286 (1978).

10) Olsen,D.K., et al., ORNL/TM-7661 (1981).

11) Chrien,R.E., et al., Nucl. Sci. Eng., 72, 202 (1979).

12) Nakagawa,T., JAERI-M 84-192 (1984).

13) Nakagawa,T., Private communication (1986).

Table 1 Experimental condition for self-shielding measurements

	Transmission experiment	Self-shielding experiment
Thickness of Ta-samples ($\times 10^{-2}$ atom/b)	0.873, 1.68, 2.62, 3.35, 3.71, 4.63, 5.31, 6.37, 8.63, 11.0, 13.3, 15.5	0.263, 0.573, 0.873 1.11, 1.67, 2.25, 3.51, 5.26, 6.69
Detector	^{10}B + 8 sets of BOG scinti..	Cap. sample: 0.46 $\times 10^{-2}$ atom/b a pair of C_6D_6 scinti.
L i n a c Pulse width	10 nsec	100 nsec
Frequency	300 Hz	200 Hz
Current	~700 mA (peak)	~700 mA (peak)
Energy	~30 MeV	~30 MeV
Foreground filter	S, Cd	S, Cd, Al, Co, Na
Background filter	S, Cd, Al, Mn, Co	- - - - - - -
Flight path	12.55 m	12.97 m
Time digitizer Channel width No. of channel	40 nsec 2048	40 nsec 2048

Fig. 1 $T(N_i)$ and $R(N_i)$ of Ta-181 at 1.0 to 2.17 keV
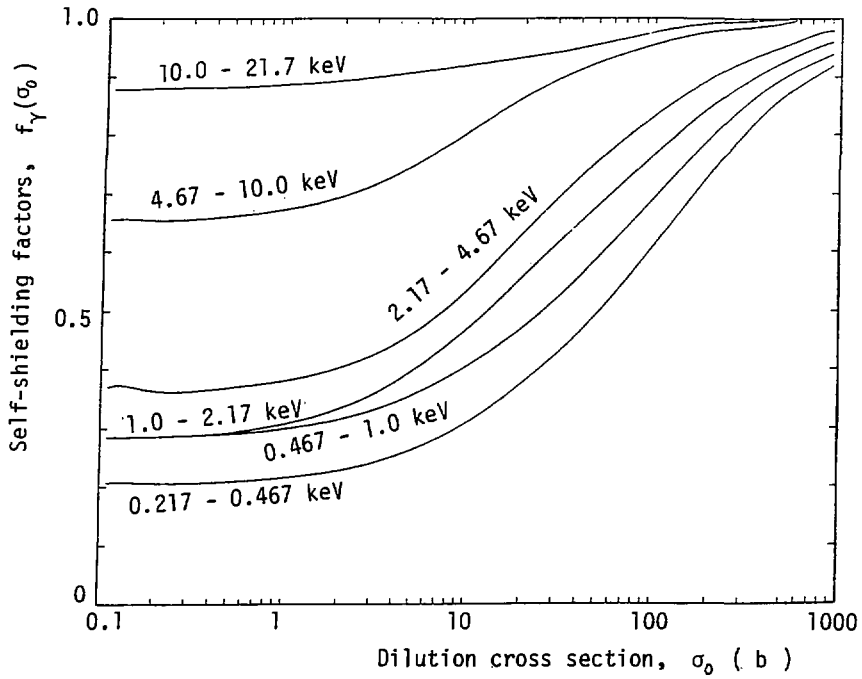
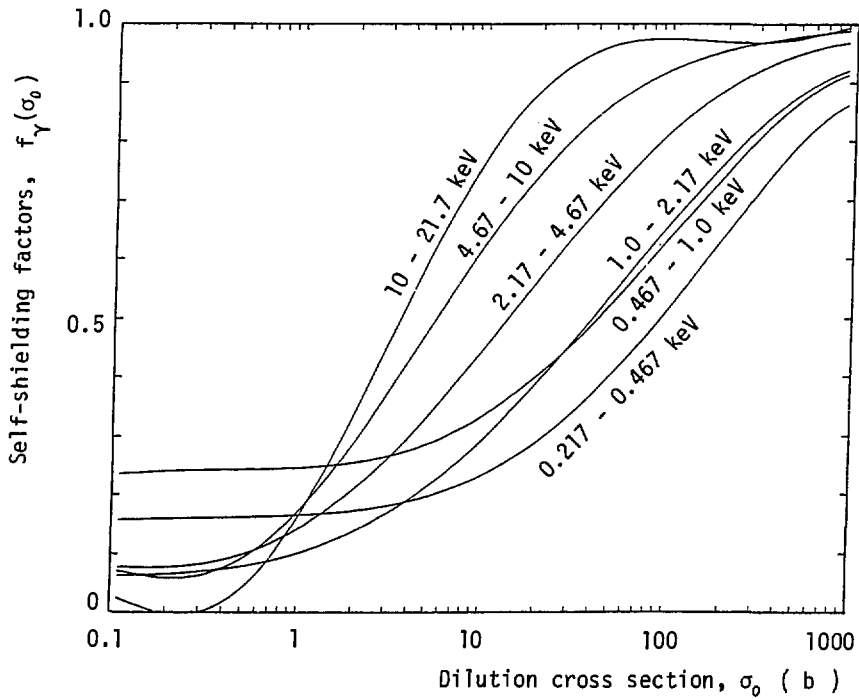Fig. 2 Self-shielding factors measured in this study

Fig. 3 Self-shielding factors calculated from JENDL-2

Table 2   Widths (meV) for the first four ^{232}Th s-wave resonances

Measurement or evaluation	21.8 eV Γ_n	21.8 eV Γ_γ	23.5 eV Γ_n	23.5 eV Γ_γ	59.5 eV Γ_n	59.5 eV Γ_γ	69.2 eV Γ_n	69.2 eV Γ_γ
Olsen (80)	2.08+.03	25.3+0.6	3.82+.06	26.9+0.7	3.86+.07	24.6+1.0	43.2+0.5	24.1+0.6
Chrien (79)	2.10+.10	24.0+1.5	3.70+.20	26.0+1.5	4.00+.30	25.0+2.0	41.2+3.0	22.6+2.0
Keyworth (78)	1.97+.05	20.9+11.3	3.72+.15	19.0+7.7	3.92+.10	20.1+7.2	44.0+1.0	22.9+1.5
Derrien (74)	2.02+.06	24.5+2.0	3.88+.40	26.6+1.5	3.90+.15	23.7+1.0	43.2+1.0	21.9+0.7
Rahn (72)	1.91+.09	20.0+2.0	3.24+.24	25.0+2.0	3.93+.23	25.0+2.0	44.0+2.0	25.0+2.0
Forman (71)					4.01+.31	22.7+6.0	42.5+1.7	21.9+2.8
Ribon (69)	1.96+.08	21.3+3.7	3.64+.12	28.2+2.9	3.93+.08	23.6+0.7	44.0+0.5	20.5+1.0
Bollinger (68)	2.09+.03	26.5+1.2	4.11+.05	25.2+1.1	3.77+.15	31.7+2.9	42.0+0.8	23.5+1.4
Bhat (67)	2.61+.17	22.4+2.4	4.17+.25	22.0+2.6	4.41+.27	16.2+2.3	42.9+2.6	21.5+4.7
Asghar (66)	1.88+.05	24.6+1.2	3.41+.08	29.9+1.6	3.34+.09	23.2+2.0	41.4+1.2	21.2+1.0
Haddad (64)	2.10+.20	21.0+5.0	4.00+.30	22.0+4.0	4.00+.40	22.0+7.0	47.0+15.	24.0+2.0
Palevsky (64)	2.60+.20	30.0+2.0	3.70+.20	27.6+1.5	4.50+.30	37.0+5.0	38.0+6.0	26.0+5.0
ENDF/8-V (80)	2.02	23.0	3.88	25.0	4.04	23.2	44.0	21.9
ENDF/8-IV (65)	2.00	25.9	3.74	25.9	4.00	25.9	42.0	25.9
JENDL-2 (84)	1.913	20.00	3.243	25.00	3.933	25.00	44.00	25.00
Previous work*	2.07+.14	24.4+2.1	4.00+.29	25.0+2.2	3.86+.27	26.0+2.9	41.7+6.6	18.3+3.5
Present work #	2.09+.03	25.2+0.7	3.88+.18	26.1+1.4	3.83+.21	25.0+2.1	42.6+1.3	22.9+1.3

* Area analysis by the present authors(1983).   # Shape analysis by the SIOB code

Table 3   Resonance parameters of ^{232}Th (meV)

Resonance energy (eV)	Present values Γ_n	Present values Γ_γ	JENDL-2 Γ_n	JENDL-2 Γ_γ	ENDF/B-IV Γ_n	ENDF/B-IV Γ_γ
21.8	2.09+.03	25.2+0.7	1.91	20.0	2.00	25.9
23.5	3.88+.18	26.1+1.4	3.24	25.0	3.74	25.9
59.5	3.83+.21	25.0+2.1	3.93	25.0	4.00	25.9
69.2	42.6+1.3	22.9+1.3	44.0	25.0	42.0	25.9
113	13.9+1.3	20.4+2.9	13.5	20.0	12.4	25.9
121	24.9+0.9	26.5+2.9	24.0	22.0	20.5	25.9
129	3.38+.75	29.6+9.5	3.41	18.0	3.50	25.9
154	.205+.044	23.0+7.9	.120	21.2	.120	25.9
170	61.9+2.8	22.1+5.8	65.0	26.0	60.0	25.9
193	17.4+1.8	22.1+4.3	18.5	17.0	15.0	25.9
199	10.2+1.5	23.9+9.3	12.6	18.0	11.0	25.9
221	26.4+3.3	25.1+7.3	30.9	22.0	29.5	25.9
251	29.9+3.9	25.7+9.4	32.0	24.0	31.0	25.9
263	22.6+4.0	24.1+10.1	24.0	19.0	20.7	25.9
286	29.8+5.0	22.4+9.5	29.9	20.0	29.2	25.9
305	23.3+4.5	25.8+9.8	26.0	20.0	27.0	25.9
329	73.1+9.6	27.4+11.5	76.0	26.0	72.0	25.9
342	35.5+7.0	26.2+9.5	36.1	19.0	37.5	25.9
365	23.0+9.3	22.6+12.9	28.1	21.0	26.0	25.9
369	24.9+10.2	25.4+12.6	25.0	22.0	26.0	25.9
401	12.1+5.2	26.6+18.0	10.4	18.0	10.8	25.9
< average Γ_γ >		< 24.7 >		< 21.3 >		< 25.9 >

Table 4 Resonance integral of ^{232}Th

Measurement in the 1/E field	86.2 $\pm$ 3.6 barn
C/E ratio for JENDL-2	0.9273
C/E ratio for ENDF/B-IV	0.9930

Calculation

	Data used	Resonance integral	Ratio
	JENDL-2	79.93	1.000
Substitution tests	Measured 4 s-waves (shape analysis)	84.36 (case-1)	1.056
	(area analysis)	82.87 (case-2)	1.037
	ENDF/B-IV	84.03 (case-3)	1.057
	ENDF/B-V	83.47 (case-4)	1.044
	Measured 21 s-waves	84.94 (case-5)	1.063
	ENDF/B-IV	85.60	1.000
Substitution tests	Measured 4 s-waves (shape analysis)	85.91 (case-6)	1.004
	(area analysis)	84.42 (case-7)	0.986
	JENDL-2	81.49 (case-8)	0.952
	ENDF/B-V	85.03 (case-9)	0.993
	Measured 21 s-waves	85.78 (case-10)	1.002

P.9 THERMAL NEUTRON CROSS SECTIONS: TRANSMISSION
EXPERIMENTS AND MODEL CALCULATIONS

J. R. GRANADA [*]

Centro Atomico Bariloche and Instituto Balseiro

8400 S.C. de Bariloche, Argentina

*A brief description is presented of some activities relat-
ed to measurement and calculation of thermal neutron cross
sections, currently underway at the Neutron Physics Divi-
sion of Centro Atomico Bariloche. Examples are given of
the application of a Synthetic Scattering Law, with special
emphasis on the evaluation of quantities of interest for
(thermal) reactor-physics calculations. Some recent trans-
mission measurements at thermal and epithermal neutron en-
ergies are also reported.*

I. INTRODUCTION

The use of thermal neutrons as a probe for the investigation of conden-
sed matter has already been established as a very powerful tool, causing
a major impact on both pure and applied science. The fundamental interest
on the atomic motions in matter as well as reactor-physics development we-
re the basic motivations for extensive studies performed in the past from
both the experimental and theoretical sides.

Although fewer groups are now involved in the determination of thermal
neutron constants, there is still a need for improved data in this energy
range, as more accurate cross section values are required in many research

----

[*] *Visiting Research Scholar, Kyoto University Research Reactor Inst.*

fields where neutron techniques are employed due to some of its unique fea-
tures[1]. Moreover, it has been pointed out that information about some
fundamental properties of the neutron itself, can be obtained from high
precision total cross section data on the thermal and epithermal neutron
energy regions[2].

II. MODEL CALCULATIONS

The basic quantity which describes the interaction of thermal neutrons
with a condensed system is the scattering law $S(Q,w)$, as it comprises all
the structural and dynamical properties of the system. The Zemach-Glauber
formalism provides an essentially exact frame for the representation of
$S(Q,w)$, but the resultant expressions are rather complicated and further-
more, a detailed knowledge of the quantum mechanical description of the
system is required. However, for many neutron-physics problems such a de-
tailed knowledge of the shape of the scattering law, over a large portion
of the energy- and momentum-transfer space, is normally unnecesary.

Therefore, motivated by the practical requirements of (thermal) reactor
physics calculations, as well as the necessity of applying inelasticity co-
rrections to the observed spectrum in neutron diffraction work on molecular
gases and liquids, a synthetic scattering function $T(Q,w;E)$ has been deve-
loped, which allows a fast and reliable evaluation of cross sections [3].
The main characteristics of the molecular dynamics are retained through the
introduction of an effective mass, and temperature and vibrational factors
which depend on the incident neutron energy E. A very simple form is thus
obtained for $T(Q,w;E)$ which yields analytic expressions for the energy –
transfer kernels and the total cross section[4].

A detailed description of the synthetic scattering function, including
its basic hypothesis and approximations was given before[3,5], therefore
only some results are presented here. Figures 1 and 2 show a comparison of
experimental data and model results for the total cross sections of H_2O
and C_6H_6 [6] respectively, over the entire thermal energy range. In each
case, the agreement between the two sets is very good, except at the lowest
energies where a collisional regime dominates the dynamics in those liquid
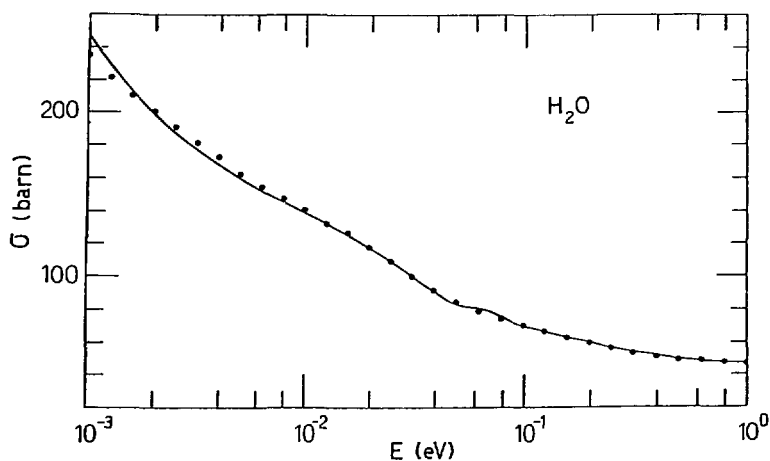systems, while the model assumes free-translation for the molecular units.

Fig.1. TOTAL CROSS SECTION OF LIGHT WATER. DOTS: EXPERIMENTAL DATA; SOLID LINE: SYNTHETIC MODEL
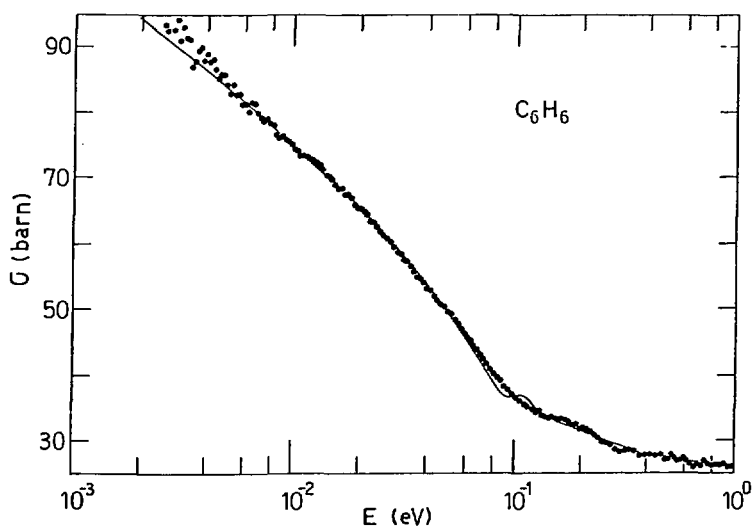

Fig.2. TOTAL CROSS SECTION OF BENZENE. DOTS: SPREVAK'S DATA; SOLID LINE: SYNTHETIC MODEL.

Figure 3 shows the isotropic energy-transfer kernel for H_2O, at three well separated incident neutron energies. The results of the analytic formula from the synthetic model are compared with GASKET-FLANGE calculations which are based on a continuos frequency spectrum. Similar agreement is obtained in the comparison of the first anisotropic kernels from both calculations.
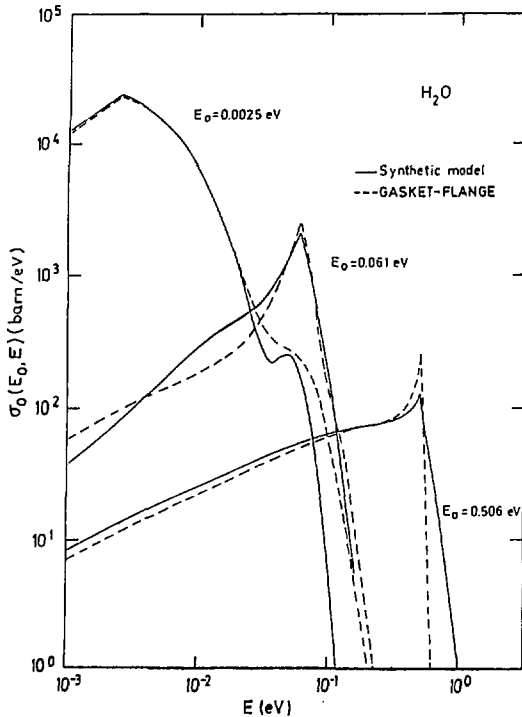
Fig.3 . THE ISOTROPIC ENERGY-TRANSFER KERNEL OF LIGHT WATER.

Besides the neutron thermalization field, the synthetic scattering function has been also applied to the evaluation of inelasticity corrections in neutron diffraction work[7]. Figure 4 shows the model results together with experimental points [8], corresponding to the observed differential cross section of H_2O as measured with a pulsed neutron source. It must be stressed that the traditional approach for the evaluation of the pedestal in this kind of measurements, based on the Placzek mass expansion, breaks down

Fig.4. THERMAL NEUTRON DIFFRACTION BY WATER. DATA FROM SOPER AND SILVER (PULSED NEUTRON SOURCE, ARGONNE, 1982).
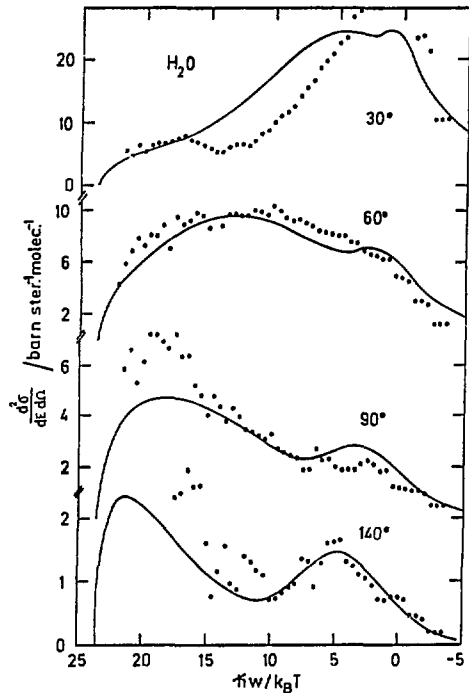
Fig.5. DOUBLE DIFFERENTIAL CROSS SECTION OF LIGHT WATER. DOTS: EXPERIMENTAL DATA FROM HARLING; SOLID LINE: SYNTHETIC MODEL.

for molecules containing light atoms. Although the synthetic model was not intended to describe the actual shape of the scattering law, but rather to give a good representation of its moments, a comparison between experimental data and model results is shown in Fig.5 for the double differential cross section of light water. It can be seen that a reasonable agreement is achieved, except at smaller angles where the quasielastic peak cannot properly be described by the model.

Neutron diffusion parameters can be readily obtained from this model by a simple integration using as a weight the Maxwellian function corresponding to the required temperature. In the Table, the results for the diffusion constant and diffusion cooling of H_2O at room temperature are compared with some results of experiments and other theories. Furthermore, Fig. 6 shows the decay constant as a function of geometrical buckling (a), and the (density removed) diffusion length as a function of temperature (b). In all cases, the agreement between measurements and model results is very good.

NEUTRON DIFFUSION PARAMETERS OF H_2O

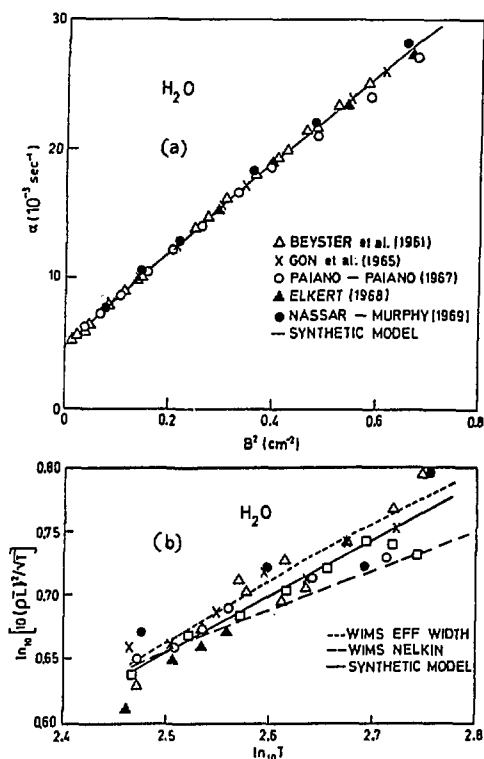| AUTHOR	D_o (cm²/s)	C (cm⁴/s)	METHOD
BANSAL ET AL. (1979)	35800	3224	CALCULAT.
MARTINHO, + (1971)	36304 +-180	3213 +-110	EXP,REAC.
DORNING (1970)	36068	2973	CALCULAT. KOPPEL M.
GODDARD, + (1969)	35620 +-230	2800 +-260	EXP,REAC.
" "	34203	2960	C: HAYWOOD
" "	36820	2920	C: NELKIN
COKINOS, + (1969)	36310 +- 78	3010 +- 80	EXP,PULSED
GRANADA, + (1985)	36310	3036	SYNTH.MOD.

Fig. 6

Finally, it is convenient to emphasize that the required input infor-
mation is minimum, and that a full calculation with the synthetic model at
a given temperature takes about 3 min of CPU time on a VAX 11/780, includ-
ing the evaluation of cross sections, scattering kernels (each a matrix of
80 x 150), and diffusion parameters.

III. TRANSMISSION EXPERIMENTS

A LINAC based pulsed neutron source is employed in combination with
time-of-flight techniques. Typical experimental conditions for transmission
measurements are:

Electron energy:	25 MeV	Target:	water cooled Pb
Repetition rate:	100 Hz	Moderator:	polypropylene
Average current: (at the target)	25 μA	Total flight path:	18 m
		Detector bank:	^{3}He tubes

Activities along this line are mainly directed towards the determina-
tion of scattering lengths and incoherent cross sections of elements and
their isotopes, as well as the characterization of structural properties
and texture effects in metals. Figure 7 shows the coherent components of
the total cross section of powdered Molybdenum, as obtained from our mea-
sured points[9] and calculated according to the CRIPO [10] computer code.
Departures from a randomly oriented
microcrystallites condition (grain
size, texture), can then be conve-
niently studied.

Examples of two recently mea-
sured total cross sections are gi-
ven in Figs. 8 and 9, corresponding
to elemental Sulphur and Gallium ,
respectively. Information quoted
in the literature about these ma-
terials (in this energy range) re-
veals a large scatter among data
points. From our measurement, we
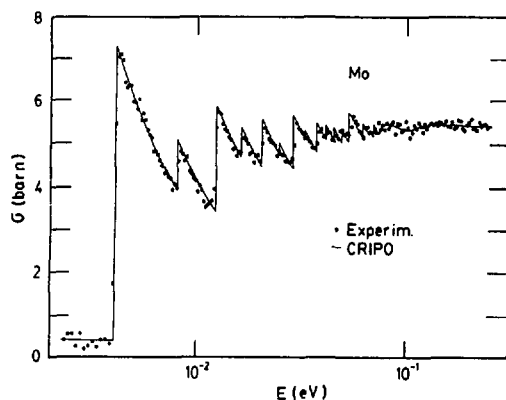obtained the value:

Fig. 7. The total cross section (absorption subtracted) of
Molybdenum in the thermal neutron range. The experi-
mental points are from [9] whereas the solid line is
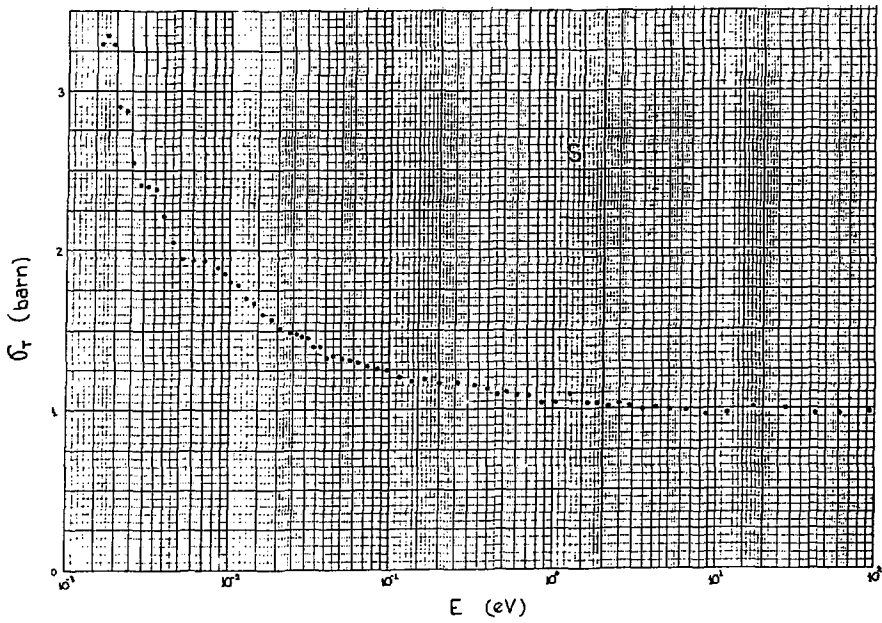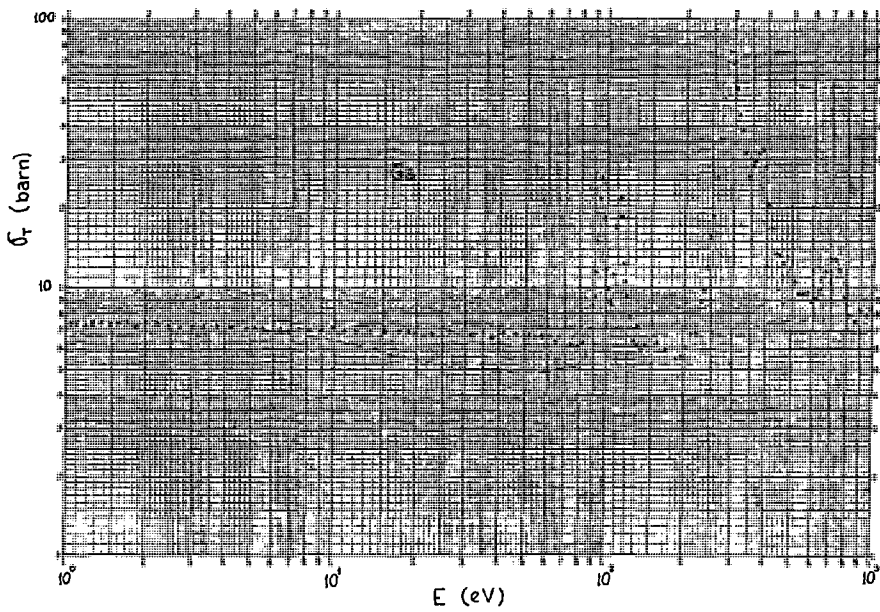calculated using the CRIPO computer code.

Fig. 8

Fig. 9

$$\sigma_{free} \ (S) = (0.9745 \ \pm \ 0.0050) \ b$$

for the free-atom scattering cross section of Sulphur.

ACKNOWLEDGMENTS

I wish to express my gratitude to Profs. S.Okamoto, I.Kimura and Y. Fujita for their kindness and hospitality during my stay at the Research Reactor Institute of Kyoto University. I also want to extend my appreciation to all members of the LINAC staff at this Institute.

1. B. Fender, *Nucl.Inst.Meth. A249, 1 (1986).*

2. L. Koester et al., *Physica 137B,282(1986).*

3. J.R. Granada, *Phys.Rev. B31,4167(1985).*

4. J.R. Granada et al., *submitted for publication.*

5. J.R. Granada, *Phys.Rev. B32,7555(1985).*

6. D. Sprevak et al., *General Atomic Report GA-8185 (USAEC,1967).*

7. J.R. Granada et al., *Physica B, in press.*

8. A.K. Soper and R.N. Silver, *Phys.Rev.Lett.,49,471(1982).*

9. F. Kropff et al., *Atomkernenergie 31,42(1978).*

10. F. Kropff and J.R. Granada, *unpublished Report (CAB-1977).*

P.10 Combined Use of Coupled-Channel, DWBA and Hauser-Feshbach

Codes for the Calculation of Neutron Inelastic Scattering

Takaaki Ohsawa

Department of Nuclear Engineering, Kyushu University

6-10-1 Hakozaki, Higashi-ku, Fukuoka 812, Japan

Abstract:

A method is proposed to calculate the neutron inelastic scattering cross sections for deformed nuclei taking into account both the direct and compound nuclear processes. The inelastic channels were divided into three classes according to the strength of coupling to the entrance channel. The coupled-channel, DWBA and Hauser-Feshbach methods were combined for use in the calculations for the three classes of channels. This prescription makes it possible to calculate the cross sections accurately without requiring lengthy computational time.

1. Introduction

Nuclear model calculation of neutron inelastic scattering has been made so far on the basis of the Hauser-Feshbach (HF) theory combined with the spherical optical model (SOM) (This method is abbreviated as SOM/HF, where width fluctuation effects are assumed to be taken into account). However, comparison of experimental data and theoretical calculations revealed considerable discrepancies, among others for partial inelastic scattering cross sections for levels of the ground-state rotational band. In addition, measured data on the angular distribution of the inelastically scattered neutrons are considerablly deviated from the symmetry about 90 at energies above 2 MeV for even-even actinide nuclei. These facts are interpreted as indications of probable existence of direct interactions (DI) in the inelastic scattering of neutrons on deformed nuclei. Thus the need is evident for a

theoretical method that allows for consistent calculation of direct and compound nuclear (CN) processes in neutron inelastic scattering.

This report presents a brief description of a new method of combining coupled-channel (CC), distorted-wave Born approximation (DWBA) and Hauser-Feshbach models for this purpose.

2. Theoretical Considerations

The reaction channels of inelastic scattering are divided into three classes according to the strength of coupling to the entrance channel(Fig.1). Our idea is to use different methods for these three classes of states; strongly coupled channels are treated with CC, moderately coupled channels with DWBA, and for weakly coupled channels only HF contributions are considered.

2.1 Strongly coupled channels

These channels include practicaly the members of ground-state rotational band of deformed nuclei. The problem of including the effect of direct processes into the HF calculations was solved[1] by consistent combination of CC and HF methods via Satchler's generalized transmission coefficients[2] ('CC/HF method', as we name it[1]).

In the case of SOM, only the diagonal elements of the S-matrix are calculated, while in the CC model the non-diagonal elements corresponding to the strongly coupled states can also be calculated. The generalized transmission coefficients are given as the 'unitarity deficit' of the average S-matrix (Fig.2). These transmission coefficients are then used for the entrance channel of the HF calculation.

Here three approximations are introduced:

(a) Use is made of the SOM transmission coefficients for the exit channels. This is justified since the role of the exit channel transmission coefficients is just to redistribute the decay probability of the compound nucleus according to the principle of detailed balance.

(b) HF model implemented with the Moldauer formalism[3] is assumed to be valid for the calculation of inelastic scattering proceeding by way of compound nucleus formation.

(c) The interference of the CN and DI processes are considered to vanish,

when average is taken over a suitable energy interval. This condition is sufficiently well fulfilled for the case of neutron inelastic scattering on actinide nuclei.

2.2 Moderately coupled channels

This class includes mainly the vibrational states of the actinide nuclei.

A possible way would be to include these states into channel-coupling. However, this choice was not taken, because this would require lengthy computational time as well as knowledge of the coupling strength for each of the states, for which information is very scarce. We thus used DWBA to calculate the DI component for these states. Since the coupling was not supposed to be so strong, the effect of loss of probability flux by way of DI was not reflected into the transmission coefficient; instead, generalized transmission coefficients obtained from CC/HF method (with coupling of strongly coupled channels only) was used to calculate the CN component of inelastic scattering cross section.

In applying the DWBA formalism, we adopted the asymmetric distorted wave approximation (ADWA), in which a spherical optical potential that reproduce the elastic scattering was used for the entrance channel, while a bare optical potential was employed for the exit channel:

$$T_{ab} = \langle \chi_b | H' | \psi_a \rangle \tag{1}$$

ψ_a = wave function generated by the SOM potential
　　 that reproduce the elastic scattering,

χ_b = wave function generated by the bare OM poten-
　　 tial(=CC-OM potential).

2.3 Weakly coupled channels

This includes higher excited states with high spin or with small reduced transition probability.

For these states it was assumed that there were no DI components. Thus CN components were calculated by the CC/HF method using the generalized trans-

mission coefficients obtained from CC calculation for the entrance channel.

3. Results and Discussion

3.1 Difference between CC/HF and SOM/HF results

Figure 3 shows the partial inelastic scattering cross sections for the 1st and 2nd excited states of Th-232. The optical potential parameters adopted are those reported by the Bruyeres group[4] , and the coupling scheme is $0^+-2^+-4^+$.
The code JUPITOR-1[5] was used for CC calculation, and ELIESE-3[6] was used for HF calculation.

Comparing the results of CC/HF and SOM/HF calculations, we note that simple summation of the SOM/HF result and DI component does not reproduce well the experimental data, nor agrees with the CC/HF calculation. This is because the CN contribution is also altered due to the difference of generalized and SOM-transmission coefficients. In fact, the energy-dependent behavior of the two kinds of transmission coefficients are significantly changed, as can be seen in Fig.4.

To summarize, the difference between the CC/HF and SOM/HF calculation is caused by two sources:

  (1) the existence of additional DI component $\left|\langle S_{ab}\rangle - \delta_{ab}\right|^2$

  (2) the change in the CN component itself $\langle\left|S_{ab}^{f\ell}\right|^2\rangle$ due

      to the alteration of the transmission coefficients.

Incidentally, in recent papers Hodgson et al.[7] applied the distorted wave formalism also to the calculation of inelastic scattering to the ground-state rotational band. They succeeded in reproducing the DI component of the cross section by empirically renormalizing the calculated value. However, there remained some discrepancies at lower energies; this is because the effect (2) above was not taken into account in their method. Thus in order to obtain good fits to the experimental data at lower energies where CN process still has greater contribution, it is necessary to consider the difference between the generalized and SOM-transmission coefficients.

3.2 Asymmetric distorted-wave approximation (ADWA)

An asymmetric form of the distorted-wave approximation for inelastic

scattering has been proposed and discussed by Satchler[8]. He found that the transition amplitude calculated with the exit channel wave function generated by the bare optical potential reproduce the exact result a little more accurately than the conventional DWBA ('DW method', according to the terminology of Satchler). Figure 5 shows a result of calculations made by the present author to test this statement. The code DWUCK[9] was used for DW calculation. It can be seen that the ADWA gives a result in better agreement with the CC calculation in the region of small beta. For larger beta, the CC result begins to saturate, because otherwise the unitarity of the S-matrix would be violated. On the other hand, in distorted wave approximations, the cross section continues to increase as β^2 if the same distorting potential is used.

Figures 6 are the results of calculations for 774.1 keV (2^+) plus 774.3 keV (3^-) and for 785.3 keV (2^+) excited levels of Th−232. The β −values deduced from reduced transition probabilities

$$B(E\lambda;I_iK_i \rightarrow I_fK_f)\uparrow$$

$$=\left(\frac{3}{4\pi}ZeR_o^\lambda\right)^2(I_i\lambda K_iK_f-K_i|I_i\lambda I_fK_f)^2\frac{\hbar}{2(B_\lambda C_\lambda)^{1/2}}\times\left\{\begin{array}{c}2\\1\end{array}\right. \tag{2}$$

$$\beta_\lambda^2=(2\lambda+1)\hbar/2(B_\lambda C_\lambda)^{1/2}\times\left\{\begin{array}{ll}2 & \text{if } K_i=0,\ K_f\neq0\\ \\ 1 & \text{otherwise}\end{array}\right. \tag{3}$$

for vibrational states of deformed nucleus[10] were used to normalize the DWUCK calculation.

4. Conclusion

A method of calculation of the neutron inelastic scattering cross sections for deformed nuclei taking into account the CN and DI processes was proposed. It was found that consistent combination of CC and HF methods (CC/HF method) gave good fits to the measurements. This is due to two effects: existence of DI component, and modification of CN component itself. For moderately coupled states, the asymmetric distorted-wave approximation

gave good results without requiring long computational time.

References

1) Ohsawa, T. et al. : Proc. of the Intern. Conf. on Nuclear
   Data for Science and Technology, Santa Fe 1985, Vol.2, p.1193
   (1986)
2) Satchler, G. : Phys. Lett. 7, 55 (1963)
3) Moldauer, P.A. : Phys. Rev. 123, 968 (1961); ibid. 135,
   B642 (1964); Rev. Mod. Phys. 36, 1079 (1964)
4) Haouat,G. et al. : Nucl. Sci. Eng., 81, 491 (1982)
5) Tamura, T. : Rev. Mod. Phys.,37, 679 (1965); ORNL-4152 (1967)
6) Igarasi, S. : JAERI-1224 (1972)
7) Hodgson, P.E., et al. : Nucl. Sci. Eng. 89, 111 (1985); ibid.
   92, 459 (1986)
8) Satchler, G. : "Direct Nuclear Reactions", Oxford University
   Press (1983)
9) Kunz, P.D. : COO-535-606 and -613 (1969)
10) Bohr, A., and Mottelson, B. : "Nuclear Structure", Vol.II,
    p.364
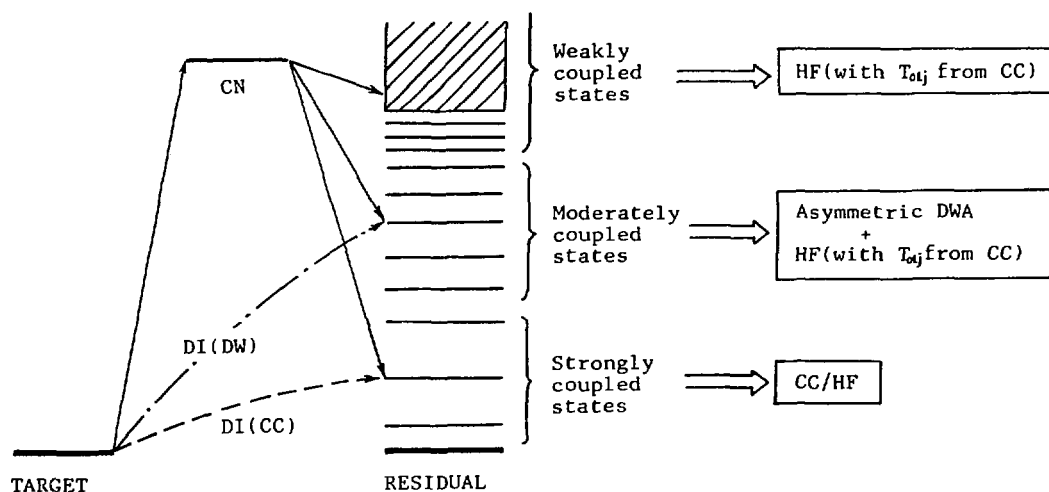
Fig.1   Three classes of reaction processes in neutron inelastic
         scattering.
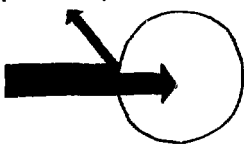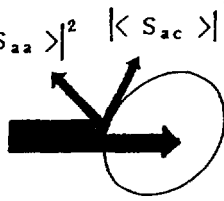
Fig.2   Schematic representation of neutron transmission coefficients
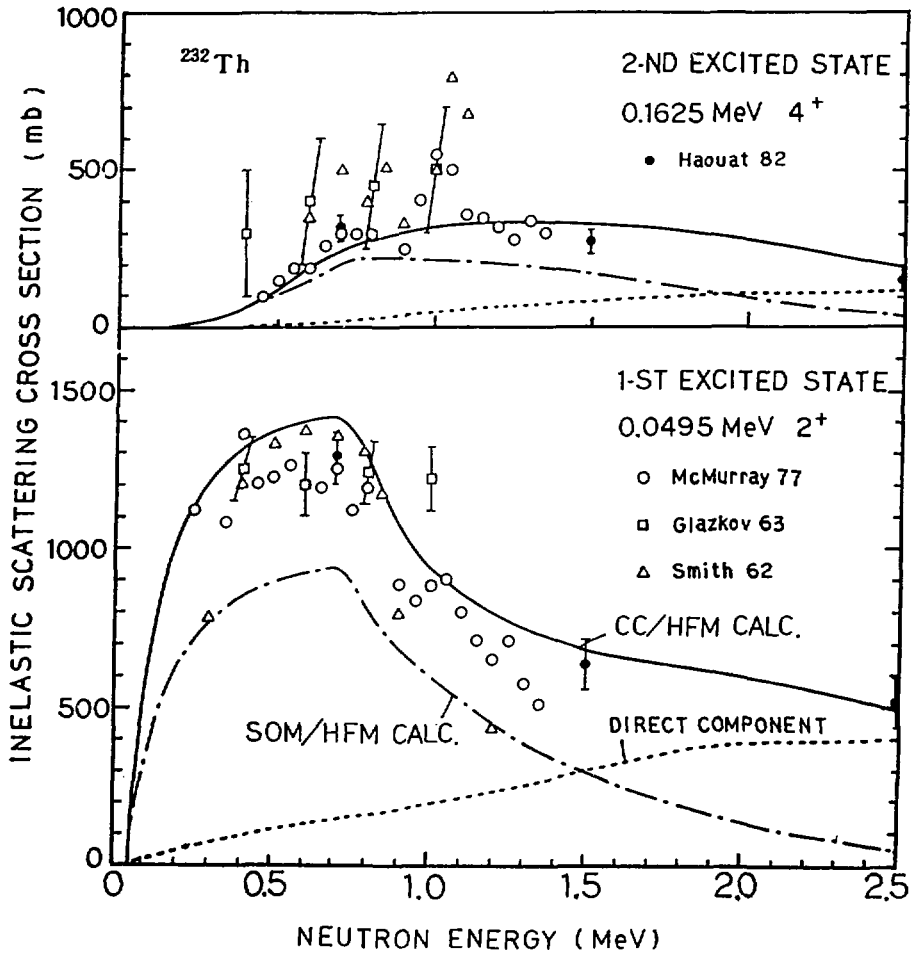   calculated with SOM and CC methods.

Fig.3   Inelastic scattering cross sections for the first and second
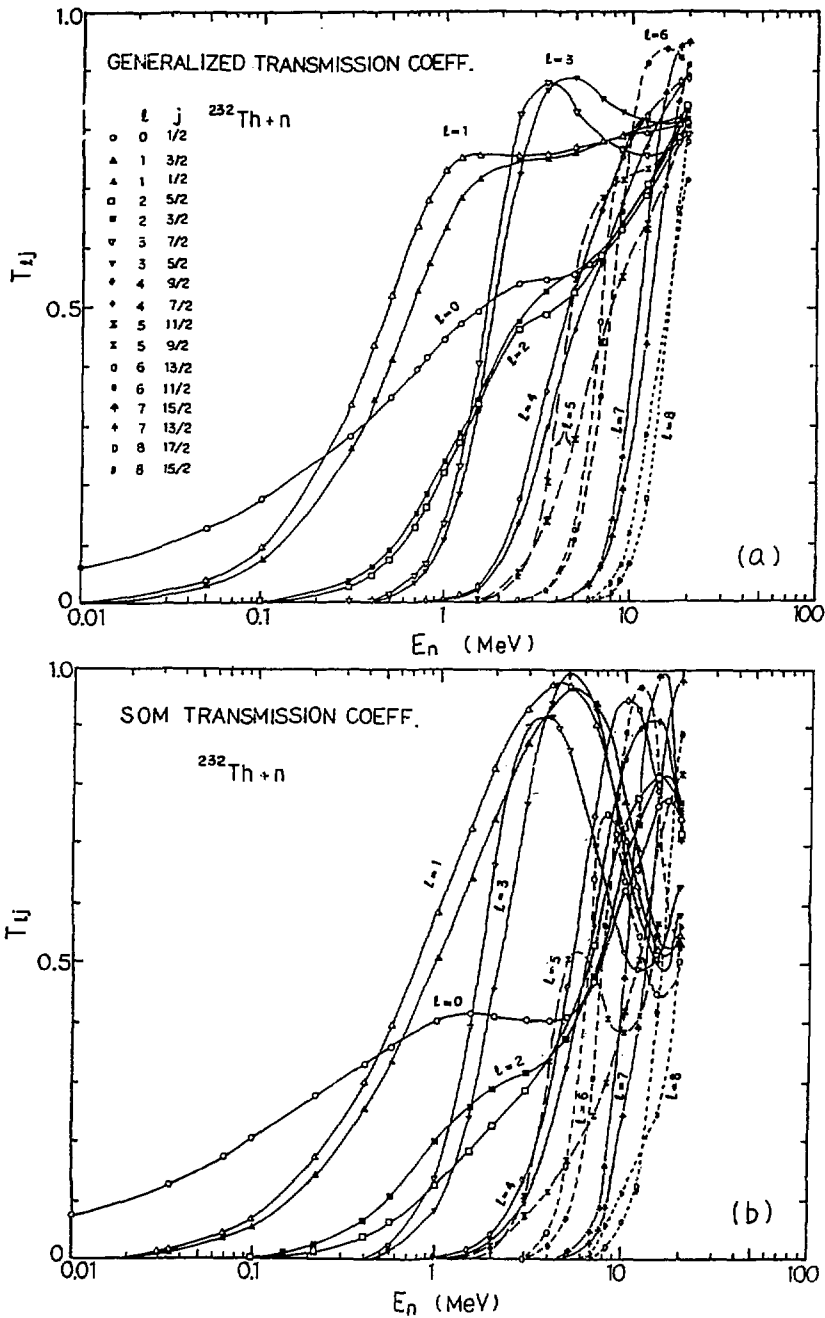   excited states of Th-232.

Fig.4   Comparison of generalized transmission coefficients (top) and
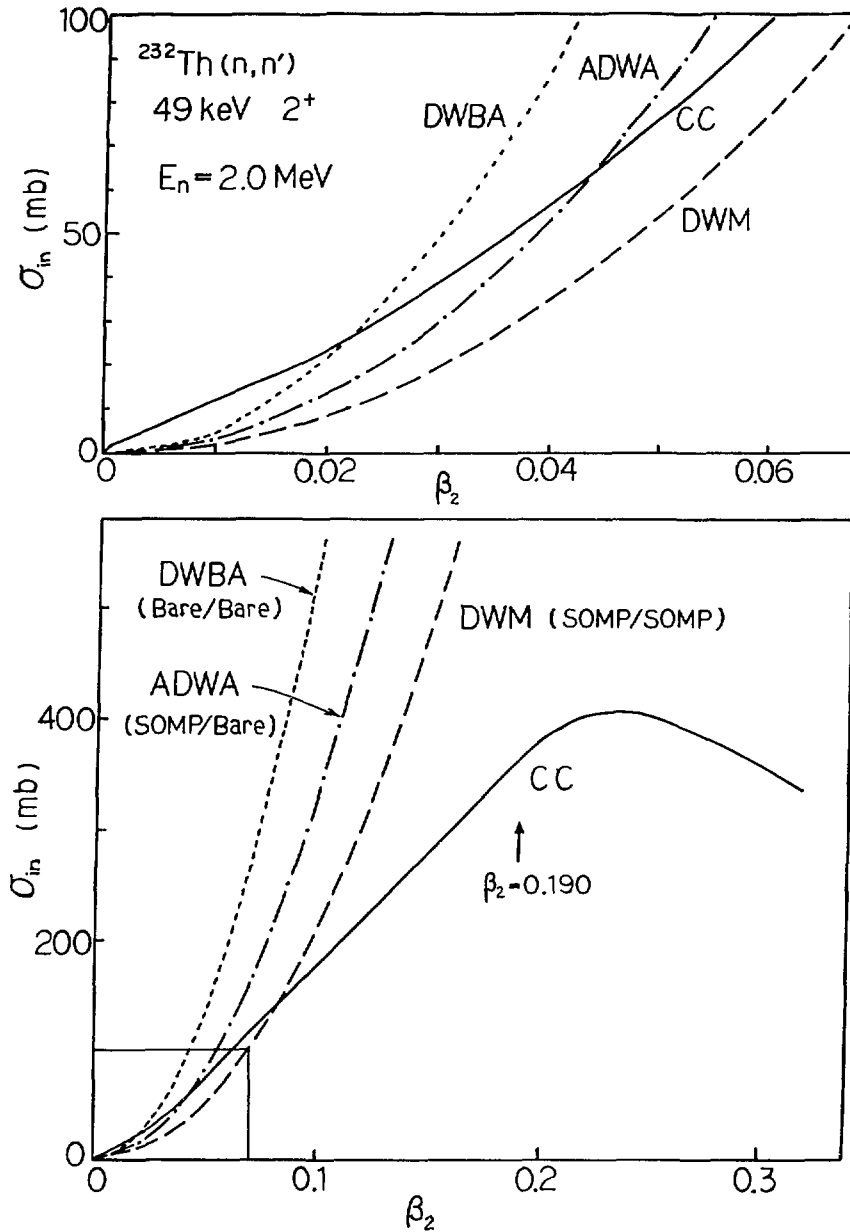SOM transmission coefficients (bottom) for Th-232.

Fig.5   Comparison of strict DWBA, ADWA, DWM and CC calculations for
        neutron inelastic scattering cross section as a function of β_2.
        In the parenthesis are shown the potentials used for the
        (entrance/exit) channels. The top figure is an enlargement
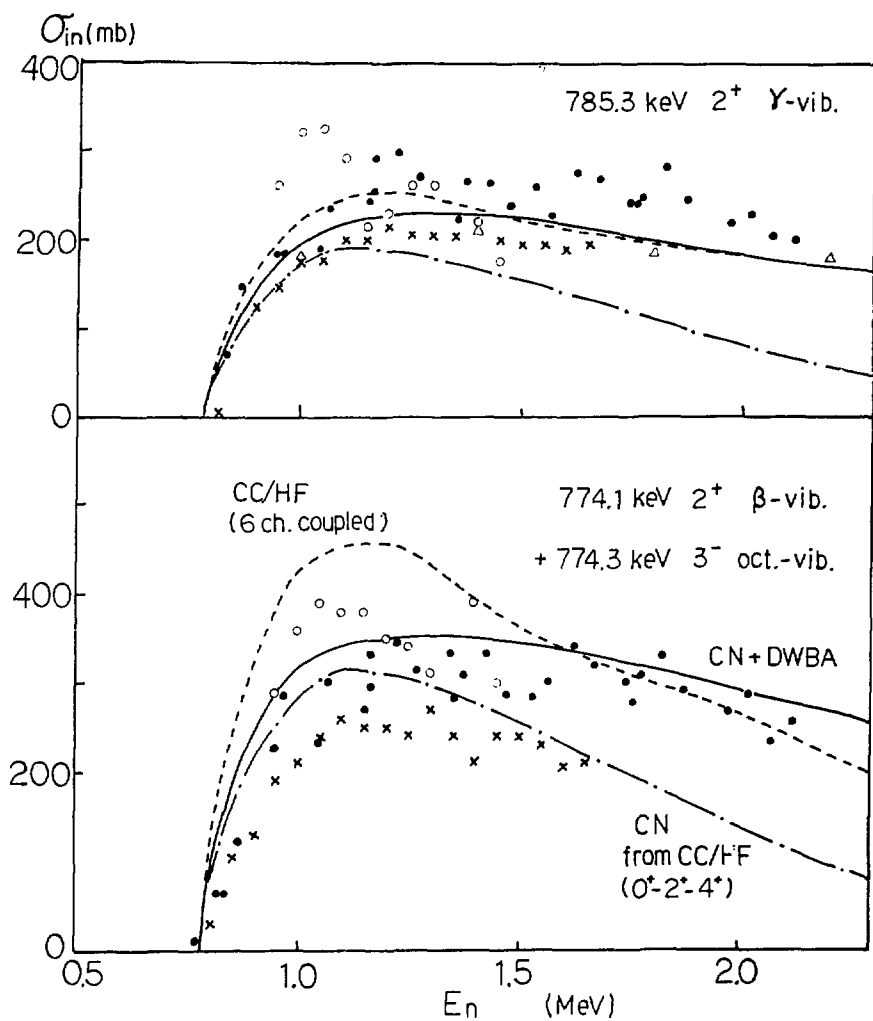   of the curves for small β_2 .

Fig.6 Neutron inelastic scattering cross sections for vibrational
       states of Th-232.

P.11 The Multistep Statistical-Model Code TNG

K. Shibata

Japan Atomic Energy Research Institute

Tokai-mura, Naka-gun, Ibaraki-ken

Abstract

Features of the TNG code are presented. Furthermore, recent improvements of the code are also discussed.

1. Introduction

The TNG code[1] is a multistep statistical-model code based on the Hauser-Feshbach theory including width-fluctuation corrections and precompound effects. This code has been used[2] for the evaluations of neutron data at the Oak Ridge National Laboratory (ORNL) since 1972. The author was engaged in evaluation work at ORNL and used TNG. This report describes several features of TNG and its recent improvements.

2. Basic Features

Several features are given as follows:

1) Width-fluctuation correction for discrete and continuum levels

The width-fluctuation correction is important for the cross-section calculation at low energies. The GNASH code[3], which has been widely used in Japan, does not have such a capability.

2) Consistent treatment of level densities in compound and precompound calculations

The particle-hole state density is consistent with the formula used in the compound part of calculations.

3) Angular-momentum conservation

Angular momentum is conserved in both the compound and precompound stages. Thus, spin populations are affected by the precompound effects. Calculations for tertiary reactions such as $(n, n\alpha)$ are quite sensitive to changes in spin populations.

4) Compound and precompound angular distributions

The precompound angular distributions are obtained[4] by using the partial random phase approximation. Figure 1 shows the angular

distributions of neutrons emitted from ^{55}Mn at 14.5 MeV[5]. It is
found that forward peaking becomes more remarkable with increasing
outgoing energies.

5) Gamma-ray production cross sections from each reaction are
available.

6) Results are stored in the ENDF format.

3. Recent Improvements[6]

The original TNG employed a constant binning method for
outgoing-particle energies. A bin width of 0.5 MeV was usually used for
incident energies between 10 and 20 MeV. The width was however too
large to calculate the neutron emission spectra accurately at low
outgoing energies, particularly near the (n,2n) and (n,3n) reaction
thresholds. Therefore, it was decided to adopt variable bins, i.e.,
smaller bins at low outgoing energies and larger ones at high outgoing
energies instead of constant bins. As an example, the neutron cross
sections of ^{56}Fe were calculated, and it was found that the neutron and
proton emission spectra at low outgoing energies are much better defined
with the variable binning than with the constant binning.

As for the (n,γ) reaction, we have been able to calculate two
additional quantities: the γ-ray production spectrum and the precompound
cross section. For calculation of the γ-ray spectra, special care was
taken to estimate the branching ratios for primary transitions from the
captured state to the discrete levels of compound nucleus. Generally
speaking, some s-wave branching ratios have been determined by
measurements but are incomplete, and hence their theoretical prediction
is required. With the new code, if the sum of the ratios determined
experimentally is less than unity, the giant-dipole model calculation is
applied in order to obtain the missing ones.

The precompound mode of the (n,γ) reaction was indispensable not
only to reproduce the experimental data in the MeV region but also to
keep consistency with particle emission. The precompound component of
the (n,γ) reaction is represented by

$$d\sigma_{n,\gamma}/d\varepsilon = \sigma_{CN}p\Sigma_h W_\gamma(p,h,\varepsilon)\int_0^T P(p,h,t)dt, \qquad (1)$$

where σ_{CN} is the compound-nucleus formation cross section and $W_\gamma(p,h,\varepsilon)$
the γ-ray emission rate with an energy ε from a nucleus in the

p-particle and h-hole state. The quantity P(p,h,t) is the occupation probability of a state with p-particles and h-holes at time t, and T is the equilibration time when all states in the composite system are equally populated. The γ-ray emission rate was derived by Akkermans and Gruppelaar[7]:

$$
W_\gamma(p,h,\varepsilon) = \frac{\varepsilon^2}{\pi^2 \hbar^3 c^2} \sigma_{inv}(\varepsilon) \frac{1}{\omega(p,h,E)} \left[\frac{\omega(1,1,\varepsilon)\omega(p-1,h-1,E-\varepsilon)}{g(p+h-2) + \omega(1,1,\varepsilon)} \right.
$$
$$
\left. + \frac{g(p+h)\omega(p,h,E-\varepsilon)}{g(p+h) + \omega(1,1,\varepsilon)} \right] \tag{2}
$$

The symbols used in eq.(2) are defined as follows:

E = the excitation energy in the compound nucleus

$\hbar$ = Planck constant

c = light velocity

$\sigma_{inv}(\varepsilon)$ = the inverse reaction cross section at an energy ε

g = the single-particle state density

$\omega(p,h,\varepsilon)$ = the state density with p-particles and h-holes at ε

The master equations solved previously in TNG were modified to start with the 1p - 0h state, because the direct capture corresponds to the 1p - 0h configuration. There is one scaling factor for the precompound (n,γ) reaction, and a good fit to experimental data can be obtained by adjusting it. The calculated (n,γ) cross sections of ^{93}Nb were found to reproduce the experimental data satisfactorily, as shown in Fig. 2.

In the case of fissionable nuclei, theoretical estimates of the fission cross sections are essential for evaluating the neutron cross sections, but the original TNG did not have such a capability. We have adopted two models to calculate the fission cross sections with TNG: the single-humped barrier and the double humped barrier models. In the single-humped barrier model, the transmission coefficient is given by[8]

$$
T_f^{J\pi} = \sum_\mu [1+\exp\{-(2\pi/\hbar\omega)(E-E_f-E_\mu^{J\pi})\}]^{-1}
$$
$$
+ \int_0^\infty d\varepsilon \rho(\varepsilon,J\pi)[1+\exp\{-(2\pi/\hbar\omega)(E-E_f-\varepsilon)\}]^{-1} \tag{3}
$$

where E is the excitation energy, E_f the fission barrier energy and $E_\mu^{J\pi}$ the discrete level energy with spin and parity of Jπ. The quantity $\rho(\varepsilon,J\pi)$ stands for the level density at ε, and $\hbar\omega$ represents the curvature of the barrier. On the other hand, in the double-humped barrier model, the transmission coefficient is given by

$$
T_f^{J\pi} = T_A^{J\pi} T_B^{J\pi} / (T_A^{J\pi} + T_B^{J\pi}), \tag{4}
$$

where A and B mean the inner and outer barriers, respectively. The quantity $T_A^{J\pi}$ (or $T_B^{J\pi}$) is calculated by using eq.(3). Concerning the level density for fission transition states, the Gilbert-Cameron's composite formula, employed for all other reaction channels, can still be used. In general, it is very difficult to determine the parameters for the density of the transition states since their direct measurement is impossible. Thus, we adopted Bjørmholm and Lynn's recommended values[9] as defaults in TNG. The calculated fission cross section of ^{242}Pu is illustrated in Fig. 3.

4. Concluding Remarks

Several basic features of the TNG code are described. The code is found to be very useful for evaluations of neutron cross sections. TNG is now available at JAERI.

References

1) Fu, C.Y.: "A Consistent Nuclear Model for Compound and Precompound Reactions with Conservation of Angular Momentum", ORNL/TM-7042 (1980).

2) For example: Hetrick, D.M., Fu, C.Y. and Larson, D.C.: "Calculated Neutron-Induced Cross Sections for ^{63,65}Cu from 1 to 20 MeV and Comparisons with Experiments", ORNL/TM-9083 (1984).

3) Young, P.G. and Arthur, E.D.: "GNASH: A Preequilibrium, Statistical Nuclear-Model Code for Calculation of Cross Sections and Emission Spectra", LA-6947 (1977).

4) Fu, C.Y.: "Development and Applications of Multi-Step Hauser-Feshbach/Pre-Equilibrium Model Theory", Proc. Symposium on Neutron Cross-Sections from 10 to 50 MeV, BNL-NCS-51245 (1980).

5) Shibata, K.: to be published.

6) Shibata, K. and Fu, C.Y.: "Recent Improvements of the TNG Statistical Model Code", ORNL/TM-10093 (1986).

7) Akkermans, J.M. and Gruppelaar, H.: Phys. Lett., 157B, 95 (1985).

8) Hill, D.L. and Wheeler, J.A.: Phys. Rev., 89, 1102 (1953).

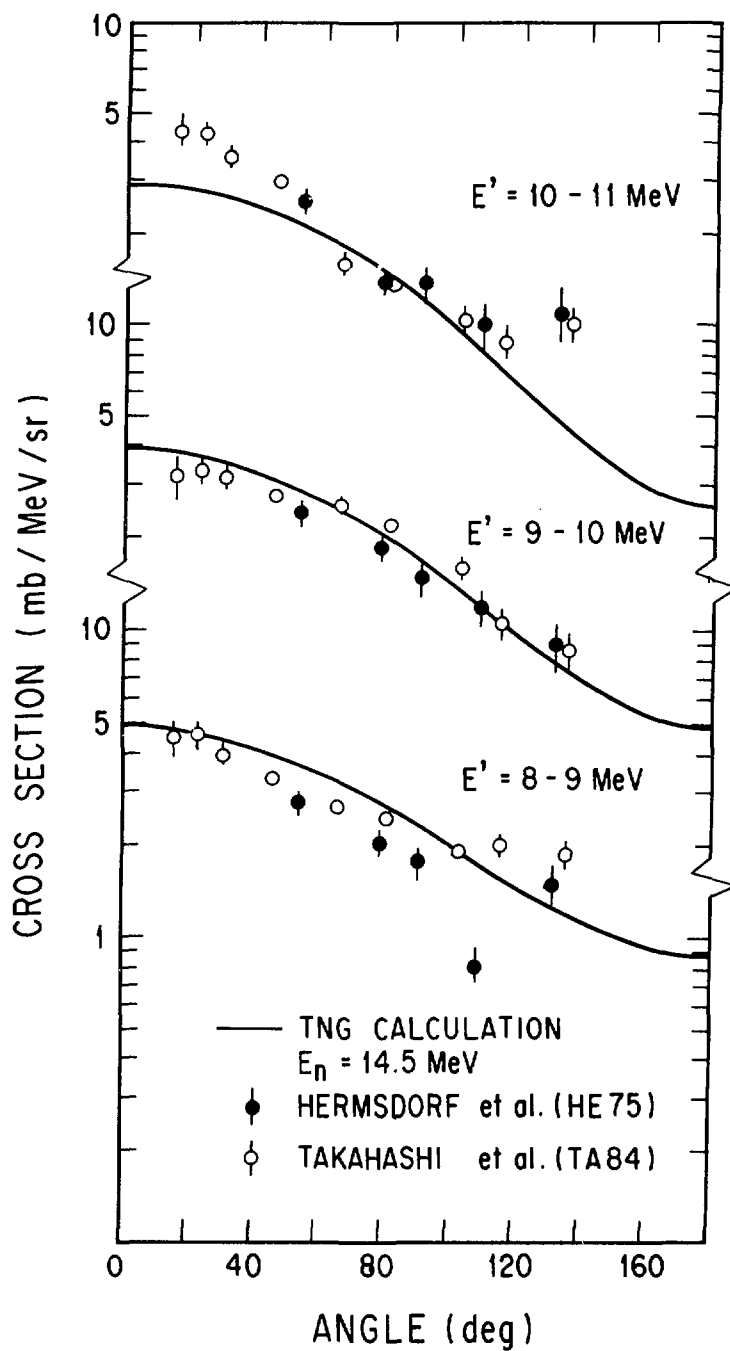9) Bjørnholm, S. and Lynn, J.E.: Rev. Mod. Phys., 52, 725 (1980).

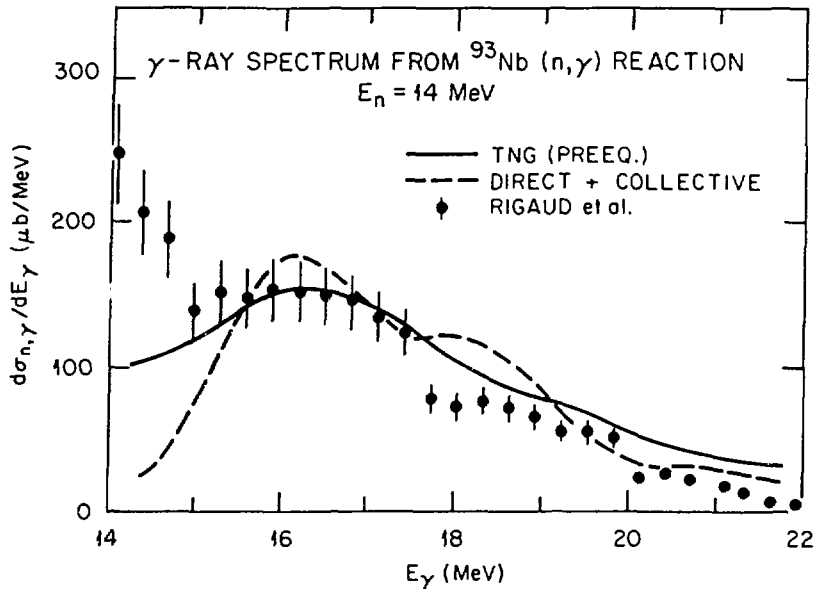Fig. 1 Angular distributions for the ^{55}Mn(n,n'x) reaction. The symbol E' stands for the outgoing energy.

ORNL-DWG 86-11640

Fig. 2 Gamma-ray spectra emitted from the ^{93}Nb(n,γ) reaction at 14.5 MeV[6]. The solid line represents the TNG calculation. The dashed line is the calculation based on the direct and collective capture models.
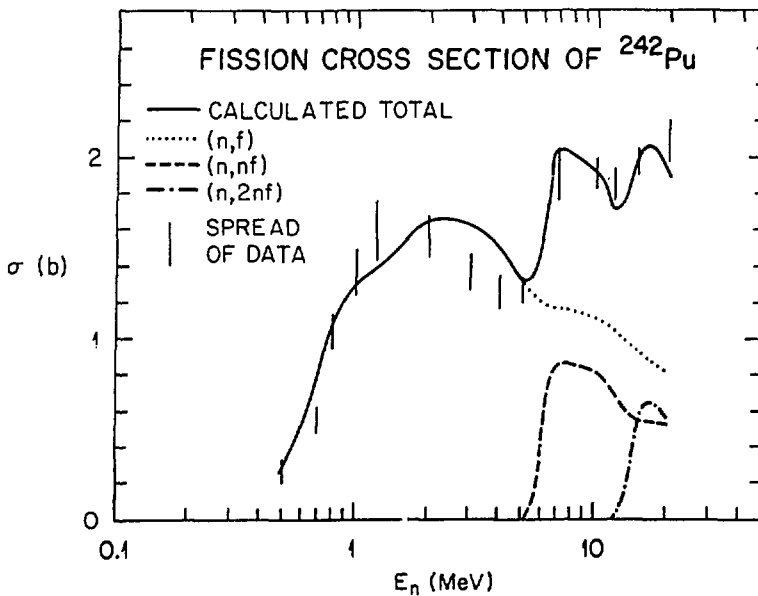
ORNL-DWG 86-11638

Fig. 3 Calculated fission cross section of ^{242}Pu[6]. The vertical bars represent the spread of the available experimental data.

P.12 Program PEGASUS, A Precompound and Multi-step Evaporation
Theory Code for Neutron Threshold Cross Section Calculation

Shungo IIJIMA[*], Teruo SUGI[**], Tsuneo NAKAGAWA[**] and Takeo NISHIGORI[$]

*) Nippon Atomic Industry Group Co.,Ltd.
**) Japan Atomic Energy Research Institute
$) Osaka University

PEGASUS, a preequilibrium and evaporation theory code, was developed
which calculates 17 neutron reaction cross sections, the particle spectra
and the double differential cross sections. The code is suited to a
rapid and scoping calculation. Theoretical model and the some results of
calculation are presented.

PEGASUS calculates neutron cross sections based on the closed form
exciton model for the preequilibrium process and the multistep
evaporation theory. The spin-parity conservation is completely ignored.
The input data to the code were made minimum making use of the parameter
data files. The data files contain the mass data of Wapstra and Bos[1],
the level density parameters of Gilbert-Cameron type, and the inverse
reaction cross sections for proton, alpha, deuteron , triton and He-3
calculated with the optical model. The neutron reaction cross section
was given by the Pearlstein's systematics formula[2]. When the mass data
is not found in Wapstra-Bos' table, the mass formula of Yamada et al.[3]
is used in the code. The built-in level density parameters are those
evaluated by the FPND and Gas Production Cross Section Evaluation working
groups of JNDC. When the level density parameters are not availble in
the data file, simple systematics formulae are used in the code. The
built-in level density parameters are easily modifiable by input data.
Main features of the code is listed in Table 1.

Table 2 illustrates the input procedure for the PC version of
PEGASUS. Fig.1 shows the inverse cross sections used to calculate iron
neutron cross sections. The ENDF/B format output cross sections are shown
in Fig. 2 for Fe-56.

Figures 3 through 5 show the comparison of the calculated and measured particle spectra from iron induced by 14 - 15 MeV neutrons. The level density parameters have been adjusted to some extent to fit the experimental data. The neutron emission spectra from iron are shown in Fig. 3 in comparison with experimental data of Vonach et al.[4] and Hermsdorf et al.[5] for incident neutron energy of 14.5 MeV. The neutron spectra from (n,n'a) and (n,an') are not depicted for the sake of the clarity of the figure.

Figure 4 gives the double differenti al neutron emission spectra for iron compared with the OKTAVIAN experimental data.[6] A nice qualitative agreement is obtained. It is noted that the neutron spectra at large angles are almost purely of the statistical nature, its intensity being reduced by the preequilibrium emission. The proton and alpha particle emission spectra initiated by 14.8 MeV neutrons are compared with the data of Grimes et al.[7] in Fig. 5.

From our experience, PEGASUS is not only a powerful tool for scoping calculations prior to a more sophisticated calculation with e.g. GNASH code.[8], but also it may be used for a quantitative prediction of cross sections at not a too low excitation energies. Further effective usages may be the application to minor nuclides such as the fission-products, and the medium energy (20 - 100 MeV) cross sections whose calculation with the sophisticated code is very time-cosuming. The code may be utilized also to make the double differential cross section file.

References :

(1) Wapstra, A.H., Boss, K. : Atomic Data and Nucl. Data Tables 19,
    No.3 (1977)

(2) Pearlstein, S. : J. Nucl. Energy 27 88 (1973)

(3) Ando, Y., Uno, M., Yamada, M. :JAERI-M 83-025 (1983)

(4) Vonach, H. et al.: BNL-NCS-51245 p.343 (1980)

(5) Hermsdorf, D. et al. : Zfk-277(U), 1977

(6) Takahashi, A. et al. :Proc. Int. Conf. Nuclear Data for Science
    and Technology, Sept.,1982, Antwerp, pp.360-367

(7) Grimes,S. M. et al. :Phys. Rev. C19 2127 (1979)

(8) Young, P. G., Arthur, E. D. :LA-6947 (1977)

(9) Iwamoto, A., Harada, K. : Phys. Rev. C26 1821 (1982)
    Sato, K., Iwamoto, A., Harada, K. :Phys. Rev. C28 1527 (1983)

(10)Mantzouranis, G., Agassi, D., Weidenmuller, H. A. :Phys. Lett. 57B
    220 (1975). Also, Akkermans, J. M. :Phys. Lett. 82B 20 (1979)

Table 1 Main Features of PEGASUS

(1) Preequilibrium (closed form excition model) plus multistep
    evaporation theory, ignoring spin–parity conservations.
    Competition with gamma–ray emission is taken into account at the
    second stage of reactions.

(2) 17 reactions are treated :
    $(n,n'),(n,p),(n,a),(n,d),(n,t),(n,He3),(n,2n),(n,n'p),(n,pn'),(n,n'a),$
    $(n,an'),(n,n'd),(n,dn'),(n,n't),(n,tn'),(n,2p),(n,3n).$

(3) The emission of cluster particles from preequilibrium stage is
    calculated with the theory of Iwamoto and Harada.[9]

(4) The angular distributions of nucleons emitted from the preequilibrium
    stage are calculated with the theory of Mantzouranis et al.[10] with
    :an infinite refraction index at the incident nuclear surface.

(5) The results are output in ENDF/B format. The threshold energiers are
    automatically inserted in the code.

(6) Fine mesh calculation ($\Delta \xi \geq 0.1$ MeV) is possible.

(7) Computational time for $E_n = 1,2, - - ,20$ MeV (every 1 MeV) is typi-
    cally 2-3 sec with large computer and 20 min. with microcomputer.

(8) Main restrictions to the code are :
    (a) Incident particle is restricted to only neutrons at present.
    (b) Competition with fission is not taken into account.
    (c) Discrete levels are not taken into account.
    (d) Neutron capture cross sections are not calculated.
    (e) Gamma–ray emission spectra are not calculated.

Table 2. Example of Input to PEGASUS PC Version.

Input from keyboard are those underlined or framed.

** PEGASUS FOR NEUTRON THRESHOLD CROSS SECTION CALCULATION

USING MULTI-STEP EVAPORATION AND PRE-EQUILIBRIUM THEORY

REVISED ON AUGUST 10 , 1986

```
TARGET NUCLIDE AND Z, A         FE-56, 26, 56
HEADING PRINT OPTION            0/ELSE (CRT/PRINTER)  | 1
LEVEL DENSITY PRINT OPTION  0/ELSE (0=NO PRINT)       | 1
INVERSE CROSS SECTION FILE NAME                       | INVFE
KALBACH K VALUE       KME (MEV^3)                     | 60
ADJUSTMENT PARAMETER FOR CLUSTER EMISSION             | 0.1
NEUTRON ENERGY INDEX - KEMIN, KEMAX AND STEP DKE      | 1, 20, 1
SPECTRUM/ANGULAR DISTIRBUTION CALCULATION   Y/ELSE    | Y
ENERGY KE FOR SPECTRUM  CLACULATION                   | 15
ENERGY KE FOR ANAGULAR DISTRIBUTION CALCULATION       | 15
ENERGY STEP FOR SPECTRUM PRINT (1 OR 2 )              | 1
```

```
K   NUCL.   REACTION    A(/MEV)      T(MEV)      C(/MEV)      EX(MEV)
-------------------------------------------------------------------------
 0  FE-57   COMPOUND    +8.910E+00   +1.100E+00   +2.230E+00   +8.638E+00

 1  FE-56   (N,N')      +7.250E+00   +1.296E+00   +6.507E-01   +1.062E+01

 2  MN-56   (N,P)       +7.950E+00   +1.171E+00   +5.902E+00   +6.944E+00

 3  CR-53   (N,ALP)     +7.790E+00   +1.100E+00   +1.092E+00   +6.993E+00

 4  MN-55   (N,D)       +7.400E+00   +1.308E+00   +2.657E+00   +9.541E+00

 5  MN-54   (N,T)       +7.300E+00   +1.210E+00   +4.072E+00   +6.555E+00

 6  CR-54   (N,TAU)     +7.390E+00   +1.260E+00   +6.951E-01   +1.009E+01

 7  FE-55   (N,2N)      +7.400E+00   +1.254E+00   +1.588E+00   +8.936E+00

 8  MN-55   (N,PN')     +7.400E+00   +1.308E+00   +2.657E+00   +9.541E+00

 9  CR-52   (N,AN')     +7.200E+00   +1.225E+00   +4.638E-01   +9.269E+00
```

** MODIFY LDP DATA ? Y/ELSE   Y

NUCLIDE NUMBER (0/1/2/..../9) , A AND T VALUES = 3, 7.186, 1.220

3 CR-53   (N,ALP)   +7.186E+00   +1.220E+00   +1.281E+00   +7.872E+00
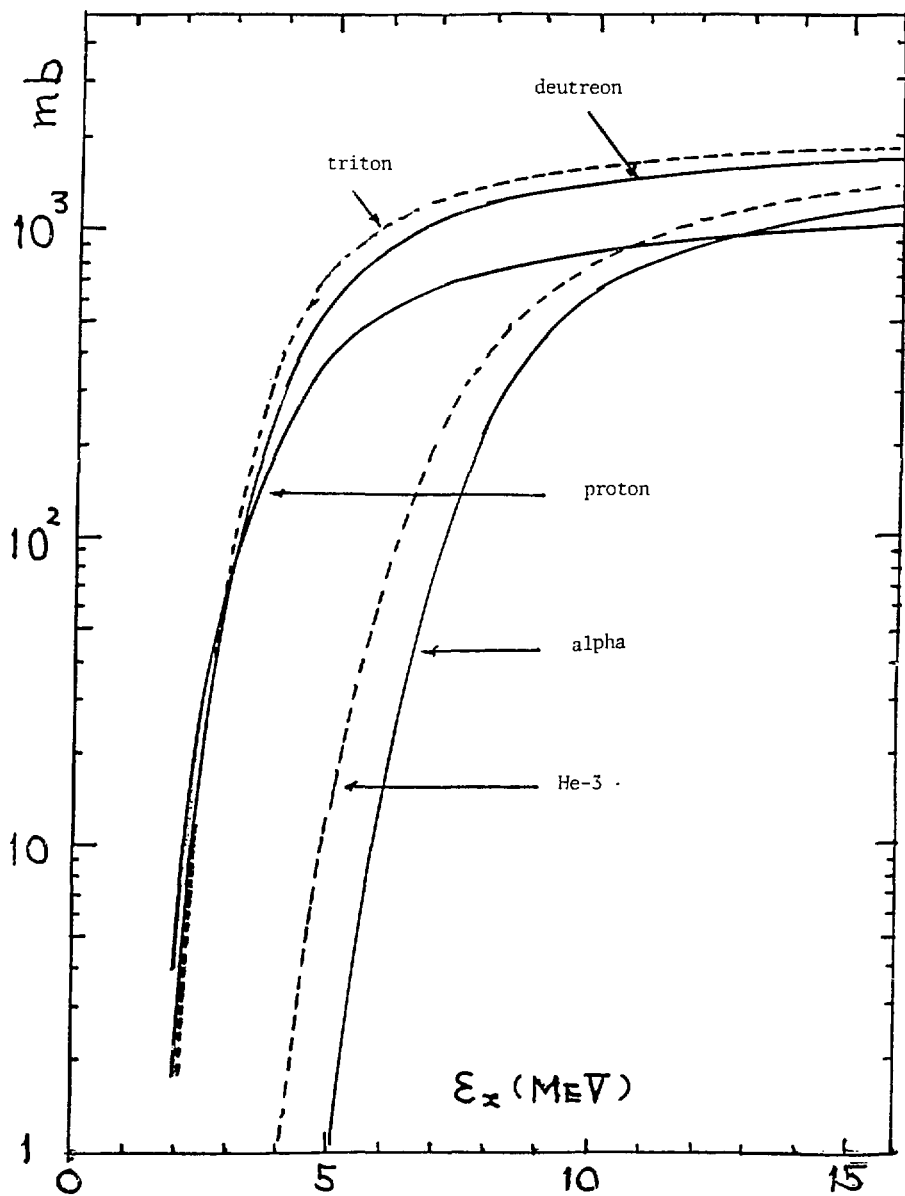
** MODIFY LDP DATA ? Y/ELSE   [CR]

Fig. 1 Inverse cross sections used for iron cross section calculation.
Inverse cross section for neutrons was assumed as given by Pearl-
stein. Optical model parameters were adopted from Perey for
protons, Huizenga and Igo for alpha particles, Lohr and
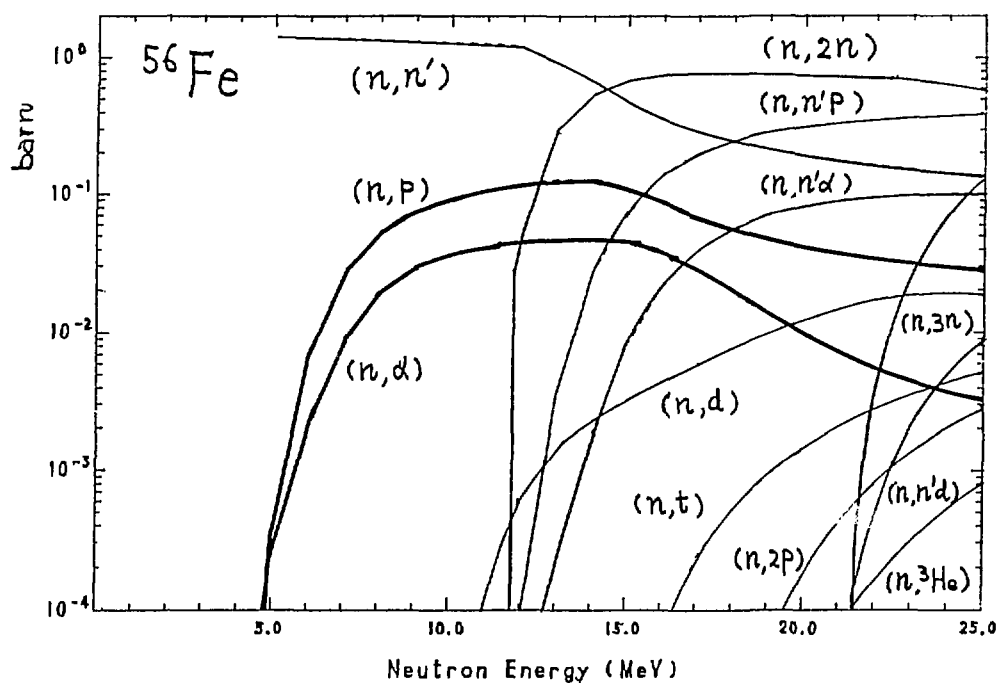Haeberli for deuterons, and Bechetti and Greenles for tritons
and He-3.

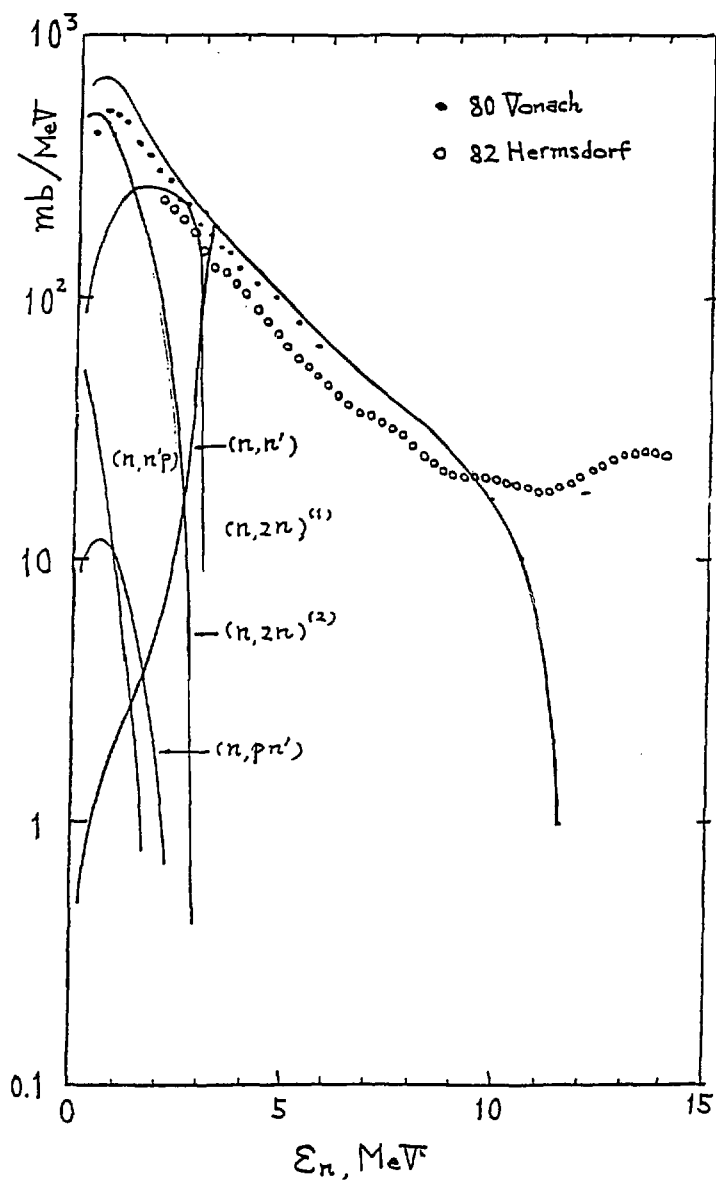Fig. 2   Calculated cross sections for Fe-56.

Fig. 3 Neutron emission spectra from iron with 14.5 MeV neutrons.
Comparison of calculation with experimental data. The curve
indicated as (n,2n)[1] is the spectra of the first neutrons.
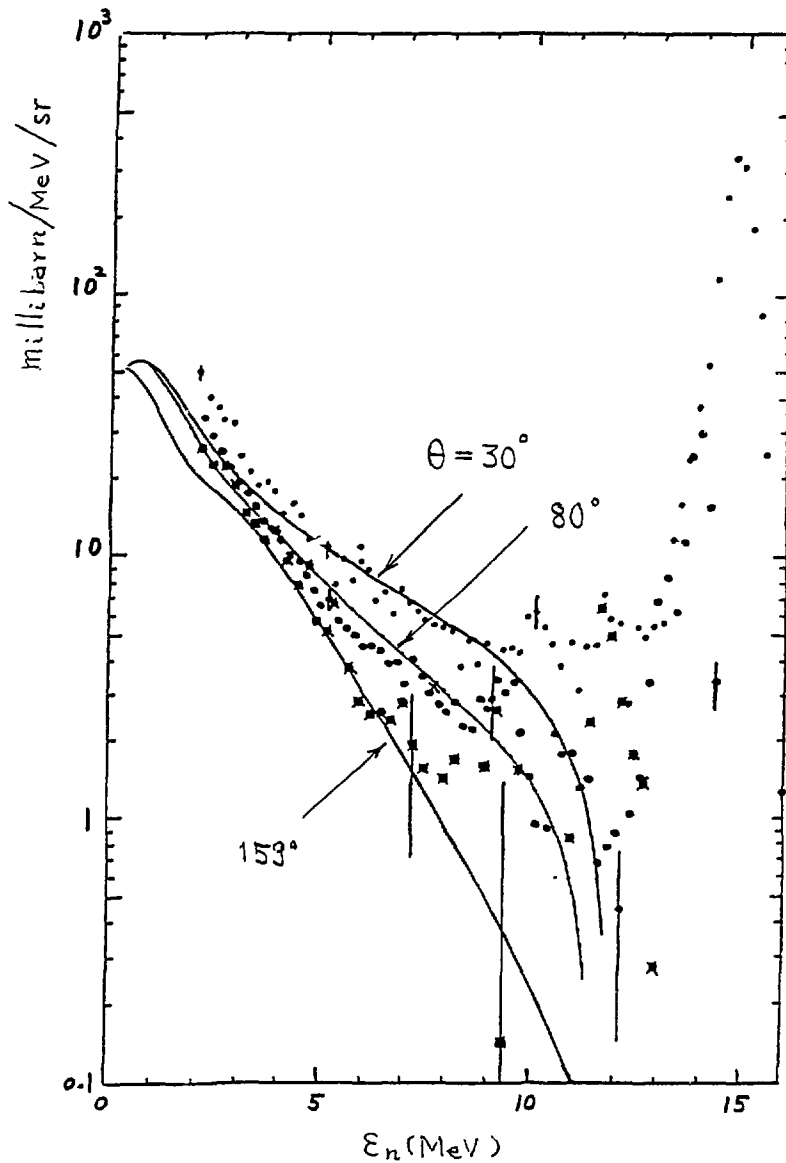The same are meant for (n,2n)[2] and (n,2n)[3].

Fig. 4 Double differential neutron spectra from iron.
Comparison of calculation with OKTAVIAN experimental data at 30,
80 and 159 degrees (the corresponding incident neutron energiers
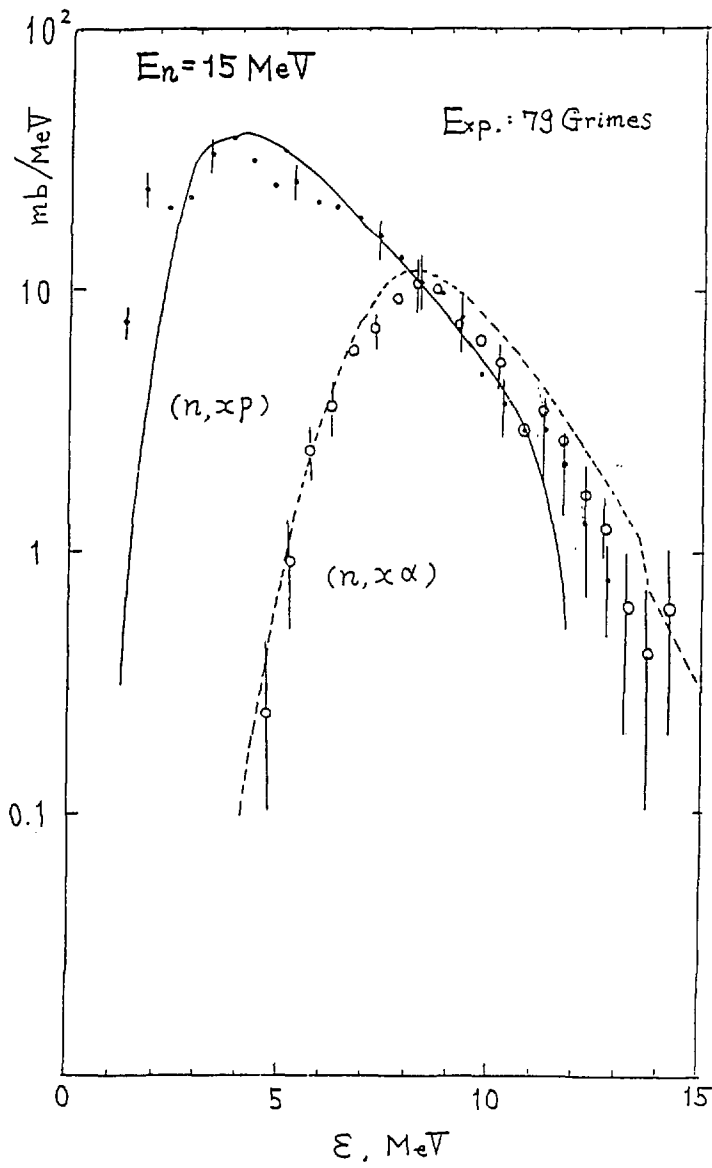being 14.8, 14.25 and 13.35 MeV).

Fig. 5 Proton and alpha particle emission spectra from Fe-56 induced by 14.8 MeV neutrons. Comparison of the calculation and the experimental data of Grimes et al.

P.13 Neutron Cross Sections Calculated by GNASH

N. Yamamuro and K. Hida

NAIG Nuclear Research Laboratory

Nippon Atomic Industry Group Company, Ltd.

Ukishima-cho, Kawasaki-ku, Kawasaki

Computer codes GNASH and CASTHY have been used for the neutron cross section calculations. The revised items for GNASH and the method of evaluation are presented. Calculated good results were obtained for copper neutron cross sections. A method of fission cross section calculation is also given.

1. GNASH – a revised version

GNASH is a preequilibrium, statistical nuclear-model code for calculation of cross sections and emission spectra developed by Young and Arthur, Los Alamos scientific laboratory.[1] We have used this code for the cross section evaluations since 1984, extending the functions of calculation and improving the method and output format. The main revised items are as follows.

(1) Options of level density formulas

In addition to the defaulted Gilbert and Cameron composite formula, the selections of spin cut-off factor are available and the partial level density formula, required from the cumulation of spin-selected levels to determine the nuclear temperature,[2] can be used (conducted by M. Kawai, NAIG)

(2) Cross section for alpha-particle pick-up process

In the preequilibrium cross section calculation, the state density is given by $g = (6/\pi^2)a$. Since the level density parameter "a" was calculated using the observed mean resonance level spacing D_0, when available, the value of "g" was usually larger than $A/13$, which is the default value of GNASH. The cross section for alpha-particle pick-up process is the dominant term of the preequilibrium calculation and depends mainly on the value of "g" of the residual nucleus for alpha-particle emission. A factor, by which the alpha-particle pick-up cross section is multiplied, is

introduced to reproduce the experimental alpha-emission spectra. The factor 0.5 was used for Co, Ni, and Cu neutron cross section calculations.

(3) Input of direct inelastic scattering cross section

The overlapping of the contribution from the direct inelastic scattering with the cross sections in the level continuum region became available in the calculation of neutron emission spectra.

(4) Output format of gamma-ray strength functions

The output format of gamma-ray strength functions was rearranged and became simpler and clearer.

(5) Expansion of particle decay channels

To treat the decay by deuteron, triton, or ^{3}He emission in addition to the gamma-ray, neutron, proton, or alpha-particle emission, the dimensions of data and variables corresponded were increased and the pointers in the subroutine LCSPCE were changed.

(6) Calculation of multi-step neutron emission spectra

The multi-step neutron emission spectra, first emissions from (n,2n), (n,n'p), and (n,n'alpha) reactions, first and second ones from (n,3n) reaction, are necessary to compile the files in the ENDF/B format. Because we have no process code from the file 12 of GNASH to the ENDF/B format, we derived directly the multi-step neutron emission spectra from the distributions of the population probabilities of excited states and transformed them into the ENDF/B format.

(7) Calculation of fission cross section

The fission cross section can be calculated when the transmission coefficient T_f for fission process is known. Section 4 will describe a method for calculating T_f and the comparison of the calculated ^{235}U cross sections with JENDL-2 evaluation.

2. Method of neutron cross section evaluation

Since the code GNASH does not carry out the resonance level-width fluctuation correction, the inelastic scattering and radiative capture cross sections in the lower neutron energy region should be calculated by the code CASTHY,[3] which can control the level-width fluctuation correction. Total and elastic scattering cross sections can be also calculated by CASTHY, where the threshold reaction cross sections obtained by the GNASH calculation are inputted as the competitive reactions for the

inelastic scattering. Cross sections for the inelastic scattering through the direct reaction process are calculated by the code DWUCK,[4] and the results are added to the equilibrium and preequilibrium inelastic scattering cross sections given by GNASH and CASTHY.

The particle transmission coefficients are calculated by the code ELIESE[5] and are used in the GNASH calculations. The flow chart of the neutron cross section evaluation is shown in Fig. 1.

3. Example of neutron cross section calculation

As an example, copper neutron cross sections evaluated by the method mentioned in Sec. 2 are briefly presented. Precisely measured particle emission spectra are useful for the determination of level density and preequilibrium process parameters. By the neutron emission spectra at 14 MeV,[6],[7] the level density parameters for ^{63}Cu and ^{65}Cu, Kalbach constant (K = 60), and the direct inelastic scattering cross sections were investigated, resulting in the good agreement between the calculated and the experimental spectra, as shown in Fig. 2. Also the charged particle emission spectra,[8] Figs. 3, 4 and 5, show the good agreement between the calculation and the experiments.

The excitation functions for level inelastic scattering (Ex = 0.669 MeV of ^{63}Cu), total inelastic scattering, (n,alpha) for ^{63}Cu, (n,p) for ^{65}Cu, (n,2n) for ^{63}Cu and ^{65}Cu, total gamma-ray production (Eg > 0.75 MeV), and radiative capture for ^{65}Cu are shown in Figs. 6 through 13, respectively. Except for ^{63}Cu(n,alpha) cross section, the agreements are very good. Considering the good result for alpha-particle total production at 15 MeV, as shown in Fig. 4, there are some problems for alpha-particle emission which should be examined.

The detail of the neutron cross section calculations for copper will appear in another report.

4. Method of fission cross section calculation

At the 1984 Seminar on Nuclear Data,[9] we presented a method to incorporate fission competition into GNASH, where the fission transmission coefficient was calculated with the double humped fission barrier (DHFB) model.[10] The calculated fission cross section of ^{238}U, however, was failed to well reproduce the experimental one. Thus, a revised method is

presented here and applied to the ^{235}U fission cross section calculation.

The fission transmission coefficient $T_f(Ex)$ at an excitation energy Ex of a compound nucleus can be derived from the fission cross section $\sigma_f(En)$ at an incident neutron energy En of the target nucleus as

$$\frac{T_f(Ex)}{T_n(Ex)} = \frac{\sigma_f(En)}{\sigma_R(En) - \sigma_f(En)} ,$$

where $T_n(Ex)$ and $\sigma_R(En)$ are the neutron transmission coefficient and the reaction cross section, respectively, calculated with the optical model. Examples are shown in Fig. 14 for the compound nuclei ^{234}U, ^{235}U, and ^{236}U responsible for the ^{235}U fission cross section calculation. Since the above method is applicable to the excitation energies corresponding to the first chance fission region only, the resultant expressions are smoothly extrapolated into the second and third chance fission regions. Below the neutron separation energy, the DHFB model is used.

By using these fission transmission coefficients, the ^{235}U neutron cross sections are calculated with GNASH and compared with JENDL-2 evaluation in Fig. 15. The neutron transmission coefficients were modified to reproduce the reaction cross section of JENDL-2, since the determination of the optical potential parameters were based not on this cross section but on the total and elastic scattering cross sections only. Agreement is good for the fission cross section, but is very poor for other reaction cross sections. The conclusion is pending for JENDL-3 evaluation of ^{235}U based on new experimental data for the (n,2n) cross section.[11]

Acknowledgment

References

(1) Young, P. G. and Arthur, E. D.: "GNASH: A Preequilibrium, Statistical Nuclear-Model Code for Calculation of Cross Sections and Emission Spectra," LA-6947 (1977).

(2) Yamamuro, N.: "Calculation of Capture Gamma-ray Spectra for Ta-181 and Au-197," Proc. Int. Conf. Nuclear Data for Basic and Applied Science, Santa-Fe, New Mexico, 1985, p.1185 (1986).

(3) Igarasi, S.: J. Nucl. Sci. Technol., 12, 67 (1975).

(4) Kunz, P. D.: "Distorted Wave Code DWUCK4," University of Colorado (1974).

(5) Igarasi, S.: "Program ELIESE-3; Program for Calculation of the Nuclear Cross Sections by Using Local and Non-Local Optical Models and Statistical Model," JAERI 1224 (1972).

(6) Baba, M.: private communication.

(7) Vonach, H, Chalupka, F., Wenninger, F., and Staffel, G.: "Measurement of the Angle-Integrated Secondary Neutron Spectra from Interaction of 14 MeV Neutrons with Medium and Heavy Nuclei," Proc. Symposium Neutron Cross Sections from 10 to 50 MeV, BNL-NCS-51245, p.343 (1980).

(8) Grimes, S. M., Haight, R. C., Alvar, K. R., Barschall, H. H., and Borchers, R. R.: Phys. Rev. C19, 2127 (1979).

(9) Hida, K.: Proc. 1984 Seminar on Nuclear Data, JAERI-M 85-035, 166 (1985).

(10) Bjørnholm, S. and Lynn, J. E.: Rev. Mod. Phys., 52, 725 (1980).

(11) Matsunobu, H.: private communication.
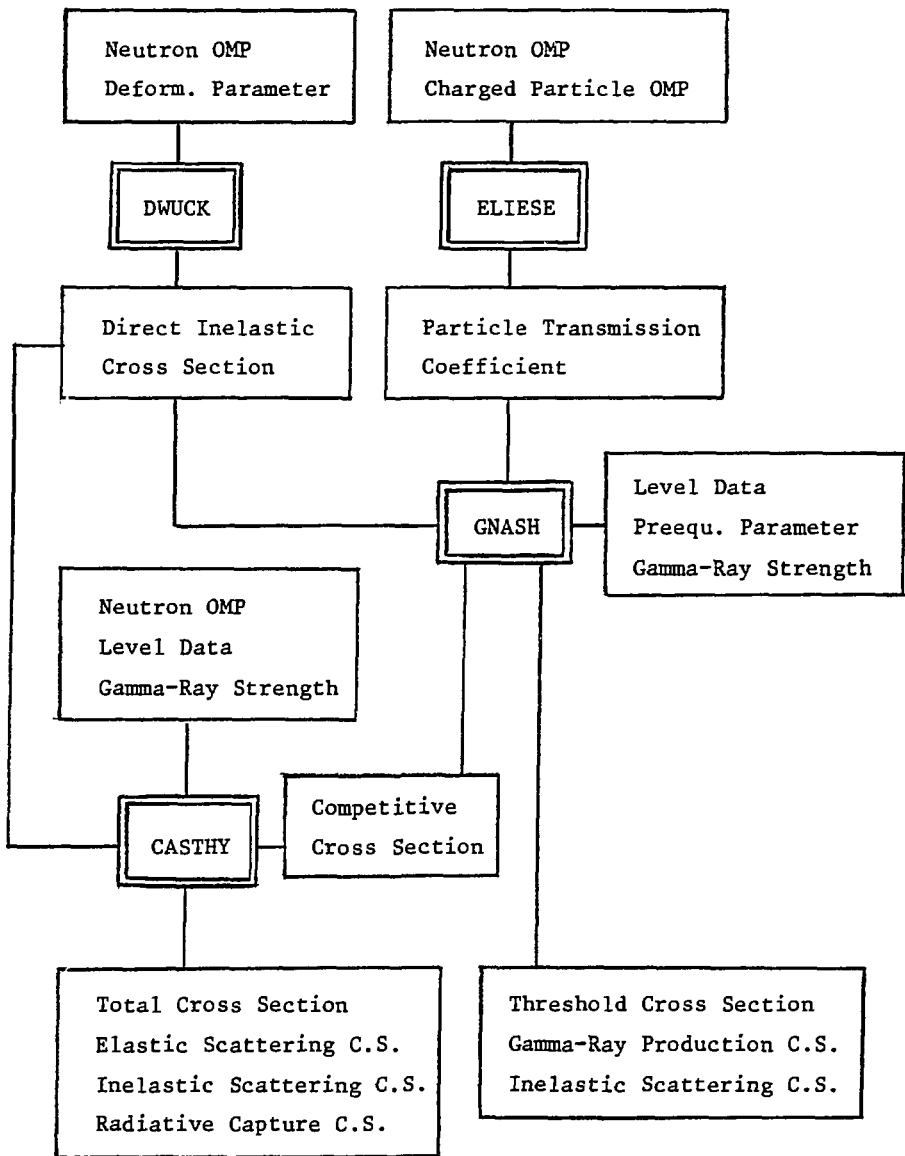
Adoption of Inelastic Scattering Cross Section

$\quad\quad$ E $\leqslant$ Ej $\quad$ CASTHY + DWUCK

$\quad\quad$ E $>$ Ej $\quad\quad$ GNASH $\;$ + DWUCK

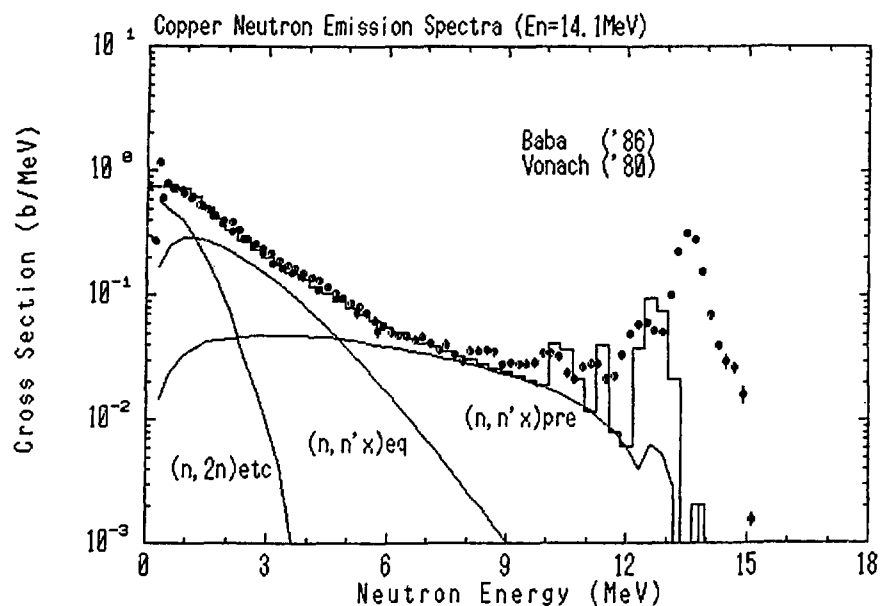Fig. 1 Flow chart of neutron cross section evaluation.

Fig. 2 Neutron emission spectra for copper calculated by GNASH compared with the data of Baba and Vonach et al.
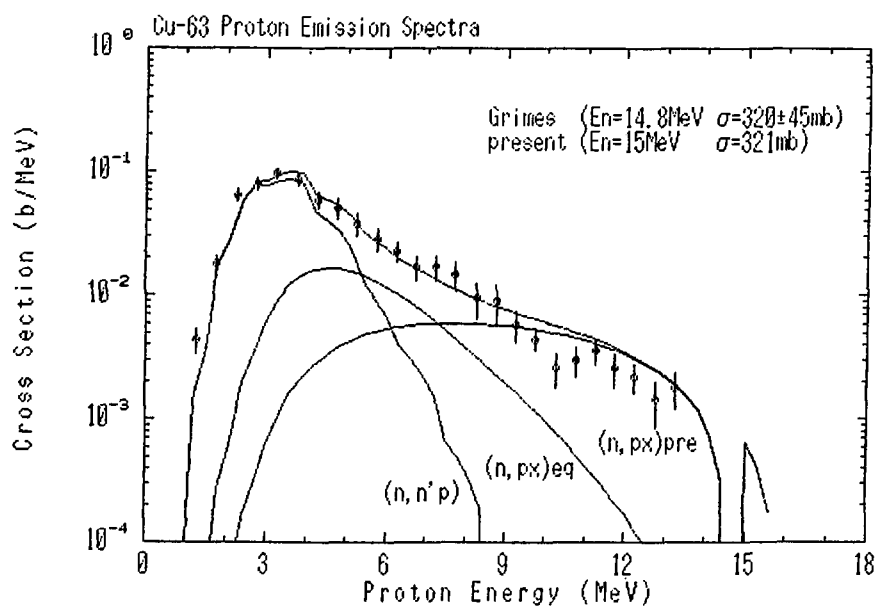

Fig. 3 Comparison of calculated and experimental proton emission spectra for ^{63}Cu.
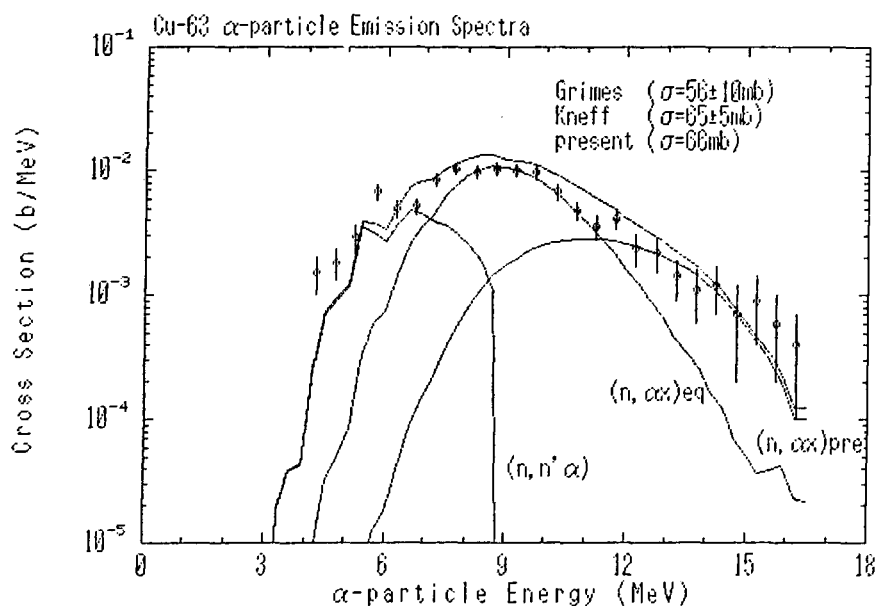
Fig. 4 Comparison of calculated and experimental alpha-particle emission
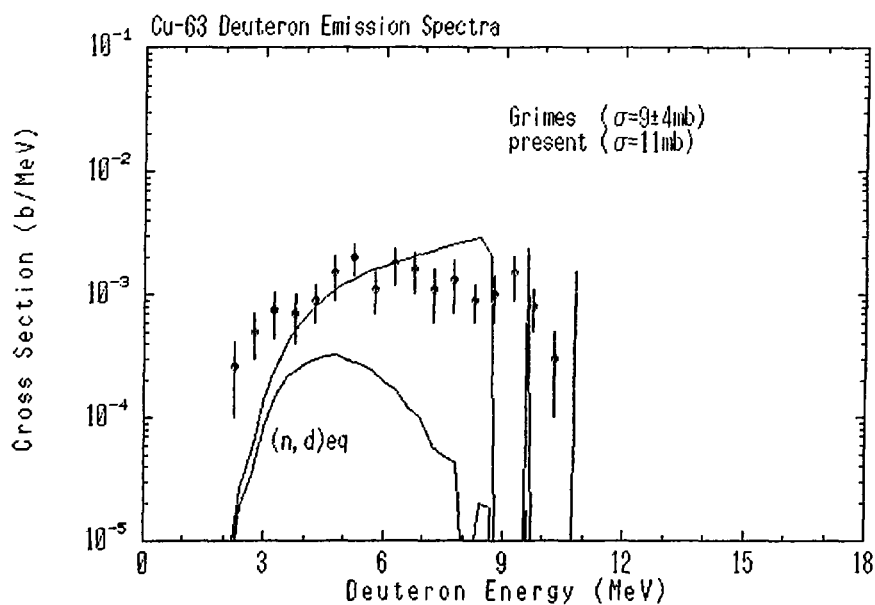spectra for ^{63}Cu.

Fig. 5 Comparison of calculated and experimental deuteron emission spectra
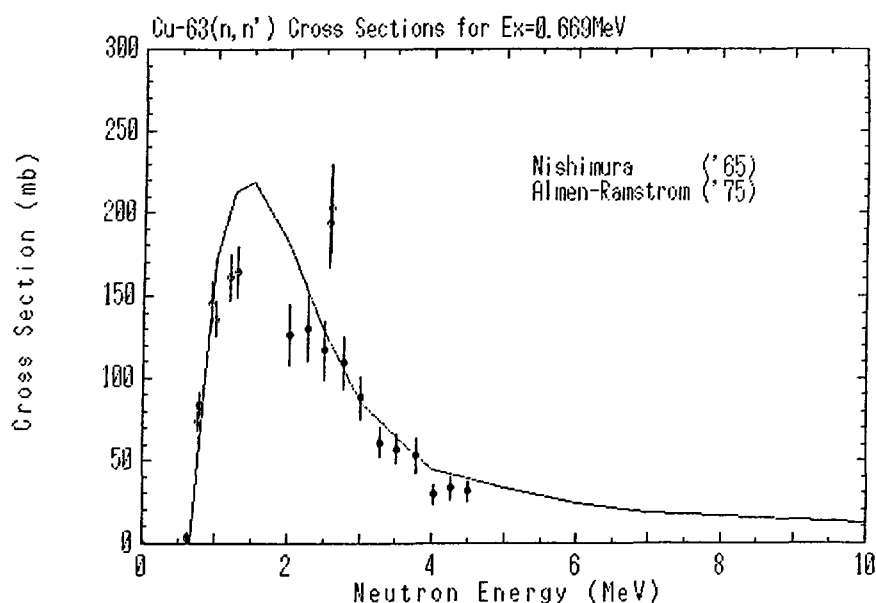for ^{63}Cu.

Cu-63(n,n') Cross Sections for Ex=0.669MeV

Fig. 6   Calculated ^{63}Cu(n,n') cross section for exciting the 0.669 MeV
level compared with experimental data.

Copper total inelastic scattering cross section
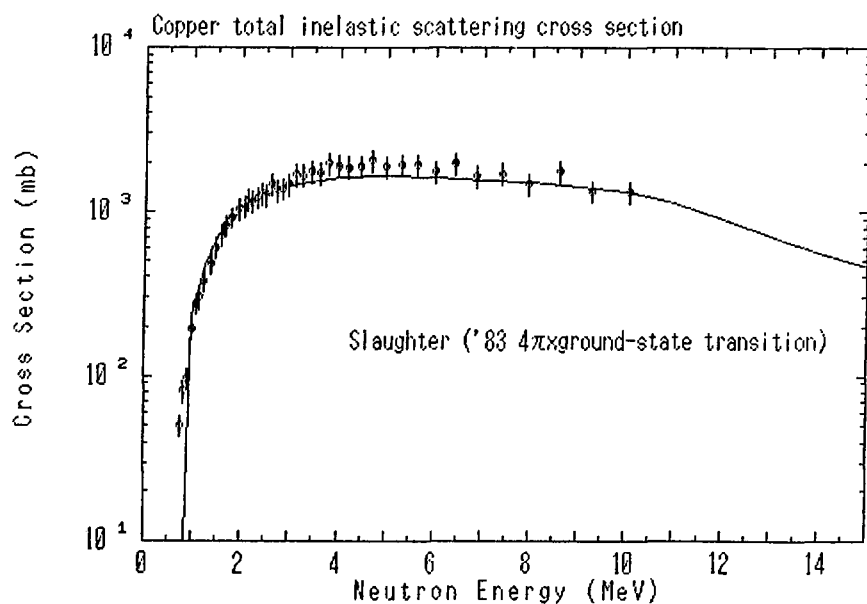

Fig. 7   Comparison of calculated and experimental total inelastic
scattering cross section for copper.
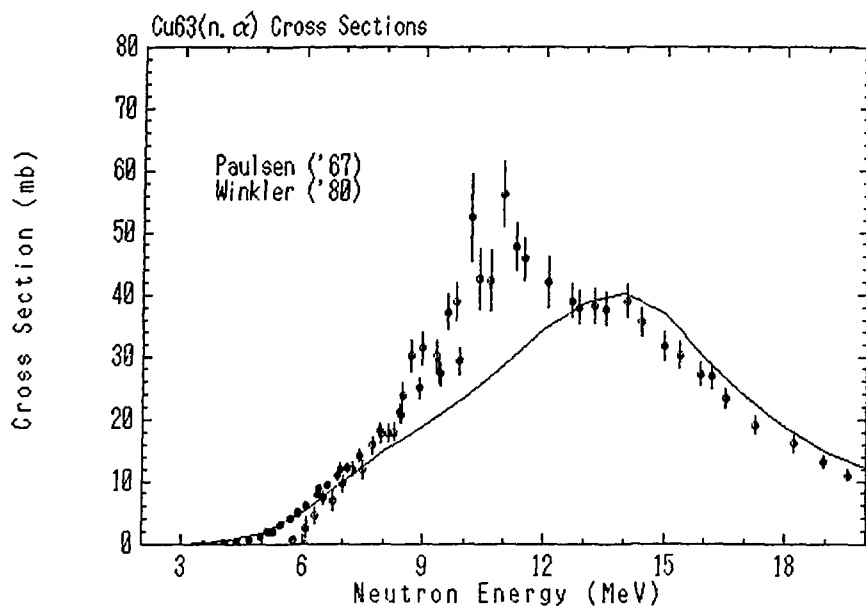
Fig. 8 ^{63}Cu(n,alpha) cross section compared with experimental data.

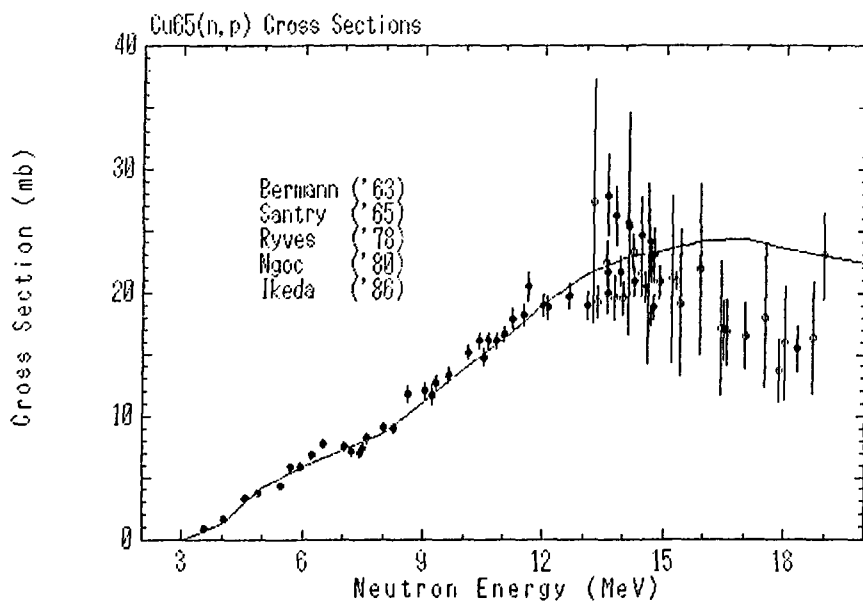Fig. 9 ^{65}Cu(n,p) cross section compared with experimental data.

Cu63(n,2n) Cross Sections
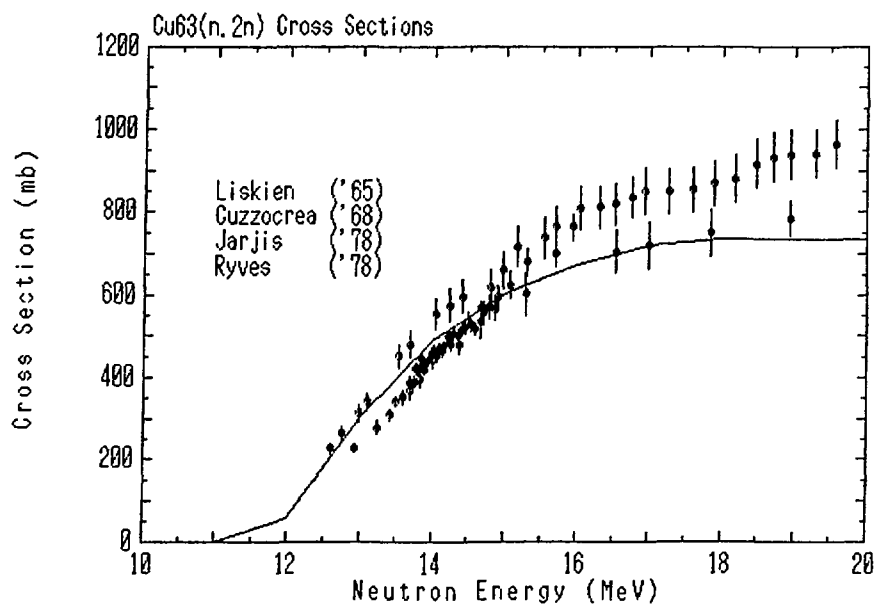
Fig.10 ^{63}Cu(n,2n) cross section compared with experimental data.

Cu65(n,2n) Cross Sections
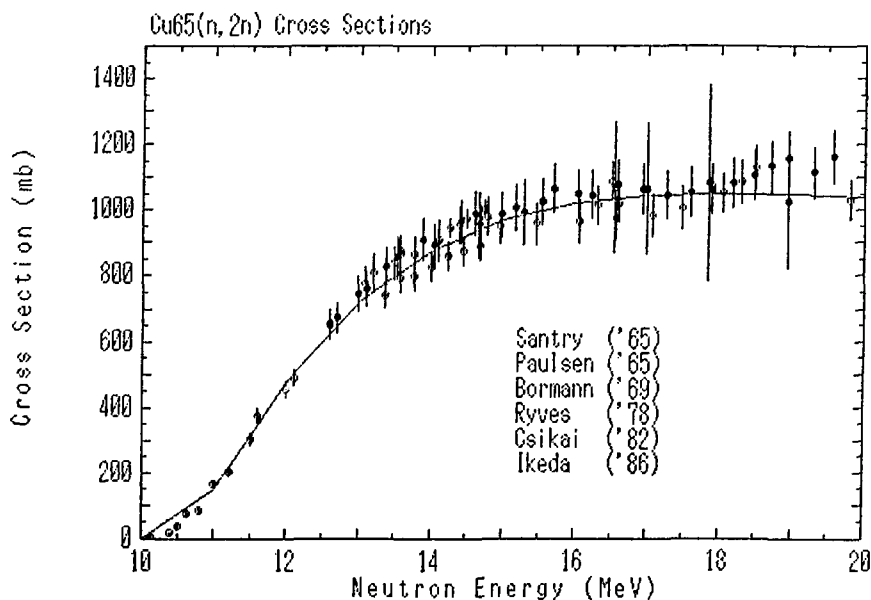
Fig.11 ^{65}Cu(n,2n) cross section compared with experimental 'ata.

Total Gamma-Ray Production Cross Sections for Copper

Eγ>0.75MeV

Dickens ('73)
Chapman ('76)
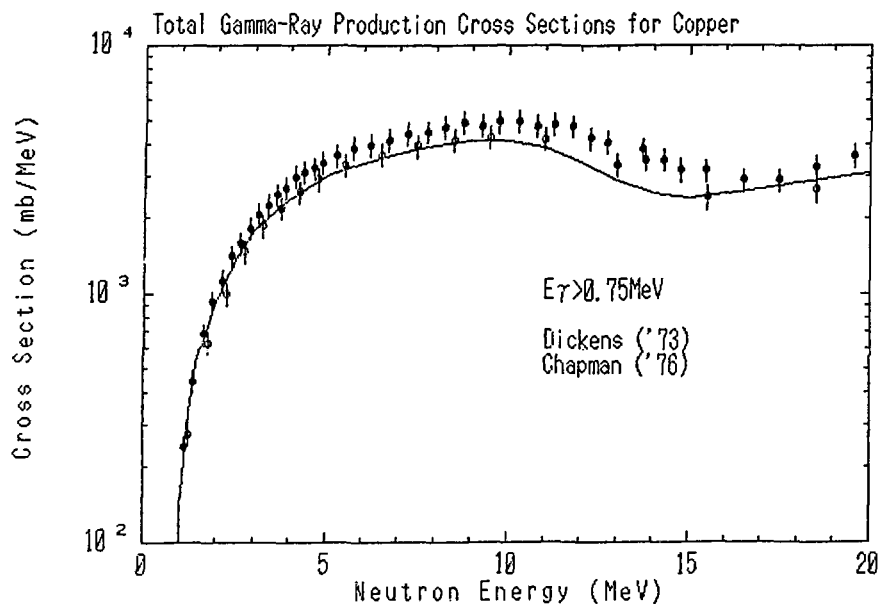
Fig.12   Total gamma-ray production cross section with Eg > 0.75 MeV
compared with data of Dickens et al. and Chapman.   Experimental
data detected at an angle 125° were multiplied by 4π.

Cu-65 Capture Cross Sections

Stavisskij ('61)
Zaikin   ('68)
Voignier ('86)
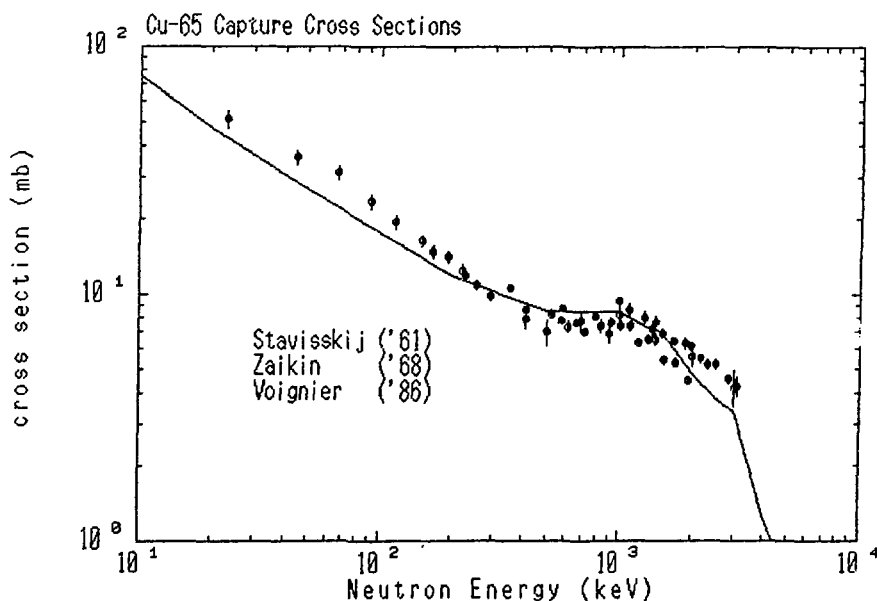
Fig.13   Comparison of calculated and experimental radiative capture cross
section for ^{65}Cu.

Excitation Energy （MeⅤ）

Fig.14 Fission-to-neutron transmission coefficient ratios for uranium
isotopes.

Fig.15 Comparison of calculated and experimental neutron cross sections for ^{235}U.

国際単位系 (SI) と換算表

表1　SI基本単位および補助単位

量	名　称	記　号
長　　さ	メ ー ト ル	m
質　　量	キ ロ グ ラ ム	kg
時　　間	秒	s
電　　流	ア ン ペ ア	A
熱力学温度	ケ ル ビ ン	K
物 質 量	モ ー ル	mol
光　　度	カ ン デ ラ	cd
平 面 角	ラ ジ ア ン	rad
立 体 角	ステラジアン	sr

表3　固有の名称をもつSI組立単位

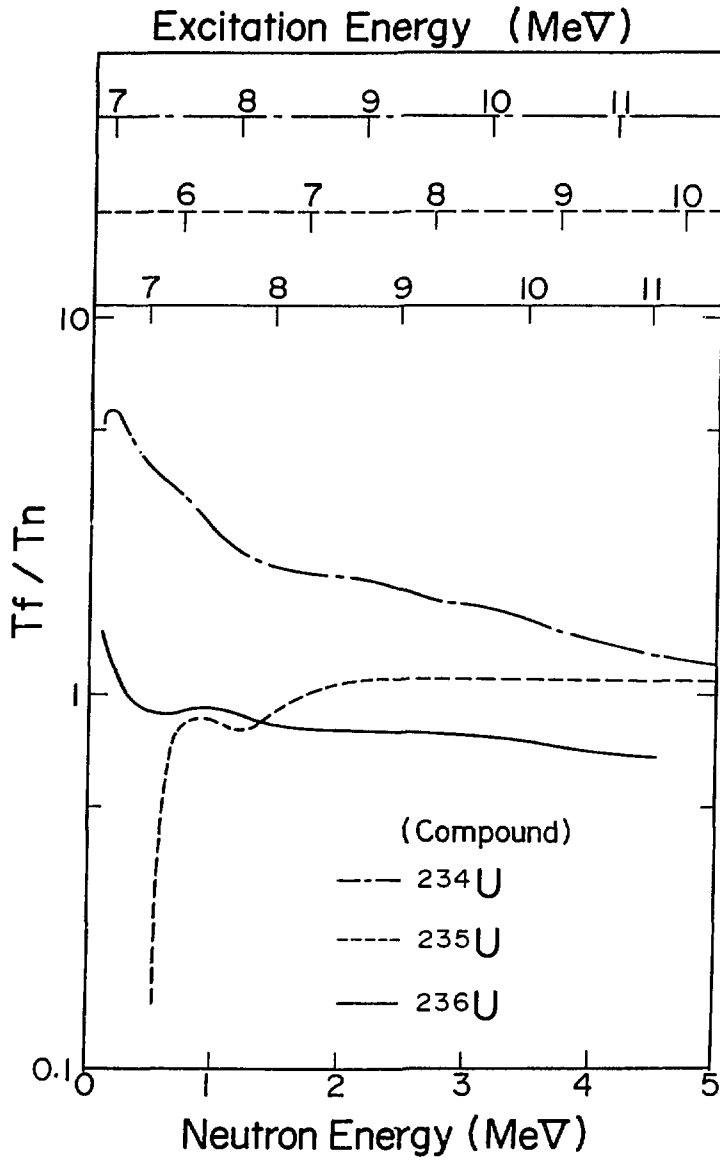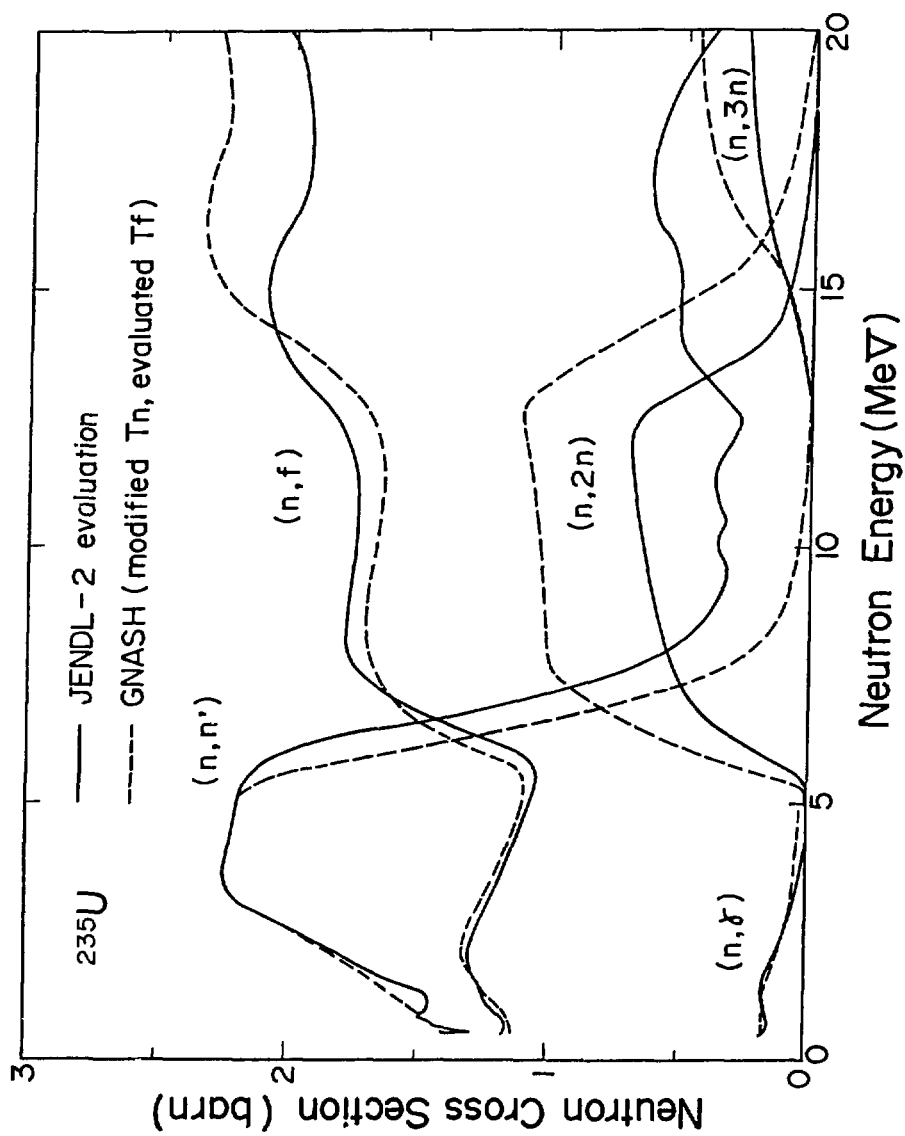| 量	名　称	記号	他のSI単位による表現
周 波 数	ヘ ル ツ	Hz	s⁻¹
力	ニュートン	N	m·kg/s²
圧力, 応力	パスカル	Pa	N/m²
エネルギー, 仕事, 熱量	ジュール	J	N·m
工率, 放射束	ワ ッ ト	W	J/s
電気量, 電荷	ク ー ロ ン	C	A·s
電位, 電圧, 起電力	ボ ル ト	V	W/A
静 電 容 量	ファラド	F	C/V
電 気 抵 抗	オ ー ム	Ω	V/A
コンダクタンス	ジーメンス	S	A/V
磁 束	ウェーバ	Wb	V·s
磁 束 密 度	テ ス ラ	T	Wb/m²
インダクタンス	ヘンリー	H	Wb/A
セルシウス温度	セルシウス度	℃	
光 束	ル ー メ ン	lm	cd·sr
照 度	ル ク ス	lx	lm/m²
放 射 能	ベクレル	Bq	s⁻¹
吸 収 線 量	グ レ イ	Gy	J/kg
線 量 当 量	シーベルト	Sv	J/kg

表2　SIと併用される単位

名　称	記　号
分, 時, 日	min, h, d
度, 分, 秒	°, ′, ″
リ ッ ト ル	l, L
ト ン	t
電子ボルト	eV
原子質量単位	u

$1 \text{ eV} = 1.60218 \times 10^{-19} \text{ J}$

$1 \text{ u} = 1.66054 \times 10^{-27} \text{ kg}$

表4　SIと共に暫定的に維持される単位

名　称	記　号
オングストローム	Å
バ ー ン	b
バ ー ル	bar
ガ ル	Gal
キ ュ リ ー	Ci
レントゲン	R
ラ ド	rad
レ ム	rem

$1 \text{ Å} = 0.1 \text{ nm} = 10^{-10} \text{ m}$

$1 \text{ b} = 100 \text{ fm}^2 = 10^{-28} \text{ m}^2$

$1 \text{ bar} = 0.1 \text{ MPa} = 10^5 \text{ Pa}$

$1 \text{ Gal} = 1 \text{ cm/s}^2 = 10^{-2} \text{ m/s}^2$

$1 \text{ Ci} = 3.7 \times 10^{10} \text{ Bq}$

$1 \text{ R} = 2.58 \times 10^{-4} \text{ C/kg}$

$1 \text{ rad} = 1 \text{ cGy} = 10^{-2} \text{ Gy}$

$1 \text{ rem} = 1 \text{ cSv} = 10^{-2} \text{ Sv}$

表5　SI接頭語

倍数	接頭語	記　号
10^{18}	エ ク サ	E
10^{15}	ペ タ	P
10^{12}	テ ラ	T
10^{9}	ギ ガ	G
10^{6}	メ ガ	M
10^{3}	キ ロ	k
10^{2}	ヘ ク ト	h
10^{1}	デ カ	da
10^{-1}	デ シ	d
10^{-2}	セ ン チ	c
10^{-3}	ミ リ	m
10^{-6}	マイクロ	μ
10^{-9}	ナ ノ	n
10^{-12}	ピ コ	p
10^{-15}	フェムト	f
10^{-18}	ア ト	a

(注)

1. 表1〜5は「国際単位系」第5版, 国際度量衡局 1985年刊行による。ただし, 1 eV および1 uの値はCODATAの1986年推奨値によった。

2. 表4には海里, ノット, アール, ヘクタールも含まれているが日常の単位なのでここでは省略した。

3. barは, JISでは流体の圧力を表わす場合に限り表2のカテゴリーに分類されている。

4. EC閣僚理事会指令ではbar, barnおよび「血圧の単位」mmHgを表2のカテゴリーに入れている。

換 算 表

力	N(=10⁵dyn)	kgf	lbf
	1	0.101972	0.224809
	9.80665	1	2.20462
	4.44822	0.453592	1

粘　度　1 Pa·s(N·s/m²) = 10 P(ポアズ)(g/(cm·s))
動粘度　1 m²/s = 10⁴ St(ストークス)(cm²/s)

圧力	MPa(=10 bar)	kgf/cm²	atm	mmHg(Torr)	lbf/in²(psi)
	1	10.1972	9.86923	7.50062×10^3	145.038
	0.0980665	1	0.967841	735.559	14.2233
	0.101325	1.03323	1	760	14.6959
	1.33322×10^{-4}	1.35951×10^{-3}	1.31579×10^{-3}	1	1.93368×10^{-2}
	6.89476×10^{-3}	7.03070×10^{-2}	6.80460×10^{-2}	51.7149	1

エネルギー・仕事・熱量	J(=10⁷erg)	kgf·m	kW·h	cal(計量法)	Btu	ft·lbf	eV
	1	0.101972	2.77778×10^{-7}	0.238889	9.47813×10^{-4}	0.737562	6.24150×10^{18}
	9.80665	1	2.72407×10^{-6}	2.34270	9.29487×10^{-3}	7.23301	6.12082×10^{19}
	3.6×10^6	3.67098×10^5	1	8.59999×10^5	3412.13	2.65522×10^6	2.24694×10^{25}
	4.18605	0.426858	1.16279×10^{-6}	1	3.96759×10^{-3}	3.08747	2.61272×10^{19}
	1055.06	107.586	2.93072×10^{-4}	252.042	1	778.172	6.58515×10^{21}
	1.35582	0.138255	3.76616×10^{-7}	0.323890	1.28506×10^{-3}	1	8.46233×10^{18}
	1.60218×10^{-19}	1.63377×10^{-20}	4.45050×10^{-26}	3.82743×10^{-20}	1.51857×10^{-22}	1.18171×10^{-19}	1

1 cal = 4.18605 J (計量法)
= 4.184 J （熱化学）
= 4.1855 J （15℃）
= 4.1868 J (国際蒸気表)

仕事率　1 PS (仏馬力)
= 75 kgf·m/s
= 735.499 W

放射能	Bq	Ci
	1	2.70270×10^{-11}
	3.7×10^{10}	1

吸収線量	Gy	rad
	1	100
	0.01	1

照射線量	C/kg	R
	1	3876
	2.58×10^{-4}	1

線量当量	Sv	rem
	1	100
	0.01	1